Conservation Laws Models in Networks and Multiscale Flow Optimization

Jean Medard Tchoukouegno Ngnotchouye

Submitted in fulfillment of the academic requirements for the degree of

DOCTOR OF PHILOSOPHY in **Applied Mathematics**

in the

School of Mathematical Sciences
University of KwaZulu-Natal
Pietermariztburg

February 2011

In the loving memory of my father, Jean Bamenyam,
who taught me that education is the key to success.
To quote him, "L'école est la clef qui ouvre toutes les portes".

Declaration

The research work described in this thesis was carried out in the School of Mathematical Sciences, University of KwaZulu-Natal Pietermaritzburg, from August 2007 to February 2011 under the supervision of Professor Mapundi K. Banda and Professor Precious Sibanda. As an external supervisor, the support of Prof Michael Herty is hereby acknowledged.

This thesis presents original work by the author and has not been submitted in any form for any degree or diploma to any University. Where use has been made of the work of others it is duly acknowledged in the text.

Pietermaritzburg, February 2nd, 2011.

Jean Medard Tchoukouegno Ngnotchouye
B.Sc (Cameroon), M. Sc. (Cameroon),
Post graduate Diploma(AIMS/UWC).

Acknowledgments

My deepest gratitude goes to my supervisor, Prof Mapundi K. Banda, for his guidance, motivation and understanding during my PhD work. Despite moving to Wits in the course of my studies, he was always available for discussions trough email or the phone when necessary. My research stays at Wits have always been very rewarding and cheerful and I thank you so much, Mapundi, for that.
I am grateful to Prof. Precious Sibanda, who accepted to co-supervise my research work. I am so grateful for his administrative support and also for the time he took to read my manuscript. My thank you goes also to Dr Anifiock Udomene at UKZN, who accepted to proofread parts of my manuscript. Your comments helped to improve the quality of my presentation.

I am very grateful to Prof. Dr. Michael Herty for his guidance and his help throughout the duration of my PhD work. I thank you Michael for inviting me to the RWTH university, Aachen for a research stay. I am thankful also to Sonja, Ute and Albert at RWTH, Aachen for their kindness and friendship during my stay in Germany.

I am thankful to Prof Banda who helped to secure the funding necessary for my PhD through the research office of the UKZN. I am very grateful to the school of mathematical sciences for funding all my local conferences trips and for providing the facilities for my research. I acknowledge the financial support of DAAD, Grant number A/08/96840 during my stay in Aachen, Germany; and of the Department of Mathematics, University of Kaizerslautern, who partially funded my one week stay in Kaizerslautern.

I owe much to staff members of the School of Mathematical Sciences of the University of KwaZulu-Natal, Pietermaritzburg for their support during this period of hard work. Thank you Prof John van den Berg, Prof J. Moori, Ms Faith Nzimande and Ms Sebe Ndlovu.

I am very grateful to my wife Mireille for her love and support during my PhD research.

I am grateful to friends and colleagues at the school of maths and statistics as well as those at CAM at Wits for their support in diverse situations. Special thanks to Ayoub, Faiz, Tekiso, Zodwa, Makhala, Pedro, Naval, Morgan.

My sincere appreciation to all the members of the Cameroonian Community in Pietermaritzburg. Thanks to you guys, in many occasions I felt at home far from home.

Finally, I am thankful to my whole family in Cameroon and abroad, including my dear mother, brothers and sisters, uncles and aunts.

My humble gratitude goes to the Scottsville Presbyterian Church in Pietermaritzburg for spiritual support.

Abstract

The flow of fluids in a network is of practical importance in gas, oil and water transport for industrial and domestic use. When the flow dynamics are understood, one may be interested in the control of the flow formulated as follows: given some fluid properties at a final time, can one determine the initial flow properties that lead to the desired flow properties?

In this thesis, we first consider the flow of a multiphase gas, described by the drift-flux model, in a network of pipes and that of water, modeled by the shallow water equations, in a network of rivers. These two models are systems of partial differential equations of first order generally referred to as systems of conservation laws. In particular, our contribution in this regard can be summed up as follows: For the drift-flux model, we consider the flow in a network of pipes seen mathematically as an oriented graph. We solve the standard Riemann problem and prove a well posedness result for the Riemann problem at a junction. This result is obtained using coupling conditions that describe the dynamics at the intersection of the pipes. Moreover, we present numerical results for standard pipes junctions. The numerical results and the analytical results are in agreement. This is an extension for multiphase flows of some known results for single phase flows. Thereafter, the shallow water equations are considered as a model for the flow of water in a network of canals. We analyze coupling conditions at the confluence of rivers, precisely the conservation of mass and the equality of water height at the intersection, and implement these results for some classical river confluences. We also consider the case of pooled stepped chutes, a geometry frequently utilized by dams to spill floodwater. Here we consider an

approach different from the engineering community in the sense that we resolve the dynamics by solving a Riemann problem at the dam for the shallow water equations with some suitable coupling conditions.

Secondly, we consider an optimization problem constrained by the Euler equations with a flow-matching objective function. Differently from the existing approaches to this problem, we consider a linear approximation of the flow equation in the form of the microscopic Lattice Boltzmann Equations (LBE). We derive an adjoint calculus and the optimality conditions from the microscopic LBE. Using multiscale analysis, we obtain an equivalent macroscopic result at the hydrodynamic limit. Our numerical results demonstrate the ability of our method to solve challenging problems in fluid mechanics.

Résumé

Les écoulements des fluides dans des réseaux sont d'une importance paticulière dans le transport des gaz ou de l' eau pour des raisons industrielles ou domestiques. Quand la dynamique de l'écoulement est comprise, l'on peut s'intéresser au control de cet écoulement formulé ainsi qu'il suit: Etant donner des propriètés d'un fluide au temps final, peut-on determiner des données initiales qui conduisent a ces propriétés désirées?

Dans cette thèse, nous considérons dans un premier temps l' écoulement d'un gaz multiphasique décrit par le modèle "drift-flux" dans un reseau de tuyaux et celui de l'eau, decrit par le model de Saint Venant ou equation en eau peu profonde dans un réseau de rivières ou de canaux. Ces deux modèles sont des equations aux dérivées partielles du premier ordre, genéralement appeler systèmes des lois de conservations. Notre contribution peut être résumer ainsi qu'il suit. Pour le modele du "drift-flux", we considérons son écoulement dans un reseau vu mathematiquement comme un graphe orienté. Nous resolvons le problème standard de Riemann et nous prouvons un resultat d'existance pour le problème de Riemann à l'intersection ou au noeud du reseau. Ce resultat est obtenu en utilisant des conditions de couplage qui descrivent la dynamique de l'écoulement au noeud du reseau de tuyaux. En plus, nous presentons des resultats numériques pour des noeuds classiques. Nos resultats analytiques et numériques coincident. Ces resultats constituent une généralisation aux modèles multiphasique de certain résultats connu pour des modèles uniphasique. Ensuite, nous considérons le modèle de Saint Venant qui décrit un écoulement d'eau, dans un reseau de canaux. Nous analysons certaines conditions de couplage a l'intersection

des canaux, précisement la conservation de la masse et l'égalité de la hauteur de l'eau, et nous presentons des resultats de simulations numériques pour des confluences classiques. Nous considérons aussi le cas des chuttes en escalier, une géométrie utilisée genéralement à des barrages pour evacuer les eaux d'inondations. Notre approche ici est différente de celle de la communauté hydraulique dans le sens ou nous résolvons la dynamique en resolvant des "problèmes de Riemann au barrage" pour les equations de Saint Venant avec des conditions de couplages appropriées.

Dans une deuxième partie, nous considérons un problème d'optimization des écoulements régit par les équations d'Euler avec une function objective du type "flow matching'. Différement des approches existentes pour la solution de ce problème, nous proposons l'utilisation d'une approximation linéaire des équations d'Euler donnée par le modèle microscopique de Boltzmann. Nous derivons l' équation adjointe et les conditions d'optimalité en utilisant le modèle microscopique de Boltzmann. En utilisant une analyse multi-echelle, nous obtenons un resultat macroscopique equivalent a la limite hydraudynamique. Nos resultats numeriques démontrent que notre approche permet de resoudre des problemes difficiles de la dynamiques des fluides.

Contents

Part I

Introduction and Preliminary Results

Chapter 1

Introduction

The mathematical study of conservations laws is an important topic that originated with the pioneering work of d'Alembert on wave equations and Euler on equations describing the evolution of a fluid. The physical concept of conservation laws appears naturally in continuum mechanics where the conservation of mass, of momentum and of energy are paramount. In general, a conservation law model appears when some physical quantity, say u, is conserved. A system of conservation laws has the form

$$\partial_t u + \partial_x f(u) = 0, \tag{1.1}$$

where the mapping f is called the *flux function* and ∂_t and ∂_x are the partial derivatives with respect to time and space, respectively. By integrating (1.1) over a space interval $[a, b]$, we have

$$\begin{aligned} \frac{d}{dt}\int_a^b u(x,t)dx &= \int_a^b \partial_t u(x,t)dx \\ &= -\int_a^b \partial_x f(u(x,t))dx \\ &= f(u(a,t)) - f(u(b,t)) \\ &= [\text{inflow at } a] - [\text{outflow at } b]. \end{aligned} \tag{1.2}$$

This says that the variation of the quantity u over the space interval $[a, b]$ depends only on the flow across the two endpoints. One can write (1.1) in the quasilinear

form

$$\partial_t u + Df(u)\partial_x u = 0, \tag{1.3}$$

where $Df(u)$ is the Jacobian matrix of the flux f. But (1.3) is equivalent to (1.1) only in the realm of smooth solutions. When the solution u is discontinuous, $\partial_x u$ is not smooth and the product in the second term of (1.3) is not defined. Therefore, our analysis will be done in the framework of weak solutions, that uses the integral form of (1.1). An important mathematical challenge associated with conservation laws is that solutions can develop discontinuities or blow-up in finite time even if the initial data is regular. To understand this challenge, one starts by studying the standard Riemann problem associated with the model equation (1.1) which consists of solving (1.1) with a Heaviside-type initial data. This is a preliminary step for the study of the Cauchy problem associated with (1.1). A proof of the existence of solutions to this Cauchy problem was first proposed by Glimm [55] using the random choice method. A deterministic proof as well as some uniqueness results were proved by Bressan and colleagues and Liu [23, 24, 21, 26, 28, 20, 81]. The main tool used in the proof was the wave-front tracking algorithm proposed by Dafermos [42]. Recently, the dynamics of systems of conservation laws in a network of pipes and canals have been of interest for many scientists. We mention the case of gas networks with the contributions of Colombo et al. [32, 33, 38] who considered the p-system and proved well-posedness for the *Cauchy problem at the junction*, of Banda et al. [6, 7, 4] who considered the isothermal Euler equations, proved the well-posedness and provide some numerical simulations. The case of the full Euler equation in standard Networks was considered by Colombo and Mauri in [41] and by Herty in [61]. Colombo and Marcellini considered the case of a pipe with discontinuous cross section in [40, 39].

In the second part of this thesis, we consider a model for multiphase flow derived from the *drift-flux model* [51] in a network of pipes. The drift-flux model is derived from the *two-fluid model* by averaging the balance laws for the momentum in the canonical form. The model is then closed with a *slip relation*, that gives an algebraic relation between the two velocities, and a pressure law, expressed in terms of the

densities [48, 51]. Here we assume that the slip function vanishes and therefore the velocities of the two phases are equal. Due to the complexity of the model for a network of pipes, we investigate separately the case of a linear pressure law and the general case where there is no restriction on the pressure law. For the two cases, we formulate some coupling conditions that serve to prove the well-posedness of the Riemann problem at the junction and we carry out some numerical simulation for a junction of two, three and four pipes. Key to our analysis are the expressions of the *Lax curves*. We prove numerically that when the exact Lax curves are replaced by their linearizations, the results are in good agreement. This result, which to the best of our knowledge is presented for the first time here, allows us to obtain well-posedness and numerical results for our model with a general equation of state. This work has led to [10, 8, 9].

The third part of the thesis deals with the flow of water in a network of canals. The flow obeys the shallow water equations and we consider different types of river confluences. We derive coupling conditions at the confluences or junctions from those proposed by Rademacher et al. [99] and compute the dynamics on common river confluences. These results appeared in [76].
Further, we consider the case of pooled stepped chutes, a geometry frequently utilized by dams to spill floodwater. Here our approach is different from that of the engineering community in the sense that we resolve the dynamics by solving some *Riemann problem at the dam* for the shallow water equations with some suitable coupling conditions. Our result compares well with the experimental results from the hydraulic literature [13, 101].

The last part of the thesis deals with the control of flow governed by a system of conservation laws. The mathematical difficulty associated with this problem is that the flow generated by systems of conservation laws is not differentiable in any classical functional space [29]. A notion of shift-differentiability have been introduced by Bressan and colleagues [22, 25, 27] and an optimality result obtained by Bressan and Shen [29] for systems and by Colombo and Groli [36, 35] for scalar conservation laws. These results nevertheless are not amenable to numerical simulations

that can help to compute the optimal solution. Key to the proofs are the control of the wave interactions that can occur between two waves or between a wave and the pipes' junctions. These wave interactions pose a serious problem for a gradient based method for the solution of this optimization problem. As a solution to this problem, we propose the use of a linear model, in the form of the lattice Boltzmann equations(LBE) that approximates the flow model given by the one dimensional Euler equations. Precisely, we use the one dimensional five velocity (D1Q5) LBE model and we prove that this microscopic model converges in the hydrodynamic limit to the Euler equations. Using the LBE, we derive an adjoint calculus and the optimality conditions for the control of the Euler equations and present the results of some numerical simulations applied to some test problems of interest. The results obtained here constitute a new approach for the control of Euler flow and avoid complicated tools as detection of discontinuity used in [64]. This work has led to [86, 87, 106].

The thesis is organized as follows: In Chapter 2, we recall some fundamental results pertaining to the mathematical analysis and numerical integration of systems of conservation laws. Due to discontinuities that arise in the solution of the flow equations, the numerical schemes need to be conservative and total variation diminishing (TVD). In Chapter 3, we present the mathematical analysis of the drift-flux multiphase flow in a network of pipes. The pressure law considered here is a linear function of the densities. We present a local well-posedness results and the constructive proof play an important role in the numerical simulations of the dynamics of the network. Chapter 4 extends the results of Chapter 3 for a general pressure law. Moreover, we analyze the effect of the *sonic speed* of each fluid on the multiphase fluid in networks. The case of a junction with a discontinuous cross section is presented.
The simulation of the dynamics of a river network is investigated in Chapter 5. Here we review some flow properties and derive some coupling conditions at the river confluences from those proposed by Rademayer et al. [99]. We present some numerical results in the case of a river and a tributary, that of three connected rivers

and that of a storage basin. In Chapter 6, we consider the case of pooled stepped chutes, a geometry frequently utilized by dams to spill floodwater. We resolve the dynamics by solving a *Riemann problem at the dam* with suitable coupling conditions. Chapter 7 deals with the optimal control of the Euler equations. Our analysis uses a kinetic model in the form of a lattice Boltzmann equation that converges in the hydrodynamic limit to the Euler equations. We derive the optimality system using the kinetic model and perform some numerical simulations that prove satisfactory on the solution of many important test problems. Finally, Chapter 8 presents the conclusions and future area of research suggested by this thesis.

PUBLICATION LIST

Journal Article

[**10**] Mapundi K. Banda, Michael Herty, **Jean Medard T. Ngnotchouye**. *Towards a mathematical analysis for drift flux multiphase models in networks.* SIAM J. Sci. Comp. Vol 31, No. 6, pp. 4633–4653, 2010.

[**8**] Mapundi K. Banda, Michael Herty, **Jean Medard T. Ngnotchouye**. *Coupling the drift-flux models with unequal sonic speeds.* Mathematical and Computational Applications, Vol. 15, No. 4, pp. 574–584, 2010.

[**87**] **Jean Medard T. Ngnotchouye**, Michael Herty, Sonja Veelken, Mapundi K. Banda. *Relaxation approaches to the optimal control of the Euler equations.* (To appear in) Computational and Applied Mathematics, 2011.

Conference proceedings

[**9**] Mapundi K. Banda, Michael Herty, **Jean Medard T. Ngnotchouye**. *Modelling and simulating multiphase drift-flux model in a networked domain.* Proceedings of the Int. Conf. on Industrial and Appl. Math. Indonesia, pp. 127-133, 2010.

[**76**] Tony Lange, Mapundi K. Banda and **Jean Medard T. Ngnotchouye**. *Time domain simulations of the dynamics of rivers networks*. Proceedings of the Mathematics in Industry Study Group, pp. 41–61, 2008.

[**86**] **Jean Medard T. Ngnotchouye**, Michael Herty and Mapundi K. Banda. *A Multi-Scale Approach to the Flow Optimization of Systems Governed by the Euler Equations*, Proceedings of the Int. Conf. on Industrial and Appl. Math. Indonesia, pp. 121-126, 2010.

[**106**] Sonja Veelken, Michael Herty, **Jean Medard T. Ngnotchouye** and Mapundi Banda. *Optimal control of the Euler equations via relaxation approaches*, Proceedings in Applied Mathematics and Mechanics, Vol. 10, pp. 595–596, 2010.

Chapter 2

Mathematical Preliminaries

In this thesis we use fluid models such as the drift-flux model, the Euler equation and the shallow water equation to formulate a model for the flow in networks of pipes or canals. These fluid models are hyperbolic systems of conservation laws. In this chapter we present the main properties and numerical schemes for hyperbolic systems of conservation laws. For more details on the topic, we refer the reader to [19, 42, 60, 83] for the theoretical analysis and to [78, 79, 102] for the numerical simulations.

We begin this chapter by recalling some definitions and properties of functions of bounded variations. It is generally in this framework that one can prove the existence of solutions to systems of conservation laws.

2.1 Functions with Bounded Variation

Definition 2.1. *Consider an interval $J \subset \mathbb{R}$ and a map $u : J \to \mathbb{R}^m$. The total variation of u is defined as*

$$TV(u) = \sup \left\{ \sum_{j=1}^{N} \|u(x_j) - u(x_{j-1})\| : N \in \mathbb{N} \setminus \{0\},\ x_j \in J,\ \text{and } x_0 < \cdots < x_N \right\}.$$

If $u \in \mathbf{L}^{\mathbf{1}}_{\mathrm{loc}}(J, \mathbb{R}^m)$ and $TV(u) < \infty$, we say that u has bounded variation, and write $u \in \mathbf{BV}(J; \mathbb{R}^m)$.

The following result, whose proof can be found for example in [19] is very important for the passage to the limits.

Theorem 2.1 (Helly)**.** *Consider a sequence of functions $u_\nu : \mathbb{R} \to \mathbb{R}^m$ and let C, M be some positive constants such that*

$$TV(u_\nu) \leq C, \quad |u_\nu(x)| \leq M \quad \text{for all } \nu, x.$$

Then there exists a function u and a subsequence u_μ such that

$$\lim_{\mu\to\infty} u_\mu(x) = u(x) \quad \text{for every } x \in \mathbb{R},$$
$$TV(u) \leq C, \quad |u(x)| \leq M \quad \text{for all } x.$$

Definition 2.2. *A function $u \in \mathbf{L^1_{loc}}(\mathbb{R}^d;\mathbb{R}^m)$ is said to be locally of bounded variation, denoted $u \in \mathbf{BV_{loc}}(\mathbb{R}^d;\mathbb{R}^m)$, if for every compact set $K \subset \mathbb{R}^d$ there exists a constant C_K such that*

$$\int_K \left| u.\frac{\partial\varphi}{\partial x_i} dx \right| \leq C_K \sup_{x\in K} \|\varphi(x)\| \quad i = 1, \ldots, d$$

for every $\mathbf{C^1}$ function φ with compact support K contained in $\mathbb{R}^d$.

Definition 2.3. *A function $u \in \mathbf{L^1}(\mathbb{R}^d;\mathbb{R}^m)$ is said to have a bounded variation, denoted $u \in \mathbf{BV}(\mathbb{R}^d;\mathbb{R}^m)$, if there exists a constant C such that*

$$\left| \int_{\mathbb{R}^d} u \cdot \frac{\partial\varphi}{\partial x_i} dx \right| \leq C \sup_{x\in\mathbb{R}^d} \|\varphi(x)\| \quad i = 1, \ldots, d$$

for every $\mathbf{C^1}$ function φ with compact support contained in $\mathbb{R}^d$.

Let $\mathcal{L}^n$ denotes the n-dimensional Lebesgue measure.

Theorem 2.2. *Let $u \in \mathbf{L^1_{loc}}(\mathbb{R}^d)$. For a fixed $k \in \{1, \ldots, d\}$, let*

$$x' = (x_1, \ldots, x_{k-1}, x_{k+1}, \ldots, x_d) \in \mathbb{R}^{d-1}$$

and set

$$u_k(x', y) = u(x_1, \ldots, x_{k-1}, y, x_{k+1}, \ldots, x_d).$$

Then $u \in \mathbf{BV_{loc}}(\mathbb{R}^d)$ if and only if the map $y \mapsto u_k(x', y)$ is in $\mathbf{BV_{loc}}(\mathbb{R})$ for $\mathcal{L}^{n-1} - a.e.\, x' \in \mathbb{R}^{d-1}$, for every $k = 1, \ldots, d$.

The following result relates the total variation of a vector valued function to that of its components.

Proposition 2.1. *Let $u : \mathbb{R}^d \to \mathbb{R}^m$. Then $u \in \mathbf{BV_{loc}}(\mathbb{R}^d; \mathbb{R}^m)$ if and only if each component $u_i \in \mathbf{BV_{loc}}(\mathbb{R}^d; \mathbb{R})$, $i = 1, \ldots, m$.*

The following theorem states the existence of trace of a **BV** function on the boundary of a measurable set. A definition of trace, of essential boundary, as well as the proof of the theorem can be found in [107, Chapter 4].

Theorem 2.3. *Let $E \subset \mathbb{R}^d$ be a measurable set, S its essential boundary. Let $u \in \mathbf{BV}(\mathbb{R}^d)$. Then the trace u^+ of u on S exists a.e. with respect to the $(n-1)$-dimensional Hausdorff measure.*

2.2 Homogeneous Systems of Conservation Laws

Let $\Omega \subset \mathbb{R}^m$ be an open set. An $m \times m$ system of conservation laws has the form

$$U_t + f(U)_x = 0, \tag{2.1}$$

with $t \in [0, T]$ and $x \in \mathbb{R}$. The map $f : \Omega \to \mathbb{R}^m$ in (2.1) is often referred to as the *flux* function. We assume in this chapter that f is at least $\mathcal{C}^1$. Let

$$A(U) \doteq Df(U) = \begin{pmatrix} \frac{\partial f_1}{\partial U_1} & \cdots & \frac{\partial f_1}{\partial U_m} \\ \vdots & \cdots & \vdots \\ \frac{\partial f_m}{\partial U_1} & \cdots & \frac{\partial f_m}{\partial U_m} \end{pmatrix}$$

be the Jacobian matrix of the map f at the point U. The system (2.1) can be written in the quasilinear form

$$U_t + A(U)U_x = 0. \tag{2.2}$$

Definition 2.4 (Classical solution)**.** *A classical solution of* (2.1) *is a continuously differentiable function $U = U(t, x)$ which satisfies* (2.1) *at every point of its domain. If an initial condition $\bar{U}(x)$ is given, U should also satisfy $U(0, x) = \bar{U}(x)$, for all x.*

For classical solutions, equations (2.1) and (2.2) are entirely equivalent. However, if at least one of the components of U has a jump at a point, say, ξ, then the left hand side of (2.2) will contain the product of a discontinuous function with a distributional derivative which contains a Dirac mass at the point ξ. In general, such a product is not well defined. Hence (2.2) is meaningful only within the class of continuous functions.

2.2.1 Weak solutions

By working with the equation in the form (2.1), we can consider discontinuous solutions interpreted in distributional sense. Indeed, we have the following definition.

Definition 2.5. *A measurable function $U(t,x)$ from an open subset Ω of $\mathbb{R}\times\mathbb{R}$ into $\mathbb{R}^m$ is a distributional solution of (2.1) if for every $\mathcal{C}^1$ function φ with compact support, one has*

$$\iint_\Omega (U_i\varphi_t + f_i(U)\varphi_x)dxdt = 0,$$

for each component U_i and $f_i(U)$ of U and $f(U)$, respectively.

A distributional solution U is not necessarily continuous, but U and $f(U)$ should be locally integrable in O. Definition 2.5 can be extended to take into account some initial data.

Definition 2.6. *Given an initial condition*

$$U(0,x) = \bar{U}(x) \tag{2.3}$$

with $\bar{U}\in \mathbf{L}^{\mathbf{1}}_{\mathrm{loc}}(\mathbb{R};\mathbb{R}^m)$, we say that a function $U:[0,T]\times\mathbb{R}\to\mathbb{R}^m$ is a distributional solution to the Cauchy problem (2.1,2.3) if for all $i=1,\dots,m$,

$$\int_0^T\int_{-\infty}^{\infty}(U_i\varphi_t + f_i(U)\varphi_x)dxdt + \int_{-\infty}^{\infty}\bar{U}_i(x)\varphi(0,x)dx = 0, \tag{2.4}$$

for each component U_i, and $f_i(U)$ of U and $f(U)$, respectively, and for every $\mathcal{C}^\infty$ function φ with compact support contained in the set $[0,T)\times\mathbb{R}$.

There is a stronger concept of discontinuous solution that requires U to be continuous as a function of time with values into $\mathbf{L}^1_{\text{loc}}(\mathbb{R})$.

Definition 2.7 (Weak solutions)**.** *A function $U : [0,T]\times\mathbb{R} \mapsto \mathbb{R}^m$ is a weak solution of the Cauchy problem (2.1, 2.3) if $U \in \mathbf{C}^0([0,+\infty[;\mathbf{L}^1_{\text{loc}}(\mathbb{R};\Omega))$, the initial condition* (2.3) *holds point wise and the restriction of U to the open strip $(0,T)\times\mathbb{R}$ is a distributional solution of* (2.1)*.*

Every weak solution is a distributional solution but the converse is clearly false.

2.2.2 Hyperbolicity, admissibility conditions and the Riemann problem

Definition 2.8. *The system of conservation laws* (2.1) *is said to be strictly hyperbolic if for every $U \in \Omega$, the Jacobian matrix $A(U) = Df(U)$ has m real distinct eigenvalues*

$$\lambda_1(U) < \lambda_2(U) < \cdots < \lambda_m(U).$$

For strictly hyperbolic systems, one can find bases of right and left eigenvectors $\{r_1(U),\ldots,r_m(U)\}$ and $\{l_1(U),\ldots,l_m(U)\}$, respectively, depending smoothly on U, and normalized such that

$$\|r_i(U)\| = 1, \text{ and } l_i(U).r_j(U) = \delta_{ij} \doteq \begin{cases} 1 & \text{if } i = j, \\ 0 & i \text{ if } i \neq j \end{cases}$$

for every $U \in \Omega$. The pair (λ_i, r_i) is referred to as the *i-th characteristic field.* The eigenvalues λ_i are also called *wave* or the *characteristic* speeds.

Definition 2.9. *For $i \in \{1,\ldots,m\}$, we say that the i-th characteristic field is genuinely nonlinear if*

$$\nabla_U \lambda_i(U).r_i(U) \neq 0 \quad \textit{for all } U \in \Omega.$$

If, on the other hand,

$$\nabla_U \lambda_i(U).r_i(U) = 0 \quad \textit{for all } U \in \Omega,$$

we say that the i-th characteristic field is linearly degenerate.

From now on, unless otherwise stated, we assume that for a given genuinely nonlinear characteristic field i, the right eigenvectors are normalized such that $\nabla_U \lambda_i(U).r_i(U) = 1$.
For brevity, we will write ∇ instead of ∇_U, for the gradient with respect to the conserved variables.

Rankine-Hugoniot Conditions

Lemma 2.1 (Rankine-Hugoniot Conditions)**.** *Let U^+, $U^- \in \Omega$, $s \in \mathbb{R}$. If the function*

$$U(t,x) = \begin{cases} U^+ & \text{if } x > s\,t, \\ U^- & \text{if } x < s\,t \end{cases} \tag{2.5}$$

is a weak solution to (2.1)*, then the Rankine-Hugoniot jump conditions*

$$f(U^+) - f(U^-) = s(U^+ - U^-). \tag{2.6}$$

hold.

The proof can be found for example in [19]. A solution of a system of conservation laws in the form (2.5) is called a *shock wave* solution and s is the shock speed. One can rewrite the Rankine-Hugoniot conditions in the following way. For any U, $V \in \Omega$, we define the averaged matrix

$$A(U,V) \doteq \int_0^1 A(\theta V + (1-\theta)U)d\theta \tag{2.7}$$

and call $\lambda_i(U,V)$, $i = 1,\ldots,m$ its eigenvalues. One can easily see that $A(U,V) = A(V,U)$ and $A(U,U) = A(U)$. The equations (2.6) can be written in the equivalent form

$$\begin{aligned} s(U^+ - U^-) = f(U^+) - f(U^-) &= \int_0^1 Df(\theta U^+ + (1-\theta)U^-)\cdot(U^+ - U^-)d\theta \\ &= A(U^-,U^+)\cdot(U^+ - U^-). \end{aligned} \tag{2.8}$$

In other words, the Rankine-Hugoniot conditions hold if and only if the jump $U^+ - U^-$ is an eigenvector of the averaged matrix $A(U^-,U^+)$ and the shock speed coincides

with the corresponding eigenvalue.
When dealing with weak solutions of systems of conservation laws, the uniqueness of solutions is lost. Indeed, consider the Burgers' equation

$$U_t + \left(\frac{U^2}{2}\right)_x = 0, \tag{2.9}$$

where U is now a scalar. Consider the Cauchy problem with initial data

$$U(0,x) = \begin{cases} 1 & \text{if } x \geq 0 \\ 0 & \text{if } x < 0. \end{cases}$$

For every $0 < \beta < 1$,

$$U_\beta(t,x) = \begin{cases} 0, & x \leq \frac{\beta}{2}t, \\ \beta, & \frac{\beta}{2}t < x < \frac{1+\beta}{2}t, \\ 1, & x \geq \frac{1+\beta}{2}t, \end{cases} \tag{2.10}$$

is a weak solution of (2.9). Indeed, the piecewise constant function U_β satisfies the equation outside the jumps. Moreover, the Rankine-Hugoniot conditions hold along the two lines of discontinuity $\{x = \frac{\beta}{2}t\}$ and $\{x = \frac{1+\beta}{2}t\}$ for all $t > 0$.

To single out the unique physically relevant solution, one uses the so called admissibility conditions. Among these are the entropy-entropy flux pair and the vanishing viscosity conditions that we present below.

Definition 2.10. *A continuously differentiable function $\eta : \Omega \to \mathbb{R}$ is called an entropy for the system* (2.1)*, with entropy flux $q : \Omega \to \mathbb{R}$, if*

$$\nabla\eta Df(U) = \nabla q(U) \quad \forall U \in \Omega.$$

The couple (η, q) is also called an entropy-entropy flux pair for (2.1)*.*

Definition 2.11. *A weak solution of* (2.1) *is entropy admissible if*

$$\eta(U)_t + q(U)_x \leq 0 \tag{2.11}$$

in the distributional sense, for every convex entropy-entropy flux pair (η, q) for (2.1)*.*

The entropy admissibility condition can be derived from the vanishing viscosity condition [19].

Vanishing viscosity A weak solution U of (2.1) is admissible in the vanishing viscosity sense if there exists a sequence of smooth solutions U^ε to

$$U_t^\varepsilon + f(U^\varepsilon)_x = \varepsilon U_{xx}^\varepsilon \tag{2.12}$$

which converges to U in $\mathbf{L}^1_{\text{loc}}$ as $\varepsilon \to 0+$.

Now we introduce the standard Riemann problem for a strictly hyperbolic system of conservation laws and investigate the construction of its solutions.

The standard Riemann problem for the system (2.1) consists of finding a weak (entropy) solution with piecewise constant initial datum

$$U(0,x) = \begin{cases} U^- & \text{if } x < 0, \\ U^+ & \text{if } x > 0, \end{cases} \tag{2.13}$$

with U^-, $U^+ \in \Omega$ some given left and right states. It is the simplest problem involving a discontinuity in the initial conditions.

Solution to the Riemann problem

If each characteristic of (2.1) is either genuinely nonlinear or linearly degenerate, it is possible to find an analytical solution to the Riemann problem (2.1,2.13). In general, this solution is either a simple wave (a shock, rarefaction or contact discontinuity wave) or a combination of these simple waves. We first consider the case of a shock wave. The shock curves are defined as followed.

Theorem 2.4. *Assume that the system* (2.1) *is strictly hyperbolic. Then for every* $U_0 \in \Omega$, *there exists* $\xi_0 > 0$ *and* m *smooth curves* $\xi \mapsto S_i(\xi; U_0)$ *defined for* $\xi \in [-\xi_0, \xi_0]$ *together with* m *scalar functions* $s_i(.; U_0) : [-\xi_0, \xi_0] \mapsto \mathbb{R}$, $i = 1, \ldots, m$ *such that*

$$f(S_i(\xi; U_0)) - f(U_0) = s_i(\xi; U_0)(S_i(\xi; U_0) - U_0)$$

for every $\xi \in [-\xi_0, \xi_0]$. *Moreover, the parameterization can be chosen such that*

$$S_i(0; U_0) = U_0, \quad s_i(0; U_0) = \lambda_i(U_0),$$

$$\frac{d}{d\xi} S_i(\xi; U_0)|_{\xi=0} = r_i(U_0).$$

The curve S_i is called the $i-$*shock curve* through U_0 and s_i is the shock speed.

An i-th shock wave solution to the Riemann problem (2.1,2.13) is given by

$$U(t,x) = \begin{cases} U^- & \text{if } x < s_i t, \\ U^+ & \text{if } x > s_i t, \end{cases} \tag{2.14}$$

where the right state U^+ and the left state U^- are connected to along the i-th shock curve:

$$U^+ = S_i(\xi; U^-) \text{ for some } \xi \in [-\xi_0, \xi_0].$$

Now we consider the case of a rarefaction wave solution to the Riemann problem. This solution is a self-similar solution, meaning that $U(t,x) = U(x/t)$.
By $\xi \mapsto R_i(\xi, U_0)$ we denote the parameterized integral curve of the eigenvector $r_i(U_0)$ through the point U_0. More precisely, $R_i(\xi, U_0)$ is the value at time $t = \xi$ of the solution to the Cauchy problem

$$\frac{dU}{dt} = r_i(U(t)), \quad U(0) = U_0.$$

The curve R_i is called the i-rarefaction curve through U_0.

Theorem 2.5. *If the initial data* U^- *and* U^+ *are such that*

$$U^+ = R_i(\xi; U^-)$$

for some ξ *and some* i, *then the following piecewise smooth function*

$$U(t,x) = \begin{cases} U^- & \text{if } \frac{x}{t} < \lambda_i(U^-) \\ U^+ & \text{if } \frac{x}{t} > \lambda_i(U^+) \\ R_i(\xi; U^-) & \text{if } \frac{x}{t} \in [\lambda_i(U^-), \lambda_i(U^+)],\ \frac{x}{t} = \lambda_i(R_i(\xi; U^-)) \end{cases} \tag{2.15}$$

is a weak solution of (2.1,2.13). This particular solution is called a rarefaction wave.

When the i-th characteristic field is linearly degenerate, then the i-th shock and rarefaction curves coincide:

$$S_i(\xi; U) = R_i(\xi; U) \text{ for all } \xi \text{ and } U$$

The resulting curve is called the *contact discontinuity curve*. The corresponding solution to the Riemann problem is called a *contact discontinuity wave*.
As pointed out before, the uniqueness of solutions of Riemann problems in the weak sense is not guaranteed and one uses admissibility conditions to single out the unique physically relevant solutions. In addition to the entropy condition and the vanishing viscosity condition presented above, we have the following conditions.

Liu condition Let $U^+ = S_i(\sigma, U^-)$ for some $\sigma \in \mathbb{R}$. The shock with left and right side U^- and U^+ is said to satisfy the Liu admissibility condition if its speed is less or equal to the speed of every smaller shock, joining U^- with an intermediary state $U^* = S_i(s, U^-)$, $s \in [0, \sigma]$.

Lax condition A shock in the i-th family, connecting states U^-, U^+ and traveling with speed $s_i = \lambda_i(U^-, U^+)$, satisfies the Lax admissibility condition if

$$\lambda_i(U^-) \geq s_i \geq \lambda_i(U^+) \tag{2.16}$$

The Liu condition was introduced by Liu in [80] and it was proven that it completely characterizes the solutions of the conservation laws which can be obtained as vanishing viscosity limits. The Lax condition says that characteristics in the i-th family disappear into the shock as time advances. We now assume that the shock curves and the rarefaction curves are chosen as to satisfy the Lax entropy condition. We then define the map

$$L_i(\xi; U_0) = \begin{cases} R_i(\xi; U_0) & \text{if } \xi \geq 0, \\ S_i(\xi; U_0) & \text{if } \xi < 0 \end{cases}$$

L_i is smooth for $\xi \neq 0$ and twice continuously differentiable at $\xi = 0$ [42]. L_i is the i-th Lax curve through U_0. The general solution of the Riemann problem is obtained as a juxtaposition of fixed states connected by the Lax curves.

Theorem 2.6. *Assume that* (2.1) *is strictly hyperbolic and each characteristic field is either genuinely nonlinear or linearly degenerate. For* $\|U^+ - U^-\|$ *sufficiently small, there exists a unique self similar solution to the Riemann problem (2.1,2.13) with small total variation. The solution comprises* $m+1$ *constant states* $U^- = U_0, U_1, \ldots, U_{m-1}, U_m = U^+$. *When the* i*-th characteristic field is linearly degenerate,* U_i *is joined to* U_{i-1} *by an* i*-contact discontinuity, while when the* i*-characteristic field is genuinely nonlinear,* U_i *is joined to* U_{i-1} *by either an* i*-(Lax) rarefaction or an* i*-(Lax) shock.*

A proof can be found in [42].
Concerning the Cauchy problem, the following result discusses the existence and stability of weak entropy solutions.

Theorem 2.7. *Let the system* (2.1) *be strictly hyperbolic with smooth coefficients, defined on an open set* $\Omega \subset \mathbb{R}^m$. *Assume that for each* $i \in \{1, \ldots, m\}$ *the* i*-th characteristic field is either genuinely nonlinear or linearly degenerate. Then there exists a positive constant* δ_0 *such that for every initial condition* $\bar{U} \in \mathbf{L^1}$ *with*

$$TV(\bar{U}) \leq \delta_0,$$

the Cauchy problem (2.1,2.3) has a weak solution $U = U(t,x)$, *defined for all* $t \geq 0$. *In addition, if the system* (2.1) *admits a convex entropy* η, *then one can find a solution which is* η*-admissible.*

The proof of this theorem, which can be found in [19] is done by constructing a sequence of approximate solutions, say, U_μ and showing that a subsequence of U_μ converges in $\mathbf{L}^1_{\text{loc}}$ to a weak solution of the Cauchy problem. The construction of an approximate solution has been done in the literature following two main approaches: the Glimm scheme [55] and the front tracking approximation [20, 23]. In general the solutions are constructed as trajectories of semi-groups.

Theorem 2.8. *Under the assumption of Theorem 2.7, there exist positive constants* δ_0, L, L', *an open set* $\mathcal{D}$ *and a map* $S : [0, +\infty[\times \mathcal{D} \to \mathcal{D}$ *with the following properties:*

(i) $\mathcal{D} \supseteq \{U \in \mathbf{L^1}(\mathbb{R};\mathbb{R}^m) : U(x) \in \Omega \text{ for } \mathcal{L}^1 - a.e.\ x \in \mathbb{R},\ TV(U) < \delta_0\}$;

(ii) *for every* $U \in \mathcal{D},\ t,\ s \geq 0$

$$S_0 U = U, \quad S_s(S_t U) = S_{s+t} U;$$

(iii) *for every* $U,\ V \in \mathcal{D},\ t,\ s \geq 0$

$$\|S_t U - S_s V\|_{\mathbf{L^1}} \leq L\|U - V\| + L'|t - s|;$$

(iv) *if* $U \in \mathcal{D}$ *is piecewise constant, then for* $t > 0$ *sufficiently small,* $S_t U$ *coincides with the juxtaposition of the weak entropy solutions to the Riemann problem centered at the points of jump of* U.

Moreover, for every $U \in \mathcal{D}$ *the map* $t \mapsto S_t U$ *is a weak solution to the Cauchy problem* (2.1) *with initial data* U. *If the system* (2.1) *admits a convex entropy* η, *then* $S_t U$ *is also* η*-admissible.*

2.3 Non-Homogeneous System of Balance Laws in Networks

This section is devoted to a review of the study of the flows governed by systems of conservation laws in a network of pipes or canals. A model used for the network is an oriented graph $(\mathcal{V}, \mathcal{E})$, where $\mathcal{E}$ is the set of edges representing the pipes or canals in the network and $\mathcal{V}$ is the set of vertices representing the intersections of the pipes or the confluences of canals. The other cases being similar, we focus below on a simple network with one intersection and, as in [41], we model a junction with n pipes as a set of non-zero vectors $\nu_j \in \mathbb{R}^3 \backslash \{0\}$ meeting at $x = 0$. Along each pipe, the space variable is $x \in \mathbb{R}^+ = [0, +\infty[$ and the junction is at $x = 0$. The flow dynamics in the pipe is governed by a system of conservation laws with a source term

$$\partial_t U_j + \partial_x f_j(U_j) = G_j(t, x, U_j) \quad \text{with} \quad \begin{cases} t \in [0, +\infty[, \\ x \in [0, +\infty[, \\ j = 1, \ldots, n. \end{cases} \tag{2.17}$$

Here U_j is the vector of conserved variables along the j-th pipe, f_j is a nonlinear flux function and G_j is the source term associated to the j-th pipe. For any j, (2.17) in an initial boundary values problem for conservation law. For the scalar case, some wellposedness results have be proven by Colombo and Groli [35, 36].

Our aim in this section is to discuss a result on the well posedness of such systems in $\mathbf{L^1}$, locally in time, for data having small total variation, like in [37]. Towards this aim, we denote by $\Omega_j \subset \mathbb{R}^m$ a non-empty set containing zero, by $f = (f_1, \ldots, f_n)$ the flux function for all arcs of the network and by $G = (G_1, \ldots, G_n)$ the source term for the network. f and G are both function of the n-tuple state $\bar{U} = (\bar{U}_1, \ldots, \bar{U}_n) \in \mathbf{\Omega}$, where $\mathbf{\Omega} = \Omega_1 \times \cdots \times \Omega_n$. We note that for all $j = 1, \ldots, n$, (2.17) can be seen as the combination of a convective part

$$\partial_t U_j + \partial_x f_j(U_j) = 0 \tag{2.18}$$

which is nothing but the system of conservation laws studied in the previous section, and a source part

$$\partial_t U_j = G_j(t, x, U_j). \tag{2.19}$$

For a given initial data U_j^0 one can solve (2.18) and obtain the solution $\bar{U}_j$ which, in turn, can be used as initial data for the solution of the ODE (2.19). This method is called the *splitting method*.
Following [37], we require the following conditions to hold true for the convective and the source part.

(F) For $j = 1, \ldots, n$, $f_j \in \mathbf{C^4}(\Omega; \mathbb{R}^n)$ is strictly hyperbolic, $Df_j(\bar{U}_j)$ is such that its minimum and maximum eigenvalue

$$\lambda^j_{\min}(\bar{U}_j) = \min \lambda_{f_j}(\bar{U}_j), \quad \lambda^j_{\max}(\bar{U}_j) = \max \lambda_{f_j}(\bar{U}_j)$$

are strictly negative and strictly positive, respectively, and each characteristic field is either genuinely nonlinear or linearly degenerate.

Under this condition **(F)**, (2.18) generates a Standard Riemann Semigroup (see [19]

and the references therein). In the following, we will use the following norms

$$\begin{array}{rl} \|U\| = \sum_{j=1}^{n} \|U_j\| & \text{for } U \in \mathbf{\Omega}, \\ \|U\|_{\mathbf{L^1}} = \int_{\mathbb{R}^+} \|U(x)\| dx & \text{for } U \in \mathbf{L^1}(\mathbb{R}^+; \mathbf{\Omega}), \\ TV(U) = \sum_{j=1}^{n} TV(U_j) & \text{for } U \in \mathbf{BV}(\mathbb{R}^+; \mathbf{\Omega}). \end{array}$$

Below, we fix a time $\hat{T} \in (0, +\infty)$ and a positive $\hat{\delta}$. For $\delta \in (0, \hat{\delta}]$, we denote

$$\mathcal{U}_\delta = \{U \in \mathbf{L^1}(\mathbb{R}^+; \mathbf{\Omega}) : TV(U) \leq \delta\}.$$

For the source term G, we require that

(G) $G : [0, \hat{T}] \times \mathcal{U}_{\hat{\delta}} \mapsto \mathbf{L^1}(\mathbb{R}^+; \mathbb{R}^n)$ is such that for suitable positive L_1, L_2 and for all $t, s \in [0, \hat{T}]$

$$\begin{array}{lrcl} \forall U, V \in \mathcal{U}_{\hat{\delta}} & \|G(t,U) - G(t,V)\|_{\mathbf{L^1}} & \leq & L_1.(\|U - V\|_{\mathbf{L^1}} + |t - s|) \\ \forall U \in \mathcal{U}_{\hat{\delta}} & TV(G(t,U)) & \leq & L_2. \end{array}$$

Interactions at the junction, which depend on time, are described by conditions on the traces of the unknown conserved variables U_j at $x = 0$, namely,

$$\Psi\left(U_1(t,0+), U_2(t,0+), \ldots, U_n(t,0+)\right) = \Pi(t), \tag{2.20}$$

for suitable smooth Ψ with n components and $\Pi : [0, T] \to \mathbb{R}^n$ a given map. We will refer below to Ψ as the *coupling conditions map*.

The Cauchy problem at the intersection consist of solving the problem

$$\begin{cases} \partial_t U_j + \partial_x f_j(U_j) = G_j(t, x, U_j) & t \in \mathbb{R}^+,\ j \in \{1, \ldots, n\} \\ \Psi\left(U(t,0)\right) = \Pi(t) & x \in \mathbb{R}^+,\ U^0 \in \mathbf{L^1}(\mathbb{R}^+; \mathbf{\Omega}) \\ U(0,x) = U^0(x) & \end{cases} \tag{2.21}$$

When the initial data U^0 is constant, the problem is referred to as the *Riemann problem at the junction*. For given coupling conditions map Ψ, the solution in the weak sense of the Cauchy problem at the junction is given below.

Definition 2.12. *Fix a map $\Psi \in \mathbf{C}^1(\Omega;\mathbb{R}^n)$. A weak solution on $[0,T]$ to (2.21) is a map $U \in \mathbf{C}^0\left([0,T];\mathbf{L}^1(\mathbb{R}^+;\Omega)\right)$ such that for all $t \in [0,T]$, $U(t) \in \mathbf{BV}(\mathbb{R}^+;\mathbf{\Omega})$ and*

(W) *$U(0) = U^0$ and for all $\varphi \in \mathbf{C}_c^\infty\left((0,T)\times]0,+\infty[;\mathbb{R}\right)$ and for $j = 1,\dots,n$ and any l-th component of U_j,*

$$\int_0^T \int_{\mathbb{R}^+} \left(U_{j,l}\partial_t\varphi + f_{j,l}(U_j)\partial_x\varphi\right) dxdt + \int_0^T \int_{\mathbb{R}^+} \varphi(t,x)G_{j,l}(t,x,U_j)dxdt = 0.$$

($\mathbf{\Psi}$) *The condition at the intersection is met: for a.e. $t \in \mathbb{R}^+$, $\Psi(U(t,0+)) = \Pi(t)$.*

The weak solution U is an entropy solution if for any entropy-entropy flux pair (η_j, q_j), for $\varphi \in \mathbf{C}_c^\infty\left((0,T)\times]0,+\infty[;\mathbb{R}\right)$ and for $j = 1,\dots,n$ and any component l of U_j^0,

$$\int_0^T \int_{\mathbb{R}^+} \left(\eta_{j,l}(U_j)\partial_t\varphi + q_{j,l}(U_j)\partial_x\varphi\right) dxdt + \int_0^T \int_{\mathbb{R}^+} D\eta_{j,l}(U_j)G_j(t,x,U_j)\varphi(t,x)dxdt \geq 0.$$

Below, we denote by $r^j_{\max}(U)$ the right eigenvector of $Df_j(U)$ corresponding to the "maximum" characteristic field. The well posedness result proposed below is in the framework of the metric space

$$X = \mathbf{L}^1(\mathbb{R}^+;\mathbf{\Omega}) \times \mathbf{L}^1(\mathbb{R}^+;\mathbb{R}^n)$$

equipped with the $\mathbf{L}^1$ distance. Let the extended variable $\mathbf{p} \equiv (U,\Pi)$ with $U = U(x)$, respectively $\Pi = \Pi(t)$, be defined for $x \geq 0$, respectively $t \geq 0$. We denote accordingly,

$$\begin{aligned} &d_X\left((U,\Pi),(\bar U,\bar\Pi)\right) = \|(U,\Pi)-(\bar U,\bar\Pi)\|_X = \|U-\bar U\|_{\mathbf{L^1}} + \|\Pi-\bar\Pi\|_{\mathbf{L^1}},\\ &TV(\mathbf{p}) = TV(U) + TV(\Pi) + \|\Psi(U(0+)) - \Pi(0+)\|,\\ &\mathcal{D}^\delta = \{\mathbf{p} : TV(\mathbf{p}) \leq \delta\}. \end{aligned} \tag{2.22}$$

Theorem 2.9. *[37] Let $n \in \mathbb{N}$, $n \geq 2$ and assume that the flux satisfies **(F)** at $\bar U$ and the source terms G satisfies **(G)**. Fix a map $\Psi \in \mathbf{C^1}(\mathbf{\Omega};\mathbb{R}^{\mathbf{m}})$ that satisfies*

$$\det\left[D_1\Psi(\bar U)r^1_{\max}(\bar U_1)\, D_2\Psi(\bar U)r^2_{\max}(\bar U_2)\, \dots\, D_n\Psi(\bar U)r^n_{\max}(\bar U_n)\right] \neq 0 \tag{2.23}$$

where $D_j\Psi = D_{U_j}\Psi$, *and let* $\bar{\Pi} = \Psi(\bar{U})$. *Then there exists positive* δ, δ', L, T, *domains* $\mathcal{D}_t$, *for* $t \in [0,T]$, *and a map*

$$\mathcal{E} := \{(\tau, t_o, \mathbf{p}) : t_o \in [0,T[,\ \tau \in [0, T-t_o],\ \mathbf{p} \in \mathcal{D}_{t_o}\} \mapsto \mathcal{D}^{\delta}$$

such that:

(i) $\mathcal{D}^{\delta'} \subset \mathcal{D}_t \subset \mathcal{D}^{\delta}$, *for all* $t \in [0,T]$;

(ii) for all $t_o \in [0,T]$ *and* $\mathbf{p} \in \mathcal{D}_{t_o}, \mathcal{E}(0,t_o)\mathbf{p} = \mathbf{p}$;

(iii) for all $t_o \in [0,T]$ *and* $\tau \in [0, T-t_o], \mathcal{E}(\tau, t_o)\mathcal{D}_{t_o} \subset \mathcal{D}_{t_o+\tau}$;

(iv) for all $t_o \in [0,T]$, $\tau_1, \tau_2 \geq 0$ *with* $\tau_1 + \tau_2 \in [0, T-t_o]$,

$$\mathcal{E}(\tau_2, t_o + \tau_1) \circ \mathcal{E}(\tau_1, t_o) = \mathcal{E}(\tau_2 + \tau_1, t_o);$$

(v) for all $(U_o, \Pi) \in \mathcal{D}_{t_o}$, *set* $\mathcal{E}(t, t_o)(U_o, \Pi) = (U(t), \mathcal{T}_t\Pi)$ *and we have that* $t \mapsto U(t)$ *is the entropy solution to the Cauchy problem* (2.17) *according to Definition 2.12 while the second component is the right translation.*

(vi) for all $t_o \in [0,T]$ *and* $\tau \in [0, T-t_o]$, *and for all* $\mathbf{p}$, $\bar{\mathbf{p}} \in \mathcal{D}_{t_o}$,

$$\begin{aligned} \|\mathcal{E}(\tau, t_o)\mathbf{p} - \mathcal{E}(\tau, t_o)\bar{\mathbf{p}}\|_{\mathbf{L^1}} \ &\leq\ L\|U - \bar{U}\|_{\mathbf{L}^1} \\ &\quad + L\int_{t_o}^{t_o+\tau} \|\bar{\Pi}(t) - \Pi(t)\| dt. \end{aligned} \tag{2.24}$$

2.4 Numerical Methods for System of Conservation Laws

In this section, we review and compare numerical methods used in the literature to solve hyperbolic system of conservation laws. We emphasize in the methods used in the problems of this thesis. For a detailed discussion on the methods presented here, we refer to [85, 78, 45, 69].

2.4.1 Finite volume methods

We consider a system of conservation laws in the form

$$\frac{\partial u}{\partial t} + \frac{\partial}{\partial x} f(u) = 0, \tag{2.25}$$

with initial conditions

$$u(x, 0) = u_0(x), \tag{2.26}$$

where u_0 is a given function of the space variable x. We discretize the space variable with a uniform mesh $x_i = i\Delta x$ with $i = 0, \ldots, N$ and width of $h = \Delta x = x_{i+1} - x_i$. The time variable is partitioned with a uniform or non uniform mesh t_n with the time step $k = \Delta t = t_{n+1} - t_n$, where k may depend on n, see Figure 2.1. A control volume or cell is the interval $I_i = [x_{i-\frac{1}{2}}, x_{i+\frac{1}{2}})$ where the cell boundaries are given by $x_{i+\frac{1}{2}} = \frac{1}{2}(x_i + x_{i+1})$.

We consider the cell averages

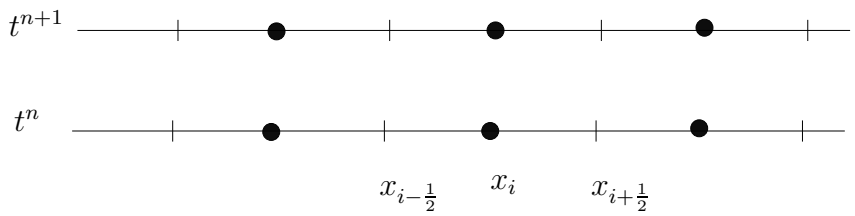

Figure 2.1: *A discretization of the space-time domain.*

$$u_i = \frac{1}{\Delta x} \int_{I_i} u(x, t) dx.$$

The idea of the finite volume methods consists of considering, in each cell I_i, a constant initial data equal to the cell average of the conserved quantities. The numerical initial conditions consist then of the piece-wise constant function

$$u^0(x) = \frac{1}{\Delta x} \int_{I_i} u_0(x) dx \doteq u_i^0, \;\; x_{i-\frac{1}{2}} \leq x < x_{i+\frac{1}{2}}. \tag{2.27}$$

One integrates the flow equations (2.25) over the control volume I_i and divides throughout by the mesh width Δx to obtain the semi-discrete numerical scheme

$$\frac{d\, u_i}{dt} = -\frac{f(u(x_{i+\frac{1}{2}}, t)) - f(u(x_{i-\frac{1}{2}}, t))}{\Delta x}, \quad u_i(t = 0) = u_i^0. \tag{2.28}$$

A simple forward integration in the time interval $[t_n, t_{n+1}]$ of (2.28) gives the explicit scheme

$$u_i^{n+1} = u_i^n - \frac{\Delta t}{\Delta x}(F_{i+\frac{1}{2}} - F_{i-\frac{1}{2}}), \tag{2.29}$$

where

$$F_{i+\frac{1}{2}} = \int_{t_n}^{t_{n+1}} f(u(x_{i+\frac{1}{2}}, t))dt$$

is called the *numerical flux* or the *cell interface flux*. The general construction of the numerical fluxes follow the Godunov method.

2.4.2 Godunov method

Godunov methods are standard methods for the integration of systems of conservation laws. For clarity in this section, we restrict ourselves to the scalar case, but the results can be easily extended to the case of systems. For Godunov methods, one computes the interface fluxes $F^n_{i+\frac{1}{2}}$ by solving the standard Riemann problem (See Section 2.2) for the conservation law with data (u_i^n, u_{i+1}^n) and taking the value along the ray $x_{i+1/2}$ in the Riemann solution. We denote this Riemann solution as $\bar{u}_{i+\frac{1}{2}} = \mathcal{R}(x_{i+1/2}, u_i, u_{i+1})$ and we omit the superscript n for simplicity. This value is constant for $t > t_n$, since the Riemann solution is a similarity solution. To fix ideas, we assume that the flux function $f(u)$ is convex (or concave), i.e., $f''(u)$ does not change sign over the range of interest of u. Then the Riemann solution consists of a single shock or rarefaction wave. For scalar conservation laws with a convex flux the Riemann solution might take five possible forms as illustrated in Figure 2.2. In

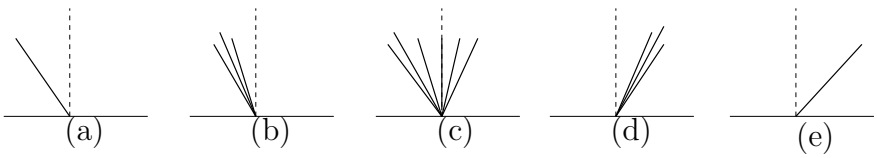

Figure 2.2: *Solution to the Riemann problem for a scalar conservation law with a convex flux.*

most cases the solution $\bar{u}^{n+1}_{i+\frac{1}{2}}$ is either u_i^n, if the solution is a shock or rarefaction

wave moving entirely to the left, as in Figure 2.2(a,b) , or u^n_{i+1}, if the solution is a shock or rarefaction wave moving entirely to the right, as in Figure 2.2(d,e). The only case where $\bar{u}^{n+1}_{i+\frac{1}{2}}$ has different value to u_i or u_{i+1} is if the solution consist of a rarefaction wave that spreads partly to the left and to the right as shown in Figure 2.2(c). We assume for example that $f''(u) > 0$ everywhere, in which case $f'(u)$ is increasing with u, so that a rarefaction wave arises if $u_i < u_{i+1}$. In this case, the situation shown in Figure 2.2(c) occurs only if

$$u_i < u_s < u_{i+1},$$

where u_s is the unique value of u for which $f'(u_s) = 0$. This is called the stagnation point, since the value u_s propagates with zero velocity. It is also called the sonic point, since in gas dynamics the eigenvalues $v \pm c$ can take the value zero only when the fluid speed $|v|$ is equal to the sound speed c. The solution shown in Figure 2.2(c) is called a transonic rarefaction since in gas dynamics, the fluid is accelerated from a subsonic velocity to a supersonic velocity through such a rarefaction. In a transonic rarefaction, the value along $x/t = x_{i+1/2}$ is simply u_s. For the case $f''(u) > 0$ we see that the Godunov numerical flux function for a convex scalar conservation law is given by

$$F_{i+\frac{1}{2}} = \begin{cases} f(u_i) & \text{if } u_i > u_s \text{ and } s > 0, \\ f(u_{i+1}) & \text{if } u_{i+1} < u_s \text{ and } s < 0, \\ f(u_s) & \text{if } u_i < u_s < u_{i+1}. \end{cases} \tag{2.30}$$

Here

$$s = \frac{f(u_{i+1}) - f(u_i)}{u_{i+1} - u_i}$$

is the shock speed. Note in particular that if $f'(u) > 0$ for both u_i and u_{i+1}, then $F_{i+1/2} = f(u_i)$ and Godunov's method reduces to the *first-order upwind* method

$$u^{n+1}_i = u_i - \frac{k}{h}[f(u_i) - f(u_{i-1})]. \tag{2.31}$$

Similar observation holds for $f'(u) < 0$ for both values of u, involving one sided differences in other directions. Only in the case where $f'(u)$ changes sign between

u_i and u_{i+1} is the formula more complicated, as we should expect since the upwind direction is ambiguous in this case and information must flow both ways. The correction in this case is called *entropy fix* and we refer the interested reader to [78]. The formula (2.30) can be written more compactly as

$$F_{i+\frac{1}{2}} = \begin{cases} \min\limits_{u_i \le u \le u_{i+1}} f(u) & \text{if } u_i \le u_{i+1}, \\ \max\limits_{u_{i+1} \le u \le u_i} f(u) & \text{if } u_{i+1} \le u_i, \end{cases} \tag{2.32}$$

since the stagnation point u_s is the global minimum or maximum of f in the convex case. This formula is valid also for the case $f''(u) < 0$ and even for non-convex fluxes, in which case there may be several stagnation points at each maximum and minimum of f (see [79]). We point out that there is one solution structure not illustrated in Figure 2.2, a stationary shock with speed $s = 0$. In this case the value $\bar{u}_{i+1/2}$ is ambiguous since the Riemann solution is discontinuous along $x = x_{i+1/2}$. However, if $s = 0$ then $f(u_i) = f(u_{i+1})$ by the Rankine-Hugoniot condition and so $F_{i+1/2}$ is still well defined and the formula (2.32) is still valid.

2.4.3 Integration in time and the CFL condition

One can integrate the semi-discrete scheme (2.28) from t_n to t_{n+1} to obtain

$$u_i^{n+1} = u_i^n - \frac{\Delta t}{\Delta x}(F^n_{i+\frac{1}{2}} - F^n_{i-\frac{1}{2}}), \tag{2.33}$$

where

$$F^n_{i+\frac{1}{2}} = \int_{t_n}^{t_{n+1}} f(u(x_{i+\frac{1}{2}}, t))dt$$

can be reasonably approximated by

$$F^n_{i+\frac{1}{2}} = \mathcal{F}(u_i^n, u_{i+1}^n)$$

where the numerical flux $\mathcal{F}$ is a function of neighboring cells. One generally imposes some basic consistency condition upon the numerical flux in the sense that if $u_i = u_{i+1} = \bar{u}$, then we have

$$\mathcal{F}(\bar{u}, \bar{u}) = f(\bar{u}).$$

Generally some requirements of Lipschitz continuity are made, that is, there exists a constant L so that

$$|\mathcal{F}(u_i, u_{i+1}) - f(\bar{u})| \leq L \max(|u_i - \bar{u}|, |u_{i+1} - \bar{u}|). \tag{2.34}$$

The CFL condition is a necessary condition that must be satisfied by any finite volume or finite difference method if we expect it to be stable and converge to the solution of the differential equation as the grid is refined. It simply states that the method must be used in such a way that information has a chance to propagate at the correct physical speeds, as determined by the eigenvalues of the flux Jacobian $f'(u)$. Precisely, a numerical method can be convergent only if its numerical domain of dependence contains the true domain of dependence of the PDE, at least in the limit as Δt and Δx go to zero. We emphasize that the CFL condition is only a necessary condition for stability and hence convergence. It is not in general sufficient to guarantee stability. The Courant number or CFL number is defined for a general system of conservation in terms of the eigenvalues of the Jacobian matrix $\lambda_1, \ldots, \lambda_m$ of the flux function

$$\nu = \frac{\Delta t}{\Delta x} \max_p |\lambda_p|. \tag{2.35}$$

For a three-point method, the CFL condition says that $\nu \leq 1$. Looking at the expression (2.33), it turns out that it is the simplest integration form of the semi-discrete equation (2.28). To gain more accuracy, one can use a more sophisticated ODE solver for the numerical integration of the semi-discrete scheme (2.28). For system of conservation laws with discontinuous solutions, this integration should be done such that the resulting scheme remains stable. This leads to method like the strong stability preserving (SSP) Runge-Kutta method [56] that is used for the numerical solution of the model in Chapter 3 and Chapter 4.

2.4.4 The Lax-Friedrichs and local Lax-Friedrichs fluxes

The Lax-Friedrichs (LxF) method has the form (2.28) with a numerical flux given by

$$F_{i+\frac{1}{2}} = \frac{1}{2}[f(u_i) + f(u_{i+1}) - a(u_{i+1} + u_i)]. \tag{2.36}$$

Therein, the *numerical viscosity* $a = \Delta x/\Delta t$ has a fixed magnitude and does not vanish near a sonic point. As a result, this method always converges to the correct vanishing viscosity solution (see Section 2.2) as the grid is refined. We note that this method is more dissipative than Godunov's method and exhibits a stair-step pattern in the vicinity of a sonic point, see [79]. An improvement to the LxF method is obtained by replacing the value of the *numerical viscosity* $a = \Delta x/\Delta t$ in (2.36) by a locally determined value,

$$F_{i+\frac{1}{2}} = \frac{1}{2}[f(u_i) + f(u_{i+1}) - a_{i+\frac{1}{2}}(u_{i+1} + u_i)], \tag{2.37}$$

where

$$a_{i+\frac{1}{2}} = \max(|f'(u)|) \text{ over all } u \text{ between } u_i \text{ and } u_{i+1}. \tag{2.38}$$

For a convex flux function, this reduces to

$$a_{i+\frac{1}{2}} = \max(|f'(u_i)|, |f'(u_{i+1})|).$$

The resulting method is the Local Lax-Friedrichs (LLF) method, also called *Rusanov's method*. It has the same form as the LxF method but the numerical viscosity $a = a_{i+\frac{1}{2}}$ is chosen locally at each Riemann problem. It is proven in [79] that this is a sufficient viscosity to make the method converge to the vanishing-viscosity solution. We point out that if the CFL condition is satisfied (which is a necessary condition for stability), then $|f'(u)|\Delta t/\Delta x \leq 1$ for each value of u arising in the whole problem, and so

$$|f'(u)| \leq \frac{\Delta x}{\Delta t}.$$

Hence, using $a = \Delta x/\Delta t$ in the standard LxF method amounts to taking a uniform viscosity that is sufficient everywhere at the expense of too much smearing in most cases.

Osher [89] first introduced the notion of *E-scheme* as one that satisfies the inequality

$$\text{sign}(u_{i+1} - u_i)[F_{i+\frac{1}{2}} - f(u)] \leq 0 \tag{2.39}$$

for all u between u_i and u_{i+1}. In particular, Godunov's method with flux $F^G_{i+1/2}$ defined by (2.32) is clearly an E-scheme. In fact it is the limiting case, in the sense

that E-schemes are precisely those for which

$$\begin{aligned} F_{i+\frac{1}{2}} &\leq F^G_{i+\frac{1}{2}} \quad \text{if } u_i \leq u_{i+1}, \\ F_{i+\frac{1}{2}} &\geq F^G_{i+\frac{1}{2}} \quad \text{if } u_i \geq u_{i+1}. \end{aligned} \tag{2.40}$$

It can be shown that any E-scheme is TVD, see below, if the Courant number is sufficiently small. Let u^n be the numerical approximation of the solution at time t_n. The total variation of u^n is defined as

$$TV(u^n) = \sum_{i=1}^{N-1} |u^n_i - u^n_{i+1}|. \tag{2.41}$$

A numerical scheme is said to be total variation diminishing(TVD) if

$$TV(u^{n+1}) \leq TV(u^n), \quad \text{for all } n. \tag{2.42}$$

Osher proved that E-schemes are convergent to the entropy satisfying weak solution. In addition, Gudunov's method, the LxF and the LLF methods are all E-schemes. Osher also showed that E-schemes are at most first order accurate.

2.4.5 Conservative properties and the Lax-Wendroff theorem

In designing numerical schemes for systems of conservation laws, the integral form of the equation plays a very important role. It guarantees that the discrete solution will be conservative in the sense that

$$u^{n+1}_i = u^n_i - \frac{\Delta t}{\Delta x}(F_{i+\frac{1}{2}} - F_{i-\frac{1}{2}}). \tag{2.43}$$

Non-conservative methods can fail as we will illustrate below. However, with conservative methods, thanks to the Lax-Wendroff theorem, see below, one has the satisfaction of knowing that if the method converges to some limiting function as the grid is refined, then this function is the weak solution.

To illustrate, consider Burger's equation

$$u_t + \frac{1}{2}(u^2)_x = 0.$$

If $u > 0$ everywhere, then the conservative upwind method (Godunov's method) takes the form

$$U_i^{n+1} = U_i^n - \frac{1}{2}\frac{\Delta t}{\Delta x}\left((U_i^n)^2 - (U_{i-1}^n)^2\right). \tag{2.44}$$

On the other hand, using the quasilinear form $u_t + uu_x = 0$, we could derive the nonconservative upwind schemes

$$U_i^{n+1} = U_i^n - \frac{\Delta t}{\Delta x}U_i^n(U_i^n - U_{i-1}^n). \tag{2.45}$$

These methods are both first-order accurate on smooth solutions, and they give comparable results.

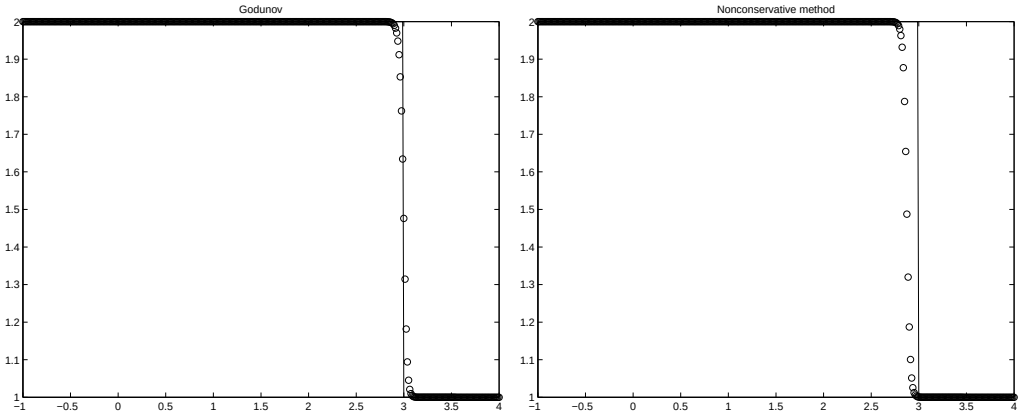

Figure 2.3: *Discontinuous solution of the Burger's equation obtained with a conservative scheme (left) and a nonconservative scheme (right).*

When the solution contains a shock wave, the method (2.45) fails to converge to the weak solution of the conservation law as depicted in Figure 2.3(right). The conservative method (2.44) gives a slightly smeared approximation to the shock, but it is smeared about the correct location as seen in Figure 2.3(left). This is justified by the fact that the method has the discrete conservation property (2.43). The non-conservative method however, gives the results shown in Figure 2.3(right). This method does not satisfy (2.43) and as the grid is refined the approximation

converges towards a discontinuous function that is not a weak solution of the conservation law.

We complete this section by stating the Lax-Wendroff theorem. It is an important theorem that says that we can have confidence in the solution we compute. Nevertheless it does not guarantee that convergence will occur, it says that as the grid is refined, if a conservative and consistent numerical scheme converges to a function, then that function is a weak solution of the conservation law. A comprehensible proof of the theorem can be found in [79].

Theorem 2.10 (Lax Wendroff)**.** *Consider a sequence of grids indexed by* $j = 1, 2, \ldots,$ *with mesh parameters* $\Delta t^{(j)}, \Delta x^{(j)} \to 0$ *as* $j \to \infty$*. Let* $U^{(j)}(x,t)$ *denote the numerical approximation computed with a consistent and conservative method on the* j*-th grid. Suppose that* $U^{(j)}$ *converges to a function* u *as* $j \to \infty$*, in the sense of the* $\mathbf{L}^1$ *norm; and for all* j*, the total variation of the map* $U^{(j)}(\cdot, t)$ *is uniformly bounded for* $0 \leq t \leq T$*. Then* $u(x,t)$ *is a weak solution of the conservation law.*

2.4.6 High resolution TVD methods

The methods described so far are only first-order accurate and are not very useful on their own. They can however be used as building blocks in developing certain high resolution methods. It is convenient to discuss high resolution method in the context of the REA algorithm [79]. This algorithm consists of reconstructing, evolving and averaging the solution at each time step. Starting with the cell averages in each cell the algorithm does the following:

Step 1 Reconstruct a piecewise polynomial function $\tilde{u}(x, t_n)$ defined for all x, from the cell averages u_j^n.

Step 2 Evolve the hyperbolic equation exactly or approximately with this initial data to obtain $\tilde{u}(x, t_{n+1})$ at time Δt later.

Step 3 Average this function over each grid cell to obtain new cell averages

$$u_i^{n+1} = \frac{1}{\Delta x} \int_{I_i} \tilde{u}(x, t_{n+1}) dx.$$

Step 1 usually uses a linear or a quadratic reconstruction based on the cell averages and some numerical derivative that are computed using limiters function. It is somehow independent of the conservation law itself. Step 2 is the main step of the algorithm. Generally here one solves approximatively the conservation law using the reconstructed data. There are two main approaches for the numerical approximation of the conservation laws. One is the upwind method where the reconstructed point values are sampled at the cell centers and waves at the cell interfaces are taken into account. The other approach is a central method where the reconstructed point values are based on neighboring cells and the solution is sampled at the cell interface. To fix ideas and with a little change of notations, we recall that we defined the cell averages as

$$\bar{u}(x,t) := \frac{1}{\Delta x}\int_{I_x} u(\xi,t)d\xi, \quad x \in I_x = \{\xi,\, |\xi - x| \leq \frac{\Delta x}{2}\}.$$

By an integration of the original conservation law (2.25) over I_x and dividing by Δx, we obtain

$$\bar{u}_t(x,t) + \frac{1}{\Delta x}\left[f(u(x+\frac{\Delta x}{2},t)) - f(u(x-\frac{\Delta x}{2},t))\right] = 0. \tag{2.46}$$

Now, with a small time step Δt, we integrate over the slab $t \leq \tau \leq t+\Delta t$ to have

$$\begin{aligned} \bar{u}(x,t+\Delta t) &= \bar{u}(x,t) - \tfrac{1}{\Delta x}\left[\int_t^{t+\Delta t} f(u(x+\frac{\Delta x}{2},\tau))d\tau \right. \\ &\quad \left. - \int_t^{t+\Delta t} f(u(x-\frac{\Delta x}{2},\tau))d\tau\right]. \end{aligned} \tag{2.47}$$

Note that (2.47) is exactly equivalent to (2.25). It is actually the integral form of (2.25) in the control volume $I_x \times [t, t+\Delta t]$. Now at time t^n, and at the first step of the REA algorithm, one can reconstruct an approximate solution, $w(\cdot, t^n)$, as a piecewise polynomial written in the form

$$w(x,t^n) = \sum p_j(x)\chi_j(x), \quad \chi_j := 1_{I_{x_j}},$$

where $p_j(x)$ is an algebraic polynomial supported at the discrete cells $I_j := I_{x_j}$, centered around the mid points $x_j = j\Delta x$. An exact evolution of $w(\cdot, t^n)$, based on

(2.47), reads

$$\begin{aligned} \bar{w}(x,t^{n+1}) &= \bar{w}(x,t^n) - \tfrac{1}{\Delta x}\left[\int_{t^n}^{t^{n+1}} f(w(x+\frac{\Delta x}{2},\tau))d\tau \right. \\ &\left. - \int_{t^n}^{t^{n+1}} f(w(x-\frac{\Delta x}{2},\tau))d\tau\right]. \end{aligned} \tag{2.48}$$

For upwind schemes, one can sample the relation (2.48) at the mid cell $x = x_i$, to obtain the scheme

$$\bar{w}_i^{n+1} = \bar{w}_i^n - \frac{1}{\Delta x}\left[\int_{t^n}^{t^{n+1}} f(w(x_{i+\frac{1}{2}},\tau))d\tau - \int_{t^n}^{t^{n+1}} f(w(x_{i-\frac{1}{2}},\tau))d\tau\right]. \tag{2.49}$$

Here it remains to recover the point values $\{w(x_{i+\frac{1}{2}},\tau)\}_i,\ t^n \le \tau \le t^{n+1}$, in terms of their known cell averages $\{\bar{w}_i^n\}_i$. The reconstruction step of the REA algorithm is used and we can write

$$w(x,t^n) = \sum_j p_j(x)\chi_j(x),\ p_i(x_i) = \bar{w}_i^n. \tag{2.50}$$

The evolution step determines the value of the interface flux from the solution of the generalized Riemann problems

$$w_t + f(w)_x = 0,\ t \ge t^n; \quad w(x,t^n) = \begin{cases} p_i(x) & x < x_{i+\frac{1}{2}}, \\ p_{i+1}(x) & x > x_{i+\frac{1}{2}}. \end{cases} \tag{2.51}$$

The solution of (2.51) is a juxtaposition of a family of nonlinear waves, left-going and right-going waves or mixed. An exact Riemann solver like the Godunov schemes presented in Section 2.2 or an approximate Riemann solver can be used to distribute these nonlinear waves between the two neighboring cells I_i and I_{i+1}. It is this distribution of waves according to their direction which is responsible for *upwind differencing* (see Figure 2.4).

For central schemes, one samples (2.48) at the interface breakpoints, $x = x_{i+\frac{1}{2}}$, which yields

$$\bar{w}_{i+\frac{1}{2}}^{n+1} = \bar{w}_{i+\frac{1}{2}}^n - \frac{1}{\Delta x}\left[\int_{t^n}^{t^{n+1}} f(w(x_{i+1},\tau))d\tau - \int_{t^n}^{t^{n+1}} f(w(x_i,\tau))d\tau\right]. \tag{2.52}$$

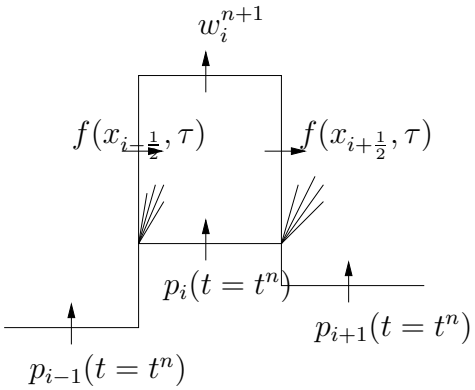

Figure 2.4: *An upwind differencing by Godunov-type scheme.*

The remaining task is to recover the point values $\{w(\cdot,t)|\, t^n \le \tau \le t^{n+1}\}$, and in particular, the staggered averages $\{\bar{w}_{i+\frac{1}{2}}\}$. As for the upwind schemes, this task is accomplished in two main steps. The reconstruction step is similar to that of the upwind method (2.50). In particular, the staggered averages on the right of (2.52) are given by

$$\bar{w}^n_{i+\frac{1}{2}} = \frac{1}{\Delta x}\left[\int_{x_i}^{x_{i+\frac{1}{2}}} p_i(x)dx + \int_{x_{i+\frac{1}{2}}}^{x_{i+1}} p_{i+1}(x)dx\right]. \tag{2.53}$$

The central scheme (2.52) then reads

$$\begin{aligned}\bar{w}^{n+1}_{i+\frac{1}{2}} &= \tfrac{1}{\Delta x}\left[\int_{x_i}^{x_{i+\frac{1}{2}}} p_i(x)dx + \int_{x_{i+\frac{1}{2}}}^{x_{i+1}} p_{i+1}(x)dx\right] \\ &\quad -\tfrac{1}{\Delta x}\left[\int_{t^n}^{t^{n+1}} f(w(x_{i+1},\tau))d\tau - \int_{t^n}^{t^{n+1}} f(w(x_i,\tau))d\tau\right].\end{aligned} \tag{2.54}$$

Next, we find the evolution of the point value along the mid-cells, $x = x_i,\ \{w(x_i,\tau \ge t^n)\}_i$ which are governed by

$$w_t + f(w)_x = 0,\ \tau \ge t^n;\ w(x,t^n) = p_i(x)\ x \in I_i. \tag{2.55}$$

Let $\{\lambda_k(u)\}_k$ denote the eigenvalues of the Jacobian $A(u) = \frac{\partial f}{\partial u}$. By hyperbolicity, information regarding the interface discontinuities at $(x_{i\pm\frac{1}{2}}, t^n)$ propagates no faster than $\max_k |\lambda_k(u)|$. Therefore, the mid-cells values governed by (2.55), $\{w(x_i,\tau \ge$

$t^n)\}_i$, remain free of discontinuities, at least for sufficiently small time step dictated by the CFL condition $\Delta t \leq \frac{1}{2}\Delta x \cdot \max_k |\lambda_k(u)|$. Consequently, since the numerical fluxes on the right of (2.54) involve only smooth integrands, they can be computed within any degree of desired accuracy by an appropriate quadrature rule.

It is the staggered averaging over the fan of left-going and right-going waves

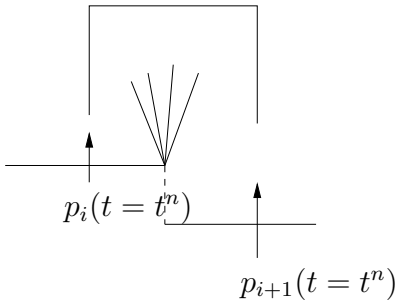

Figure 2.5: *A central reconstruction*

centered at the cell interfaces $(x_{i+\frac{1}{2}}, t^n)$ which characterizes the *central differencing*, see Figure 2.5. A main feature of these central schemes, in contrast to upwind ones, is the computation of smooth numerical fluxes along the cell centers, which avoid the costly (approximate) Riemann solvers.

2.4.7 Entropy condition and nonlinear stability

The use of a conservative and a consistent method does not guarantee that the computed weak solution satisfies an entropy condition. Recall that this condition singles out the unique solution or the physically relevant solution when many weak solutions exist.

If a system of conservation laws possesses an entropy function $\eta(u)$ with the entropy flux $q(u)$, then the following inequality holds in the weak sense

$$\frac{\partial}{\partial t}\eta(u(x,t)) + \frac{\partial}{\partial x}q(u(x,t)) \leq 0, \tag{2.56}$$

i.e., for all $\varphi \in \mathcal{C}_0^1$ with $\varphi(x,t) \geq 0$ for all x, t :

$$\int_0^\infty \int_{\mathbb{R}} \left[\varphi_t(x,t)\eta(u(x,t)) + \varphi_x(x,t)q(u(x,t))\right] dxdt + \int_{\mathbb{R}} \varphi(x,0)\eta(u(x,0))dx \geq 0. \tag{2.57}$$

For a weak solution $u(x,t)$ obtained as the limit of a sequence $u^{(j)}$ to satisfy such inequality, one can prove that a discrete entropy inequality holds, of the form

$$\eta(u_i^{n+1}) \leq \eta(u_i^n) - \frac{\Delta t}{\Delta x}\left(Q_{i+\frac{1}{2}}^n - Q_{i-\frac{1}{2}}^n\right). \tag{2.58}$$

Here $Q_{i+\frac{1}{2}}^n = Q(u_i^n, u_i^{n+1})$, where $Q(u_l, u_r)$ is some numerical entropy flux function that must be consistent with q in the same manner that we require the numerical flux $\mathcal{F}$ to be consistent with the flux f. It is proven in [79, Chapter 12] that for Godunov method, numerical approximation will always satisfy the entropy condition provided that the Riemann solution used to define the flux in each cell interface satisfy the entropy condition. Key to the proof is the correct treatment of transonic rarefaction for the scalar case, and of the case of resonance for systems, where some eigenvalues of the jacobian of the flux function vanish.

The Lax-Wendroff theorem introduced in Section 2.4.5 does not treat the convergence of the method, it only says that if a sequence of approximations converges, then the limit is a weak solution. To ensure convergence, one needs a form of stability, in the sense that the approximation remains bounded as time varies. One can achieve this, for example, with a numerical method that is total variation diminishing as defined in (2.41) and (2.42). This property says that the total variation of the approximate solution at time t_{n+1} does no increase faster than that of the approximate solution at time t_n. This is a major form of stability for nonlinear systems. Other numerical stability properties include the monotonicity of a numerical schemes, the L^1 contracting and the total variation boundedness. We refer the interested reader to [79] for more details on these forms of numerical stability.

2.4.8 Approximate Riemann solvers

The application of Godunov's method to a system of equations requires the similarity solution of a Riemann problem at each cell interface, that is, a state denoted

$RP(\frac{x}{t}, u_l, u_r)$ along $\frac{x}{t} = 0$ based on Riemann data u_l and u_r. In general, one does not need the entire structure of the Riemann problem. Typically, this state is one of the intermediary states in the Riemann solution obtained in the process of connecting u_l to u_r by a sequence of shocks or rarefactions or contact discontinuity. Many approximate Riemann solvers have been proposed that can be applied more cheaply than the exact Riemann solver and yet give results that in many cases are equally good when used in the Godunov or high resolution methods.

The key idea behind the definition of approximate Riemann solver is to replace the nonlinear problem $u_t + f(u)_x = 0$ by some linearized problem defined locally at each cell interface,

$$\hat{u}_t + \hat{A}_{i+\frac{1}{2}}\hat{u}_x = 0. \tag{2.59}$$

The matrix $\hat{A}_{i+\frac{1}{2}}$ is chosen to be some approximation of the Jacobian matrix of the flux $f'(u)$ valid in the neighborhood of the data u_i and u_{i+1}. The linear problem (2.59) is easy to solve using the technique described in Section 2.2. The problem now is to choose the matrix $\hat{A}_{i+\frac{1}{2}}$ such that the approximate system (2.59) is locally equivalent to the original system. Roe suggested in [78] the following conditions on $\hat{A}_{i+\frac{1}{2}}$

(i) $\hat{A}_{i+\frac{1}{2}}$ is diagonalizable with real eigenvalues so that (2.59) is hyperbolic,

(ii) $\hat{A}_{i+\frac{1}{2}} \to f'(\bar{u})$ smoothly as u_i, $u_{i+1} \to \bar{u}$,

(iii) $\hat{A}_{i+\frac{1}{2}}(u_{i+1} - u_i) = f(u_{i+1}) - f(u_i)$.

Condition (iii) ensures that if u_i and u_{i+1} are connected in the exact solution of the Riemann problem by a single wave, then the jump $u_{i+1} - u_i$ should also be an eigenvector of the matrix $\hat{A}_{i+\frac{1}{2}}$. The general way to construct the matrix $\hat{A}_{i+\frac{1}{2}}$ was introduced by Roe, Harten, Lax and consists in choosing an appropriate integration path in the phase plane connecting u_i and u_{i+1} and writing the flux difference as an integral of the Jacobian of the flux computed along this path [79]. To illustrate the general construction, we present below the Roe solver for the shallow water equation.

Roe solver for the shallow water equations

We use here the notation v for the velocity of the water waves and h for the water height. The shallow water equations have the form (2.25) with

$$u = \begin{bmatrix} h \\ hv \end{bmatrix} = \begin{bmatrix} u^1 \\ u^2 \end{bmatrix}, \quad f(u) = \begin{bmatrix} hv \\ hv^2 + \frac{1}{2}gh^2 \end{bmatrix} = \begin{bmatrix} u^2 \\ (u^2)^2/u^1 + \frac{1}{2}g(u^1)^2 \end{bmatrix}$$

and

$$f'(u) = \begin{bmatrix} 0 & 1 \\ -(u^2/u^1)^2 + gu^1 & 2u^2/u^1 \end{bmatrix} = \begin{bmatrix} 0 & 1 \\ -v^2 + gh & 2v \end{bmatrix}.$$

As a parameter vector, we take

$$z = h^{-1/2}u, \text{ so that } \begin{bmatrix} z^1 \\ z^2 \end{bmatrix} = \begin{bmatrix} \sqrt{h} \\ \sqrt{h}v \end{bmatrix}. \tag{2.60}$$

We can then see that

$$u(z) = \begin{bmatrix} (z^1)^2 \\ z^1 z^2 \end{bmatrix} \Rightarrow \frac{\partial u}{\partial z} = \begin{bmatrix} 2z^1 & 0 \\ z^2 & z^1 \end{bmatrix} \tag{2.61}$$

and

$$f(z) \doteq f(u(z)) = \begin{bmatrix} z^1 z^2 \\ (z^2)^2 + \frac{1}{2}g(z^1)^4 \end{bmatrix} \Rightarrow \frac{\partial f}{\partial z} = \begin{bmatrix} z^2 & z^1 \\ 2g(z^1)^3 & 2z^2 \end{bmatrix}. \tag{2.62}$$

We now consider the path

$$z^p = Z_i^p + (Z_{i+1}^p - Z_i^p)\xi \text{ for } p = 1, 2$$

where $Z_i = z(u_i)$ and integrate each element of these matrices from $\xi = 0$ to $\xi = 1$. Except for the (2,1) element of $\partial f/\partial z$ which is cubic, all elements are linear in ξ. Integrating the linear term $z^p(\xi)$ yields

$$\int_0^1 z^p(\xi)d\xi = \frac{1}{2}(Z_i^p + Z_{i+1}^p) \equiv \bar{Z}^p,$$

simply the average between the endpoints. For the cubic term we obtain

$$\begin{aligned}\int_0^1 (z^1(\xi))^3 d\xi &= \tfrac{1}{4}\left(\frac{(Z^1_{i+1})^4 - (Z^1_i)^4}{Z^1_{i+1} - Z^1_i}\right) \\ &= \tfrac{1}{2}(Z^1_i + Z^1_{i+1})\tfrac{1}{2}\left[(Z^1_i)^2 + (Z^1_{i+1})^2\right] \\ &= \bar{Z}^1\bar{h},\end{aligned}$$

where

$$\bar{h} = \frac{1}{2}(h_i + h_{i+1}).$$

Hence the Roe matrix can be computed as the product of the two matrices

$$\hat{B}_{i+1/2} = \begin{bmatrix} 2\bar{Z}^1 & 0 \\ \bar{Z}^2 & \bar{Z}^1 \end{bmatrix}, \quad \hat{C}_{i+1/2} = \begin{bmatrix} \bar{Z}^2 & \bar{Z}^1 \\ 2g\bar{Z}^1\bar{h} & 2\bar{Z}^2 \end{bmatrix} \tag{2.63}$$

as

$$\hat{A}_{i+1/2} = \hat{C}_{i+1/2}\hat{B}^{-1}_{i+1/2} = \begin{bmatrix} 0 & 1 \\ -(\bar{Z}^2/\bar{Z}^1)^2 + g\bar{h} & 2\bar{Z}^2/\bar{Z}^1 \end{bmatrix} = \begin{bmatrix} 0 & 1 \\ -\hat{v}^2 + g\bar{h} & 2\hat{v} \end{bmatrix}. \tag{2.64}$$

Here $\bar{h}$ is the arithmetic average of h_i and h_{i+1}, but $\hat{v}$ is a different sort of average of the velocities, the *Roe average*:

$$\hat{v} = \frac{\bar{Z}^2}{\bar{Z}^1} = \frac{\sqrt{h_i}v_i + \sqrt{h_{i+1}v_{i+1}}}{\sqrt{h_i} + \sqrt{h_{i+1}}}. \tag{2.65}$$

One can see that the matrix $\hat{A}_{i+1/2}$ is simply the Jacobian matrix $f'(\hat{u})$ evaluated at the special state $\hat{u} = (\bar{h}, \bar{h}\hat{v})$. In particular, if $u_i = u_{i+1} = u$, then $\hat{A}_{i+1/2}$ reduces to $f'(u)$.

When solving the shallow water equations with an upwind method, at each cell interface, the approximate Riemann problem (2.59) is solved using the method described in Section 2.2 and this constitutes the approximate Riemann solver of Roe for the shallow water equations.

2.4.9 Relaxation methods for system of conservation laws

In this section, we investigate the relaxation methods for the solution of system of conservation laws in the form (2.1):

$$u_t + f(u)_x = 0 \tag{2.66}$$

The motivation for relaxation methods comes from physics. Indeed, in many physical problems there is an equilibrium relationship between the variables that is essentially maintained at all times. If the solution is perturbed away from this equilibrium, then it rapidly *relaxes* back towards the equilibrium, see [79]. A simple relaxation model for (2.66) is given by the system [69]

$$\begin{aligned} u_t + v_x &= 0 \\ v_t + A^2 u_x &= -\tfrac{1}{\varepsilon}(v - f(u)) \end{aligned} \tag{2.67}$$

where v is a relaxation variable, ε the relaxation parameter and $A^2 = diag(a_1^2, \ldots, a_N^2)$ is a diagonal matrix of real numbers. When ε goes to zero, we obtain from the second equation in (2.67) that $v = f(u)$ and (2.67) reduces to (2.66). Therefore, we can obtain approximate solutions of the system (2.66) as solution of (2.67) for small values of ε. In fact, this is true provided the *sub-characteristic condition* is satisfied

$$Df(u)^2 - A^2 \leq 0. \tag{2.68}$$

This inequality means that for each eigenvalue $\lambda_i(u)$ of the Jacobian matrix $Df(u)$, we have $\lambda_i(u)^2 \leq a_i^2$. The derivation of (2.68) is done using the Chapman Enskog expansion. Indeed, we can expand the variable v as

$$v = f(u) + \varepsilon v_1 + \varepsilon^2 v_2 + \ldots \tag{2.69}$$

and substituting in the first equation in (2.67), we have

$$u_t + \left[f(u) + \varepsilon v_1 + \varepsilon^2 v_2 + \ldots \right]_x = 0 \tag{2.70}$$

or

$$u_t + f(u)_x = -\varepsilon (v_1)_x - \varepsilon^2 (v_2)_x + \ldots \tag{2.71}$$

Inserting (2.69) in the second equation of (2.67), we obtain

$$\left[f(u) + \varepsilon v_1 + \varepsilon^2 v_2 + \ldots \right]_t + A^2 u_x = -\left(v_1 + \varepsilon v_2 + \ldots \right) \tag{2.72}$$

or

$$\begin{aligned} & Df(u)\left[-Df(u)u_x - \varepsilon (v_1)_x - \varepsilon^2 (v_2)_x + \ldots \right] + \varepsilon (v_1)_t + \varepsilon^2 (v_2)_t + \cdots + A^2 u_x \\ = \; & -\left(v_1 + \varepsilon v_2 + \ldots \right). \end{aligned} \tag{2.73}$$

Collecting the first order terms obtained for $\varepsilon \ll 1$ gives

$$(A^2 - Df(u)^2)u_x = -v_1$$

and then, using (2.71), we obtain

$$u_t + f(u)_x = \varepsilon \left[(A^2 - Df(u)^2)u_x\right]_x + \mathcal{O}(\varepsilon^2). \tag{2.74}$$

This system is dissipative if and only if

$$A^2 - Df(u)^2 \geq 0.$$

This condition says that the characteristic speed a_i^2 of (2.67) interlaces with those of the system (2.66). When the sub-characteristic condition is violated, then for some cases, the solution will blow up along the characteristic of the relaxing system.

2.4.10 The relaxation scheme of Jin and Xin

The discretization of the relaxation system (2.67), which depend on the relaxation rate ε are called *relaxing schemes* and their zero relaxation limits are called *relaxed schemes*. The relaxed schemes are theoretically stable and conservative discretization of the original balance law. Thus they are independent of ε and the artificial variable v. To obtain the relaxing schemes, one uses the spatial discretization of (2.67) given by

$$\begin{array}{rcl} \partial_t u_j + \frac{1}{h}(v_{j+\frac{1}{2}} - v_{j-\frac{1}{2}}) & = & 0, \\ \partial_t v_j + \frac{1}{h}A^2(u_{j+\frac{1}{2}} - u_{j-\frac{1}{2}}) & = & -\frac{1}{\varepsilon}(v_j - F_j), \end{array} \tag{2.75}$$

where the average quantities

$$F_j = \frac{1}{h}\int_{x_{j-\frac{1}{2}}}^{x_{j+\frac{1}{2}}} f(u)dx = f\left(\frac{1}{h}\int_{x_{j-\frac{1}{2}}}^{x_{j+\frac{1}{2}}} u dx\right) + O(h^2) = F(u_j) + O(h^2). \tag{2.76}$$

The point value quantities $u_{j+\frac{1}{2}}$ and $v_{j+\frac{1}{2}}$ are defined below using the variables characteristics

$$v \pm Au$$

of the system (2.67). A second order scheme for the approximations of (2.67) uses the piecewise linear interpolation which, applied to the p-th components of $v \pm Au$, denoted as $v \pm a_p u$, gives respectively

$$\begin{aligned} (v + a_p u)_{j+\frac{1}{2}} &= (v + a_p u)_j + \tfrac{1}{2} h s_j^+ \\ (v - a_p u)_{j+\frac{1}{2}} &= (v - a_p u)_{j+1} + \tfrac{1}{2} h s_{j+1}^-. \end{aligned} \tag{2.77}$$

Here $s_j^\pm$ is the slope of $v \pm au$ on the jth cell. The slopes are given by

$$s_j^\pm = \frac{1}{h}(v_{j+1} \pm a_p u_{j+1} - v_j \mp a_p u_j)\phi(\theta_j^\pm), \tag{2.78}$$

$$\theta_j^\pm = \frac{v_j \pm a_p u_j - v_{j-1} \mp a_p u_{j-1}}{v_{j+1} \pm a_p u_{j+1} - v_j \mp a_p u_j}. \tag{2.79}$$

The map ϕ is the slope-limiter and it satisfies the general condition [100]

$$0 \leq \frac{\phi(\theta)}{\theta} \leq 2 \text{ and } 0 \leq \phi(\theta) \leq 2 \tag{2.80}$$

for the scheme (2.75) to be total variation diminishing. Examples of slopes limiters are given by the minmod limiter and the van Leer limiter

$$\phi(\theta) = \max(0, \min(1, \theta)), \text{ and } \phi(\theta) = \frac{|\theta| + \theta}{1 + |\theta|},$$

respectively. Solving (2.77) for $u_{j+\frac{1}{2}}$ and $v_{j+\frac{1}{2}}$ gives

$$\begin{aligned} u_{j+\frac{1}{2}} &= \tfrac{1}{2}(u_j + u_{j+1}) - \tfrac{1}{2a_p}(v_{j+1} - v_j) + \tfrac{h}{4a_p}(s_j^+ + s_{j+1}^-) \\ v_{j+\frac{1}{2}} &= \tfrac{1}{2}(v_j + v_{j+1}) - \tfrac{a_p}{2}(u_{j+1} - u_j) + \tfrac{h}{4}(s_j^+ + s_{j+1}^-). \end{aligned} \tag{2.81}$$

By inserting these values in the numerical scheme (2.75), we obtain the semi-discrete form of the relaxation scheme. We point out that when the slope $s^\pm = 0$, the scheme (2.75) reduces to a first order upwind scheme. For time discretization, we use the second order TVD Runge-Kutta splitting scheme introduced by Jin [68]. It takes two implicit stiff source steps and two explicit convection step alternatively. If we denote

$$D_+ w_j = \frac{1}{\Delta x}(w_{j+\frac{1}{2}} - w_{j-\frac{1}{2}}),$$

the fully discrete relaxation scheme reads with initial data $U^n = (u_j^n)_j$ and $V^n = f(U^n) = (f(u_j^n))_j$

$$\begin{aligned}
U^* &= U^n, && (2.82)\\
V^* &= V^n + \frac{\Delta t}{\varepsilon}(V^* - f(U^*)); && (2.83)\\
U^{(1)} &= U^* - \Delta t D_+ V^* + \Delta t S(U^*), && (2.84)\\
V^{(1)} &= V^* - \Delta t A^2 D_+ U^*; && (2.85)\\
U^{**} &= U^{(1)}, && (2.86)\\
V^{**} &= V^{(1)} - \frac{\Delta t}{\varepsilon}(V^{**} - f(U^{**})) - 2\frac{\Delta t}{\varepsilon}(V^* - f(U^*)); && (2.87)\\
U^{(2)} &= U^{**} - \Delta t D_+ V^{**} + \Delta t S(U^{**}), && (2.88)\\
V^{(2)} &= V^{**} - \Delta t A^2 D_+ U^{**}; && (2.89)\\
U^{n+1} &= \frac{1}{2}(U^n + U^{(2)}), && (2.90)\\
V^{n+1} &= \frac{1}{2}(V^n + V^{(2)}). && (2.91)
\end{aligned}$$

Because of the implicit treatment of the source term, this time discretization is stable, independently of ε, given that the CFL condition from the convective part is satisfied. As $\varepsilon \to 0$, $V = f(U)$ and the relaxing schemes (2.82)–(2.91) converge to a consistent and stable discretization of the original balance law, see [69]. If we assume that $\varepsilon \ll 1$ and $\varepsilon/\Delta x \ll 1$, $\varepsilon/\Delta t \ll 1$, then we can prove as in Jin [68] that

$$V^* = f(U^*) + O(\frac{\varepsilon}{\Delta t}), \quad V^{**} = f(U^{**}) + O(\frac{\varepsilon}{\Delta t}). \tag{2.92}$$

Applying (2.92) to the scheme (2.82)–(2.91) we obtain, ignoring the error $O(\frac{\varepsilon}{\Delta t})$, the relaxed schemes

$$\begin{aligned}
U^{(1)} &= U^n - \Delta t D_+ V^n|_{V^n = f(U^n)} + \Delta t S(U^n),\\
U^{(2)} &= U^{(1)} - \Delta t D_+ V^{(1)}|_{V^{(1)} = f(U^{(1)})} + \Delta t S(U^{(1)}), && (2.93)\\
U^{n+1} &= \tfrac{1}{2}(U^n + U^{(2)}).
\end{aligned}$$

2.5 Concluding Remarks

We have introduced in this chapter the general theory on systems of conservation laws in one dimension, and the extensions for a network of pipes. We collected results on the well-posedness of the standard Riemann problem and the Riemann problem at the junction. We have also discussed briefly the Cauchy problem. We have reviewed the current state of the art numerical methods for the computation of the approximate solution of system of conservation laws. Since the solutions are usually discontinuous, we have introduced numerical schemes that are conservative, stable and consistent with the continuous model. These properties ensure the convergence of the method.

A few results on the well-posedness of scalar conservation laws in the multi-dimensional case exist in the literature. We refer to the remarkable work of Kružkov [73] and the more recent publications [104, 105, 42]. Many authors have investigated numerical integration of multidimensional system of conservation laws. We refer for example to the book by Leveque [79] where the case of the Euler equations and the shallow water equations are investigated. Jin and Xin [69] and Banda [3] used a relaxation approach for the integration of the multidimensional systems.

Part II

The Drift-flux Multiphase Model in Networks of Pipes

Chapter 3

Towards a Mathematical Analysis for Drift-Flux Multiphase Flow Models in Networks

This chapter deals with the dynamics of the multiphase *drift-flux* model in a network of pipes. We formulate the model equations from the two-fluid model and obtain a model with a conservation of mass for each of the two phases and a conservation of momentum. The system is closed with an equation of state which gives a formula of the pressure in terms of the densities of the two phases. This chapter focuses on a linear pressure law derived under the assumption that the pressure of each phase is a linear function of the densities. In the next chapter, we will consider a more general pressure law defined as an arbitrary function of the densities. When the model equation for the fluid is adopted, we consider a junction of a network as a set of vectors intersecting at the origin. The vector length represents the pipe and their meeting point is the junction. The dynamic of the flow of the fluid at the junction is stable only if some suitable coupling conditions are prescribed. These are usually derived from the physics of the problem and they play an important role in the proof of the well-posedness of the Riemann problem at the junction. The main results of this chapter are the well-posedness of the Riemann problem at the

junction and numerical simulations of the dynamics of the flow at the junction for the cases of three and four connected pipes. These results appeared in [10].

3.1 Introduction

We consider an *isothermal no-slip drift-flux* model for multiphase flows of the form:

$$\partial_t \rho_1 + \partial_x(\rho_1 u) = 0 \tag{3.1a}$$

$$\partial_t \rho_2 + \partial_x(\rho_2 u) = 0 \tag{3.1b}$$

$$\partial_t(u(\rho_1+\rho_2)) + \partial_x\left((\rho_1+\rho_2)(u^2+\frac{a^2}{2})\right) = 0 \tag{3.1c}$$

where ρ_1 and ρ_2 are the density of phase 1 and phase 2, respectively, u is the common velocity of the two phases and a is a constant which depends on both phases. This model is derived from the drift-flux model [51] by making the simplifying assumption that the closure law, the so called *slip condition*, has a vanishing *slip function*. The slip condition is an algebraic relation that relates the two velocities of the two phases. The drift-flux model in turn is derived from the *two-fluid* model by summing up the balance laws for the momentum, in canonical form, for each phase. The choice of this model has been motivated by the fact that we would like to concentrate on some basic aspects of the model in order to analyze coupling conditions of pipes at a junction in a network and devise a computational approach for approximating flow at a junction.

The *no-slip* condition was considered by Evje and Flåtten [50] when extending the Weakly Implicit Mixture Flux (WIMF) scheme originally developed for the *two-fluid* model, to the *drift-flux* model. In [52] Evje and Karlsen used the same simplification as a basis for proving global existence of weak solutions for the viscous form of the drift-flux model. This model has many applications in the chemical, petroleum and nuclear industries [48, 46]. As a result there has been intense research on such multiphase flows in the recent past. Different models for multiphase flows have been proposed [1, 54, 63, 46, 51] and numerical methods for such models have

been investigated [48, 49, 47, 46]. The mathematical study of the flow of gases in networks is a young field of research and has been under investigation only recently. The reader is referred to [32, 33, 41, 6, 7], in the context of gas networks. Work has also been undertaken in the context of traffic flow networks, see for example [62].
In this chapter, we investigate the flow of an *isothermal no-slip drift-flux* model (3.1) in a network of pipes. Firstly, using the properties of Riemann problems for general one dimensional systems of conservation laws, we derive a Riemann solver for the model equation (3.1). Secondly, we consider the flow of (3.1) at the junction of a network of pipes and prove the well-posedness of the resulting Riemann problem at the vertex. Our proof relies on suitable conditions which couple the models from each pipe at the junction. These coupling conditions are motivated by consideration from the physics of the flow. For example, the conservation of mass at the junction forms the cornerstone of such considerations. Similar work has been done for the p-system by Colombo et al. [32, 33] and on the isothermal Euler equations by Banda et al. [6, 7]. Here we consider the case of a multiphase fluid. The constructive proof of our main result allows us to do some numerical simulations of junctions connecting up to four pipes.
This chapter is organized as follows: In Section 3.2, we derive the model equation given in (3.1), study the wave curves in one pipe and define a Riemann solver for the model equation. Section 3.3 is devoted to the modeling of pipe to pipe intersections and the proof of well-posedness of the model at an uncontrolled junction of a network. Finally, we describe in Section 3.4 a numerical method used to solve the isothermal no-slip drift-flux model on networks. Computational results on some carefully chosen examples are presented and compared with theoretical results.

3.2 Modeling of a single pipe flow and preliminary discussion

In this section we will briefly introduce the no-slip drift-flux model as discussed in [51]. Mathematical properties of this model will be discussed. We will conclude with the solution of a Riemann Problem for such a model in a single pipe. We consider a multi-component fluid in a pipe modeled by the so–called drift-flux model. The model arises from general two–fluid models like those presented in [51] by assuming that the pressure for both phases is equal. We denote the volume fraction, the density and the velocity of phase i at position x and time t, where $i \in \{1, 2\}$ by $\alpha_i = \alpha_i(x,t)$, $\varrho_i(x,t)$, $u_i(x,t)$, respectively. We have

$$\alpha_1 + \alpha_2 = 1,$$

and letting p be the common pressure for both phases, the drift-flux model reads

$$\frac{\partial}{\partial t}(\varrho_1\alpha_1) + \frac{\partial}{\partial x}(\varrho_1\alpha_1 u_1) = 0; \tag{3.2a}$$

$$\frac{\partial}{\partial t}(\varrho_2\alpha_2) + \frac{\partial}{\partial x}(\varrho_2\alpha_2 u_2) = 0; \tag{3.2b}$$

$$\frac{\partial}{\partial t}(\varrho_1\alpha_1 u_1 + \varrho_2\alpha_2 u_2) + \frac{\partial}{\partial x}(\varrho_1\alpha_1 u_1^2 + \varrho_2\alpha_2 u_2^2 + p) = Q. \tag{3.2c}$$

Here, the momentum sources that act on both phases are given by

$$Q := -(\varrho_1 + \varrho_2)g\sin\theta - f_1\varrho_1 u_1|u_1| - f_2\varrho_2 u_2|u_2| + \mu(u_{\text{mix}})_{xx},$$

where g is the gravitational constant, θ is the inclination of the pipe, f_i the friction factor, $\mu > 0$ is the diffusion coefficient and $u_{\text{mix}} = \alpha_1 u_1 + \alpha_2 u_2$. The phasic momentum satisfies a slip relation of the form $u_1 - u_2 = \Phi(p, u_1, u_2)$.

As a further simplification, we discuss the case of a no–slip condition $\Phi \equiv 0$ [52], no source term $Q \equiv 0$, and an isothermal equation of state given by

$$p = \frac{a^2}{2}(\rho_1 + \rho_2). \tag{3.3}$$

Remark 3.1. *The pressure law in* (3.3) *can be derived as follows: we assume that the compressibility factors* a_1 *and* a_2 *of the two phases are equal and satisfy* $a_1^2 = a_2^2 = \frac{a^2}{2}$. *Since each phase is isothermal, its pressure is given by*

$$p_i = a_i^2 \varrho_i, \ i \in \{1, 2\}, \ a_i = \text{const.}$$

Moreover, we assume that the pressure p *of the multiphase flow is such that* $p = p_1 = p_2$. *From the volume fraction relation* $\alpha_1 + \alpha_2 = 1$, *we obtain*

$$\frac{\rho_1}{\varrho_1} + \frac{\rho_2}{\varrho_2} = \frac{a_1^2 \rho_1}{p} + \frac{a_2^2 \rho_2}{p} = 1.$$

Hence with the above assumption on the compressibility, we obtain (3.3). *Moreover, in the case where we have different compressibility for the two phases (i.e.* $a_1^2 \neq a_2^2$*) the pressure takes the form* $p = a_1^2 \rho_1 + a_2^2 \rho_2$. *This latter pressure laws is investigated in detail in Chapter 4.*

Under these assumptions the model in (3.2) simplifies to the form

$$\begin{aligned} \frac{\partial \rho_1}{\partial t} + \frac{\partial (\rho_1 u)}{\partial x} &= 0, && \text{(3.4a)} \\ \frac{\partial \rho_2}{\partial t} + \frac{\partial (\rho_2 u)}{\partial x} &= 0, && \text{(3.4b)} \\ \frac{\partial I}{\partial t} + \frac{\partial}{\partial x}\left[\hat{\rho}(u^2 + \frac{a^2}{2})\right] &= 0, && \text{(3.4c)} \end{aligned}$$

where

$$\rho_1 := \varrho_1 \alpha_1, \quad \rho_2 := \varrho_2 \alpha_2, \quad \hat{\rho} = \rho_1 + \rho_2, \quad I = \hat{\rho} u.$$

Remark 3.2. *For smooth solutions with* $\rho_1 + \rho_2 \neq 0$, *one can derive an evolution equation for the common velocity* u *in conservative form for both phases as*

$$\partial_t u + \partial_x \left(\frac{1}{2} u^2 + \frac{a^2}{2} \log(\rho_1 + \rho_2) \right) = 0. \tag{3.5}$$

In the following we study the system (3.4a), (3.4b), (3.4c) in terms of the conservative variables

$$U := (\rho_1, \rho_2, I).$$

We refer to [42, 78] for a general reference on the theory of hyperbolic equations.

The Jacobian matrix of the flux function

$$f(U) = \begin{bmatrix} \rho_1 u \\ \rho_2 u \\ \hat{\rho}(u^2 + \frac{a^2}{2}) \end{bmatrix}$$

of the system (3.4) is given by

$$Jf(U) = \begin{bmatrix} \frac{u\rho_2}{\rho_1+\rho_2} & -\frac{u\rho_1}{\rho_1+\rho_2} & \frac{\rho_1}{\rho_1+\rho_2} \\ -\frac{u\rho_2}{\rho_1+\rho_2} & \frac{u\rho_1}{\rho_1+\rho_2} & \frac{\rho_2}{\rho_1+\rho_2} \\ \frac{a^2}{2} - u^2 & \frac{a^2}{2} - u^2 & 2u \end{bmatrix}.$$

The eigenvalues for the Jacobian of the flux function are given by

$$\lambda_1(U) = u - \frac{a}{\sqrt{2}}, \quad \lambda_2(U) = u, \quad \lambda_3(U) = u + \frac{a}{\sqrt{2}} \tag{3.6}$$

and the corresponding eigenvectors by

$$r_1 = \begin{bmatrix} \rho_1 \\ \rho_2 \\ \hat{\rho}\lambda_1 \end{bmatrix}, \; r_2 = \begin{bmatrix} -1 \\ 1 \\ 0 \end{bmatrix}, \; r_3 = \begin{bmatrix} \rho_1 \\ \rho_2 \\ \hat{\rho}\lambda_3 \end{bmatrix}.$$

The first and the third field are genuinely nonlinear since $\nabla\lambda_{1,3} \cdot r_{1,3} = \mp\frac{a}{\sqrt{2}} \neq 0$, and the second field is linearly degenerate since $\nabla\lambda_2 \cdot r_2 = 0$, see Section 2.2.2.

For a given state U^0 and $i = 1, 2, 3$, we denote by $\xi \to L_i^+(\xi; U^0)$ the $i-$th forward Lax–curve through U^0 and by $\xi \to L_i^-(\xi; U^0)$ the i-th backwards Lax–curve through U^0 corresponding to the i-th characteristic field. We choose the parameterization of the Lax-curves in such a way that $L_i^{\pm}(1; U^0) = U^0$ and $L_i^{\pm}(0; U^0)$ correspond to a vacuum state. We assume for the rest of the Chapter that $\xi > 0$ so that no vacuum state is considered. For a given state U^0, the states that can be connected to the right of U^0 by a $1-$Lax curve are given by

$$L_1^+(\xi; U^0) = \begin{cases} \xi(\rho_1^0, \rho_2^0, 0)^T + (0, 0, I^0\xi - \hat{\rho}^0(\xi - 1)\sqrt{\xi}\frac{a}{\sqrt{2}})^T, & \xi \geq 1; \\ \xi(\rho_1^0, \rho_2^0, 0)^T + (0, 0, I^0\xi - \hat{\rho}^0\frac{a}{\sqrt{2}}\xi\log(\xi))^T, & \xi < 1. \end{cases} \tag{3.7a}$$

The states that can be connected to the right of U^0 by 3−Lax curves satisfy

$$L_3^+(\xi;U^0)=\begin{cases}\xi(\rho_1^0,\rho_2^0,0)^T+(0,0,I^0\xi+\hat{\rho}^0(\xi-1)\sqrt{\xi}\frac{a}{\sqrt{2}})^T, & \xi\leq 1;\\ \xi(\rho_1^0,\rho_2^0,0)^T+(0,0,I^0\xi+\hat{\rho}^0\frac{a}{\sqrt{2}}\xi\log(\xi))^T, & \xi>1.\end{cases} \tag{3.7b}$$

The state that can be connected to a state U^0 by a contact discontinuity belongs to the curve defined by

$$L_2(\xi,U^0)=(\rho_1^0\xi,(1-\xi)\rho_1^0+\rho_2^0,I^0)^T,\ \xi\in\mathbb{R}. \tag{3.7c}$$

For a given state U^0, the states that can be connected to the left of U^0 by a 1−Lax curve and a 3−Lax curve, are given by

$$L_1^-(\xi;U^0)=\begin{cases}\xi(\rho_1^0,\rho_2^0,0)^T+(0,0,I^0\xi-\hat{\rho}^0(\xi-1)\sqrt{\xi}\frac{a}{\sqrt{2}})^T, & \xi\leq 1,\\ \xi(\rho_1^0,\rho_2^0,0)^T+(0,0,I^0\xi-\hat{\rho}^0\frac{a}{\sqrt{2}}\xi\log(\xi))^T, & \xi>1;\end{cases} \tag{3.7d}$$

and

$$L_3^-(\xi;U^0)=\begin{cases}\xi(\rho_1^0,\rho_2^0,0)^T+(0,0,I^0\xi+\hat{\rho}^0(\xi-1)\sqrt{\xi}\frac{a}{\sqrt{2}})^T, & \xi\geq 1;\\ \xi(\rho_1^0,\rho_2^0,0)^T+(0,0,I^0\xi+\hat{\rho}^0\frac{a}{\sqrt{2}}\xi\log(\xi))^T, & \xi<1,\end{cases} \tag{3.7e}$$

respectively. Note that we obtain 1–shocks for $\xi>1$ on L_1^+ and for $\xi<1$ on L_1^-. Similarly, for $\xi<1$, we obtain a 3–shock along L_3^+ and on L_3^- we obtain a 3–shock for $\xi>1$. The shock speeds are given by

$$s_{1,3}(\xi;U)=\frac{I}{\hat{\rho}}\mp\frac{a}{\sqrt{2}}\sqrt{\xi}.$$

Further the contact discontinuity travels with speed

$$s_2(\xi;U)=\lambda_2(\xi;U)=u(\xi)=\frac{I}{\hat{\rho}}.$$

Remark 3.3. *If we considered equations (3.4a), (3.4b) and (3.5) instead, the conserved variable would be $U=(\rho_1,\rho_2,u)$ and we would obtain the shock speeds $\bar{s}_{1,3}$*

$$\bar{s}_{1,3}\Big(\xi;\begin{bmatrix}\rho_1\\ \rho_2\\ u\end{bmatrix}\Big)=u\mp\frac{a}{\xi^2-1}\xi\sqrt{(\xi^2-1)\log(\xi)}.$$

Locally, around $\xi = 1$*, an expansion in a series gives, up to order* $(\xi - 1)^2$*,*

$$\bar{s}_{1,3}(\xi;\cdot) \approx u \mp a\left(\frac{1}{\sqrt{2}} + \frac{\sqrt{2}}{4}(\xi - 1) + \dots\right)$$

and similarly for $s_{1,3}$

$$s_{1,3}(\xi;\cdot) \approx u \mp \frac{a}{\sqrt{2}}\left(1 + \frac{1}{2}(\xi - 1) + \dots\right).$$

A Riemann problem for (3.4a, 3.4b, 3.4c) is a Cauchy problem for $(x,t) \in \mathbb{R}\times\mathbb{R}^+$ with Heaviside initial data given by

$$U(x,0) = \begin{cases} U^l, & \text{if} \quad x \le 0; \\ U^r, & \text{if} \quad x > 0, \end{cases}$$

for constant states U^l and U^r. For the rest of the discussion, we assume that there is no vacuum, that is, $\rho_i^l, \rho_i^r > 0$ for $i \in \{1,2\}$. Hence, the system of partial differential equations is strictly hyperbolic, the existence and uniqueness of a self–similar solution $U(x,t) = V(x/t)$ for $\|U^l - U^r\| \ll 1$ is guaranteed by classical results, see for example [42].

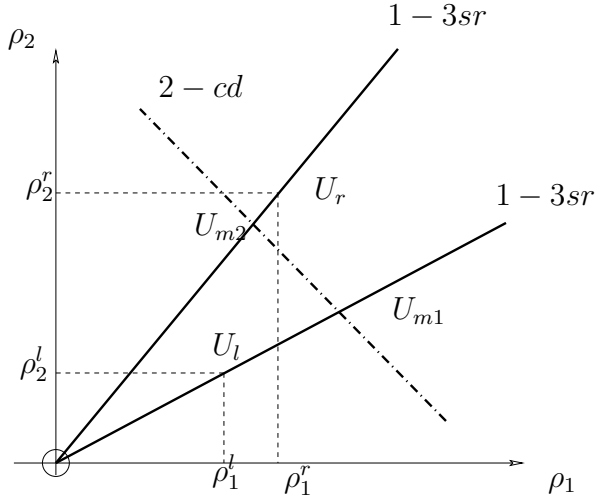

Figure 3.1: *Projected Lax–curves in the* $\rho_1 - \rho_2$ *plane*

If there is no vacuum state, i.e., $\rho_i^l, \rho_i^r > 0$, then the solution can be easily constructed by the following procedure in the $\rho_1 - \rho_2-$phase space (see Figure 3.1).

First we observe the following: in the $\rho_1-\rho_2-$plane the projections of the 1– and the 3–Lax–curves are straight lines and the projection of the rarefaction and shock coincide; furthermore, the *projections* of the 1–Lax curve and the 3–Lax curves coincide. Hence we consider a given left state $U^l = (\rho_1^l, \rho_2^l, I^l)$ and a given right state $U^r = (\rho_1^r, \rho_2^r, I^r)$. We distinguish two cases:

(a) If $\hat{\rho}^l = \hat{\rho}^r$ and $I^l = I^r$, then U^l and U^r can be connected by a single 2-contact discontinuity. The speed of the rarefaction is then $s = \frac{I^l}{\hat{\rho}^l}$, recall that $\hat{\rho}^l = \rho_1^l + \rho_2^l$.

(b) Denote by $U_{m_1} = L_1^+(\xi_{m_1}; U^l)$ for some $\xi_{m_1} \in \mathbb{R}^+$ and $U_{m_2} = L_3^-(\xi_{m_2}; U^r)$ for some $\xi_{m_2} \in \mathbb{R}^+$. We determine (ξ_{m_1}, ξ_{m_2}) such that $U_{m_1} = (\rho_1^{m_1}, \rho_2^{m_1}, I^{m_1})$ and U_{m_2} are connected by a 2–contact discontinuity. We solve the following equations for (ξ_{m_1}, ξ_{m_2})

$$I^{m_1}(\xi_{m_1}) = I^{m_2}(\xi_{m_2}), \tag{3.8a}$$

$$\hat{\rho}^{m_1}(\xi_{m_1}) = \hat{\rho}^{m_2}(\xi_{m_2}). \tag{3.8b}$$

In the case of no vacuum, the system (3.8) reduces to solving the nonlinear equation (3.9) for $\xi \in \mathbb{R}^+$. Note that due to the particular structure of the Lax–curves we have $\hat{\rho}^{m_1}(\xi_{m_1}) = \xi_{m_1}\hat{\rho}^l = \rho_1^l + \rho_2^l$. The solutions of (3.8) are obtained as $\xi_{m_1} = \dfrac{\hat{\rho}^r}{\hat{\rho}^l}\xi$ and $\xi_{m_2} = \xi$, where

$$I^{m_1}\left(\frac{\hat{\rho}^r}{\hat{\rho}^l}\xi\right) - I^{m_2}(\xi) = 0. \tag{3.9}$$

In the numerical results later on, equation (3.9) is solved locally using Newton's method. The solution to the Riemann problem is a wave of the first family connecting U^l to U_{m_1}, a contact discontinuity connecting U_{m_1} and U_{m_2} and a wave of the third family connecting U_{m_2} and U^r. Depending on the sign of $\xi_{m_1} - 1$ and $\xi_{m_2} - 1$, we either obtain shock or rarefaction waves, see (3.7).

Finally, we introduce the region of subsonic states in the phase–space that will be critical in establishing the well-posedness of the model at the intersection of the

pipes. We state the sets in terms of $u = \frac{I}{\hat{\rho}}$.

$$\begin{aligned} A_0^+ &:= \{(\rho_1, \rho_2, I) \in \overset{\circ}{\mathbb{R}}_+ \times \overset{\circ}{\mathbb{R}}_+ \times \mathbb{R} : u + \tfrac{a}{\sqrt{2}} \geq 0 \text{ and } u \leq 0\}, \\ A_0^- &:= \{(\rho_1, \rho_2, I) \in \overset{\circ}{\mathbb{R}}_+ \times \overset{\circ}{\mathbb{R}}_+ \times \mathbb{R} : \ u \leq 0\}, \\ A_0^\# &:= \{(\rho_1, \rho_2, I) \in \overset{\circ}{\mathbb{R}}_+ \times \overset{\circ}{\mathbb{R}}_+ \times \mathbb{R} : u - \tfrac{a}{\sqrt{2}} \leq 0 \text{ and } u \geq 0\}. \end{aligned} \tag{3.10}$$

The following elementary result characterizes the speed of forward 1-shock and backward 3-shock for subsonic initial data and will be used later for solutions at a pipe–to–pipe intersection.

Lemma 3.1. *Let U^0 be in the interior of $A_0^\#$ or in the interior of A_0^- (respectively, A_0^+) and assume that U^0 is not a vacuum state. Then, the velocity of a 1–shock wave (respectively, 3–shock wave) connecting U^0 and U has non–positive (respectively, non–negative) speed provided that $\|U - U^0\|_\infty$ is sufficiently small.*

Proof. Consider a (right) state $U = L_1^+(\xi; U^0)$ connected to the left state U^0 by a 1–Lax–shock, hence $\xi \geq 1$. The shock speed is

$$s_1(\xi; U^0) = u^0 - \frac{a}{\sqrt{2}}\sqrt{\xi} \leq u^0 - \frac{a}{\sqrt{2}} \leq 0.$$

Similarly, we obtain $s_3(\xi; U^0) \geq 0$, for $\xi \geq 1$, for $U^0 \in A_0^+$ and a (left) state $U = L_3^-(\xi; U^0)$ ∎

Note that any state connected to U^0 in the interior of A_0^+ by a 3–wave has non–negative speed due to (3.6). Similarly, any state U^0 in the interior of A_0^- connected to a left state U by a 1– or 2– wave has non–positive speed. This will be a key point for verifying well–posedness for pipe–to–pipe conditions.

3.3 Modeling of pipe–to–pipe intersections

As in [32, 38], we model a single pipe–to–pipe intersection by a set of distinct vectors $\nu_j \in \mathbb{R}^2 \setminus \{\mathbf{0}\}, j = 1, \ldots, n$, with $\nu_{j,1} \geq 0$. Each ν_j is directed along the pipe j and represents the direction of the pipe. We further choose ν_j such that $\|\nu_j\|$ equals the

cross–section of the pipe. Each $j = 1, \ldots, n$ belongs either to the set $\delta^- \subset \mathbb{N}$ of incoming arcs or to the set $\delta^+ \subset \mathbb{N}$ of outgoing arcs, see Figure 3.2 for an example. We assume that there is at least one incoming and one outgoing pipe, which means that $|\delta^\pm| \geq 1$, where $|A|$ is the number of elements of the set A. The jth pipe is parameterized by $x \in \mathbb{R}^-$, if $j \in \delta^-$ and by $x \in \mathbb{R}^+$, if $j \in \delta^+$, see Figure 3.2. The parametrization is such that the vertex is located at $x = 0$ for all pipes. Along each

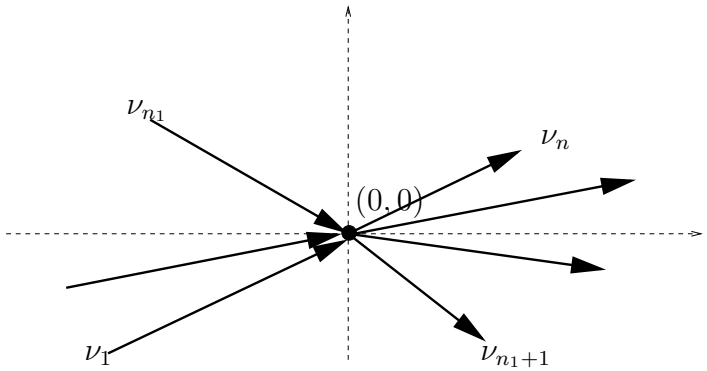

Figure 3.2: *Junction with n pipes demonstrating the parametrization: the cross section ν_j and sets $\delta^\pm$ with $\delta^- = \{1, \ldots, n_1\}$ and $\delta^+ = \{n_1 + 1, \ldots, n\}$*

pipe $j \in \{1, 2, \ldots, n\}$, we assume the flow is modeled by a no-slip drift-flux model, that is, for $x \in \mathbb{R}^-(j \in \delta^-)$ or $x \in \mathbb{R}^+(j \in \delta^+)$ and $t > 0$,

$$\partial_t \begin{pmatrix} \rho_1^j \\ \rho_2^j \\ I^j \end{pmatrix} + \partial_x \begin{pmatrix} \rho_1^j u^j \\ \rho_2^j u^j \\ \hat{\rho}^j \left((u^j)^2 + \frac{a^2}{2} \right) \end{pmatrix} = \begin{pmatrix} 0 \\ 0 \\ 0 \end{pmatrix} \tag{3.11}$$

along with initial conditions

$$U_j(x, 0) = (\rho_{1,0}^j, \rho_{2,0}^j, I_0^j)(x), \ \forall x \in \mathbb{R}^{\pm(j)}. \tag{3.12}$$

We further prescribe algebraic conditions at the junction $x = 0$ coupling the dynamics on adjacent edges. Several possibilities for prescribing such conditions exist. Our conditions in the context of the two–component model are motivated as follows: It is assumed that neither mass of component one nor mass of component

two is lost when passing through the junction. This yields the two conditions (**M1**) and (**M2**) below. Furthermore, we assume that the junction does not introduce an acceleration to the combined velocity. It follows that for the two gas components in the adjacent pipes near the junctions, velocity differences vanish. This can be modeled by assuming that the flux of the momentum remains constant along all pipes near the intersection leading to the condition (**Q**). These assumptions could also be obtained in a rigorous way by a similar procedure as in [77]:

(M1) Conservation of mass of phase 1: for $t > 0$ a.e.,

$$\sum_{j\in\delta^-} \|\nu_j\|(\rho_1^j u^j)(0,t) = \sum_{j\in\delta^+} \|\nu_j\|(\rho_1^j u^j)(0,t).$$

(M2) Conservation of mass of phase 2: for $t > 0$ a.e.,

$$\sum_{j\in\delta^-} \|\nu_j\|(\rho_2^j u^j)(0,t) = \sum_{j\in\delta^+} \|\nu_j\|(\rho_2^j u^j)(0,t).$$

Furthermore, we require as an additional condition which correspond to an equal momentum along $\sum_j \nu_j$:

(Q) The *flux of the momentum* density remains constant at the intersection: for $t > 0$ a.e.,

$$\left(\hat{\rho}^j\left((u^j)^2 + \frac{a^2}{2}\right)\right)(0,t) = \left(\hat{\rho}^i\left((u^i)^2 + \frac{a^2}{2}\right)\right)(0,t) = P^*(t),\ \forall i \neq j.$$

Conditions **(M1)** and **(M2)** are compulsory and resemble Kirchoff's law at the intersection. They can be obtained by considering the weak formulation of (3.11). Condition **(Q)** is also obtained from the weak formulation of (3.11) using a special class of test functions as in [77]. However, other conditions can be proposed to replace **(Q)**, see also [41, 61, 7, 95]. Clearly, in the case $n = 2,\ \nu_1 = -\nu_2 = -(1,0)^T$, **(Q)** is equivalent to assuming:

(Q') There is a *single pressure* p^* at the intersection

$$\frac{a^2}{2}\left(\hat{\rho}^j\right)(0,t) = p^*,\ \forall j.$$

If we consider the sum of **(M1)** and **(M2)** we obtain $\sum_{j=1}^{2} \|\nu_j\| \hat{\rho}^j u^j = 0$ and therefore $\frac{2p_*}{a^2}\|\nu\| \sum_{j=1}^{2} u_j = 0$ and $\sum_{j=1}^{2} u_j = 0$. Combining this last equality and the equality of momentum immediately yields **(Q)**.

Remark 3.4. *We present some discussion on condition* **(Q)** *similar to [32]. Condition* **(Q)** *implies that the momentum over time* $[t_1, t_2]$*:*

$$\int_{t_1}^{t_2} P^j dt := \int_{t_1}^{t_2} \hat{\rho}^j ((u^j)^2 + \frac{a^2}{2})(0,t) dt = \int_{t_1}^{t_2} P^* dt \equiv \kappa.$$

Therefore, we obtain

$$\int_{t_1}^{t_2} \sum_{j \in \delta^\pm} P^j \nu_j dt = \kappa \sum_{j \in \delta^\pm} \nu_j.$$

This is equivalent to the following:

$$\forall \eta \in \left(\sum_{j \in \delta^\pm} \nu_j \right)^\perp, \quad \left(\sum_{j \in \delta^\pm} P^j \nu_j \right) \cdot \eta = 0.$$

Hence, the linear momentum orthogonal to $\sum_{j \in \delta^\pm} \nu_j$ *is conserved and the constraint acts parallel to* $\sum_{j \in \delta^\pm} \nu_j$*.*

In recent years there has been an intense discussion on existence of solutions to coupled systems of hyperbolic conservation laws. Without giving a complete list of references we mention the publications by Colombo et. al. [41, 33, 32]. Therein, for gas and traffic flow networks, existence of solutions to a Riemann problem and, depending on the application, to the Cauchy problem has been proven. We apply the technique derived in [41] to prove existence to a Riemann problem under conditions **(M1)** – **(Q)** for the no–slip multiphase model. As expected, the result is essentially a perturbation result for constant data. The assertions are restrictive since the data has to belong to certain sub–critical sets. Nevertheless, the importance of the result

is the construction of a solution at the junction. This construction is used and implemented later in the numerical scheme to compute the boundary values at the junction and prevent boundary layer effects.

Proposition 3.1. *Given n distinct vectors $\nu_j \in \mathbb{R}^2\backslash\{\mathbf{0}\}, \nu_{j,1} \geq 0$, and coupling conditions given by* **(M1)**, **(M2)** *and* **(Q)**. *Let $j = 1 \in \delta^-$ and assume constant initial data $\bar{U}_{j,0}$ with the following properties: $\bar{U}_{1,0} \in \overset{\circ}{A}{}_0^+$, $\bar{U}_{j,0} \in \overset{\circ}{A}{}_0^{\#}$ for $j \in \delta^-\backslash\{1\}$, $\bar{U}_{j,0} \in \overset{\circ}{A}{}_0^+$ for $j \in \delta^+$ and let the constant states $\bar{U}_{j,0}$ satisfy the conditions* **(M1)**, **(M2)** *and* **(Q)**. *Moreover, assume that the initial data satisfies the technical condition* $\det M \neq 0$ *for M given by* (3.14) *below.*

Then, there exists $\delta, C > 0$ such that, for all states V_j with $\|V_j - \bar{U}_{j,0}\| \leq \delta$, there exists self–similar functions $U_j(x,t)$ satisfying the weak formulation of (3.4a, 3.4b, 3.4c), the initial condition $U_j(x,0) = \bar{U}_j$ and such that the trace of U_j at $x = 0$ satisfies **(M1)**, **(M2)** *and* **(Q)**; *furthermore, U satisfies the stability condition*

$$\|U_j - U_{j,0}\|_{L^\infty(\mathbb{R}\times[0,\infty),\overset{\circ}{\mathbb{R}}_+\times\overset{\circ}{\mathbb{R}}_+\times\mathbb{R})} \leq C\|V_j - U_{j,0}\|, \text{ for all } j \in \delta^- \cup \delta^+. \tag{3.13}$$

The matrix M in Proposition 3.1 is given by

$$M := \begin{pmatrix} A_0 & A_1 & A_2 & A_3 & \dots & A_n \\ B_0 & B_1 & B_2 & B_3 & \dots & B_n \\ b_0 & b_1 & 0 & 0 & \dots & -b_n \\ 0 & 0 & b_2 & 0 & \dots & -b_n \\ \vdots & \vdots & \vdots & \vdots & \vdots & \vdots \\ 0 & \dots & \dots & \dots & b_{n-1} & -b_n \end{pmatrix} \tag{3.14}$$

where

$$\begin{aligned} & A_0 = \|\nu_1\|\lambda_2(U_{1,0})\rho_1^{1,0}, \quad B_0 = \|\nu_1\|\lambda_2(U_{1,0})\rho_2^{1,0}, \quad b_0 = \lambda_2(U_{1,0})I^{1,0}, \\ i \in \delta^-,\ i \geq 1: \quad & A_i = \|\nu_i\|\lambda_1(U_{i,0})\rho_1^{i,0}, \quad B_i = \|\nu_i\|\lambda_1(U_{i,0})\rho_2^{i,0}, \quad b_i = \lambda_1^2(U_{i,0})\hat{\rho}^{i,0}, \\ i \in \delta^+,\ i \geq 1: \quad & A_i = -\|\nu_i\|\lambda_3(U_{i,0})\rho_1^{i,0}, \quad B_i = -\|\nu_i\|\lambda_3(U_{i,0})\rho_2^{i,0}, \quad b_i = \lambda_3^2(U_{i,0})\hat{\rho}^{i,0}. \end{aligned}$$

Proof. (*of Proposition 3.1*) Assume $\delta^- := \{1, \dots, n_1\}$ and $\delta^+ := \{n_1+1, \dots, n\}$. Consider a perturbation of $\bar{U}_{j,0}$, V_j, such that $V_1 \in \overset{\circ}{A}{}_0^+$, $V_j \in \overset{\circ}{A}{}_0^{\#}$ for $j \in \delta^-\backslash\{1\}$,

$V_j \in \overset{\circ}{A}{}_0^+$ for $j \in \delta^+$. Let $U_j = (\rho_1^j, \rho_2^j, I^j)$ and consider the map $\tilde{\Psi} : \mathbb{R}^{3n} \to \mathbb{R}^{n+1}$ given by

$$\tilde{\Psi}((U_j)_{j=1}^n) := \begin{pmatrix} \sum_{j=1}^{n_1} \|\nu_j\| \rho_1^j u^j - \sum_{j=n_1+1}^{n} \|\nu_j\| \rho_1^j u^j \\ \sum_{j=1}^{n_1} \|\nu_j\| \rho_2^j u^j - \sum_{j=n_1+1}^{n} \|\nu_j\| \rho_2^j u^j \\ \hat{\rho}^1((u^1)^2 + \frac{a^2}{2}) - \hat{\rho}^n((u^n)^2 - \frac{a^2}{2}) \\ \vdots \\ \hat{\rho}^{n-1}((u^{n-1})^2 + \frac{a}{2}) - \hat{\rho}^n((u^n)^2 - \frac{a^2}{2}) \end{pmatrix}$$

Thanks to Lemma 3.1 we obtain for any fixed state V, parameters

$$(\sigma, \xi_1, \dots, \xi_n) = (\sigma, (\xi_1, \dots, \xi_{n_1}), (\xi_{n_1+1}, \dots, \xi_n)) \in (\mathbb{R}^+)^{n+1}$$

such that

$$\begin{aligned} &\Psi((\sigma, \xi_1, \dots, \xi_n), (V_j)) := \tilde{\Psi}(L_2(\sigma; L_1^+(\xi_1, V_1)), L_1^+(\xi_2, V_2), \dots \\ &\dots, L_1^+(\xi_{n_1}, V_{n_1}), L_3^-(\xi_{n_1+1}, V_{n_1+1}), \dots, L_3^-(\xi_n, V_n)) = 0. \end{aligned} \tag{3.15}$$

Note that the function Ψ depends on the parameterization $\sigma, \xi_1, \dots, \xi_n$ and the perturbed state V_i. For $\sigma = \xi_1 = \dots = \xi_n = 1$ and $V_i = \bar{U}_{j,0}$ we have that Ψ vanishes due to the assumption that $\bar{U}_{j,0}$ satisfies the coupling conditions. We want to apply the implicit function theorem and obtain a parameterization in terms of the perturbed state V_i. We compute the determinant of $D_{(\sigma,\xi_1,\dots,\xi_n)}\Psi$ at $\sigma = \xi_1 = \dots = \xi_n = 1$ and obtain

$$\det \Psi(\cdot) = \det \begin{bmatrix} A_0 & A_1 & & \dots & & & A_n \\ B_0 & B_1 & & \dots & & & B_n \\ b_0 & b_1 & 0 & \dots & & & -b_n \\ 0 & 0 & b_2 & 0 & \dots & & -b_n \\ 0 & 0 & 0 & \ddots & & & -b_n \\ \vdots & & & & & & \\ 0 & 0 & 0 & 0 & \dots & b_{n-1} & -b_n \end{bmatrix}$$

where

$$
\begin{aligned}
& & A_0 &= \|\nu_1\|\lambda_2(U_{1,0})\rho_1^{1,0} \le 0, \\
& & B_0 &= \|\nu_1\|\lambda_2(U_{1,0})\rho_2^{1,0} \le 0, \\
& & b_0 &= \lambda_2(U_{1,0})I^{1,0} \ge 0, \\
i \in \delta^-,\ i \ge 1 & & A_i &= \|\nu_i\|\lambda_1(U_{i,0})\rho_1^{i,0} \le 0,\ B_i = \|\nu_i\|\lambda_1(U_{i,0})\rho_2^{i,0} \le 0, \\
& & b_i &= \lambda_1^2(U_{i,0})\hat{\rho}^{i,0} \ge 0,\ i \ge 1 \\
i \in \delta^+,\ i \ge 1: & & A_i &= -\|\nu_i\|\lambda_3(U_{i,0})\rho_1^{i,0} \le 0,\ B_i = -\|\nu_i\|\lambda_3(U_{i,0})\rho_2^{i,0} \le 0,\ i \ge 1, \\
& & b_i &= \lambda_3^2(U_{i,0})\hat{\rho}^{i,0} \ge 0,\ i \ge 1
\end{aligned}
$$

Since the initial data is in the interior of the subsonic sets (3.10), the inequalities are strict, i.e., A_i, B_i are negative and b_i are positive. Due to the assumption, this determinant is non–zero. Hence, for any perturbation V_i of $U_{j,0}$ with $\|V_i - U_{j,0}\|$ sufficiently small, we obtain values $\sigma = \xi_1 = \cdots = \xi_n$ such that the coupling conditions are fulfilled. The solution to the Riemann problem at the junction is now constructed by using the states:

$$
\widetilde{V}_1 = L_2(\sigma; L_1^+(\xi_1; V_1)),\ \widetilde{V}_j = L_1^+(\xi_j; V_j) \text{ for } j \in \delta^- \setminus \{1\},\ \widetilde{V}_j = L_3^-(\xi_j; V_j) \text{ for } j \in \delta^+ \tag{3.16}
$$

for σ, ξ_j given by (3.15). Then for $j \in \{1, \ldots, n\}$, the solution U_j is given by the restriction to the real half–line of the solution to the Riemann problem

$$
U_j = (\rho_1^j, \rho_2^j, u_j)(x,0) = \begin{cases} V_j, & x \le 0 \\ \widetilde{V}_j, & x > 0 \end{cases} \quad j \in \delta^- \text{ and} \tag{3.17}
$$

$$
U_j = (\rho_1^j, \rho_2^j, u_j)(x,0) = \begin{cases} \widetilde{V}_j, & x < 0 \\ V_j, & x \ge 0 \end{cases} \quad j \in \delta^+. \tag{3.18}
$$

By construction, the trace of the solution at the junction satisfies the coupling conditions. The stability estimate (3.13) is derived from the C^1–regularity of the map Ψ. ∎

3.4 Numerical Results

In this section we present practical tests of the coupling conditions that we propose in Section 3.3. To achieve that, we design the section to serve two purposes: we firstly verify that the numerical schemes we apply are appropriate for this kind of problems; secondly we test the coupling conditions on different junction types and discuss the qualitative behavior of the approach.

The numerical schemes we use to approximate homogeneous no-slip drift-flux multiphase fluid flow models as defined in (3.4) are the second-order relaxed schemes which were first developed in [69] and also discussed in [3]. In general, we assume the pipes' diameters to be $\|\nu\| = 1$ and the sound speed is $a = 6$ for all pipes in all examples. Initial conditions are selected carefully in order for the conditions of the proposition (Proposition 3.1) to be satisfied. Newton's method is used to solve the system in equation (3.15) which gives the values of the parameters used to define the Lax-curves defining the coupling of flow fields at the junctions. We wish to point out that the coupling conditions are necessary for defining boundary conditions at the internal nodes of the network and populating the cells that are used in approximating flow close to the junction i.e. to couple multiple pipes at the junction. The coupling conditions in Section 3.3 must be satisfied and at each time step, the system of coupling conditions is solved for the intermediate state $\tilde{V}$ (see (3.16)), the construction of such a solution is undertaken as described in the proof of Proposition 3.1.

For time integration a semi-discrete approach is used and a second-order Runge-Kutta scheme with strong-stability preserving (SSP) [56] property is applied. The time step size is given dynamically by

$$\Delta t = \frac{0.75\Delta x}{\max(\varrho(\partial f(U)/\partial U))}$$

where the maximum is taken over all computational grid-points. The spatial step-width is Δx and $\varrho(\partial f(U)/\partial U))$ is the spectral radius of the Jacobian of the flux function $f(U)$ with respect to the conserved variables, U.

For the external (inlet to network or outlet from network) boundary conditions, transparent boundary conditions are imposed.

3.4.1 Solution of two-phase Riemann problems

In this section, we test the numerical schemes that we use to approximate two-phase problems. In [52] global existence of solutions for a viscous two-phase model for no-slip drift-flux two-phase flow problems were discussed. Numerical results for both inviscid and viscous extensions of the model were presented. In [52], it is assumed that liquid phase is much heavier than the gas phase, $\rho_l/\rho_g \approx 10^3$, where ρ_l is the liquid density and ρ_g is the gas density. As a result, the gas phase is ignored in the mixture momentum equation (3.2c). In addition a non-linear pressure law is employed which is in contrast to a linear pressure law applied here in (3.3).

The following example (persistent discontinuity in [52]) will be used to test if the numerical schemes reproduce the expected results. In the subsequent sections the numerical scheme will be used to test the practical validity of the coupling conditions.

We consider a two phase Riemann problem with the data [52]:

$$U(x,0) = \begin{cases} U_l = (500/9, 0.95/18, 0.17982), & x < 0.5 \\ U_r = (500/10, 1/20, 0.1998), & x > 0.5 \end{cases}$$

Take note that the last component of U_l and U_r is the common velocity.

Results are presented in Figure 3.3 on a mesh size of $N \in \{400, 800, 1600\}$. We present the densities, the common velocity and the pressure of the two phases. The plots of the densities demonstrate the two-phase characteristic of the flow as noted in [52]. The difference is that the discontinuities are no longer persistent but are transported in the same direction as documented in [52]. This demonstrates that the numerical scheme is capable of producing correct results. Notably the shock speeds and shock strengths were in general well resolved. The difference captured in comparison to [52] can be attributed mainly to the non-linear pressure laws applied there.

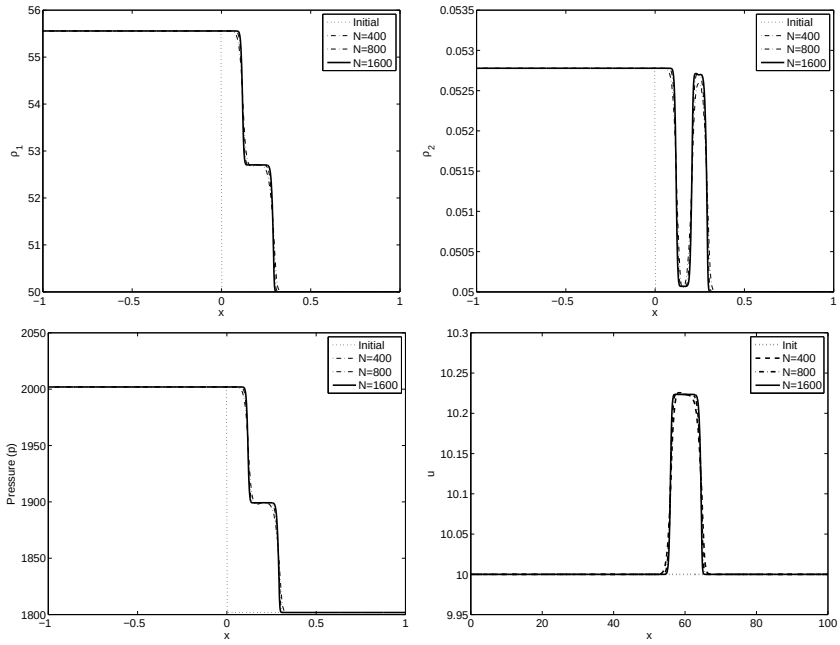

Figure 3.3: *Snapshots of densities ρ_1 and ρ_2, the common velocity $v_1 = v_2 = u$, the common pressure p, at $t = 1.0$.*

The results of the relaxation scheme were also compared to the results of the central schemes in [75, 70]. The two schemes produced very similar results in the picture norm as shown in Figure 3.4.

3.4.2 Shock-tube problem and the case of one incoming and one outgoing pipe

This example will be used as a tool to verify the qualitative behavior of the coupling conditions. The results of the shock tube problem will be compared with the results of coupling two connected horizontal pipes. Here we consider the Riemann data

$$U_l = (1.81832, 1.44174, -0.751082), \quad U_r = (2.01667, 1.22004, -1.584711). \quad (3.19)$$

The mesh size of $N = 400$ was employed in a single pipe on which the standard Riemann solver was applied. For the coupled pipes the mesh size of $N = 200$

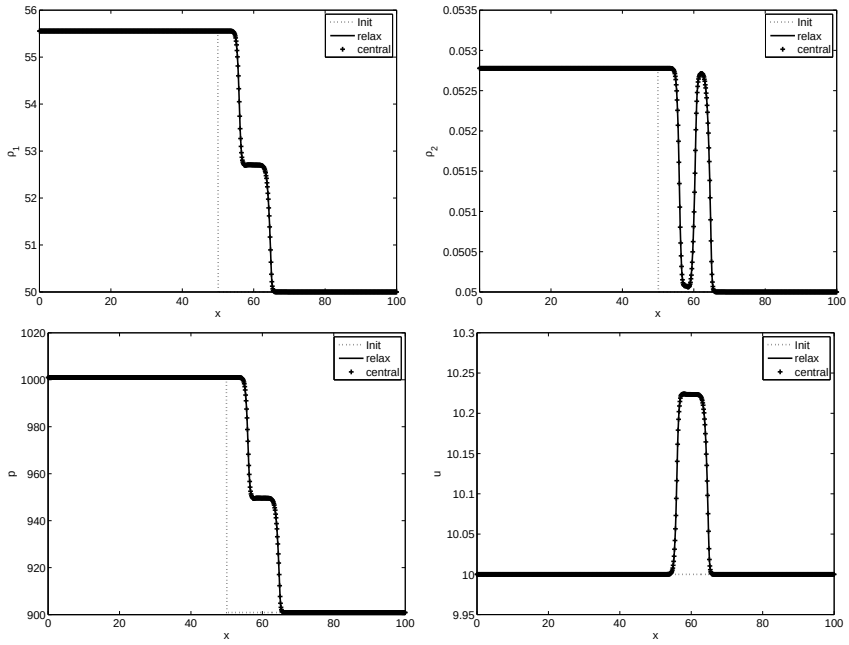

Figure 3.4: *Snapshots of densities ρ_1 and ρ_2, the common velocity $v_1 = v_2 = u$, the common pressure p, at $t = 1.0$. A comparison of relaxation schemes (relax) and central schemes (central).*

was applied in each pipe. The initial conditions for the Riemann problem at the intersection is done as follows. We consider equal initial conditions in each pipe

$$\bar{U}_{1,0} = \bar{U}_{2,0} = (1.5259, 0.7536, -0.9621),$$

so that the conditions of Proposition 3.1 are trivially satisfied. Then we perturb the initial conditions with some little noise in each pipe in such a way that it remains in the prescribed subsonic sets. The perturbed data are given by $V_1 = U_l$ and $V_2 = U_r$ as in (3.19). With this new initial data, we solve numerically the Riemann problem at the junction. The results are presented in Figure 3.5.

The densities, velocities and pressure are qualitatively similar in terms of the wave profiles in the solution. This demonstrates that in the case of two coupled pipes, the Riemann problem at the intersection reduces to the standard Riemann problem. This is an important observation that validates our choice of the coupling

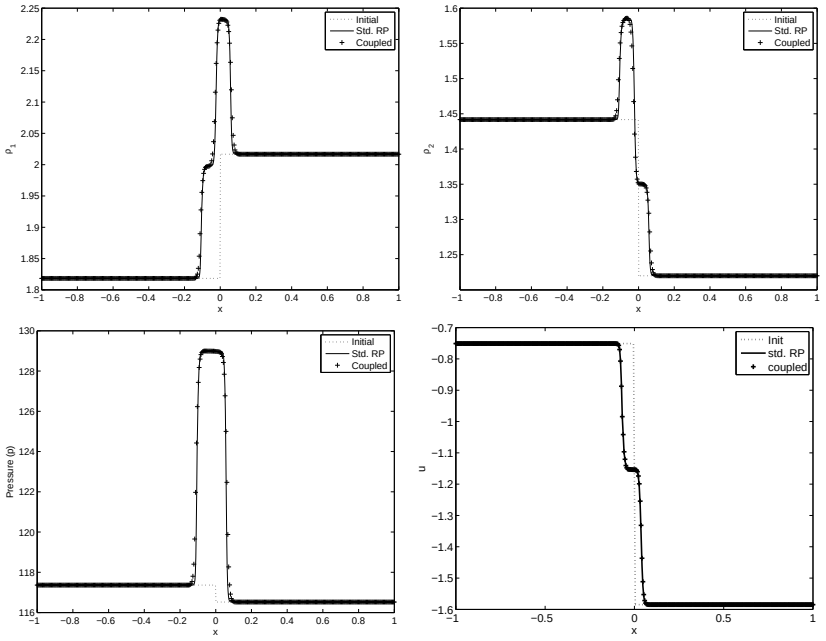

Figure 3.5: *Snapshots of densities ρ_1 and ρ_2, the common velocity $v_1 = v_2 = u$, the common pressure p, at $t = 0.013$. A comparison of solutions computed by standard relaxation schemes (std. RP.) with relaxation schemes in which coupling conditions are applied at the junction (coupled).*

conditions as it was done in [7]. We can then have confidence in the application of our coupling conditions for junctions with more than two pipes. Before we present such examples, we perform a grid convergence analysis for our numerical scheme for the solution of the flow equations. This ensures us that as the grid is refined, our flow solver produce a more accurate solution of the flow equations, that is the drift-flux model.

3.4.3 Grid convergence example

We simulate the dynamics of a junction with one incoming and one outgoing pipe with initial data given by (3.19) on four different meshes with the number of grid-points $N \in \{40, 80, 160, 320\}$. We compute up to time $t = +0.013$ and present the

density and velocity profile in Figure 3.6. For comparison, the quantities of the same variables for the standard Riemann problem are plotted which is used as a reference solution for comparing qualitative behavior. The reference solution is computed using a mesh size of $N = 2000$. We note that the qualitative behavior for all mesh sizes demonstrates convergent behavior. This justifies the choice of the mesh size $N = 200$ in the previous and subsequent examples.

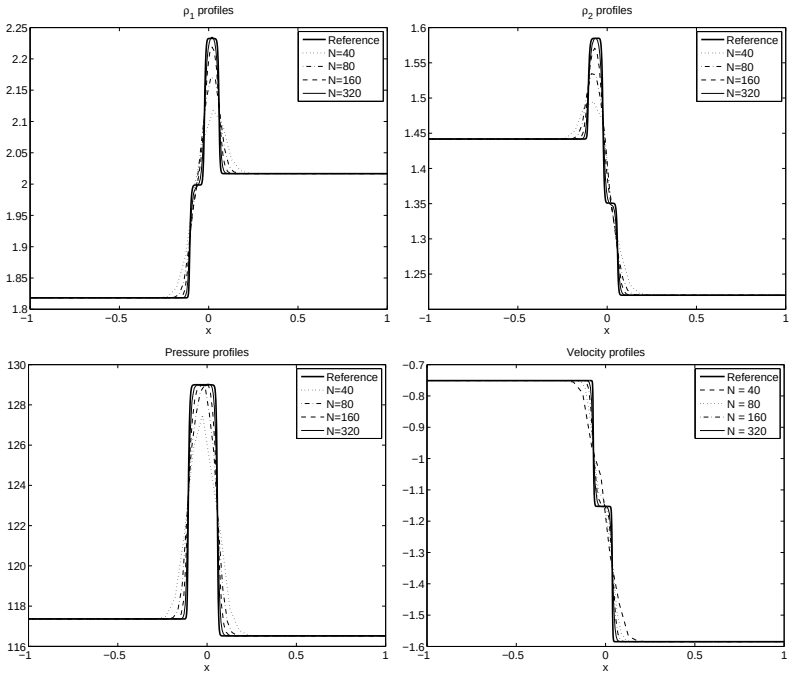

Figure 3.6: *Densities of each phase, common pressures and velocities for different mesh size at time* $t = 0.013$.

3.4.4 Case of one incoming and two outgoing pipes

We consider three coupled pipes with one incoming and two outgoing forming a 'T' junction. Such junctions are very common in flow networks.The network is described with the vectors $\nu_1 = (-1, 0),\ \nu_2 = (0, +1)$ and $\nu_3 = (0, -1)$ with the junction at

$x = 0$. The initial conditions applied here are

$$\bar{U}_{1,0} = (1.0500, 2.8050, -11.2401),$$
$$\bar{U}_{2,0} = (2.03, 3.3578, -5.2842),$$
$$\bar{U}_{3,0} = (0.9534, 4.3508, -5.9559).$$

These initial data are chosen so as to satisfy the conditions of Proposition 3.1. As discussed in Section 3.4.2, we perturb these initial data with a small random vector in such a way that the states remain in the required subsonic regions given in (3.10). We use the states

$$V_1 = (1.1722, 2.8192, -11.1772),$$
$$V_2 = (2.1517, 3.3928, -5.1600),$$
$$V_3 = (1.0026, 4.4683, -5.8547).$$

We then solve numerically the Riemann problem at the intersection with initial conditions in pipe j, V_j. We present the snapshots of the densities (Figure 3.7), the velocities and the pressures (Figure 3.8) in each pipe for times $0 \leq t \leq 0.2$. The dynamics of the flow in the pipes are well resolved. As expected we have some waves moving out of each pipes. The contact discontinuity wave is well resolved by our numerical scheme and can be observed in the plots of the densities in Figure 3.7. The wave pattern in each pipe is seen more clearly in the contour lines of the densities where we clearly observe, as expected, two waves in pipe 1 and single waves in the other pipes as shown in Figure 3.9. The pressure profile for the pipes is also presented in Figure 3.10.

3.4.5 Case of four connected pipes

Here we consider a network with four connected pipes. The discretization of the space variable is such that $\nu_1 = (-1, 0),\ \nu_2 = (+1, 0),\ \nu_3 = (0, +1)$ and $\nu_4 = (0, -1)$ with the junction at $x = 0$. If we assume, for example, that we have one incoming and three outgoing pipes, then we consider the following initial conditions which satisfy coupling conditions:

$$\begin{aligned} &\bar{U}_{1,0} = (0.7836, 0.7737, -6.2500), \quad \bar{U}_{2,0} = (1.0987, 1.0587, -5.5508), \\ &\bar{U}_{3,0} = (1.1210, 1.8262, -0.04386), \quad \bar{U}_{4,0} = (1.7112, 1.2384, -0.2606). \end{aligned} \tag{3.20}$$

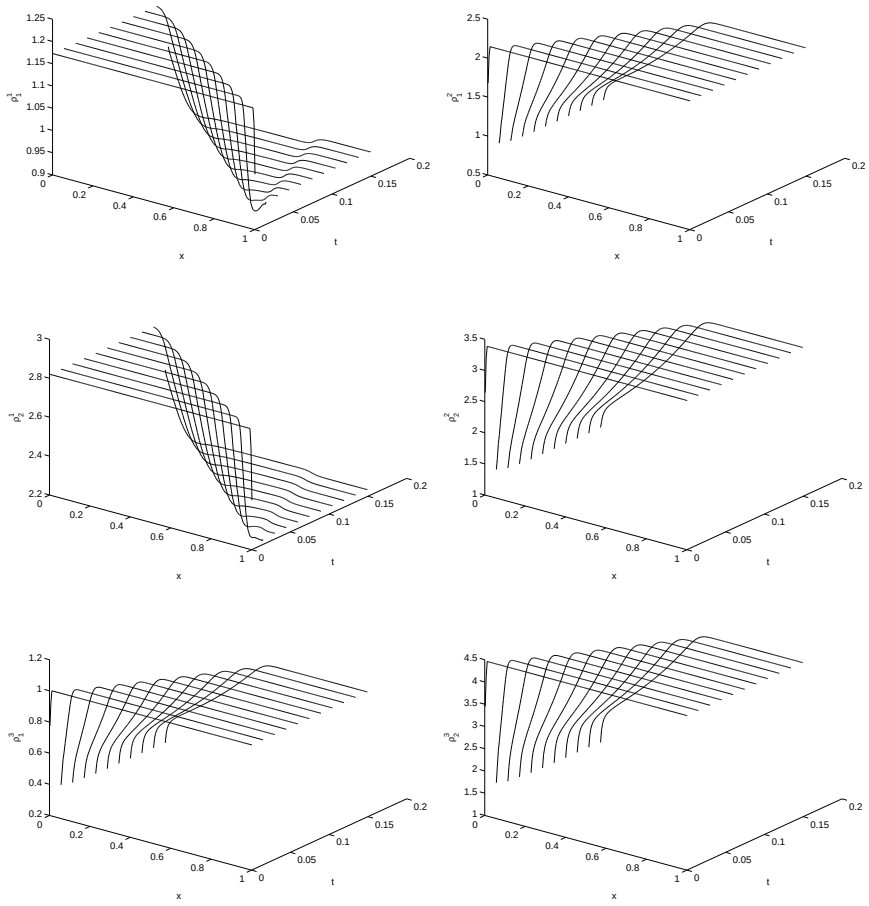

Figure 3.7: *Snapshots of densities for three coupled pipes with one incoming and two outgoing pipes at different times t.*

The perturbed data for the simulations are given by

$$V_1 = (0.7939, 0.7894, -6.2093), \quad V_2 = (1.1395, 1.0640, -5.4566),$$
$$V_3 = (1.1360, 1.8646, -0.4075), \quad V_4 = (1.7281, 1.3280, -0.2283).$$

Using Proposition 3.1, the solution of the Riemann problem at the junction can be constructed from the V_j. The snapshots of the densities in each pipe for $0 \leq t \leq 0.1$ are given in Figure 3.12. We see two waves moving in Pipe 1 while there is only one wave in the other pipes. The dynamics in Pipe 1 is more complex than in the other

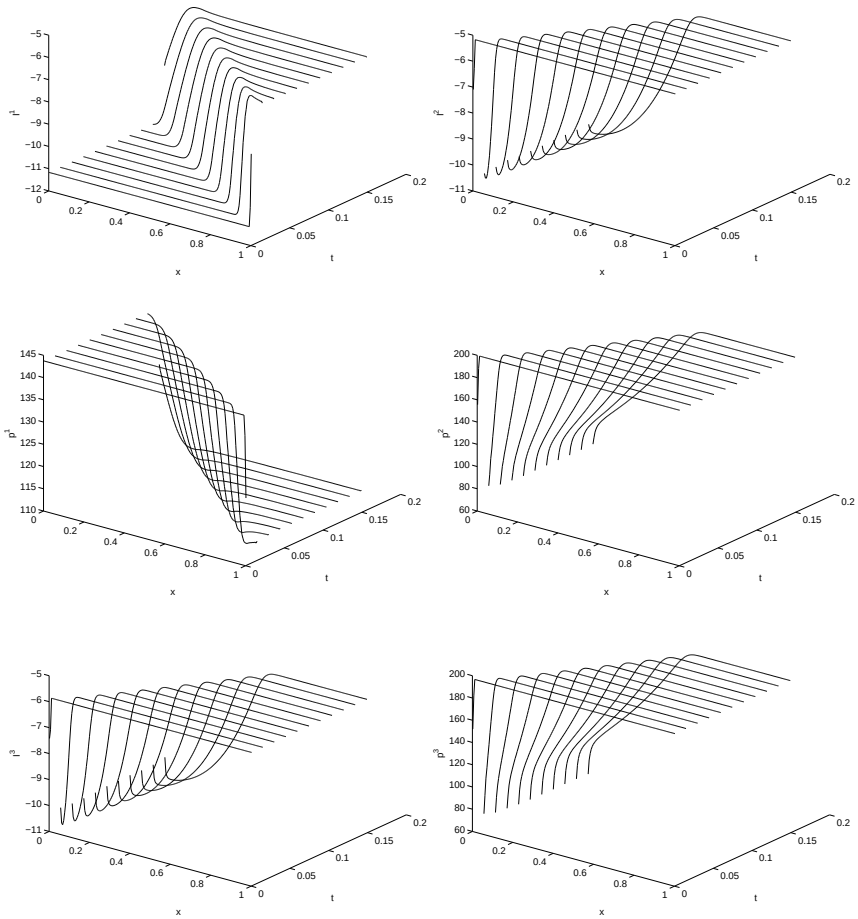

Figure 3.8: *Snapshots of momentum and pressure for three coupled pipes with one incoming and two outgoing pipes at different times t.*

pipes. This can be explained by the fact that Pipe 1 is the only incoming pipe while the other pipes are outgoing.

See also Figure 3.11 for the pressure profiles. The other configurations give qualitatively similar results. This is not surprising since the wave pattern in each pipe is prescribed *a-priori* in our main result: we always have two waves in the first pipe and one wave in each of the other pipes. Above, the existence of a solution is confirmed by the numerical results and the expected qualitative behavior is reproduced.

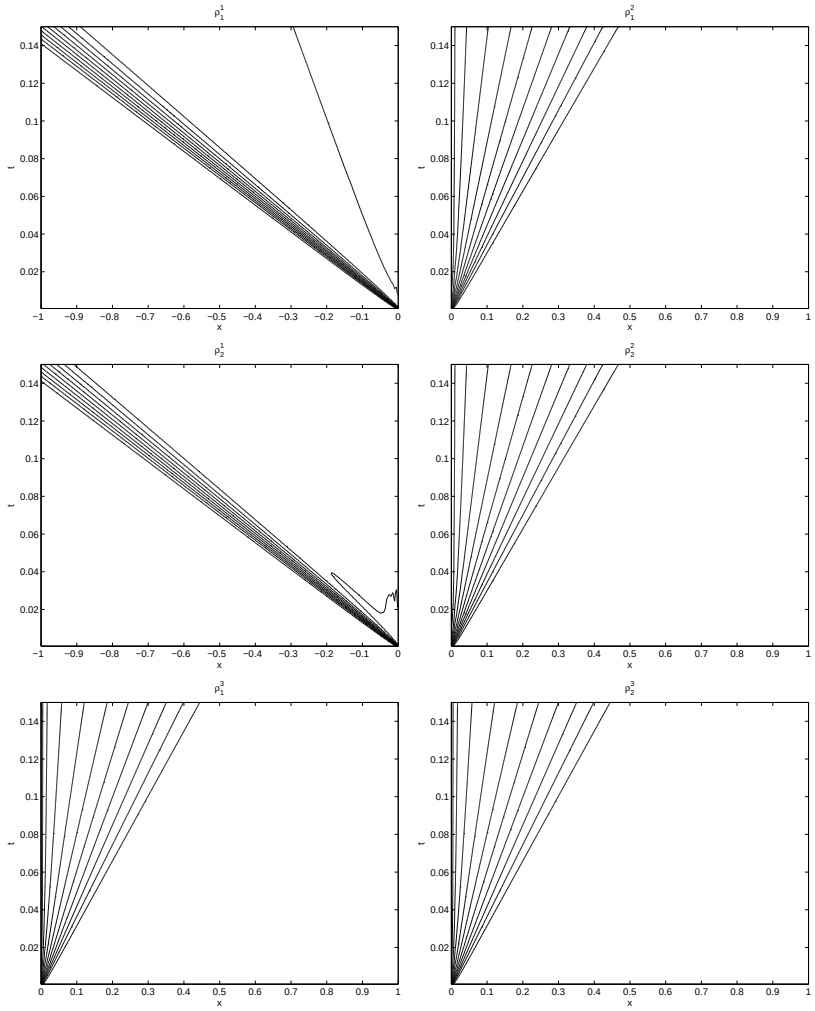

Figure 3.9: *Contour lines of densities for three coupled pipes with one incoming and two outgoing pipes.*

3.5 Concluding Remarks

We derived a conservative model for multiphase flow from the two-fluid model and proposed some general coupling conditions at junctions in a network of pipes. A well–posedness result at the intersection of the pipes was proposed and proved. Numerical tests were designed and applied for different pipes configurations. This

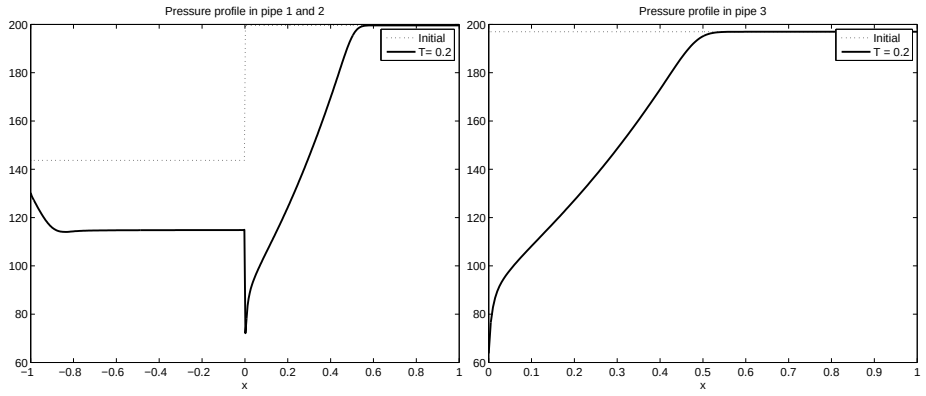

Figure 3.10: *Snapshots of pressure for three coupled pipes with one incoming and two outgoing pipes.*

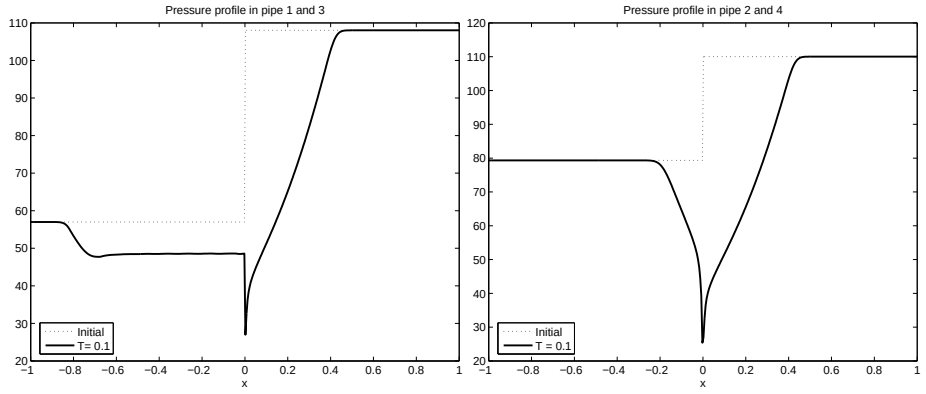

Figure 3.11: *Snapshots of pressure for four coupled pipes with one incoming and three outgoing pipes at different times t.*

served as a way of realizing the theoretical results in a practical setting. The numerical results conform with the expected theoretical results. However, the model seems to be restrictive since it assumes isothermal flow and equal velocity of different phases. The isothermal condition is dropped in the next chapter where we also consider the case of a discontinuous junction, that is, a junction where the connecting pipes have different cross sections.

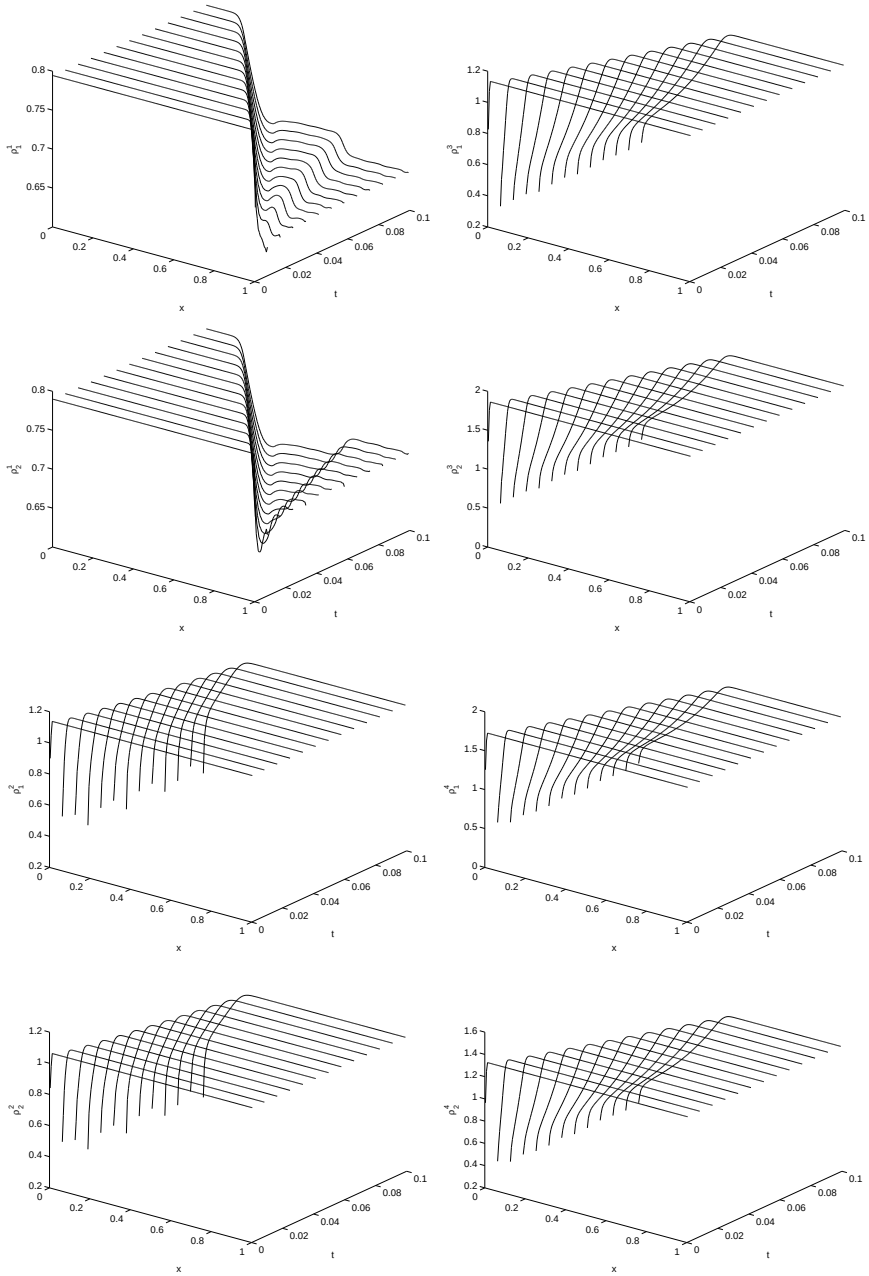

Figure 3.12: *Snapshots of densities for four coupled pipes with one incoming and three outgoing pipes at different times t.*

Chapter 4

The Multiphase Drift-Flux Model with a General Equation of State in Networks

In this chapter, we consider the drift-flux model describing a subsonic multiphase fluid in a network of pipes. Differently from the work presented in Chapter 2, the pressure law of the multiphase fluid is taken in a general form and it is expressed in terms of the sonic speeds and densities of each phase. We discuss the well-posedness of the Riemann problem at the junction and present some computational results on the dynamics of the multiphase fluid in a network of pipes. Some results for a discontinuous junction are presented. Some of the results presented in this chapter appeared or are to appear in [9, 8].

4.1 Introduction

We consider the flow in a network of pipes of a no-slip drift-flux model for multiphase flow in the form

$$\begin{aligned} \partial_t \rho_1 + \partial_x(\rho_1 u) &= 0 \\ \partial_t \rho_2 + \partial_x \rho_2 u &= 0 \\ \partial_t[(\rho_1+\rho_2)u] + \partial_x\left((\rho_1+\rho_2)u^2 + p(\rho_1,\rho_2)\right) &= 0 \end{aligned} \tag{4.1}$$

where ρ_1 and ρ_2 are the density of phase 1 and 2, respectively, u is the common velocity of the two phases and $p(\rho_1, \rho_2)$ is the pressure of the model given as a function of the densities. This flow model is derived from the *two-fluid* model by averaging the balance law for the momentum in the canonical form.
The mathematical study of flow of fluid in networks of pipes is a young field of research and has been under investigation only recently. We refer the reader to [32, 33, 41, 6, 7] for the case of gas networks, to [77, 99] for water networks and [62] for traffic networks. The study of the multiphase case was first introduced in [10] where the isothermal drift-flux model was considered. Therein, the physical motivations of the coupling conditions, which are necessary for the solution of the Cauchy problem or Riemann problem at the junction, were given. The coupling conditions comprise the conservation of mass at the junction. Depending on the fluid properties, one can add the equality of the so-called *dynamic pressure* or the pressure itself at the junction. As was pointed out by Colombo et al. [33], the equality of pressure for the p-system can lead to the loss of uniqueness of the solution of the Cauchy problem at the junction.

In this chapter, we investigate the flow of the drift-flux model (4.1) in a network of pipes. We first determine the admissible Lax curves that are paramount in the single wave solution of the standard Riemann problem (RP). Secondly, we consider the model (4.1) at the junction of a network of pipes. Using the coupling conditions proposed in [10], we prove the well-posedness of the Riemann problem at the junction for the case of two connected pipes and discuss briefly the general case. An important contribution of this chapter is the use of a linearization of the Lax curves for the

solution of the Riemann problem at the junction. This is motivated by the fact that for some equations of state (pressure law as a function of densities), one can not obtain an analytical expression of the rarefaction curves. We justify this approach by solving numerically the Riemann problem at the junction for the isothermal model whose solution is known. We find that the results are comparable and we then use this new approach for the numerical solution of the isentropic drift-flux model at a junction with three connected pipes.

The rest of the chapter is organized as follows. In Section 4.2, we briefly discuss the derivation of the flow model equations and we solve the standard Riemann problem. A junction of pipes in a network is considered in Section 4.3. We give a rigorous definition of the Riemann problem at the junction and prove the well-posedness of the Riemann problem at a junction of two connected pipes. We discuss briefly the general case of a junction with m incoming pipes and p outgoing pipes. Section 4.5 is devoted to some numerical simulations and results. We start by investigating the effect of the sound speed of the two phases on the junction. Then we present the linearization of the Lax curves and apply it to the solution of the Riemann problem at the junction of three connected pipes. An example with a discontinuous junction is presented.

4.2 Model Formulation and Preliminary results

We consider a mixture of two fluids with density, volume fraction, velocity and pressure denoted by ϱ_i, α_i, v_i, p_i, respectively. A common model for this multiphase fluid is the drift-flux model [47] which reads

$$\frac{\partial}{\partial t}(\varrho_1\alpha_1) + \frac{\partial}{\partial x}(\varrho_1\alpha_1 u_1) = 0, \tag{4.2a}$$

$$\frac{\partial}{\partial t}(\varrho_2\alpha_2) + \frac{\partial}{\partial x}(\varrho_2\alpha_2 u_2) = 0, \tag{4.2b}$$

$$\frac{\partial}{\partial t}(\varrho_1\alpha_1 u_1 + \varrho_2\alpha_2 u_2) + \frac{\partial}{\partial x}(\varrho_1\alpha_1 u_1^2 + \varrho_2\alpha_2 u_2^2 + p) = Q. \tag{4.2c}$$

Here, Q represents the sum of the momentum and source forces such as wall friction or gravity acting on each phase separately. We assume that the two fluids are immiscible and, therefore, denote the total density of each phase as $\rho_1 = \alpha_1\varrho_1$ and $\rho_2 = \alpha_2\varrho_2$. We assume for the analysis that $Q = 0$. This is not a restriction since a system of conservation laws with source terms can be handled with the fractional step method [79] which consists in considering separately the convective part and the source part of the equation. For simplicity, we restrict ourselves to a flow regime where the pressure and the velocity of the two phases are equal [52]. This leads to the system of equations

$$\begin{aligned} \partial_t \rho_1 + \partial_x \tfrac{\rho_1 I}{\rho_1+\rho_2} &= 0 \\ \partial_t \rho_2 + \partial_x \tfrac{\rho_2 I}{\rho_1+\rho_2} &= 0 \\ \partial_t I + \partial_x \left(\tfrac{I^2}{\rho_1+\rho_2} + p(\rho_1,\rho_2) \right) &= 0. \end{aligned} \tag{4.3}$$

where $I = (\rho_1 + \rho_2)u$ is the momentum of the mixture. The system (4.3) needs to be completed by an equation of state expressing the pressure of the multiphase fluid in terms of the density of each phase. Keeping the general case in mind, we will use for illustrations the following two equations of state.

Isothermal drift-flux model

Assume that each phase is isothermal with an equation of state of the form

$$p \doteq p_i(\varrho_i) = a_i^2 \varrho_i, \ i \in \{1, 2\}, \tag{4.4}$$

where the positive constant a_i is the compressibility factor or sound speed of phase i. The relation $\alpha_1 + \alpha_2 = 1$ can then be written as

$$\frac{\rho_1}{\varrho_1} + \frac{\rho_2}{\varrho_2} = \frac{\rho_1 a_1^2}{p} + \frac{\rho_2 a_2^2}{p} = 1.$$

Hence

$$p = \rho_1 a_1^2 + \rho_2 a_2^2. \tag{4.5}$$

When we substitute (4.5) in (4.3), we obtain the isothermal drift-flux model. When $a_1^2 = a_2^2 = a^2/2$, we obtain the model presented in Chapter 3.

Isentropic drift-flux model

For isentropic gases $p = \hat{\kappa}\rho^\gamma$ where $\hat{\kappa}$ and γ are constants. We assume that each component of the multiphase fluid is isentropic with the equation of state of the form

$$p \doteq p_i(\varrho_i) = a_i^2 \varrho_i^\gamma,\ i \in \{1, 2\}, \tag{4.6}$$

where the positive constant a_i is as above. For simplicity, we take for the two phases the same ratio of the specific heats γ. One can consider different γ's for each phase in a similar way. The relation $\alpha_1 + \alpha_2 = 1$ leads to

$$\frac{\rho_1}{\varrho_1} + \frac{\rho_2}{\varrho_2} = \frac{\rho_1}{\left(p/a_1^2\right)^{1/\gamma}} + \frac{\rho_2}{\left(p/a_2^2\right)^{1/\gamma}} = 1.$$

Hence

$$p = \left[\rho_1 a_1^{\frac{2}{\gamma}} + \rho_2 a_2^{\frac{2}{\gamma}}\right]^\gamma. \tag{4.7}$$

Before discussing in details the dynamics of a junction of pipes, we start by solving the standard Riemann problem for the model equation (4.3). The exact solution is constructed as a set of constant states separated by some wave curves, see Section 2.2.

The eigenvalues $\lambda_{1,2,3}$ and the eigenvectors $r_{1,2,3}$ of the drift-flux model (4.3) are given by

$$\lambda_{1,3}(U) = \frac{I}{\hat{\rho}} \mp \sqrt{\frac{\rho_1 \partial_1 p + \rho_2 \partial_2 p}{\hat{\rho}}}, \quad \lambda_2(U) = \frac{I}{\hat{\rho}}.$$

$$r_{1,3}(U) = \begin{bmatrix} \rho_1 \\ \rho_2 \\ \hat{\rho}\lambda_{1,3}(U) \end{bmatrix}, \quad r_2(U) = \begin{bmatrix} \partial_2 p \\ -\partial_1 p \\ (\partial_2 p - \partial_1 p)\lambda_2(U) \end{bmatrix}. \tag{4.8}$$

The 2-field is always linearly degenerate (see Section 2.2) since $\nabla\lambda_2(w).r_2(U) \equiv 0$. For the 1- and 3-field, we have that

$$\nabla\lambda_{1,3}(U).r_{1,3}(U) = \mp\frac{\rho_1^2\,\partial_{11}p + \rho_2^2\,\partial_{22}p + 2\rho_1\rho_2\,\partial_{12}p + 2(\rho_1\,\partial_1 p + \rho_2\,\partial_2 p)}{2\sqrt{\hat{\rho}\,(\rho_1\partial_1 p + \rho_2\partial_2 p)}}, \tag{4.9}$$

where we have used the notations

$$\begin{aligned} \partial_1 p = \tfrac{\partial}{\partial \rho_1} p(\rho_1, \rho_2), \quad \partial_2 p = \tfrac{\partial}{\partial \rho_2} p(\rho_1, \rho_2), \quad \partial_{12} p = \tfrac{\partial^2}{\partial \rho_2 \partial \rho_2} p(\rho_1, \rho_2) \\ \partial_{11} p = \tfrac{\partial^2}{\partial \rho_1^2} p(\rho_1, \rho_2), \quad \partial_{22} p = \tfrac{\partial^2}{\partial \rho_2^2} p(\rho_1, \rho_2). \end{aligned} \tag{4.10}$$

To ensure hyperbolicity and genuine nonlinearity (Section 2.2), we consider pressure laws which satisfy

$$\rho_1 \partial_1 p + \rho_2 \partial_2 p > 0, \ \forall \rho_1, \rho_2 > 0 \tag{4.11}$$

and

$$\rho_1^2 \partial_{11} p + \rho_2^2 \partial_{22} p + 2\rho_1 \rho_2 \partial_{12} p + 2(\rho_1 \partial_1 p + \rho_2 \partial_2 p) \neq 0. \tag{4.12}$$

The conditions (4.11) and (4.12) are both fulfilled if we choose a pressure law $p(\rho_1, \rho_2)$ satisfying

$$p(0,0) = 0, \ \partial_1 p(\rho_1, \rho_2), \partial_2 p(\rho_1, \rho_2) > 0 \text{ and } \mathrm{Hess}(p) \text{ is semi-positive definite,} \tag{4.13}$$

where $\mathrm{Hess}(p)$ is the Hessian of the map p. Condition (4.13) is a direct generalization for multiphase flow of a similar condition for single phase flow, see [32, 61, 41]. Indeed, this condition is fulfilled by the isothermal pressure law given in (4.5) and the isentropic pressure law in (4.7).

Remark 4.1.

- *For completeness we present the derivatives of the isentropic pressure law.*

$$\begin{aligned} \partial_1 p &= \gamma a_1^{2/\gamma} (a_1^{2/\gamma} \rho_1 + a_2^{2/\gamma} \rho_2)^{\gamma - 1}; \\ \partial_2 p &= \gamma a_2^{2/\gamma} (a_1^{2/\gamma} \rho_1 + a_2^{2/\gamma} \rho_2)^{\gamma - 1} \\ \partial_{11} p &= \gamma(\gamma - 1) a_1^{4/\gamma} (a_1^{2/\gamma} \rho_1 + a_2^{2/\gamma} \rho_2)^{\gamma - 2}; \\ \partial_{12} p &= \gamma(\gamma - 1) a_1^{2/\gamma} a_2^{2/\gamma} (a_1^{2/\gamma} \rho_1 + a_2^{2/\gamma} \rho_2)^{\gamma - 2}; \\ \partial_{22} p &= \gamma(\gamma - 1) a_2^{4/\gamma} (a_1^{2/\gamma} \rho_1 + a_2^{2/\gamma} \rho_2)^{\gamma - 2}. \end{aligned}$$

- *If one takes $\gamma_1 \neq \gamma_2$ the pressure law now satisfies*

$$a_1^{2/\gamma_1} \rho_1 p^{\frac{\gamma_1 - \gamma_2}{\gamma_1 \gamma_2}} - p^{1/\gamma_2} + a_2^{2/\gamma_2} \rho_2 = 0.$$

The partial derivatives needed for the discussion above can be calculated implicitly using the following equations:

$$
\begin{aligned}
&a_1^{2/\gamma_1}\Big[p^{(\gamma_1-\gamma_2)/(\gamma_1\gamma_2)}+\Big(\frac{\gamma_1-\gamma_2}{\gamma_1\gamma_2}\Big)\rho_1 p^{(\gamma_1-\gamma_2)/(\gamma_1\gamma_2)-1}\partial_1 p\Big]-\gamma_2^{-1}p^{1/\gamma_2-1}\partial_1 p=0;\\
&a_1^{2/\gamma_1}\Big(\frac{\gamma_1-\gamma_2}{\gamma_1\gamma_2}\Big)\rho_1^{(\gamma_1-\gamma_2)/(\gamma_1\gamma_2)-1}\partial_2 p-\gamma_2^{-1}p^{1/\gamma_2-1}\partial_2 p+a_2^{2/\gamma_2}=0;\\
&a_1^{2/\gamma_1}\Big[\Big(\frac{\gamma_1-\gamma_2}{\gamma_1\gamma_2}\Big)p^{(\gamma_1-\gamma_2)/(\gamma_1\gamma_2)-1}\partial_1 p+\Big(\frac{\gamma_1-\gamma_2}{\gamma_1\gamma_2}\Big)\Big\{p^{(\gamma_1-\gamma_2)/(\gamma_1\gamma_2)-1}\partial_1 p+\\
&\Big(\frac{\gamma_1-\gamma_2}{\gamma_1\gamma_2}-1\Big)\rho_1 p^{(\gamma_1-\gamma_2)/(\gamma_1\gamma_2)-2}(\partial_1 p)^2+\rho_1 p^{(\gamma_1-\gamma_2)/(\gamma_1\gamma_2)-1}\partial_{11}p\Big\}\Big]\\
&-\gamma_2^{-1}\Big((\gamma_2^{-1}-1)p^{1/\gamma_2-2}(\partial_1 p)^2+p^{1/\gamma_2-1}\partial_{11}p\Big)=0;\\
&a_1^{2/\gamma_1}\Big(\frac{\gamma_1-\gamma_2}{\gamma_1\gamma_2}\Big)\Big(\frac{\gamma_1-\gamma_2}{\gamma_1\gamma_2}-1\Big)\rho_1 p^{((\gamma_1-\gamma_2)/(\gamma_1\gamma_2)-2)}\partial_2 p^2+\\
&p^{((\gamma_1-\gamma_2)/(\gamma_1\gamma_2)-1)}\partial_{22}p-\gamma_2^{-1}\Big((\gamma_2^{-1}-1)p^{1/\gamma_2-2}\partial_2 p+p^{1/\gamma_2-1}\partial_{22}p\Big)=0;\\
&a_1^{2/\gamma_1}\Big(\frac{\gamma_1-\gamma_2}{\gamma_1\gamma_2}\Big)\Big[p^{((\gamma_1-\gamma_2)/(\gamma_1\gamma_2)-1)}\partial_2 p+\\
&\Big(\frac{\gamma_1-\gamma_2}{\gamma_1\gamma_2}-1\Big)\rho_1 p^{((\gamma_1-\gamma_2)/(\gamma_1\gamma_2)-2)}\partial_1 p p_2+\rho_1 p^{((\gamma_1-\gamma_2)/(\gamma_1\gamma_2)-1)}\partial_{12}p\Big]\\
&-\gamma_2^{-1}\Big((\gamma_2^{-1}-1)p^{1/\gamma_2-2}\partial_1 p\partial_2 p+p^{1/\gamma_2-1}\partial_{12}p\Big)=0.
\end{aligned}
$$

These can be solved using appropriate numerical approaches. In the following discussion we only consider the case where $\gamma_1=\gamma_2$.

Now we discuss the Lax curves as a preliminary step for the solution of the standard Riemann problem for (4.3).

4.2.1 Shock curves

The Lax shock curves are derived from the Rankine-Hugoniot jump conditions as presented in Section 2.2.2. Indeed, let U be a given state and assume that another state $\bar{U}$ is connected to U by a 1,3-shock wave of shock speed s. Then U and $\bar{U}$ satisfy

$$f(U)-f(\bar{U})=s(U-\bar{U}). \tag{4.14}$$

This system defines a one-parameter family of curves found to be

$$S_{1,3}(\xi;U) = (\rho_1\xi, \rho_2\xi, I_{1,3}(\xi))^T \tag{4.15}$$

with

$$I_{1,3}(\xi) = I\xi \mp \sqrt{\hat{\rho}\,(\xi^2-\xi)\,(p(\rho_1\xi,\rho_2\xi)-p(\rho_1,\rho_2))} \tag{4.16}$$

and the shock speed is given by

$$s_{1,3}(\xi;U) = \frac{I}{\hat{\rho}} \mp \frac{\sqrt{\xi(p(\rho_1\xi,\rho_2\xi)-p(\rho_1,\rho_2))}}{\sqrt{\hat{\rho}(\xi-1)}}. \tag{4.17}$$

For the isothermal pressure law given in (4.5), the shock curves are given by

$$S_{1,3}(\xi;U) = \begin{bmatrix} \rho_1\xi \\ \rho_2\xi \\ I\xi \mp (\xi-1)\sqrt{\xi}\sqrt{\hat{\rho}(a_1^2\rho_1 + a_2^2\rho_2)} \end{bmatrix} \tag{4.18a}$$

with shock speed

$$s_{1,3}(\xi;U) = \frac{I}{\hat{\rho}} \mp \sqrt{\xi}\sqrt{\frac{a_1^2\rho_1 + a_2^2\rho_2}{\hat{\rho}}} = \frac{I}{\hat{\rho}} \mp \sqrt{\xi}\sqrt{\frac{p(\rho_1,\rho_2)}{\hat{\rho}}}. \tag{4.18b}$$

Using the Lax admissibility conditions (see Section 2.2), the forward and backward admissible 1-shock curves are obtained as $S_1(\xi;w)$ in (4.18) with $\xi \geq 1$ and $\xi \leq 1$, respectively. Similarly, the forward and backward 3-shock curves are given by $S_3(\xi;w)$ in (4.18) with $\xi \leq 1$ and $\xi \geq 1$, respectively.

4.2.2 Contact discontinuity

Let $\bar{U}$ be a given state. We want to find the set of states that can be connected to $\bar{U}$ on the contact discontinuity curve. Using the linear degeneracy of the 2-field and the Rankine-Hugoniot jump condition (4.14), we show that a state U belongs to the 2-curve or the 2-contact discontinuity curve emanating from $\bar{U}$ if

$$U - \bar{U} = \xi r_2(\bar{U}), \quad \xi \in \mathbb{R}.$$

Hence,

$$\begin{aligned}\rho_1 &= \bar{\rho}_1 + \xi\partial_2\bar{p},\\ \rho_2 &= \bar{\rho}_1 - \xi\partial_1\bar{p},\\ I &= \bar{I} + \xi(\partial_2\bar{p} - \partial_1\bar{p})\lambda_2(\bar{U}).\end{aligned}$$

Therein, the notations $\partial_1\bar{p} = \partial_1 p(\bar{\rho}_1, \bar{\rho}_2)$ and $\partial_2\bar{p} = \partial_2 p(\bar{\rho}_1, \bar{\rho}_2)$ are used. We eliminate ξ in this system and after a suitable scaling, we show that the contact discontinuity wave emanating from any state U is given by the curve

$$L_2(\xi; U) = \frac{1}{\partial_2 p}\begin{bmatrix}\partial_2 p\rho_1\xi\\ \partial_2 p\rho_2 - \partial_1 p(\xi-1)\rho_1\\ \frac{I}{\hat{\rho}}\left(\partial_2 p(\rho_1+\rho_2) + (\partial_2 p - \partial_1 p)\rho_1(\xi-1)\right)\end{bmatrix}, \tag{4.19}$$

and with speed

$$u = \frac{\frac{I}{\hat{\rho}}\left(\partial_2 p(\rho_1+\rho_2) + (\partial_2 p - \partial_1 p)\rho_1(\xi-1)\right)}{\rho_1(\partial_2 p - \partial_1 p)\xi + (\rho_1\partial_1 p + \rho_2\partial_2 p)} = \frac{I}{\rho_1+\rho_2} = \lambda_2(U).$$

For the pressure law given in (4.5), the contact discontinuity curve is found to be

$$L_2(\xi; U) = \frac{1}{a_2^2}\begin{bmatrix}a_2^2\rho_1\xi\\ a_2^2\rho_2 + a_1^2(1-\xi)\rho_1\\ \frac{I}{\hat{\rho}}\left(a_1^2\rho_1 + a_2^2\rho_2 + (a_2^2 - a_1^2)\rho_1\xi\right)\end{bmatrix}. \tag{4.20}$$

Note that we have continuity of the pressure along the contact discontinuity as for the Euler equations.

4.2.3 Rarefaction curves

As introduced in Section 2.2.2, the rarefaction curves are the integral curves of the eigenvectors of the flux function, in the sense that they solve the ordinary differential equation

$$\frac{dU}{d\xi} = \frac{r_{1,3}(U(\xi))}{\nabla\lambda_{1,3}(U(\xi)).r_{1,3}(U(\xi))}, \quad \xi \geq \xi_{1,3},$$

with $\xi_{1,3} = \lambda_{1,3}(U)$. This yields

$$\frac{d}{d\xi}\begin{bmatrix}\rho_1\\ \rho_2\\ I\end{bmatrix} = \mp\frac{2\sqrt{\hat{\rho}\left(\rho_2\,\partial_2 p + \rho_1\,\partial_1 p\right)}}{\rho_1^2\,\partial_{11}p + \rho_2^2\,\partial_{22}p + 2\rho_1\rho_2\,\partial_{12}p + 2(\rho_1\,\partial_1 p + \rho_2\,\partial_2 p)}\begin{bmatrix}\rho_1\\ \rho_2\\ \hat{\rho}\lambda_\mp(U)\end{bmatrix}, \quad \xi \geq \xi_\mp.$$

This system of ODEs is difficult to solve for a general pressure law. However, for a pressure law satisfying (4.13), a solution exists, see [59]. For the simple case of the isothermal pressure law given in (4.5), the rarefaction curves are given by

$$R_{1,3}(\xi;U) = \begin{bmatrix} \rho_1\xi \\ \rho_2\xi \\ I\xi \mp \xi\log(\xi)\sqrt{\hat{\rho}(a_1^2\rho_1 + a_2^2\rho_2)} \end{bmatrix}. \tag{4.21}$$

The forward and backward admissible 1-rarefaction curves for (4.21) are obtained using the Lax admissibility condition as $R_1(\xi;w)$ with $\xi < 1$, and $\xi > 1$, respectively. Similarly, the forward and backward 3-rarefaction curves are given by $S_3(\xi;w)$ with $\xi > 1$, and $\xi < 1$, respectively.
In summary the Lax-curves for the model (4.3) with the equation of state (4.5) are given by

$$L_1^+(\xi;U) = \begin{cases} S_1(\xi;U), & \xi \geq 1; \\ R_1(\xi;U), & \xi < 1; \end{cases} \qquad L_3^+(\xi;U) = \begin{cases} S_3(\xi;U), & \xi \leq 1; \\ R_3(\xi;U), & \xi > 1; \end{cases} \tag{4.22a}$$

$$L_1^-(\xi;U) = \begin{cases} S_1(\xi;U), & \xi \leq 1; \\ R_1(\xi;U), & \xi > 1; \end{cases} \qquad L_3^-(\xi;U) = \begin{cases} S_3(\xi;U), & \xi \geq 1; \\ R_3(\xi;U), & \xi < 1; \end{cases} \tag{4.22b}$$

4.2.4 Solution to the standard Riemann problem

The solution to the standard Riemann problem for a system of conservation laws has been presented extensively for example in the books [42, 78, 79].

Proposition 4.1. *We consider the Riemann problem for* (4.3) *with initial data*

$$U(x,0) = \begin{cases} U^+ & \text{if } x > 0, \\ U^- & \text{if } x < 0. \end{cases} \tag{4.23}$$

For $|U^+ - U^-|$ sufficiently small, there exist a unique weak self-similar solution to this Riemann problem with small total variation. This solution comprises 4 *constant states $U_0 = U^-, U_1, U_2, U_3 = U^+$. When the i-th characteristic family is genuinely nonlinear U_i is joined to U_{i-1} by either an i-rarefaction wave or an i-shock, while*

when the i-characteristic family is linearly degenerate, U_i is joined to U_{i-1} by an i-contact discontinuity.

We briefly discuss the construction of the solution of the Riemann problem for the model (4.1) with the pressure law given in (4.5). We assume that the left and right states U^- and U^+ are given and satisfy the conditions of Proposition 4.1. We call U_1 and U_2 the intermediary states. We can then find ξ_1, ξ_2 and ξ_3 such that

$$U_1 = L_1^+(\xi_1; U^-), \quad \text{and} \quad U_2 = L_2(\xi_2; U_1), \quad \text{and} \quad U_2 = L_3^-(\xi_3; U^+). \tag{4.24}$$

For simplicity, we denote the momentum components of U_1 and U_2 as $I_1(\xi_1; U^-)$ and $I_3(\xi_3; U^+)$, respectively. The solution for the Riemann problem is found if we can solve for ξ_1, ξ_2 and ξ_3 the system

$$\left\{ \begin{array}{lcl} \rho_1^+ \xi_3 & = & \rho_1^- \xi_1 \xi_2, \\ \rho_2^+ \xi_3 & = & \rho_2^- \xi_1 + \frac{a_2^2}{a_1^2}(1-\xi_2)\rho_1^- \xi_1, \\ I_3(\xi_3; U^+) & = & \frac{I_1(\xi_1;U^-)}{a_2^2(\rho_1^- + \rho_2^-)\xi_1} \left((a_1^2 \rho_1^- + a_2^2 \rho_2^-)\xi_1 + (a_2^2 - a_1^2)\rho_1^- \xi_1 \xi_2 \right). \end{array} \right. \tag{4.25}$$

One can solve the first two equations in (4.25) and find ξ_2 and ξ_3 in terms of ξ_1.

$$\xi_2 = \frac{\rho_1^+}{\rho_1^-} \frac{p(\rho_1^-, \rho_2^-)}{p(\rho_1^+, \rho_2^+)}, \quad \xi_3 = \frac{\rho_1^-}{\rho_1^+} \xi_1 \xi_2 = \frac{p(\rho_1^-, \rho_2^-)}{p(\rho_1^+, \rho_2^+)} \xi_1. \tag{4.26}$$

Replacing these expressions in the third equation in (4.25), we obtain a scalar equation to solve for ξ_1 given by

$$I_3 \left(\frac{p(\rho_1^-, \rho_2^-)}{p(\rho_1^+, \rho_2^+)} \xi_1; U^+ \right) = \frac{I_1(\xi_1; U^-)}{a_2^2(\rho_1^- + \rho_2^-)} \left(p(\rho_1^-, \rho_2^-) + (a_2^2 - a_1^2)\rho_1^+ \frac{p(\rho_1^-, \rho_2^-)}{p(\rho_1^+, \rho_2^+)} \xi_1 \right). \tag{4.27}$$

If we assume for example that U_1 is connected to U^- with a 1-shock curve and that U_2 is connected to U^+ by a 3-rarefaction curve (see Figure 4.1), we find that the map

$$\begin{array}{rcl} g(\xi_1; U^-, U^+) & = & I_3 \left(\frac{p(\rho_1^-, \rho_2^-)}{p(\rho_1^+, \rho_2^+)} \xi_1; U^+ \right) \\ & & - \frac{I_1(\xi_1;U^-)}{a_2^2(\rho_1^- + \rho_2^-)} \left(p(\rho_1^-, \rho_2^-) + (a_2^2 - a_1^2)\rho_1^+ \frac{p(\rho_1^-, \rho_2^-)}{p(\rho_1^+, \rho_2^+)} \xi_1 \right) \end{array} \tag{4.28}$$

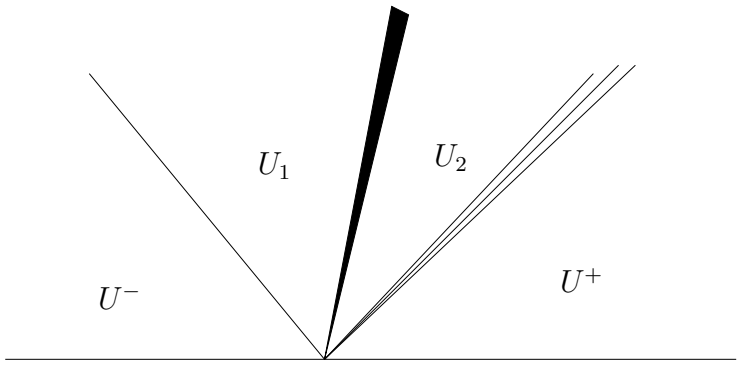

Figure 4.1: *Wave structure for the solution of the Riemann problem for the Drift-flux model in the $x-t$ plane.*

satisfy $g(1;U,U)=0$ and

$$\frac{\partial g}{\partial \xi_1}(\xi_1,U^-,U^+)|_{(\xi_1=1,U,U)}=\frac{\rho_1 I}{\hat{\rho}}\frac{a_1^2-a_2^2}{a_2^2}+2\sqrt{a_1^2\rho_1^2+a_1^2\rho_1\rho_2+a_2^2\rho_2}\neq 0$$

provided that U satisfy the condition of Lemma 4.1 below. The cases corresponding to other wave structures in the solution lead to the same conditions. We have then proven the following result.

Lemma 4.1. *Assume that we have a multiphase fluid described with the equation of state in the form $p=p(\rho_1,\rho_2)$. Let U be a state that satisfies the following condition*

$$\frac{\rho_1\, I}{\hat{\rho}}\frac{\partial_1 p-\partial_2 p}{\partial_2 p}+2\sqrt{\hat{\rho}(\rho_1\partial_1 p+\rho_2\partial_2 p)}\neq 0. \tag{4.29}$$

Then, for U^- and U^+ close to U, the standard Riemann problem with data (U^-,U^+) admits a solution.

4.3 Pipe-to-pipe intersections

The network of pipes is considered as an oriented graph with the arcs representing the pipes and the vertices representing the pipe intersections. Moreover, we consider a junction as a set of non-zero vectors of $\mathbb{R}^3$ meeting at the origin considered as the

junction. Along the arcs, the flow is governed by a copy of the drift-flux model (4.3). At the junction located at $x = 0$, some coupling conditions in the form

$$\Psi\left(U_I(t,0-);U_O(t,0+)\right) = 0 \tag{4.30}$$

are prescribed. In (4.30), $U_I(t,0-)$ (respectively $U_O(t,0+)$) represents the traces of the flow in all the incoming (respectively outgoing) pipes at the junction. In many physical systems related for example to gas dynamics the stationary solutions of the flow equation (4.3) play an important role in the precise definition of the coupling condition map Ψ. For the drift-flux model, they satisfy

$$\begin{array}{rcl} \partial_x \frac{\rho_1 I}{\rho_1+\rho_2} & = & 0, \\ \partial_x \frac{\rho_2 I}{\rho_1+\rho_2} & = & 0, \\ \partial_x \left(\frac{I^2}{\rho_1+\rho_2} + p(\rho_1+\rho_2) \right) & = & 0. \end{array} \tag{4.31}$$

4.3.1 A junction connecting two pipes

In this section and the rest of the chapter, we will use the notations $\mathbb{R}^+ = [0,+\infty[$ and $\overset{\circ}{\mathbb{R}}{}^+ =]0,+\infty[$. We consider only one junction here. A more complex network can be treated by considering each junction separately. The flow in each pipe is governed by the drift-flux model equations (4.3) written in the compact form

$$\partial_t(U) + \partial_x(f(U)) = 0, \tag{4.32a}$$

with

$$U = \begin{bmatrix} \rho_1 \\ \rho_2 \\ I \end{bmatrix}, \quad f(U) = \begin{bmatrix} \frac{\rho_1 I}{\hat\rho} \\ \frac{\rho_2 I}{\hat\rho} \\ \frac{I^2}{\hat\rho} + p(\rho_1,\rho_2) \end{bmatrix}, \tag{4.32b}$$

and

$$\hat\rho = \rho_1 + \rho_2, \quad I = u\hat\rho. \tag{4.32c}$$

At the junction, we assume that some coupling conditions in the form

$$\Psi\left(U^-(t,0-);U^+(t,0+)\right) = 0 \tag{4.33}$$

are prescribed. Therein, U^- and U^+ are the flow variable in the left and right pipe, respectively. We assume that the junction is located at $x = 0$. The map Ψ will be called the map of the coupling conditions. Note that in general, Ψ has as many arguments as the number of pipes meeting at the junction. For clarity, we develop the theory below for a junction of two connected pipes. In Remark 4.2, we will discuss briefly the general case of a junction with more than two pipes.

We will require the state variables to belong in the subsonic region defined as

$$A_0 = \{U \in \overset{\circ}{\mathbb{R}}^+ \times \overset{\circ}{\mathbb{R}}^+ \times \mathbb{R} : \lambda_1(U) < 0 < \lambda_2(U) < \lambda_3(U)\}. \tag{4.34}$$

For later use, we define the quantities

$$\begin{aligned} &\text{Flow of the density of phase 1:} && M(U) = \tfrac{\rho_1 I}{\rho_1+\rho_2}, \\ &\text{Flow of the density of phase 2:} && N(U) = \tfrac{\rho_2 I}{\rho_1+\rho_2}, \\ &\text{Flow of the linear momentum:} && P(U) = \tfrac{I^2}{\rho_1+\rho_2} + p(\rho_1,\rho_2). \end{aligned}$$

We have the following elementary lemma.

Lemma 4.2. *Let $U = (\rho_1, \rho_2, I) \in A_0$ and assume that the Lax curves are defined as in* (4.22)*. The following hold.*

(i) $\frac{d}{d\xi} P\left(L_{1,3}(\xi;U)\right)_{|_{\xi=1}} = \lambda_{1,3}^2(U)\hat{\rho}$;

(ii) $\frac{d}{d\xi} M\left(L_1(\xi;U)\right)_{|_{\xi=1}} = \lambda_1(U)\rho_1, \quad \frac{d}{d\xi} M\left(L_3(\xi;U)\right)_{|_{\xi=1}} = \lambda_3(U)\rho_1$;

(iii) $\frac{d}{d\xi} N\left(L_1(\xi;U)\right)_{|_{\xi=1}} = \lambda_1(U)\rho_2, \quad \frac{d}{d\xi} N\left(L_3(\xi;U)\right)_{|_{\xi=1}} = \lambda_3(U)\rho_2$;

(iv) $\frac{d}{d\xi} M\left(L_2(\xi;U)\right)_{|_{\xi=1}} = \lambda_2(U)\rho_1,$
$\frac{d}{d\xi} M\left(L_2(\xi;U)\right)_{|_{\xi=1}} = \lambda_2(U)\rho_2, \quad \frac{d}{d\xi} P\left(L_2(\xi;U)\right)_{|_{\xi=1}} = \frac{\partial_2 p - \partial_1 p}{\partial_1 p}\lambda_2(U)^2\rho_1.$

Proof.

(i) By the chain rule, we may write

$$\begin{aligned} \frac{d}{d\xi} P\left(L_{1,3}(\xi;U)\right) \;=\; & \frac{\partial P}{\partial \rho_1}\left(L_{1,3}(\xi;U)\right) \frac{d}{d\xi}\left(L_{1,3}^1(\xi;U)\right) \\ & + \frac{\partial P}{\partial \rho_2}\left(L_{1,3}(\xi;U)\right) \frac{d}{d\xi}\left(L_{1,3}^2(\xi;U)\right) \\ & + \frac{\partial P}{\partial I}\left(L_{1,3}(\xi;U)\right) \frac{d}{d\xi}\left(L_{1,3}^3(\xi;U)\right) \end{aligned}$$

where $L^i_{1,3}$ is the i-th component of $L_{1,3}$. Proceeding with the calculations, we have

$$\begin{aligned}
&\frac{d}{d\xi}P\left(L_{1,3}(\xi;U)\right)_{|_{\xi=1}}\\
=\;& \rho_1\left(-\frac{I^2}{(\rho_1+\rho_2)^2}+\partial_1 p\right)+\rho_2\left(-\frac{I^2}{(\rho_1+\rho_2)^2}+\partial_2 p\right)+\frac{2I}{\rho_1+\rho_2}\hat{\rho}\lambda_{1,3}(U)\\
=\;& \frac{I}{\rho_1+\rho_2}(2\hat{\rho}\lambda_{1,3}(U)-I)+\rho_1\partial_1 p+\rho_2\partial_2 p\\
=\;& 2I\lambda_{1,3}(U)-\frac{I^2}{\hat{\rho}}+\rho_1\partial_1 p+\rho_2\partial_2 p\\
=\;& \hat{\rho}\left(\frac{2I\lambda_{1,3}(U)}{\hat{\rho}}-\frac{I^2}{\hat{\rho}^2}+\frac{\rho_1\partial_1 p+\rho_2\partial_2 p}{\hat{\rho}}\right)\\
=\;& \hat{\rho}\left(\frac{2I}{\hat{\rho}}\left(\frac{I}{\rho}\mp\frac{1}{\rho}\sqrt{\rho_2^2\,\partial_2 p+\rho_1\left(\partial_2 p+\partial_1 p\right)\rho_2+\rho_1^2\,\partial_1 p}\right)\right.\\
&\left.-\frac{I^2}{\hat{\rho}^2}+\frac{\rho_1\partial_1 p+\rho_2\partial_2 p}{\hat{\rho}}\right)\\
=\;& \hat{\rho}\left(\frac{I^2}{\hat{\rho}^2}\mp\frac{2I}{\hat{\rho}^2}\sqrt{\rho_2^2\,\partial_2 p+\rho_1\left(\partial_2 p+\partial_1 p\right)\rho_2+\rho_1^2\,\partial_1 p}+\frac{\rho_1\partial_1 p+\rho_2\partial_2 p}{\hat{\rho}}\right)\\
=\;& \hat{\rho}\left(\lambda_{1,3}(U)\right)^2.
\end{aligned}$$

(ii) Likewise to (i) above, we have

$$\begin{aligned}
&\frac{d}{d\xi}N\left(L_1(\xi;U)\right)_{|_{\xi=1}}\\
=\;& \rho_1\left(\frac{I}{\rho_1+\rho_2}-\frac{\rho_1 I}{(\rho_1+\rho_2)^2}\right)+\rho_2\left(-\frac{\rho_1 I}{(\rho_1+\rho_2)^2}\right)+\frac{\rho_1}{\rho_1+\rho_2}\hat{\rho}\lambda_1(U)\\
=\;& \frac{\rho_1 I}{\rho_1+\rho_2}-\rho_1 I\frac{\rho_1+\rho_2}{(\rho_1+\rho_2)^2}+\rho_1\lambda_1(U)\\
=\;& \rho_1\lambda_1(U)
\end{aligned}$$

(iii) change the roles of ρ_1 and ρ_2 in (ii).

(iv) Similar to the previous case.

■

In general, for two connected pipes at a junction, we are interested in Ψ-solutions, that is, weak solutions depending on the coupling conditions map Ψ. We consider a map $\hat{U}$ defined as

$$\hat{U}(x) = \begin{cases} \hat{U}^- & \text{if } x < 0 \\ \hat{U}^+ & \text{if } x > 0 \end{cases} \quad \text{with} \quad \begin{array}{l} \Psi(\hat{U}^-; \hat{U}^+) = 0, \\ \hat{U}^-,\, \hat{U}^+ \in A_0. \end{array} \tag{4.35}$$

The existence of $\hat{U}^+$ for a given $\hat{U}^-$ is guaranteed by Lemma 4.3 below. The following definition is a direct extension for the model (4.1) of [40, Definition 2.2].

Definition 4.1. *A weak Ψ-solution of (4.3,4.33) is a map*

$$\begin{gathered} U \in \mathbf{C}^0\left(\mathbb{R}^+; \hat{U} + \mathbf{L}^1(\mathbb{R}; \overset{\circ}{\mathbb{R}}^+ \times \overset{\circ}{\mathbb{R}}^+ \times \mathbb{R})\right) \\ U(t) \doteq U(t,\cdot) \in \mathbf{BV}(\mathbb{R}; \overset{\circ}{\mathbb{R}}^+ \times \overset{\circ}{\mathbb{R}}^+ \times \mathbb{R}) \quad \textit{for a.e. } t \in \mathbb{R}^+ \end{gathered} \tag{4.36}$$

such that

(i) for all $\varphi \in \mathbf{C}^1_c\left(\overset{\circ}{\mathbb{R}}^+ \times \mathbb{R}; \mathbb{R}\right)$ whose support does not intersect $x = 0$

$$\int_{\mathbb{R}^+} \int_{\mathbb{R}} \left(\begin{bmatrix} \rho_1 \\ \rho_2 \\ I \end{bmatrix} \partial_t \varphi + \begin{bmatrix} \frac{\rho_1 I}{\hat{\rho}} \\ \frac{\rho_1 I}{\hat{\rho}} \\ P(U) \end{bmatrix} \partial_x \varphi \right) dx dt = 0; \tag{4.37}$$

(ii) for a.e. $t \in \mathbb{R}^+$, the coupling condition is fulfilled

$$\Psi(U(t,0-); U(t,0+)) = 0.$$

In a neighborhood of the junction, one can integrate the stationary solution of (4.3) given by (4.31) and obtain the coupling conditions map

$$\Psi\left(U^-; U^+\right) = \begin{bmatrix} M(U^+) - M(U^-) \\ N(U^+) - N(U^-) \\ P(U^+) - P(U^-) \end{bmatrix}, \tag{4.38}$$

which express the conservation of mass of each phase and the equality of the dynamic pressure at the junction. Similar conditions were obtained in [32, 33, 61]. We prove that when a stationary flow U^- is prescribed in the incoming pipe, we can solve for the flow in the outgoing pipe which is also stationary. Indeed, we have the following result.

Lemma 4.3. *Let $\bar{U} \in A_0$. Then there exists a positive constant $\bar{\delta}$ and a Lipschitz map*

$$\mathcal{T} : B(\bar{U}; \bar{\delta}) \to A_0, \tag{4.39}$$

where $B(\bar{U}; \bar{\delta})$ is the ball centered at $\bar{U}$ and radius $\bar{\delta}$, such that

$$\left.\begin{array}{l} \Psi\left(U^-; U^+\right) = 0 \\ U^-,\, U^+ \in B(\bar{U}, \bar{\delta}) \end{array}\right\} \Leftrightarrow U^+ = \mathcal{T}(U^-). \tag{4.40}$$

Proof. The proof is straightforward and uses the implicit function theorem. We obviously have that $\Psi(\bar{U}; \bar{U}) = 0$ and moreover we have that

$$\begin{aligned}
&\mathrm{Det}\left(D_{U^+}\Psi\left(U^-; U^+\right)\right)_{|_{(\bar{U};\bar{U})}} \\
&= \left|\begin{array}{ccc} D_{\rho_1^+}M(U^+) & D_{\rho_2^+}M(U^+) & D_I M(U^+) \\ D_{\rho_1^+}N(U^+) & D_{\rho_2^+}N(U^+) & D_I N(U^+) \\ D_{\rho_1^+}P(U^+) & D_{\rho_2^+}P(U^+) & D_I P(U^+) \end{array}\right|_{|_{(\bar{U};\bar{U})}} \\
&= \left|\begin{array}{ccc} \frac{\rho_2^+}{\hat{\rho}^+}\lambda_2(U^+) & -\frac{\rho_1^+}{\hat{\rho}^+}\lambda_2(U^+) & \frac{\rho_1^+}{\hat{\rho}^+} \\ -\frac{\rho_2^+}{\hat{\rho}^+}\lambda_2(U^+) & \frac{\rho_1^+}{\hat{\rho}^+}\lambda_2(U^+) & \frac{\rho_2^+}{\hat{\rho}^+} \\ D_{31} & D_{32} & (\lambda_2(U^+) + p^+) \end{array}\right|_{|_{(\bar{U};\bar{U})}} \\
&= \lambda_1(\bar{U})\lambda_2(\bar{U})\lambda_3(\bar{U}) \neq 0.
\end{aligned}$$

with

$$D_{31} = -\lambda_1(U^+)\lambda_3(U^+) + \partial_1 p^+ - \frac{\rho_1^+\partial_1 p^+ + \rho_2^+\partial_2 p^+}{\hat{\rho}^+}$$

and

$$D_{32} = -\lambda_1(U^+)\lambda_3(U^+) + \partial_2 p^+ - \frac{\rho_1^+ \partial_1 p^+ + \rho_2^+ \partial_2 p^+}{\hat{\rho}^+}$$

■

This result is similar to a result presented by Colombo and Marcellini [40] in the context of the p-system. Therein, the pipe was considered as being of variable cross-section. Moreover, Lemma 4.3 ensures for the case of the Riemann problem at the junction the "additivity" property as for the Standard Lax Riemann solver [42, 33] which states that if (U^-, U^o) and (U^o, U^+) are Riemann data for a stationary solution of the Riemann problem at the junction, then so is the case for (U^-, U^+). Now we present another approach for the well-posedness of the Riemann problem at the junction. The argument used here is standard and has been developed in [32, 7] for the case of isothermal Euler equations and in [61, 41] for the case of the Euler equations. The importance of this result comes from the extension to the case of a junction with more than two pipes. For the case of the drift-flux model, more conditions are needed on the initial data in each pipe as presented in the following result.

Proposition 4.2. *Let $\hat{U}_1, \hat{U}_2 \in A_0$ be the data in the incoming and outgoing pipes connected at $x = 0$. We assume further that the following condition is satisfied:*

$$\frac{1}{a_1^2}\lambda_1(\hat{U}_1)\,\lambda_2(\hat{U}_2)\,\lambda_3(\hat{U}_2)\left(\lambda_2(\hat{U}_2)\rho_1^2(a_2^2 - a_1^2) - \lambda_3(\hat{U}_2)p(\hat{\rho}_1^2, \hat{\rho}_2^2)\right)(\hat{\rho}_1^1\hat{\rho}_2^2 - \hat{\rho}_2^1\hat{\rho}_1^2) \neq 0. \tag{4.41}$$

Then, there exists a constant $\delta > 0$ such that for any states $\bar{U}_1$ and $\bar{U}_2$ with $|\bar{U}_i - \hat{U}_i| < \delta$ for $i = 1, 2$, the Riemann problem at the junction with data $(\bar{U}_1, \bar{U}_2)$ has a unique solution.

Proof. Consider some perturbations V_1 and V_2 of $\hat{U}_1$ and $\hat{U}_2$ which belong to the subsonic space A_0. We want to find some states $\tilde{V}_1$ and $\tilde{V}_2$ such that the restriction of the solution of the standard Riemann problem with data $(V_1, \tilde{V}_1)$ on $x < 0$ consists of waves of non-positive speed only and the restriction of the solution of the standard Riemann problem with data $(\tilde{V}_2, V_2)$ on $x > 0$ consists of waves of non-negative speed

only. Based on the expressions of the Lax waves curves presented in the previous section, the possible choices for $\tilde{V}_1$ and $\tilde{V}_2$ are the following:

$$\tilde{V}_1 = L_1^+(\xi_1; \hat{U}_1), \quad \text{and} \quad \tilde{V}_2 = L_3^-(\xi_3; L_2(\xi_2; \hat{U}_2)).$$

Moreover, we want the states $\tilde{V}_1$ and $\tilde{V}_2$ to satisfy the coupling conditions given in (4.38). This results in a system of three equations for the three unknowns ξ_1, ξ_2 and ξ_3. The determinant D of the Jacobian matrix of the resulting map satisfies, using Lemma 4.2,

$$\begin{aligned} D &= \begin{vmatrix} -\lambda_1(\hat{U}_1)\hat{\rho}_1^1 & \lambda_2(\hat{U}_2)\hat{\rho}_1^2 & \lambda_3(\hat{U}_2)\hat{\rho}_1^2 \\ -\lambda_1(\hat{U}_1)\hat{\rho}_2^1 & \lambda_2(\hat{U}_2)\hat{\rho}_2^2 & \lambda_3(\hat{U}_2)\hat{\rho}_2^2 \\ -(\lambda_1(\hat{U}_1))^2(\hat{\rho}_2^1 + \hat{\rho}_2^2) & (\lambda_2(\hat{U}_2))^2\hat{\rho}_1^2 & (\lambda_3(\hat{U}_2))^2(\hat{\rho}_1^2 + \hat{\rho}_2^2) \end{vmatrix} \\ &= \tfrac{1}{a_1^2}\lambda_1(\hat{U}_1)\,\lambda_2(\hat{U}_2)\,\lambda_3(\hat{U}_2)\left(\lambda_2(\hat{U}_2)\rho_1^2(a_2^2 - a_1^2) - \lambda_3(\hat{U}_2)p(\hat{\rho}_1^2, \hat{\rho}_2^2)\right)(\hat{\rho}_1^1\hat{\rho}_2^2 - \hat{\rho}_2^1\hat{\rho}_1^2) \end{aligned}$$

By using the implicit function theorem and the condition (4.41), and proceeding as in the proof of Proposition 3.1 in Chapter 3, we obtain an existence and uniqueness result for the ξ_i and then for the $\tilde{V}_i$ in the neighborhood of the data $\hat{U}_1$ and $\hat{U}_2$. ■

This result can be extended in a straightforward way to a sequence of junctions in a linear pipe. This can be interpreted as a junction with a piece-wise constant cross-section. Before giving more details on the piece-wise constant cross section case, we discuss some remarks on a junction with more than two pipes.

Remark 4.2. *Let us consider a junction with m incoming pipes with the flow variables in those pipes denoted by $U_1, \ldots, U_m$ and p outgoing pipes with the flow variables denoted by $U_{m+1}, \ldots, U_{m+p}$. One example of the coupling condition map here*

is given by

$$\Psi(U_1,\dots,U_m,U_{m+1},\dots,U_{m+p}) = \begin{pmatrix} \sum_{i=1}^{m} M(U_i(t,0-)) & - & \sum_{i=1}^{p} M(U_{m+i}(t,0+)) \\ \sum_{i=1}^{m} N(U_i(t,0-)) & - & \sum_{i=1}^{p} N(U_{m+i}(t,0+)) \\ P(U_1(t,0-)) & - & P(U_2(t,0-)) \\ & \vdots & \\ P(U_{m-1}(t,0-)) & - & P(U_m(t,0-)) \\ P(U_m(t,0-)) & - & P(U_{m+1}(t,0+)) \\ P(U_{m+1}(t,0+)) & - & P(U_{m+2}(t,0+)) \\ & \vdots & \\ P(U_{m+p-1}(t,0+)) & - & P(U_{m+p}(t,0+)) \end{pmatrix}.$$

The first two rows of Ψ are compulsory. They express the conservation of mass of each phase at the junction. The last $m+p-1$ rows of Ψ express the equality of the dynamic pressure at the junction. Similar conditions have been proposed in [33, 32, 7]. Some other conditions used in the literature are the equality of the pressure at the junction. For the p-system, many other conditions were proposed and compared in [34]. The proof of the well-posedness of the Riemann problem at the junction in this general case proceeds as in the proof of Proposition 4.2 or in the proof of the main result of Chapter 3. It consists of considering the waves in each pipe to be described by some Lax curves and considering a composition of these Lax curves and the coupling condition map Ψ. This is done in such a way that one can solve $\Psi = 0$ for some parameters of the Lax curve. This gives some intermediary states (like the $\tilde{v}$ in the proof of Proposition 4.2) that ensure the well-posedness and play an important role in the numerical simulation of the dynamics of the fluid in the pipes. With this approach in mind, it is therefore important to have an expression for the Lax curves for any system we want to investigate. As pointed out above, the exact solution of the ODE giving the rarefaction curve is not easy. We next propose an approach which consists of linearizing the Lax curves in order to compute the solution of the Riemann problem at the junction.

4.4 Linearization of the Lax curves

The technique that we have described above for the solution of the Riemann problem at the junction fails in general when one cannot find an exact expression for the Lax curves. It turns out that this is generally the case when the pressure law for the drift-flux model is nonlinear. The integration of the differential equation describing the rarefaction curve is not trivial and therefore one can not have the exact expression for the rarefaction curve. We claim that one can still solve numerically the problem in this case. Indeed, we propose the use of the linearized Lax curves. We recall that the Lax curves through a given state $\bar{U}$ are given for example by

$$L_i(\xi;\bar{U}) = \begin{cases} S_i(\xi;\bar{U}), & \xi \geq 1 \\ R_i(\xi;\bar{U}), & \xi < 1 \end{cases} \tag{4.42}$$

where $\xi \mapsto S_i(\xi;\bar{U})$ and $\xi \mapsto R_i(\xi;\bar{U})$ are the i-shock and the i-rarefaction curves through U, respectively. With the parameterization of these curves, they have a tangency of second order at the point U, i.e.

$$R_i(\xi;\bar{U}) - S_i(\xi;\bar{U}) = \mathcal{O}(\xi^3). \tag{4.43}$$

Hence, the composite function, $L_i(\xi;\bar{U})$ in (4.42) is smooth for $\xi \neq 1$, and twice continuously differentiable at $\xi = 1$. Moreover, its second derivatives are Lipschitz-continuous functions of ξ and $\bar{U}$, see [19]. We then write the Taylor expansion of $L_i(\xi;\bar{U})$ about $\xi = 1$ as

$$\tilde{L}_i(\xi;\bar{U}) = \bar{U} + (\xi - 1)r_i(\bar{U}) + \mathcal{O}((\xi-1)^2)), \tag{4.44}$$

where $r_i(\bar{U})$ are the eigenvectors given in (4.8). For ξ close to 1, we use the expression of the Lax curves in (4.44) instead of the exact Lax curves for the computation of the solution of the Riemann problem at the junction.

Dynamics for a pipe with a piece-wise constant cross-section

We now consider a pipe with a piecewise constant section

$$c = c_0\chi_{]-\infty,x_1]} + \sum_{j=1}^{n-1} c_j\chi_{]x_j,x_{j+1}]} + c_n\chi_{]x_n,+\infty[}$$

for a suitable number n of discontinuities in the cross-section map c. The fluid in each pipe obeys the balance law (4.3) and at each junction x_j, the coupling conditions now have the form

$$\Psi(c_{j-1}, U_j^-; c_j, U_j^+) = 0 \text{ for all } j = 1, \ldots, n \text{ and } U_j^{\pm} = \lim_{x \to x_j \pm} U_j(t, x), \text{ for all } t \geq 0. \tag{4.45}$$

Now, the coupling condition map has the form

$$\Psi\left(c^-, U^-; c^+, U^+\right) = \begin{bmatrix} c^+ M(U^+) - c^- M(U^-) \\ c^+ N(U^+) - c^- N(U^-) \\ c^+ P(U^+) - c^- P(U^-) \end{bmatrix}.$$

When $c^- = c^+ = 1$, we recover the previous coupling conditions: $\Psi\left(1, U^-; 1, U^+\right) \equiv \Psi\left(U^-; U^+\right)$. The solution of the Riemann problem in the pipe is an iteration of Definition 4.1 at each point of jump x_j of the cross sectional map $c(x)$. We will show a numerical result for this case in the next section. Since the coupling conditions apply locally in the neighborhood of the junction, the analysis presented in the case of a smooth junction above can be extended to this case iteratively in a straightforward way.

4.5 Numerical simulations and results

The set up for this section is similar to that of Chapter 3, Section 3.4. The numerical integration of the multiphase fluid flow model defined in (4.3) is done with a second-order relaxed scheme [69]. In this section, we assume in general that the pipes have a constant cross-section and the sound speed, unless stated otherwise, for phase 1 is taken as $a_1^2 = 16.0$ and for phase 2, $a_2^2 = 1.0$. Initial conditions are usually some perturbation of some stationary solutions. Newton's method is used to solve the system in equation (4.38) combined with the Lax curves as described in the proof of Proposition 4.2 which gives the boundary conditions at the internal nodes of the network at the junction. This insures that at every time step, the coupling conditions at the junction are satisfied. For the external (inlet to network or outlet

from network) boundary conditions, we use the transparent boundary conditions. For time integration we use a second-order Runge-Kutta scheme with the strong-stability preserving (SSP) [56] property. The time step size is given dynamically by

$$\Delta t = \frac{0.75\Delta x}{\max(\varrho(\partial f(W)/\partial W))}$$

where the maximum is taken over all computational grid-points. We recall that Δx is the spatial step-width and $\varrho(\partial f(W)/\partial W))$ is the spectral radius of the Jacobian of the flux function $f(W)$ with respect to the conserved variables, W.

4.5.1 Two connected pipes and the standard Riemann problem

This section serves to verify the qualitative behavior of the coupling conditions and to validate the use of the linearized Lax curves for a junction connecting two pipes. To achieve that goal, we consider the isothermal pressure law in (4.5) which is the same as the isentropic pressure law (4.7) for $\gamma = 1$. We solve independently the standard Riemann problem, the Riemann problem at the junction with two horizontal pipes and with the exact Lax curves and then with the linearized Lax curves. It is expected that the three results will agree. The choice of the isothermal pressure law for this test is motivated by the fact that we have already determined the exact expressions for the Lax curves. Here we consider the Riemann data

$$U_l = (1.4712300, 2.2832400, 3.2928117), \quad U_r = (0.8070800, 1.2525284, 2.2928117). \tag{4.46}$$

For the Riemann problem at the junction, $U_1 = U_l$ and $U_2 = U_r$ are considered as the data in each pipe such that the conditions of Proposition 4.2 are satisfied. The mesh size of $N = 400$ was employed on a single pipe on which the standard Riemann solver was applied. For the Riemann problem at the junction, the mesh size of $N = 200$ was applied in each pipe. The results computed at time $t = 0.05$ for the standard Riemann, the Riemann problem at the junction with the exact Lax curves and the linearized Lax curves are presented in Figure 4.2. These two

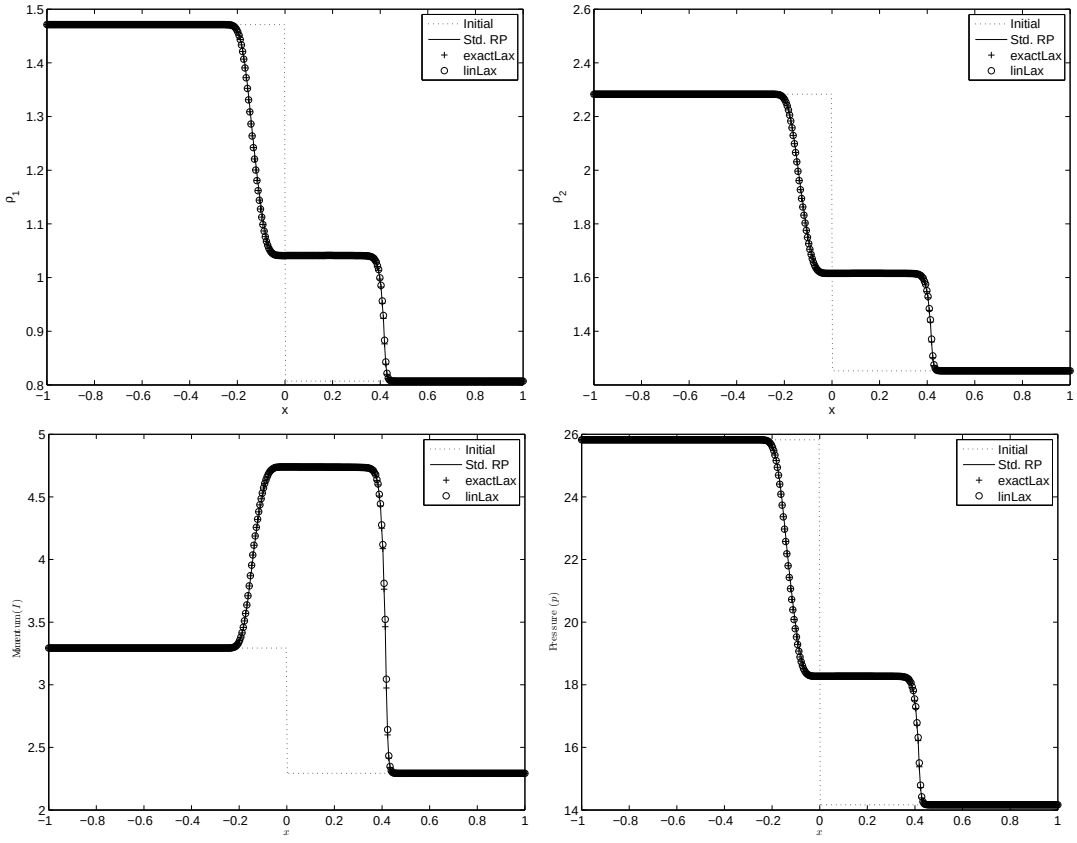

Figure 4.2: *Profiles of the densities ρ_1 and ρ_2, the momentum I, the common pressure p for the standard Riemann problem (continuous line), the Riemann problem at the junction with the use of the exact Lax curves (crosses) and the linearized Lax curves (circles).*

results are in good agreement. This proves two things. First, that qualitatively the solution of Riemann problem at the junction with the coupling conditions proposed here is the same as the solution of the Sod shock tube problem and secondly, that the linearization of the Lax curves is a good approximation for the solution of the Riemann problem at the junction.

Now we consider an example with the isentropic pressure law. Here, we take $\gamma = 5/3$

and we consider the following initial data

$$U_1 = (1.81832, 1.44174, -0.751082), \quad U_2 = (2.01667, 1.22004, -1.584711) \quad (4.47)$$

which is the same as the data used in Chapter 3, Eq. (3.19). The results are presented in Figure 4.3. We see here that the results for the solution of the standard Riemann problem and the coupled pipes are in good agreement. The shock and rarefaction waves are well resolved. There is a small error in the position of the contact discontinuity. We suspect that this is due to the linearization of the Lax curves.

4.5.2 Effect of the sound speed on the flow

Here we consider the case of a standard Riemann problem for the model equation (4.3) with the isentropic pressure law (4.7) and with $\gamma = 5.0/3$. We investigate the effect of changes in the compressibility factors of each phase on the multiphase model. The Riemann data is taken as

$$U(x,0) = \begin{cases} U^- = (3.17123, 3.38324, 3.71816) & x < 0.5; \\ U^+ = (2.70708, 4.0434, 3.5629) & x > 0.5. \end{cases} \quad (4.48)$$

We present in Figure 4.4 the plots of the densities, the momentum and the pressure at time $t = 0.1$, for the sound speed ratio $\frac{a_2^2}{a_1^2} = 1$ with $a_1^2 = 6$, $\frac{a_2^2}{a_1^2} < 1$ with $a_1^2 = 16$ and $a_2^2 = 1$, and $\frac{a_2^2}{a_1^2} > 1$ with $a_1^2 = 1$ and $a_2^2 = 16$. The results for the case $\frac{a_2^2}{a_1^2} = 1$ compare well with those obtained in [10]. We note also that the qualitative behavior of the solution for $a_1^2 < a_2^2$ is comparable to the case $a_1^2 = a_2^2$. Also, the flow is more compressive for $a_1^2 < a_2^2$.

4.5.3 A pipe with piece-wise constant cross section

Here we consider two connected pipes with a jump in the cross section. We investigate the effect of the discontinuity of the cross-section on the flow. We recall that the analytical setup here was discussed in Section 4.4. The initial conditions are taken to be

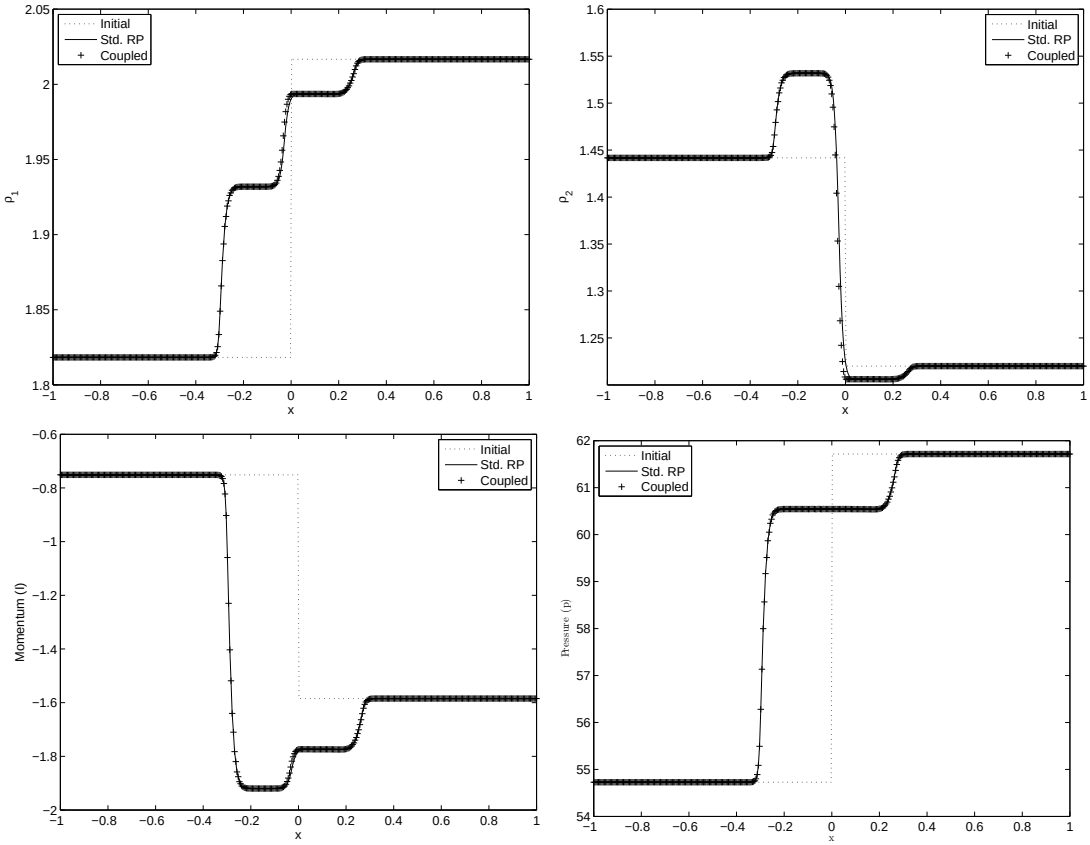

Figure 4.3: *Profiles of the densities ρ_1 and ρ_2, the momentum I, the common pressure p for the solution of standard Riemann problem (continuous line) and the Riemann problem at the junction with the use of the linearized Lax curves (crosses).*

$$U_1 = (2.2173,\ 1.3735,\ 1.5805), \quad U_2 = (0.4362,\ 1.5711,\ 3.7245).$$

The cross sections at the left and at the right of the junction are given by

$$c^- = 0.50, \quad c^+ = 1.5, \tag{4.49}$$

respectively. In Figure 4.5, we display for comparison the results for the pipes with the cross sections given in (4.49) and for the case $c^- = c^+$. It is clear that the change in the pipes cross sections influences the flow in the pipes. The jump in the junction decreases the pressures in the pipes.

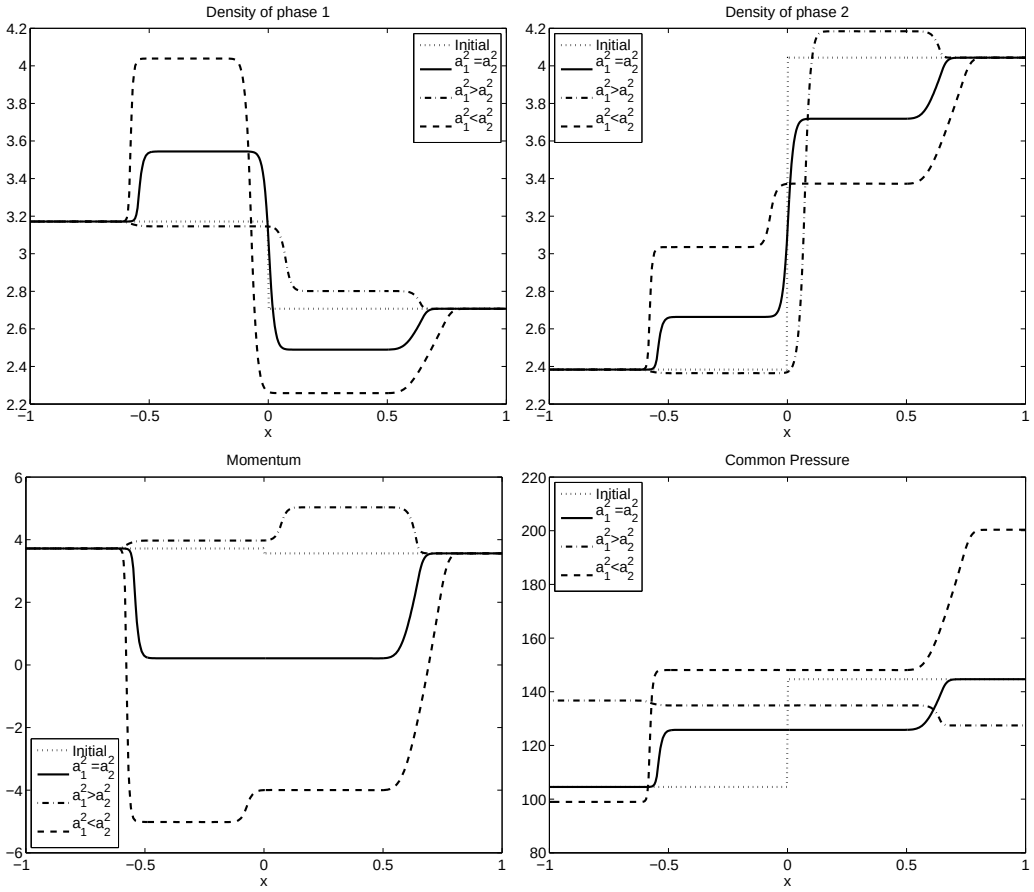

Figure 4.4: *Profiles of the densities, the momentum and the pressure for the Riemann problem for the drift flux model with different compressibility factors plotted at time* $t = 0.1$.

4.5.4 A junction with one incoming and two outgoing pipes

In this section we consider the nonlinear pressure law given in (4.7) and a junction with three pipes with one incoming and two outgoing pipes. We use for the numerical solution of the Riemann problem at the junction the linearization of the Lax curves

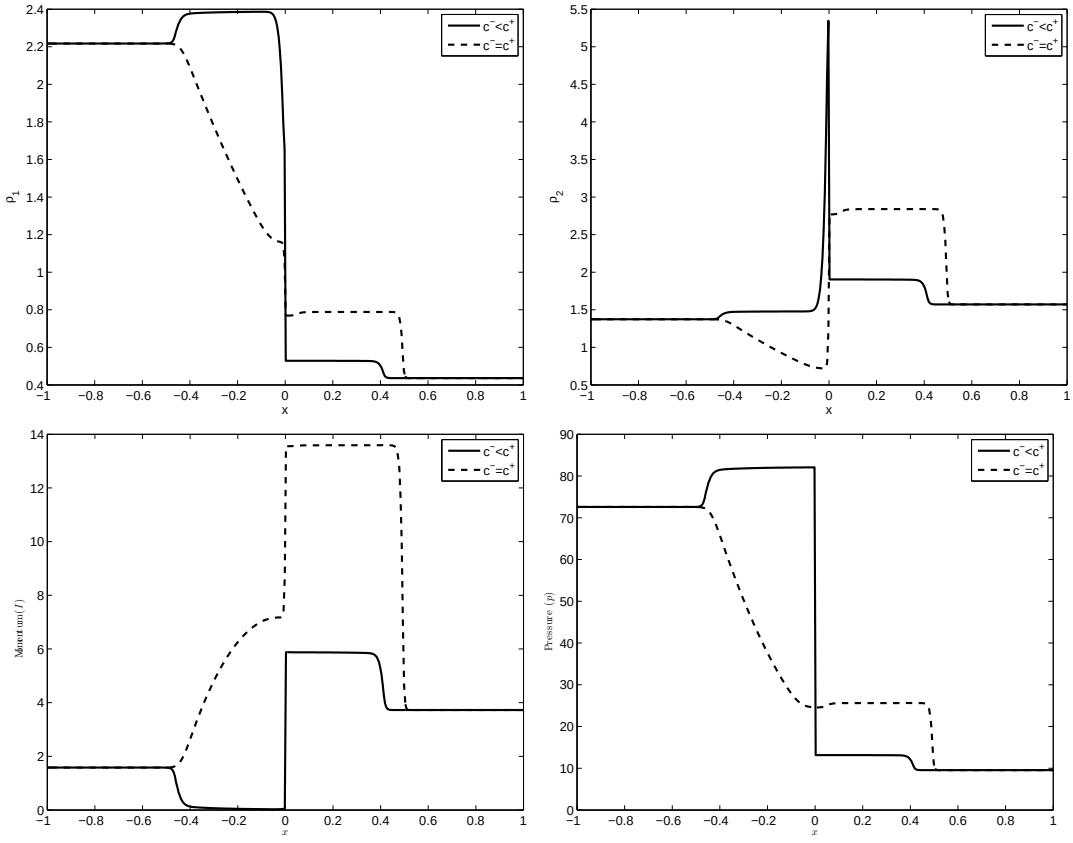

Figure 4.5: *Profiles of the densities, momentum and the pressure for a continuous and a discontinuous junction plotted at time* $t = 0.08$.

described above. The initial data in the pipes are taken as

$$\begin{aligned} U_1 &= (3.4500000,\ 2.4050000,\ 6.5056726); \\ U_2 &= (2.1300000,\ 4.1578000,\ 3.5720977); \\ U_3 &= (2.2534000,\ 2.4191412,\ 2.9335749). \end{aligned} \tag{4.50}$$

is stable and our simulation results agree with some real life observations.

These initial data satisfy the coupling conditions and belong to the subsonic region (4.34). The results are presented in Figure 4.6 for the densities and in Figure 4.7 for the momentum and pressure for times $0 \leq t \leq 0.08$. The dynamics are stable and we can see a wave moving in each pipe. Similar results were observed for the sim-

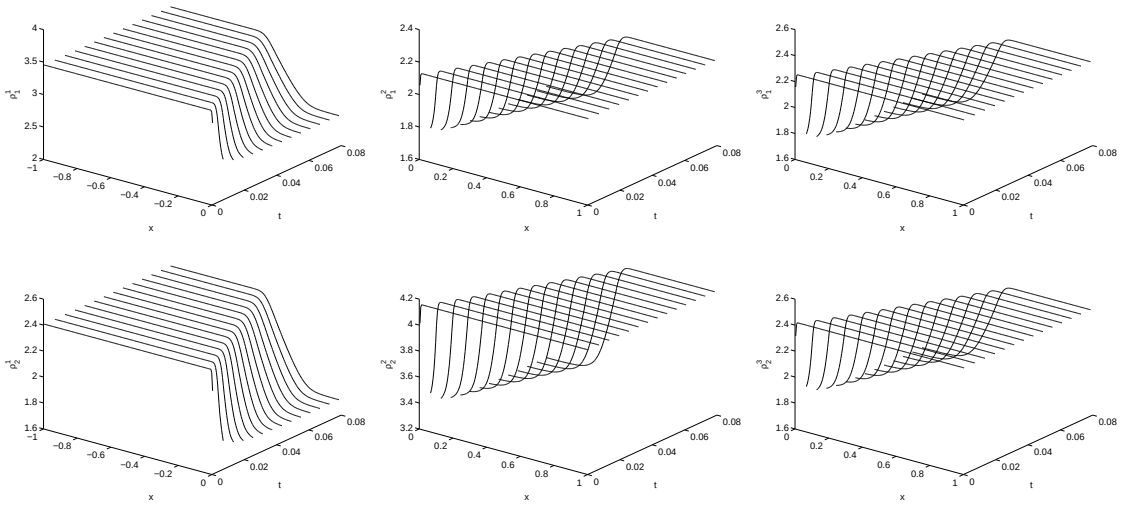

Figure 4.6: *Snapshots of the densities for the solution of the Riemann problem at the junction with one incoming and two outgoing pipes. The coupling conditions and the linearization of the Lax curves are used.*

ulation of the isothermal Euler equation in [7, 6]. Therein, the coupling conditions map were combined with the demand and supply function. Here the linearization of the Lax curves combined with the coupling conditions produce comparable results for the drift-flux model.

4.6 Concluding Remarks

In this chapter, the Riemann problem at a junction for the drift flux model with a general pressure law was solved. The linearization of the Lax curves have been used in an efficient way to compute the numerical solutions for some standard junctions. We have investigated the influence of the sonic speeds of each phase of the gas at the junction. We have proven that when the inflow is given and the coupling conditions are defined in a suitable way, one can solve for the outflow in the outgoing pipe.

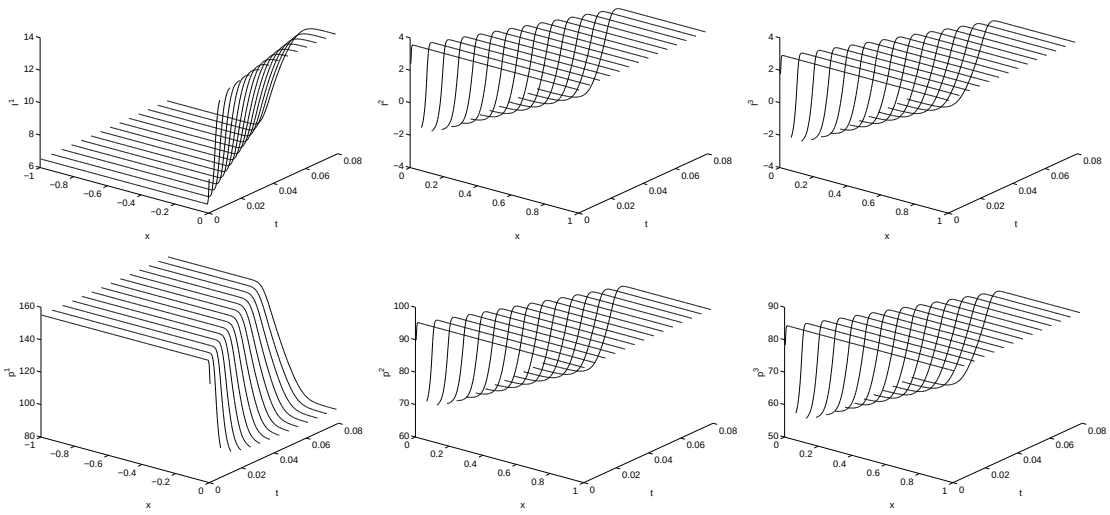

Figure 4.7: *Snapshots of the momentum (top) and pressure (bottom) in each pipe for the solution of the Riemann problem at the junction with one incoming and two outgoing pipes.*

Part III

The Use of the Shallow Water Equations for the Simulation of Water Networks and Pooled Stepped Chutes

Chapter 5

Time Domain Simulations of the Dynamics of River Networks

This chapter deals with the modeling and simulations of river networks. For each component of the network, the flow of water is described by the shallow water equations. At the intersections of connected rivers, we propose some coupling conditions that express, for example, the conservation of the mass of water or the equality of the water height. These coupling conditions are then used for the simulation of some classical river confluences. The results presented in this chapter appeared in [76].

5.1 Introduction

We consider the simulation over time of the dynamics of river networks. We assume that the flow in each river is described by the shallow water equations [43] and we resolve the dynamics by using some coupling conditions at the confluences of the rivers. Other approaches have been considered in the literature. Schulz and Steinebach [97] propose the use of two dimensional models in the case study of the Rhine river in Germany. Rissoan et al. [94] and Goutal et al. [57] suggested the use of a coupling of a two dimensional model and a one dimensional model at the confluence of the rivers.

Here we consider a one dimensional shallow water equations for the flow of water in each component of the network and at the confluence or junction, we use the the coupling conditions proposed by Rademacher et al. [99].

These coupling conditions are algebraic equations describing the relationship between the connected rivers at the intersection. The dynamics of the volume of water in a reservoir or a storage basin is modeled by a function of the flux of water into and out of the reservoir. This can be described by a system of differential equations.

The numerical integration of the shallow water equation plays an important role in the numerical simulations. Here we use a well-balanced upwind scheme. There exists several numerical methods for the numerical solution of the shallow water equations. The basic ideas have been discussed in Section 2.4. Moreover, these schemes need to satisfy some specific conditions, namely, the well-balanced property which requires that for steady state solutions, the convective part of the system of conservation law balances the source term; the positivity of the water height property which requires that at each step of the computation, the water height remain positive. This later property ensures that the computed solution remain physically relevant. Examples of such schemes can be found in [85, 108, 44, 45] or in the recent publications [2, 18].

The rest of this chapter is organized as follows. In Section 5.2, we introduce the formulation of the shallow water equations used to model the flow of water in the rivers. The properties of this system of conservation laws is reviewed and some parameters describing the characteristics of the flow are introduced. In Section 5.3, we present the coupling conditions used at the confluence of rivers' reaches. These are mainly the continuity of the water level at the intersection and the conservation of mass of water through the junction. In Section 5.4, numerical schemes used to solve the flow equation and the implementation of the coupling conditions are discussed. Some numerical examples are used to demonstrate the robustness and the efficiency of this approach.

5.2 Modeling the Dynamics of a River

An open channel flow is a flow system in which the top surface of the fluid is exposed to the atmosphere. Rivers and dams fall under this definition. In this section, we will present the modeling of the rivers, dams and thereafter define the coupling conditions necessary for a network.

5.2.1 The Shallow Water Model

To model the flow of water in a river the conservation of mass and momentum of the flow is considered. The model is derived from the depth averaging of the incompressible flow models. In general, to model the conservation of mass along the flow direction in a channel of arbitrary cross-section one considers the cross-sectional area of water $A\ [L^2]$, at time $t[s]$ and point $x\,[L]$ as presented in Figure 5.1. At any position x along the river, the rate of change of the cross-sectional area of the river is a result of the gradient of the total volume flow rate also known as discharge Q. This might be balanced by other mass source or sink terms S_m (for example, rainfall, evaporation, seepage, runoff) to give equation (5.1a) in which ∂_t is a partial derivative with respect to time and ∂_x is a partial derivative with respect to space. One also refers to $S_m\,[L^2/T]$ as the volume flux per unit length into the stream. Equation (5.1b) describes the balance of momentum: the rate of change of the discharge depends on the flow of momentum, Q^2/A, the hydrostatic pressure term I_1, the effect of the forces exerted by the channel walls on the flow I_2, the bottom slope of the channel S_0, and the frictional forces at the bottom S_f.

$$\partial_t A + \partial_x Q = S_m \tag{5.1a}$$

$$\partial_t Q + \partial_x \left(\frac{Q^2}{A} + gI_1 \right) = g\left(I_2 + A(S_0 - S_f)\right). \tag{5.1b}$$

Here, $A(x,t)$ is the wetted cross-section area:

$$A(x,t) = \int_{B(x)}^{B(x)+h(x,t)} \sigma(x,y)\, dy,$$

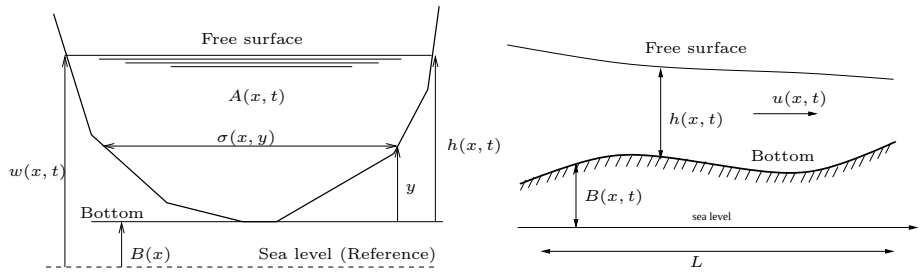

Figure 5.1: *Cross section at x (left) and side view of the river (right)*

while x is the longitudinal position in the river. The river is assumed to be of length L and t is time. The hydrostatic pressure term, $I_1 = I_1(x,h)$ is defined as

$$I_1 = \int_{B(x)}^{B(x)+h} (h-y)\sigma(x,y)dy, \tag{5.2}$$

where σ is the channel breadth, h the channel depth and y the coordinate in the vertical direction. On the other hand $I_2 = I_2(x,h)$ is the term that accounts for the forces exerted by the channel walls at the contractions and expansions due to longitudinal width variations

$$I_2 = \int_{B(x)}^{B(x)+h} (h-y)\frac{\partial \sigma}{\partial x}(x,y)dy. \tag{5.3}$$

Note that $h = h(x,A)$ is the water depth. Due to their geometric interpretation, we have that

$$\sigma(x,y) > 0 \text{ for all } x \in [0,L] \text{ and } y \geq 0. \tag{5.4}$$

The bottom slope S_0 is given by

$$S_0 = -\frac{dB}{dx}(x) \tag{5.5}$$

where $B = B(x)$ describes the bottom topography (bottom elevation) of the channel. Any erosion effects are likely to happen in a much longer time scale than the dynamics of interest in this chapter. The friction term is given as

$$S_f = -\frac{n_m^2 Q|Q|}{A^2 R^{4/3}} \tag{5.6}$$

where n_m is the Manning's roughness coefficient, given in tables, see for example [84]; and the hydraulic radius $R = A/P$, P being the wetted perimeter of the river at position x.

When the channel cross section is locally rectangular, triangular or trapezoidal, the pressure force integrals I_1 and I_2 can be expressed as

$$I_1 = h^2\left(\frac{\sigma_0}{2} + \frac{hZ}{3}\right), \quad I_2 = h^2\left(\frac{1}{2}\frac{\partial\sigma_0}{\partial x} + \frac{h}{3}Z_x\right)$$

where σ_0 is the channel bottom width (with $\sigma_0 = \sigma$ for rectangular channel) and Z is the slope of the channel (vertical to horizontal). For the case of rectangular cross section, the model (5.1) takes the simplified form

$$\begin{aligned} \partial_t A + \partial_x Q &= S_m && \text{(5.7a)} \\ \partial_t Q + \partial_x\left(\frac{Q^2}{A} + \frac{1}{2}g\sigma h^2\right) &= gh\left(\frac{1}{2}h\sigma' - \sigma B'\right), && \text{(5.7b)} \end{aligned}$$

where the prime stands for the derivative with respect to the space variable x. The convective part of the model (5.7), that is the model (5.7), with a vanishing right hand side, is strictly hyperbolic. Indeed, the Jacobian matrix of the flux function is given by

$$J = \begin{pmatrix} 0 & 1 \\ g\frac{A}{\sigma} - u^2 & 2\,u \end{pmatrix},$$

where $u = Q/A$ is the stream-wise velocity of the fluid. The eigenvalues and eigenvectors are given by $\lambda_\mp = u \mp \sqrt{gA/\sigma}$ and $e^\mp = (1,\, \lambda_\mp)^T$, respectively. Therefore when $A/\sigma > 0$, the system (5.7) is strictly hyperbolic.

We assume a rectangular channel, so that

$$A = \sigma\, h \quad \text{and} \quad Q = A\, u = \sigma\, h\, u$$

and substituting in (5.7) we recover, by dividing by σ and assuming that $S_m = 0$, the usual form of the shallow water equations in terms of the water height h,

$$\begin{aligned} \partial_t h + \partial_x(hu) &= 0 \\ \partial_t(hu) + \partial_x\left(h\,u^2 + \tfrac{g}{2}h^2\right) &= -ghB'. \end{aligned} \qquad (5.8)$$

In the rest of this chapter, we will be mainly interested in the water height $w = h+B$ (see Figure 5.1) and the quantity hu that we denote again for clarity as $Q = hu$. Simple algebra helps to transform (5.8) to

$$\begin{aligned} \partial_t w + \partial_x Q &= 0 \\ \partial_t Q + \partial_x \left(\frac{Q^2}{w-B} + \frac{g}{2}(w-B)^2 \right) &= -g(w-B)B'. \end{aligned} \tag{5.9}$$

It is this form of the shallow water equations that we will later use for the numerical simulations.

Since the original form of the shallow water equations [44] are derived under the assumptions of the conservation of the volume of water without taking into account the effect of rainfall, evaporation and seepage, we choose the source term in the mass balance equation to account for these effects. To fix ideas, we choose a source term that takes into account rainfall, evaporation, seepage and infiltration. This information is obtained by measurement and is given in the literature by coarse models derived from the interpolation of data [57, 65] . The rainfall rate, $r(t)$, can be obtained from a meteorological station situated near the river. The evaporation rate, $e(t)$ depends on the surface of the river and the weather. Seepage and infiltration rate, $s(t)$, depend on soil water content and groundwater resources. Putting these together, the source term is then given by

$$S_m(t) = r(t) - e(t) - s(t).$$

We conclude this section by pointing out some flow behaviors that arise in the simulation of river flows.

5.2.2 Characteristics of the flow

We briefly discuss the characteristic of the flow in open-channels. One parameter that characterizes the flow in an open channel is the Reynolds number. It is given by

$$N_R = \frac{|u|R}{\nu} \tag{5.10}$$

where u is the average velocity of the flow, R is the hydraulic radius and ν is the kinematic viscosity of the fluid. Laminar flow occurs when $N_R < 500$ and turbulent flow occurs when $N_R > 2000$. The transition region corresponds to the Reynolds number in the range 500 to 2000, see [84]. Besides the viscosity versus inertial forces that are captured by the Reynolds number, the ratio of inertial forces to gravity forces, given by the Froude number, plays an important role in the characterization of open channel flows. It is given by

$$N_F = \frac{|u|}{\sqrt{g y_h}} \tag{5.11}$$

where y_h, called the hydraulic depth, is given by $y_h = A/T$ with A being the wetted cross-section area and T being the width of the free surface of the fluid at the top of the channel. When the Froude number is equal to 1.0, that is, when $|u| = \sqrt{g y_h}$, the flow is called a critical flow. When $N_F < 1.0$, the flow is subcritical (or fluvial) and the flow is dubbed supercritical (or torrential) when $N_F > 1.0$, see [84].

When one consider a channel with a locally rectangular cross section, the Froude number simplifies to

$$N_F = \frac{|u|}{\sqrt{gh}},$$

where h is the water height. This expression is closely related to the eigenvalues of the flux function of the shallow water equations in this case.

5.3 Coupling of confluencing rivers

We index the rivers and the quantities associated with them by $i \in \mathcal{I} = \{1, \ldots, n\}$. We label the locations of the end points of the canals and dams, which we shall refer to as nodes, by $j \in \mathcal{J} = \{1, \ldots, m\}$. We distinguish between multiple nodes, indexed by $j \in \mathcal{J}_M$, at which various rivers come together, and simple nodes, indexed by $j \in \mathcal{J}_S$, which are endpoints of a single river. For $j \in \mathcal{J}$, we introduce

$$\mathcal{I}_j = \{i \in \mathcal{I} : \text{the } i^{\text{th}} \text{river meets the } j^{\text{th}} \text{ node}\}.$$

For each river $i \in \mathcal{I}$, the dynamics is described by the model (5.9), that is,

$$\partial_t w_i + \partial_x Q_i = 0, \tag{5.12a}$$

$$\partial_t Q_i + \partial_x \left(\frac{Q_i^2}{w_i - B} + \frac{1}{2} g (w_i - B_i)^2 \right) = -g(w_i - B_i) B_i', \tag{5.12b}$$

where B_i is the bottom elevation in channel i. We will look at different common types of intersection that are encountered in real life water networks.

5.3.1 Intersection of three rivers with the same strength

Here we consider three rivers of equal strength (i.e. similar breadths and wetted cross-sectional areas) meeting at a node 1. The configuration is depicted in Figure 5.2.

In this case, we prescribe the Rankine-Hugoniot condition at the junction:

$$Q_3 = Q_1 + Q_2.$$

This condition simply ensures that the volume flux in reach 3 at the intersection is equal to the volume flux from reach 1 and reach 2. We also impose equal water level at the intersection, that is, we have at the junction,

$$w_3 = w_2 = w_1.$$

These conditions are physically motivated and ensure the conservation of mass of water as well as the continuity of the water height at the junction.

5.3.2 Intersection of a river and a tributary

Now we consider the confluence of a large river and a small tributary as shown in Figure 5.3. The width of the tributary is assumed to be small compared to that of the main river. We are mainly interested in the influence of the tributary on the main river downstream from the confluence point. One can consider a model for which the water flow in the tributary is computed first and then, the data is used as

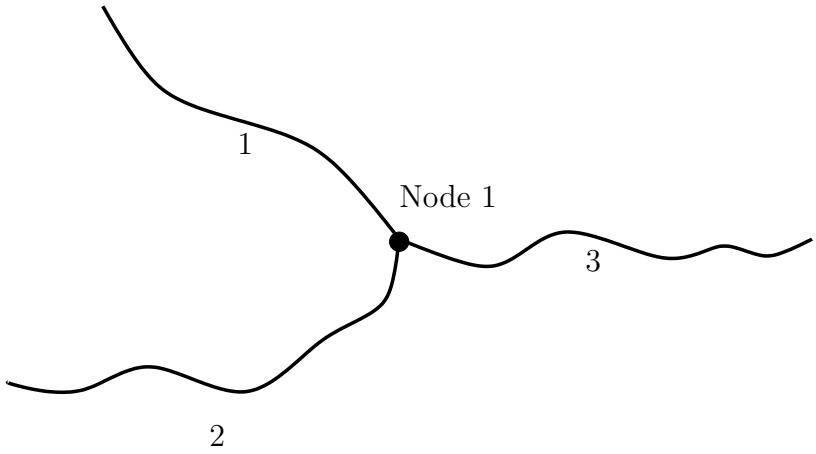

Figure 5.2: *Junction of three rivers of equal strength*

a source term for the computation in the main river. With this one way coupling, it is hardly possible to take into account flow information from the large river into the model of the tributary. We will assume here that the rivers are well instrumented. Precisely, we assume that there is a gauge station located directly downstream the relevant tributary at the confluence point . Therefore, the water level information $w_g(t)$, from the gauge station is used for a lower boundary condition for the tributary,

$$w_1(t, \bar{x}) = w_g(t). \tag{5.13}$$

Once the tributary model has been run, its calculated outflow at the junction $Q_1(t, \bar{x})$ must be considered as a lateral inflow

$$S_{m2} = \begin{cases} 0 & \text{if } x < \bar{x}, \\ Q_1(t, \bar{x})/(x - \bar{x}) & \text{if } x > \bar{x}, \end{cases}$$

to the main river after the confluent point. This ensures that the tributary affects the main river near to the junction only. Far from the junction, the effect of the tributary on the main river vanishes. For the implementation, the condition $x - \bar{x} < 0$ may be replaced by the more practical one $|x - \bar{x}| < \varepsilon$ where $\varepsilon > 0$ is a very small number.

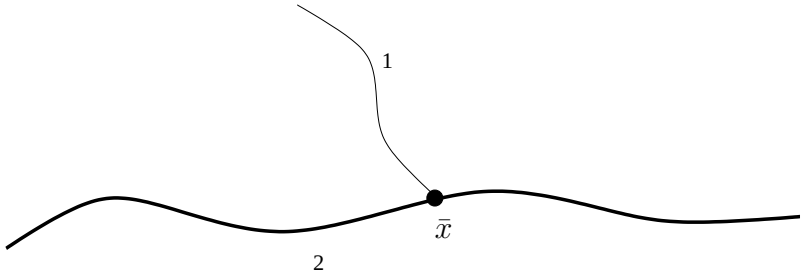

Figure 5.3: *A river and its tributary*

5.3.3 Coupling conditions for a weir and a storage basin

A weir is modeled by splitting the river into a reach upstream and a reach downstream the weir. The downstream boundary condition of the upstream reach is given as in (5.13), that is

$$w_{\text{upstream}} = f(Q_{\text{upstream}}, t).$$

Some rivers are steered in a way that the water level directly upstream of the weir is practically constant over time. This translates in the new coupling condition

$$w_{\text{upstream}} = \text{Constant}.$$

In any case, the upstream water level at the downstream reach needs to be smaller than the water level downstream of the upstream reach. When floods occur, this condition can be violated. Then, to ensure a good resolution of the flow equation, the boundary condition at the downstream of the upstream reach needs to have the form [99]:

$$w_{\text{upstream}}(t) = \max\left\{w_{\text{downstream}}(t), f(Q_{\text{upstream}}, t)\right\}.$$

For the discharge, we prescribe naturally the conservation of mass at the interface:

$$Q_{\text{upstream}} = Q_{\text{downstream}}.$$

The effective flow area is treated as interconnecting storage basins, for which a relation between storage volume and water level is known or assumed. The flow calculation between the basins is based on the continuity of volume for each basin

and non-inertial flow laws between basins. Continuity of volume in a reservoir or storage basin j is expressed as [57]

$$\frac{\partial V_j}{\partial t} = \sum_{i=1}^{n} Q_{ij}, \tag{5.14}$$

where $V_j\,[m^3]$ is the volume of water in the basin j; n is the number of connections leading to basin j, $Q_{ij}[m^3/s]$ is the discharge from basin i to basin j or from river i to basin j.

5.4 Numerical Approach to Approximate Network Dynamics

A simple discretization of the shallow water equation may follow a standard finite volume approach as presented in Section 2.2. From the cell averages

$$v_j = \frac{1}{\Delta x_j} \int_{x_{j-1/2}}^{x_{j+1/2}} v(x,t)dx$$

an integration of the non homogeneous conservation law

$$\partial_t v + \partial_x f(v) = g(v)$$

over $I_j = [x_{j-1/2}, x_{j+1/2}]$ leads to

$$\partial_t v_j = -\frac{1}{\Delta x_j}\left(f(v(x_{j+1/2},t)) - f(v(x_{j-1/2},t))\right) + \frac{1}{\Delta x_j}\int_{x_{j-1/2}}^{x_{j+1/2}} g(v)dx. \tag{5.15}$$

As in Section 2.4, one can write the scheme (5.15) in the semi-discrete form

$$\frac{d}{dt}\mathbf{V}_j = -\frac{H_{j+\frac{1}{2}} - H_{j-\frac{1}{2}}}{\Delta x} + G_j \tag{5.16}$$

where $H_{j+\frac{1}{2}}$ is the numerical flux and G_j is an approximations of the source term in the cell I_j,

$$G_j \approx \frac{1}{\Delta x_j}\int_{x_{j-1/2}}^{x_{j+1/2}} g(v)dx.$$

G_j can be obtained with an integration quadrature. Here we use the mid-point rule. The shallow water equation admits steady states solution (lake at rest, for example); therefore a numerical solution should preserve such a solution and, more generally, its small perturbations. A numerical scheme that satisfies this condition is known as a *well-balanced* scheme. Another desirable property for a numerical scheme for the shallow water equation is that of positivity preserving. This property ensures a correct resolution of dry bed where the water depth is very small. In this case, due to inherent numerical oscillations, the water height can take a non-positive value and can lead to nonphysical solutions. Some example of schemes satisfying these properties are presented in [108, 44, 45, 74]. In [45] the numerical solution of the shallow water equation was found as the kinetic limit of a relaxation system.

For the simulation of confluencing rivers, we discretize the simulation time t_s according to the mesh $t_n = n\Delta t$ for $n = 0, 1, ..., N$ where N satisfies $t_s = N\Delta t$. For each simulation step, we solve the flow equation for $t \in [t_n, t_{n+1}]$, we adjust the coupling and boundary conditions and iterate the process. These steps are summarized in the flow diagram presented in Table 5.1.

- Start with initial data in each river such that the coupling and boundary conditions are satisfied.
- For each simulation time interval $[t_n, t_{n+1}]$ do the following:
  - Solve the flow equation for each river for $t \in [t_n, t_{n+1}]$;
  - Adjust the boundary and coupling conditions.

Table 5.1: *Flow diagram for the computer program for the simulations*

5.5 Numerical Examples and Results

Now we consider some examples of water network simulations.

5.5.1 Dam-break wave simulation

We consider the dam-break problem in a rectangular channel with flat bottom $B = 0$. This is a well known problem in water waves simulation. For more details, we refer the interested reader to [44, 108, 98].
We compute the solution on a channel with length $L = 2000\,m$ for time $t = 20$s and with initial condition

$$u(x,0) = 0,$$
$$h(x,0) = \begin{cases} h_1, & x \leq 1000 \\ h_0, & x > 1000. \end{cases}$$

with $h_1 > h_0$. We consider two cases both with $h_1 = 10$ m: Case (a) the depth ratio $h_0/h_1 = 0.7$ and case (b) the depth ratio $h_0/h_1 = 0.01$. The dam collapse at time $t = 0$ and we have a shock wave (bore) traveling downstream, a rarefaction wave (depression wave) traveling upstream (see Figure 5.4).

For case(a), the flow remains subcritical throughout the channel where as for case (b) the flow is supercritical in the vicinity of the dam and subcritical far away from the dam which is situated at $x = 1000$, see Figure 5.5.

5.5.2 Simulation of three connected rivers of equal strength

The setup for this simulation is as described in Section 5.3.1. We consider three rivers of equal strength meeting at the junction. The flow in each river reach is simulated by the numerical discretization of the shallow water as described above and the coupling conditions are introduced as interior boundary conditions. Here as in the case of the dam-break wave simulation, we assume that the rivers have a flat bottom. To drive the flow, we introduce a dam–break in each river.

We assume that the three rivers have equal length $L = 2000$m. The bottom topography is the same in each river i.e $B_1 = B_2 = B_3 = 0.5$ m. The first and second river are incoming to the junction and the third river is outgoing. The confluence is at $x = 0$. The results for the numerical simulations for the water levels and the discharges in each river are shown in Figure 5.6 and Figure 5.7. There appears a

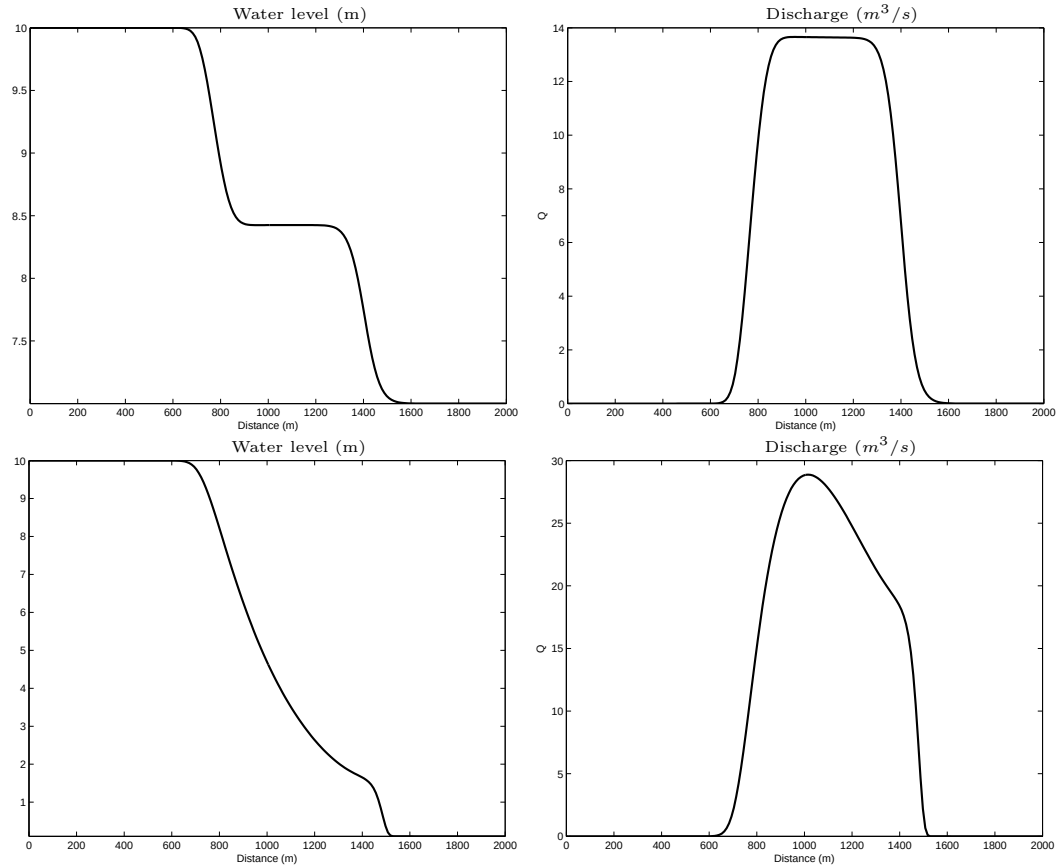

Figure 5.4: *Water level (left) and discharge (right) for the dam-break problems*

hydraulic jump in the first river which dissipates at the intersection. The flow in the third river is more uniform. This results from the effect of the intersection. The complex dynamics in the first river and the second river lead to a more stable and uniform flow in the third river.

5.5.3 Simulation of a main river with a tributary

Here we use the coupling mechanism presented in Section 5.3.2. The width of the tributary is chosen so that it is a tenth of the width of the main river. The elevations of the river beds are assumed to be constant. Here we are interested in the effect of

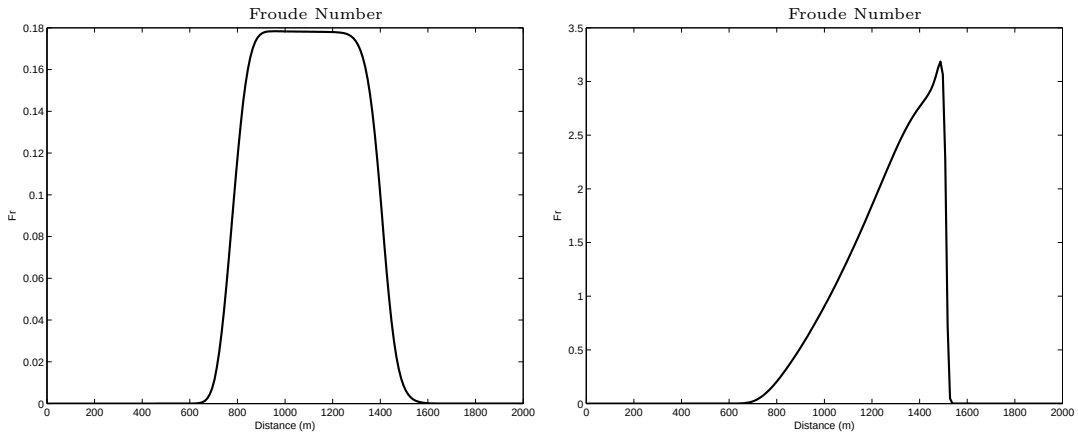

Figure 5.5: *Froude Number for the dam-break problem with the depth ratio* $h_0/h_1 = 0.7$ *(left) and* $h_0/h_1 = 0.01$ *(right)*

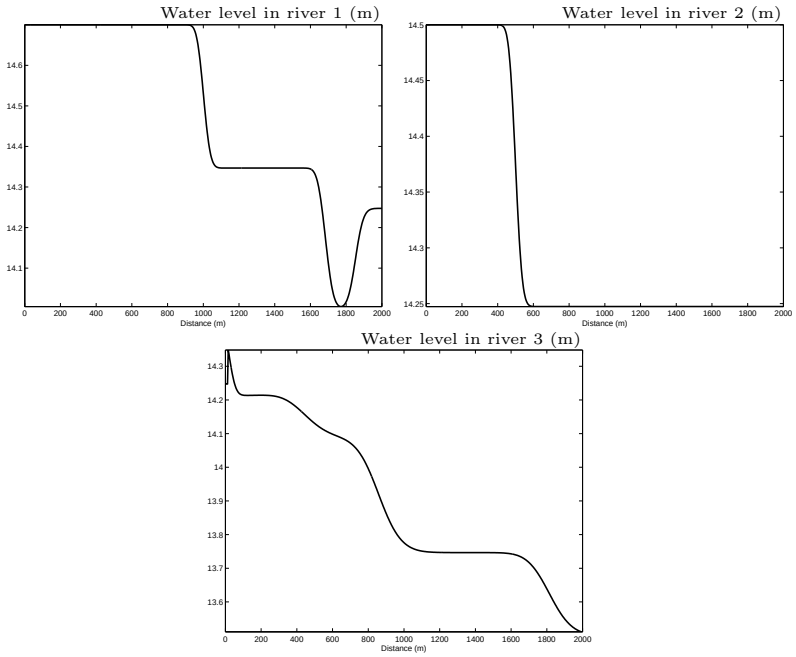

Figure 5.6: *Water level in each river at time* $t = 40s$ *for the simulation of three rivers of same strength*

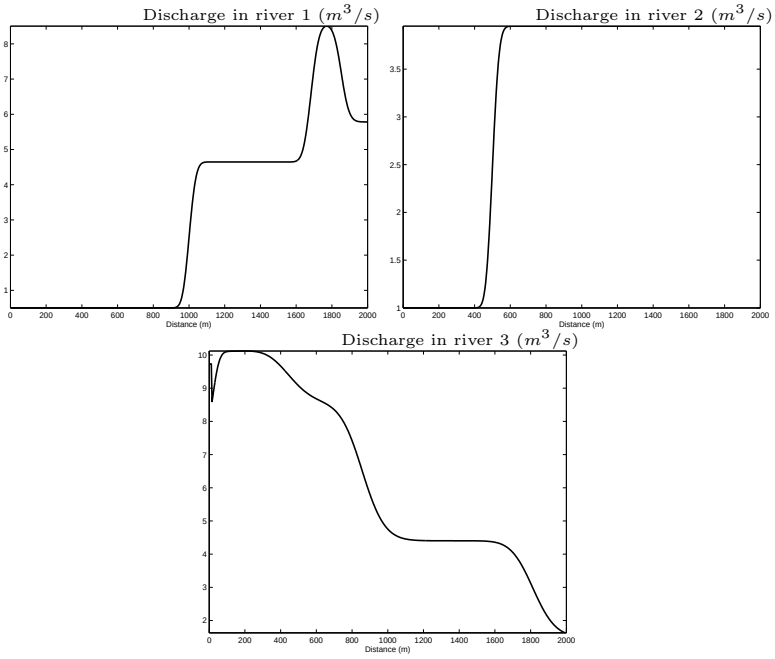

Figure 5.7: *Discharge in each river for the simulation of three rivers of same strength*

the tributary on the main river. A dam break is driving the flow in the tributary river with the downstream initial water height being $h = 4\,m$. We start the simulation with water flowing at constant height and velocity in the main river. The initial water height is $h = 4.0\,m$ and the initial discharge is $q = 0.45\,m^2/s$. We plotted in Figure 5.8 the water levels and the discharge in the main river. We can see that the influence of the tributary on the main river is limited to the neighborhood of the confluence region located at $x = 1000\,m$ downstream the main river.

5.5.4 Simulation of a reservoir or a storage basin

Here we consider a reservoir with arbitrary geometry. We assume that a river, say river 1 flows into the reservoir and another river, river 2, flows out of the reservoir. We are interested in the volume of water in the reservoir. The dynamics of that volume of water follows the model equation (5.14) with $n = 2$. Here one can assume

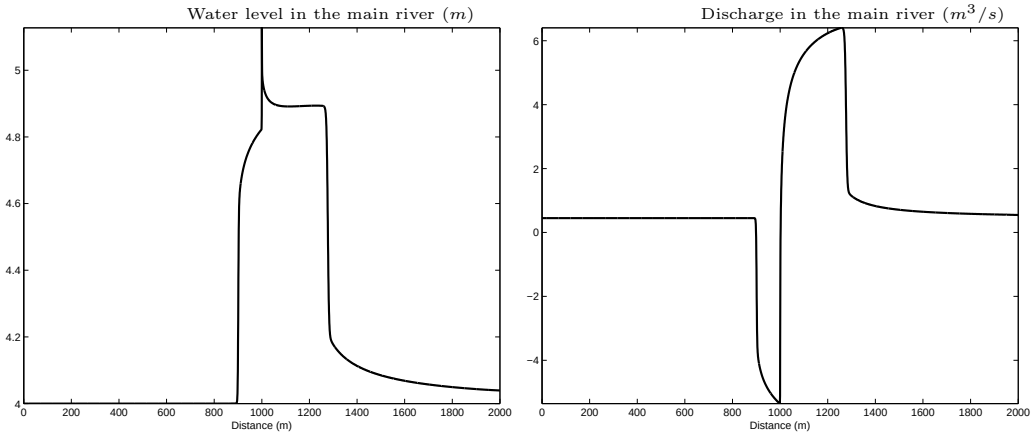

Figure 5.8: *Water height (left) and discharge (right) in the main river at time* $t = 15s$. *The influence of the tributary on the main river is more relevant about* $x \in (950, 1200)$, *that is a neighborhood of the location of the tributary.*

that there is a pumping station located upstream of river 1. When the filling capacity of the reservoir is reached, the pump is switched off and the water level in river 1 and river 2 remain constant with the same discharge; leading to a constant volume of water in the reservoir. This behavior is well seen in the simulation results presented in Figure 5.9. The initial volume of water in the reservoir is given by $V_0 = 1000\text{m}^3$ and the simulation is carried out for time span of $t_s = 80$ seconds.

5.6 Concluding Remarks

In this Chapter, we have reviewed and implemented some coupling mechanisms at the confluences of a river network. The proposed coupling conditions for the case of three confluencing rivers are very similar to the cases studied by Colombo et al. [33, 32, 38] for the p-system or by Banda et al [10] for the multiphase drift-flux model. These authors considered the case of a network of pipes. Further work will include the coupling of supercritical flow, or the case of time dependent flow beds.

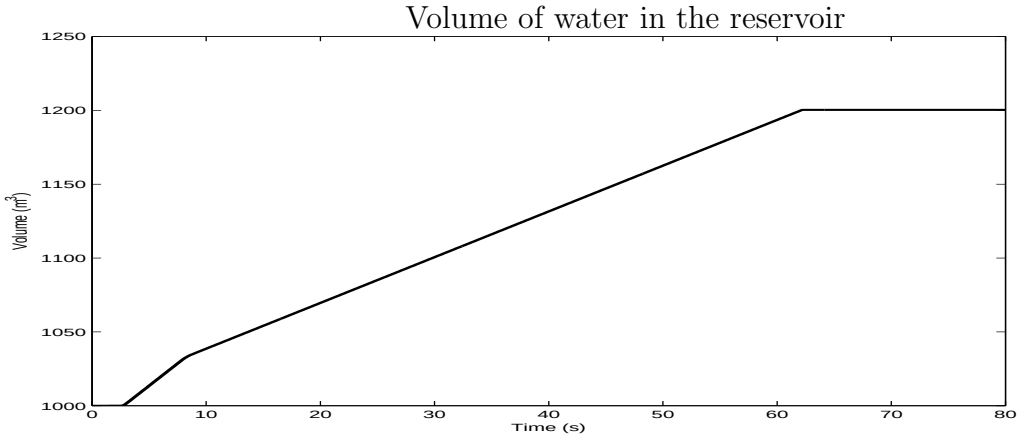

Figure 5.9: *Evolution of the volume of water in the reservoir with time*

Chapter 6

The Use of the Shallow Water Equations for the Simulation of Pooled Stepped Chutes

6.1 Introduction

In recent years, stepped spillways have become more popular to discharge flood waters because of their good energy dissipation and low cavity risks. Important research in the hydraulic community has focused on the investigation of the complex flow and provided guidelines for the design of such hydraulic structures. These structures have been tested and validated experimentally, and some empiric formula were derived by Boes and Hager [13] to find the water height at any point in a canal with pooled stepped chutes.

In this chapter, we consider the flow of water in such canals with pooled stepped chutes. Differently from the hydraulic community, we consider that the water flow is modeled by the shallow water equations. Moreover, we compute independently the water flow between the horizontal steps and we coupled the dynamics using suitable coupling conditions. This work has two important objectives. Firstly, we validate the coupling conditions of the type discussed in the previous chapters with

the results from the literature and secondly, we propose a new computational tool for the analysis of pooled stepped chutes. The rest of the chapter is organized as follows. The formulation of the water model is presented in Section 6.2. Also, in the same section, we solve analytically and numerically the standard Riemann problem. This is an important preliminary step for the solution for coupled rivers. In Section 6.3, we present the dynamics for two coupled rivers in the framework of a Riemann problem at the dam. We propose some coupling conditions motivated by the physics of the problem and we prove a result for the existence of a solution satisfying some technical conditions. In Section 6.4, we present some numerical results of the simulation of the dynamics. Moreover we compare the water height at the dam obtained with the coupling conditions and an empirical formula obtained in the hydraulic community via experiments. The two results agree in the sense that the error is "small".

6.2 Model formulation and preliminary results

Here we are interested in the shallow water equation in 1D given by

$$\begin{cases} \partial_t h + \partial_x q &= 0, \\ \partial_t q + \partial_x (\frac{q^2}{h} + \frac{1}{2} g h^2) &= 0, \end{cases} \tag{6.1}$$

where h is the water height and $q = hu$ is the discharge. A source term that accounts for the bottom topography or friction can be added to this model depending on the applications. As discussed in Chapter 5, the flow is generally characterized by the Froude number defined as

$$Fr = \frac{u}{\sqrt{gh}}.$$

The flux function for the shallow water equation $f(h, q) = (q, hu^2 + \frac{1}{2} g h^2)^T$ enjoys the following properties. The eigenvalues and eigenvectors of the Jacobian matrix

of the flux function are given by

$$\begin{aligned} \lambda_1(h,q) &= \tfrac{q}{h} - \sqrt{gh}, \quad r_1(h,q) = \begin{pmatrix} 1 \\ \lambda_1(h,q) \end{pmatrix}; \\ \lambda_2(h,q) &= \tfrac{q}{h} + \sqrt{gh}, \quad r_1(h,q) = \begin{pmatrix} 1 \\ \lambda_2(h,q) \end{pmatrix}. \end{aligned} \tag{6.2}$$

In the rest of the chapter, we restrict ourselves to the subsonic region of the states (h,q) such that

$$\lambda_1(h,q) < 0 < \lambda_2(h,q). \tag{6.3}$$

The 1- and the 2- field are genuinely nonlinear since $\nabla\lambda_1(h,q)\cdot r_1(h,q) = -\frac{3}{2}\sqrt{\frac{g}{h}}$ and $\nabla\lambda_2(h,q)\cdot r_2(h,q) = \frac{3}{2}\sqrt{\frac{g}{h}}$. The (standard) Riemann problem for (6.1) consists of the conservation law equation (6.1) and a Heaviside-type initial data

$$(h,q)(x,0) = \begin{cases} (h_l,q_l) & \text{if} \quad x<0, \\ (h_r,q_r) & \text{if} \quad x>0, \end{cases} \tag{6.4}$$

where the left state $U_l = (h_l, q_l)$ and the right state $U_r = (h_r, q_r)$ are given. The construction of the exact solution of the Riemann problem follow the standard techniques. One introduces the admissible Lax shock curves, $S^{\pm}_{1,2}$, emanating from a state $(\bar{h},\bar{q})$ as the solution of the Rankine-Hugoniot jump condition [78] and the admissible rarefaction curves, $R^{\pm}_{1,2}$, as integral curves of the eigenvectors r_1 and r_2 and obtain the admissible Lax curves given by

$$L_1^+(h,\bar{h},\bar{q}) = \begin{cases} S_1^+(h,\bar{h},\bar{q}) = \frac{\bar{q}}{\bar{h}}h - \frac{(h-\bar{h})}{2h}\sqrt{2g(\bar{h}^2h+\bar{h}h^2)} & h \geq \bar{h} \\ R_1^+(h,\bar{h},\bar{q}) = \frac{\bar{q}}{\bar{h}}h - 2\sqrt{g}(\sqrt{h}-\sqrt{\bar{h}})h & h \leq \bar{h}; \end{cases} \tag{6.5a}$$

$$L_1^-(h,\bar{h},\bar{q}) = \begin{cases} S_1^-(h,\bar{h},\bar{q}) = \frac{\bar{q}}{\bar{h}}h - \frac{(h-\bar{h})}{2h}\sqrt{2g(\bar{h}^2h+\bar{h}h^2)} & h \leq \bar{h} \\ R_1^-(h,\bar{h},\bar{q}) = \frac{\bar{q}}{\bar{h}}h - 2\sqrt{g}(\sqrt{h}-\sqrt{\bar{h}})h & h \geq \bar{h}; \end{cases} \tag{6.5b}$$

$$L_2^+(h,\bar{h},\bar{q}) = \begin{cases} S_2^+(h,\bar{h},\bar{q}) = \frac{\bar{q}}{\bar{h}}h + \frac{(h-\bar{h})}{2h}\sqrt{2g(\bar{h}^2h+\bar{h}h^2)} & h \leq \bar{h} \\ R_2^+(h,\bar{h},\bar{q}) = \frac{\bar{q}}{\bar{h}}h + 2\sqrt{g}(\sqrt{h}-\sqrt{\bar{h}})h & h \geq \bar{h}; \end{cases} \tag{6.5c}$$

$$L_2^-(h,\bar{h},\bar{q}) = \begin{cases} S_2^-(h,\bar{h},\bar{q}) = \frac{\bar{q}}{\bar{h}}h + \frac{(h-\bar{h})}{2h}\sqrt{2g(\bar{h}^2h+\bar{h}h^2)} & h \geq \bar{h} \\ R_2^-(h,\bar{h},\bar{q}) = \frac{\bar{q}}{\bar{h}}h + 2\sqrt{g}(\sqrt{h}-\sqrt{\bar{h}})h & h \leq \bar{h}. \end{cases} \tag{6.5d}$$

The shock speeds are given by

$$s_{1,2} = \frac{\bar{q}}{\bar{h}} \mp \frac{\sqrt{g}}{\bar{h}\sqrt{2}} \sqrt{h\bar{h}(h+\bar{h})}. \tag{6.6}$$

The solution of the Riemann problem is then found as a juxtaposition of fixed states separated by the Lax curves. For given left and right states, the solution for the Riemann problem is constructed as in Figure 6.1 where we present also a numerical computation of the water height using a Godunov scheme. As expected the solution consists of a rarefaction wave traveling to the left and a shock wave moving to the right.

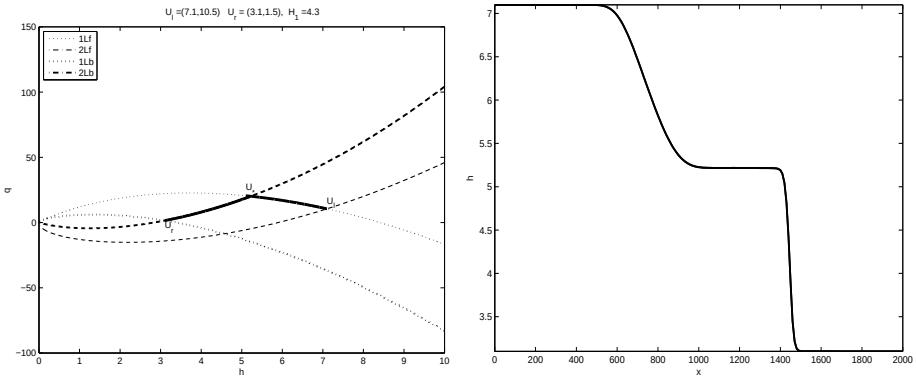

Figure 6.1: *The exact construction of the solution of the Riemann problem for the shallow water equation via the Lax curves(left) and a computed numerical solution (right).*

Remark 6.1. *From the subsonic hypotheses* (6.3)*, we see that waves traveling on the 1-Lax curve have non-positive speed. Indeed, we have*

$$\frac{ds_1}{dh}(h, \bar{h}, \bar{q}) = -\frac{1}{4} \frac{\sqrt{2}g(\bar{h}+2h)}{\sqrt{gh\bar{h}(h+\bar{h})}} < 0 \quad \forall h, \bar{h} > 0. \tag{6.7}$$

Therefore, along the 1-shock curve, the shock speed is decreasing. Moreover, $s_1(\bar{h}, \bar{h}, \bar{q}) = \lambda_1(\bar{h}, \bar{q}) < 0$*. Hence, the shock speed remains non-positive for* $h \geq \bar{h}$*. The rarefaction curves travel at the characteristic speed* $\lambda_1(h, q)$ *which is non-positive in the subsonic region* (6.3)*.*

6.3 Dynamics at the stepped chute

Now we consider a pooled stepped chute as illustrated in Figure 6.2. We assume that the upstream reach (or river) is represented by the interval $x < 0$ and the downstream reach by $x > 0$ and the step, that we call a *dam*, is located at $x = 0$. This is a standard step in a pooled stepped chute canal. The step has a height of $H_2\, m$ and a weir of height $H_1\, m$ is added above the step. In each river, the shallow

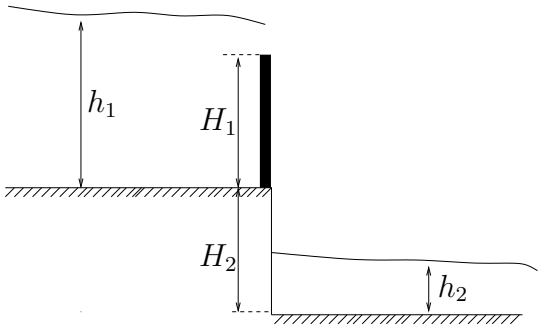

Figure 6.2: *A pooled stepped chute with a weir(dam).*

water equation is assumed to govern the flow. The Riemann problem at the dam is defined as followed.

Definition 6.1. *The Riemann problem at the dam consists of the shallow water model* (6.1)

$$\begin{cases} \partial_t h + \partial_x q &= 0, \\ \partial_t q + \partial_x(\frac{q^2}{h} + \frac{1}{2}gh^2) &= 0, \end{cases}$$

in the upstream river $x < 0$ from the dam and in the downstream river $x > 0$ from the dam with constant initial data, that is, $U(x,0) = U_{1,0} = (h_{1,0}, q_{1,0})$ for $x < 0$ and $U(x,0) = U_{2,0} = (h_{2,0}, q_{2,0})$ for $x > 0$.

It is clear that the case $H_2 = H_1 = 0$ corresponds to the standard Riemann problem presented in the previous section. We start the analysis of the problem by considering the case where $H_2 = 0$. This leads to the situation presented in Figure 6.3. The solution of the Riemann problem at the dam is defined as follows.

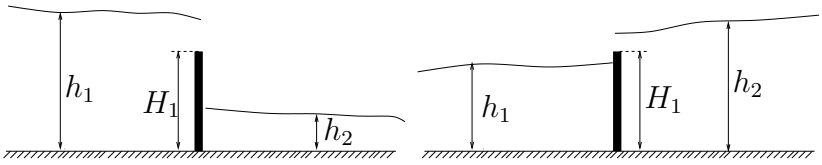

Figure 6.3: *Two connected rivers with a dam and* $H_2 = 0$.

Definition 6.2. *A function* $U : \mathbb{R} \times [0,T] \to \mathbb{R}^+ \times \mathbb{R}$ *is said to be a solution to the Riemann problem at the dam with initial data* $U_{1,0} = (h_{1,0}, q_{1,0})$ *and* $U_{2,0} = (h_{2,0}, q_{2,0})$ *if* U *coincides with the restriction on* $x < 0$ *of the solution to the standard Riemann problem with initial data*

$$U(x,0) = \begin{cases} U_{1,0} & \text{if} \quad x < 0 \\ \lim\limits_{x \to 0^-} U(x,t) & \text{if} \quad x > 0 \end{cases}$$

and with the restriction for $x > 0$ *of the solution to the standard Riemann problem with initial data*

$$U(x,0) = \begin{cases} \lim\limits_{x \to 0^+} U(x,t) & \text{if} \quad x < 0 \\ U_{2,0} & \text{if} \quad x > 0 \end{cases}$$

and the left and right limits $\{\lim\limits_{x \to 0^-} U(x,t), \lim\limits_{x \to 0^+} U(x,t)\}$ *satisfy coupling conditions to be defined below .*

We are interested in finding suitable coupling conditions for the construction of an admissible solution of the Riemann problem at the dam. As the first possible and straightforward coupling condition, we prescribe the conservation of the mass of water and conservation of momentum at the dam. We do that in a very subtle way since we are modeling a flooding phenomenon. Unlike the case of flow of gas at an intersection of pipes where the conservation of mass assume that all the gas that comes in goes out, here only the mass of water that is above the dam of height H_1 is conserved at the dam. So the coupling conditions read

$$[(h_1 - H_1)u_1](0,t) - (h_2 u_2)(0,t) = 0 \quad \forall t \geq 0, \tag{6.8}$$

$$\left[(h_1 - H_1)u_1^2 + \frac{1}{2}g(h_1 - H_1)^2\right](0,t) - \left[h_2 u_2^2 + \frac{1}{2}g h_2^2\right](0,t) = 0, \quad \forall t \geq 0. \tag{6.9}$$

The coupling conditions (6.8) and (6.9) can be written in the form of a map, omitting $(0,t)$

$$\Psi(h_1, q_1, h_2, q_2; H_1) = (\Psi_1, \Psi_2) = 0, \tag{6.10}$$

where the two components of Ψ, Ψ_1 and Ψ_2 are given respectively by the left hand side of the equalities (6.8) and (6.9).

It is expected that in the absence of the dam, the two connected rivers behave like a standard Riemann problem. Therefore, we consider intermediary states $U_l^* = (h_l^*, q_l^*)$ on the forward 1-curve through U_l and $U_r^* = (h_r^*, q_r^*)$ on the backward 2-curves through U_r :

$$q_l^* = L_1^+(h_l^*, h_l, q_l), \tag{6.11a}$$

$$q_r^* = L_2^-(h_r^*, h_r, q_r), \tag{6.11b}$$

and the Riemann problem at the dam is solved if these intermediary states satisfy the coupling conditions, i.e.,

$$\Psi(h_l^*, q_l^*, h_r^*, q_r^*; H_1) = 0.$$

There are two cases to consider in this analysis. One is when the upstream water height is above the dam $h_l > H_1 > h_r$ and the other case corresponds to the situation when the water height at both sides of the dam are less than the dam height i.e. $h_l < H_1$ and $h_r < H_1$. In this later case, we have simply two uncoupled half line boundary value problems. We then focus below only on the first case that is of interest here

6.3.1 Case 1: $h_l > H_1 > h_r$

We assume that

$$H_1 = h_r + \alpha(h_l - h_r), \quad \alpha \in (0,1)$$

such that we obviously have $h_r < H_1 < h_l$. We want to find the states U_r^* and U_l^* as in (6.11) which satisfy the coupling conditions (6.8)-(6.9). We assume that the intermediary states U_l^* belong to the forward 1-rarefaction through U_l and U_r^* to the

2-shock curve through U_r. When we instead have a 1-shock connection to the left state U_l and a 2-rarefaction connection to the right state U_r, similar arguments apply.

We have that

$$\frac{d}{dh}R_1^+(h;h_l,q_l) = \frac{q_l}{h_l} - 3\sqrt{gh} + 2\sqrt{gh_l} \quad \text{and} \quad \frac{d^2}{dh^2}R_1^+(h;h_l,q_l) = -\frac{3g}{2\sqrt{h}}.$$

Moreover, we know that $\frac{d}{dh}R_1^+(0;h_l,q_l) = \frac{q_l}{h_l} + 2\sqrt{gh_l} > 0$ and $\frac{d}{dh}R_1^+(h_l;h_l,q_l) = \frac{q_l}{h_l} - \sqrt{gh_l} = \lambda_1(U_l) \leq 0$ thanks to the subsonic conditions (6.3). Therefore, $\frac{d}{dh}R_1^+(h;h_l,q_l)$ is a decreasing function ranging from a positive number to a negative number. We can then find a water height value $\tilde{h}$ such that $\frac{d}{dh}R_1^+(\tilde{h};h_l,q_l) = 0$. $\tilde{h}$ can be determined explicitly as

$$\tilde{h} = \frac{1}{g}\left(\frac{q_l}{3h_l} - \frac{2}{3}\sqrt{gh_l}\right)^2.$$

We choose h_l^* such that $h_l^* \in (\tilde{h}, h_l)$ and h_r^* such that $h_r^* \in [h_r, h_r + \varepsilon)$.

To conclude, we use the implicit function theorem in the open set $(\tilde{h}, h_l + \varepsilon) \times (h_r - \varepsilon,\, h_r + \varepsilon)$ with $\varepsilon > 0$ a small number, and the map

$$\Phi(h,k,U_l,U_r) \doteq \Psi\left(h, L_1^+(h;h_l,q_l), k, L_2^-(k;h_r,q_r), H_1\right).$$

Provided the initial data satisfy the coupling conditions, we have

$$\Phi(h_l,q_l,h_r,q_r;H_1) = 0$$

and the Jacobian matrix

$$J \doteq \frac{D\Phi(h,k,U_l,U_r)}{D(h,k)}|_{(h,k)=(h_l,h_r)} \tag{6.12}$$

satisfy

$$\begin{aligned}\mathrm{Det}(J) \;=\; & -\frac{1}{h_l^{5/2}}\left(h_l^2\lambda_1(U_l)\lambda_2(U_r)\left[\lambda_2(U_r)\sqrt{h_l} + \sqrt{g}(h_l - H_1)\right]\right. \\ & \left. +\sqrt{h_l}\left(\lambda_2(U_r)\sqrt{g}h_l^{3/2}H_1 - q_l^2\right) + (h_l - H_1)\sqrt{g}q_r q_l h_r h_l\right).\end{aligned}$$

One can choose the data U_l and U_r as well as the dam height such that $\mathrm{Det}(J) \neq 0$. By the implicit function theorem, we obtain the existence of a unique solution of the equation $\Psi(h_l^*, q_l^*, h_r^*, q_r^*; H_1) = 0$. We have then proven the following result.

Theorem 6.1. *Let U_l and U_r be two subsonic states satisfying the coupling conditions* (6.8)–(6.9) *and such that $h_l > H_1 > h_r$. Assume, furthermore, that $Det(J) \neq 0$, where J is the Jacobian matrix in* (6.12). *Then the Riemann problem at the dam admits a solution in the sense of Definition 6.2.*

Other coupling conditions can be prescribed instead of (6.9). As in the case of the p-system, a model which share many properties with the shallow water model, in [7], we assume the equality of pressure at the dam and then have instead of (6.9)

$$(h_1 - H_1)^2 = h_2^2. \tag{6.13}$$

Note that this expression comes from the fact that the hydrostatic pressure at a location is proportional to the water height. Also, due to gravitational forces, we might expect that the momentum in the downstream river results from the momentum in the upstream river and a momentum due to an additional gravitational energy. This additional momentum is proportional to the height difference between the upstream reach and the downstream reach at the junction. If we call β the proportionality constant, we obtain the following coupling conditions

$$\left[(h_1 - H_1)u_1^2 + \frac{1}{2}g(h_1 - H_1)^2\right](0,t) + \beta g(h_1 - h_2)(0,t) - \left[h_2u_2^2 + \frac{1}{2}gh_2^2\right](0,t) = 0. \tag{6.14}$$

The constant β is determined from the fraction of the mass of the water that flows from the upstream reach to the downstream reach.
These coupling conditions are combined with the Lax curves determined above to find intermediary states that are used as internal boundary conditions for the numerical solution of the dynamics of the flow at the dam.

Remark 6.2. *If $u_1 = u_2$, then the coupling conditions (6.8, 6.9) are equivalent to (6.8, 6.13). Indeed, by* (6.8), *we have*

$$(h_1 - H_1)u_1 = h_2u_2 \text{ or } (h_1 - H_1)u_1^2 = h_2u_2u_1.$$

Now (6.9) *reads*

$$(h_1 - H_1)u_1^2 + \frac{1}{2}g(h_1 - H_1)^2 - (h_2u_2^2 + \frac{1}{2}gh_2^2) = 0$$

which is equivalent to

$$h_2u_2u_1 + \frac{1}{2}g(h_1 - H_1)^2 - (h_2u_2^2 + \frac{1}{2}gh_2^2) = 0$$

or

$$\frac{1}{2}g(h_1 - H_1)^2 - \frac{1}{2}gh_2^2 = h_2u_2(u_2 - u_1) = 0$$

and the last equation is the same as (6.13).

It is worth noting that when the initial data satisfy $h_l > H_1 > h_r$, then the intermediary states h_l^* and h_r^* satisfy the same condition.This is made precise in the following result.

Proposition 6.1. *Let $U_l^0 = (h_l^0, q_l^0)$ and $U_r^0 = (h_r^0, q_r^0)$ be given subsonic states such that $h_l^0 > H_1 > h_r^0$ and furthermore satisfy the coupling conditions* (6.10)*:*

$$\Psi(h_l^0, q_l^0, h_r^0, q_r^0; H_1) = 0 \tag{6.15}$$

as well as $Det(J) \neq 0$ where J is the Jacobian matrix in (6.12)*. Then there exists a constant $\delta > 0$ and neighborhoods of the states U_l^0 and U_r^0 such that for any initial data U_l^* and U_r^* in the respective neighborhood, the Riemann problem at the dam, see Definition 6.1, admits a solution (U_1, U_2) in the sense of Definition 6.2, with $h_1 > H_1 > h_2$.*

Proof. Let us consider some perturbations $U_l = (h, q_l)$ and $U_r = (k, q_r)$ of $U_l^0 = (h_l^0, q_l^0)$ and $U_r^0 = (h_r^0, q_r^0)$, respectively, such that

$$q_l = L_1^+(h; U_l^0) \quad \text{and} \quad q_r = L_2^-(k, U_r^0).$$

Since the initial data satisfy the coupling conditions, we then have that the map

$$(h, k) \mapsto \Psi(h, q_l, k, q_r; H_1)$$

is smooth and satisfy

$$\Psi(h_l^0, q_l^0, h_r^0, q_r^0; H_1) = 0 \quad \text{and} \quad |\frac{D\Psi}{D(h,k)}(h_l^0, q_l^0, h_r^0, q_r^0; H_1)| \neq 0.$$

By the implicit function theorem, we can find some neighborhoods of the states U_l^0 and U_r^0, denoted as B_l^0 and B_r^0, respectively, and a constant $\delta > 0$ such that for all $(U_l^*, U_r^*) \in B_l^0 \times B_r^0$, there exists some heights $(h, k) \in B_\delta(h_l^0, h_r^0)$ and the solution to the Riemann problem at the dam (U_1, U_2) is constructed as the restrictions to the dam of the standard Riemann problem with data U_l^* and $(h, L_1^+(h; U_l^*))$ for the upstream reach and $(k, L_2^-(h; U_r^*))$ and U_r^* for the downstream reach. Moreover, we can choose δ such that $h_1 > H_1 > h_2$. This complete the proof of the proposition. ■

6.3.2 The general case with $H_2 \neq 0$

A sketch of the situation here is depicted in Figure 6.2. We denote by $\tilde{h}_1 = h_1 + H_2$ the water height in the upstream reach of the river from the common reference level taken to be the bottom level of the downstream river. One can take the water velocity in the upstream river to be the same as that of the case $H_2 = 0$ so that $\tilde{u}_1 = u_1$. By inserting $(\tilde{h}_1, \tilde{u}_1)$ in the shallow water equations, we obtain an evolution equation for $(\tilde{h}_1, \tilde{u}_1)$ as

$$\partial_t \tilde{h}_1 + \partial_x(\tilde{h}_1 \tilde{u}_1) = H_2 \partial_x \tilde{u}_1 \tag{6.16a}$$

$$\partial_t(\tilde{h}_1 \tilde{u}_1) + \partial_x \left[\tilde{h}_1 \tilde{u}_1^2 + \frac{1}{2} g \tilde{h}_1^2 \right] = H_2 \partial_t(u_1 + \partial_x \tilde{u}_1^2 - g \partial_x \tilde{h}_1). \tag{6.16b}$$

This resulting system is not conservative due to the presence of a source term that involves the derivatives of the flow variables. This situation poses serious problems in the analysis due to the fact that for steady state solutions, we need to balance the source term with the flow gradient. One can solve the problem by directly solving the flow equation for the case $H_2 = 0$ to obtain (h_1, u_1) and then obtain the flow variable in the case $H_2 \neq 0$ as $\tilde{h}_1 = h_1 + H_2$ and $\tilde{u}_1 = u_1$.

6.4 Numerical Results

Here, we test the efficiency of the coupling conditions proposed above by implementing some examples. We discretize in the finite volume framework the shallow water

equation using a Godunov type scheme. The space domain is subdivided into cells $I_i = [x_{i-\frac{1}{2}}, x_{i+\frac{1}{2}}]$, with a constant mesh size $\Delta x = x_{i+\frac{1}{2}} - x_{i-\frac{1}{2}}$ and the time domain in cells $[t_n, t_{n+1}]$, with the time step $\Delta t = t_{n+1} - t_n$ chosen so as to satisfy the CFL condition [79]. Considering the cell averages

$$\bar{v}_i(t) = \frac{1}{\Delta x} \int_{I_i} v(x,t), dx$$

the first order Godunov scheme for a conservation law $\partial_t v + \partial_x f(v) = 0$ reads

$$\bar{v}^{n+1} = \bar{v}^n - \frac{\Delta t}{\Delta x} \left(F_{i+\frac{1}{2}} - F_{i-\frac{1}{2}} \right). \tag{6.17}$$

Therein, the numerical flux function $F_{i+\frac{1}{2}} = \mathcal{F}(\bar{v}_i, \bar{v}_{i+1})$ is a map that depends on the values of the flow in the neighboring cells of the interface $x_{i+1/2}$ as was discussed in Chapter 2. For the simulations, at each time step, we evolve the flow equations for each river reach and adjust the boundary conditions. For the external boundary conditions, we use the transparent boundary conditions. At the dam, we solve numerically the coupling conditions presented in the previous section to obtain the intermediary states that are used as internal boundary conditions at the dam. The nonlinear solver used is a Broyden's method with a Sherman-Morrison formula, see [53].

6.4.1 The Riemann problem at the dam and the pooled stepped chutes

To validate the coupling conditions proposed here for the shallow water equations at the dam, we use some heuristic formulas from the engineering literature. These formulas come from experiments and play an important role in the dynamics of pooled stepped chutes.

The set up here is a channel with some pooled stepped chutes where each of the steps has the form presented in Figure 6.4. From the hydraulic literature, see for example [13, 101], one can compute the water height at any point x of the channel with the formula [101]

$$\frac{z}{H} = k_A (\frac{x}{H})^2 + k_B \frac{x}{H} + k_C \tag{6.18}$$

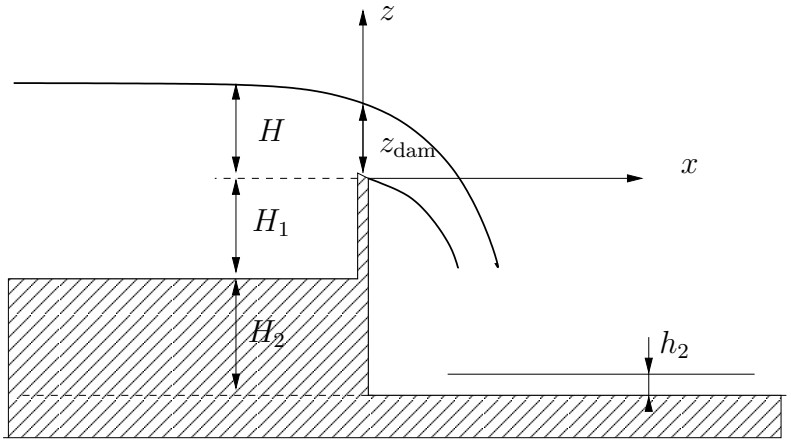

Figure 6.4: *Geometry of the step with a dam.*

and

$$\frac{z}{H} = k_A(\frac{x}{H})^2 + k_B\frac{x}{H} + k_C + k_D, \tag{6.19}$$

with the constant k_A, k_B, k_C, k_D given as

$$\begin{aligned}
k_A &= -0.43 + 0.25\frac{u^2}{2gH} \\
k_B &= 0.41 - 1.60\frac{u^2}{2gH} - \sqrt{1.57(\frac{u^2}{2gH})^2 - 0.89\frac{u^2}{2gH} + 0.13} \\
k_C &= 0.15 - 0.45\frac{v^2}{2gH} \\
k_D &= 0.57 - 2\left(\frac{u^2}{2gH} - 0.21\right)^2 \mathrm{e}^{10(u^2/(2gH)-0.21)}.
\end{aligned}$$

Here z is the water height at $x = 0$, H is the water height above the dam initially and u is the velocity of the water at the dam, see Figure 6.4.

As we have seen before, the coupling conditions given by the equality of the dynamic pressure and that of the equality of the water height give the same results provided that the velocity on the left of the dam and on the right are equal. So we consider in the numerical simulations only the two cases corresponding to (6.8, 6.9) and (6.8, 6.14). In this section, we compare the result obtained with the coupling conditions described above with the formula from the hydraulic literature (6.18)

and (6.19). We assume that the upstream river corresponds to the interval $[-20, 0]$ and the downstream river corresponds to $[0, 20]$ with the step or dam sitting at $x = 0$. The results obtained with (6.19) compare well with that obtained with the coupling conditions (6.8,6.9) and (6.8,6.14), see Table 6.1 and Table 6.2. In the tables, the first column represent the dam height H_1, the second column the initial water height upstream the dam, the third column represent water height at the dam z^1_{dam} obtained with our simulation routine, the fourth column is the water height at the dam z^2_{dam} obtained from the experimental formula (6.19) and the last column shows the absolute value of the difference of the two water heights at the dam $|z^2_{\text{dam}} - z^1_{\text{dam}}|$. We see in these tables that the absolute error increases with the dam height. However, the relative error with respect to the dam height, that is not shown in the table, remains in the same range for the different dam heights.

Table 6.1: *The water height at the dam obtained with the coupling conditions and the experiments. The Lax curves and the coupling conditions* (6.8),(6.9) *are used.*

H_1	h_1	z^1_{dam} (simulation)	z^2_{dam} (experiments, (6.19))	$\lvert z^2_{\text{dam}} - z^1_{\text{dam}}\rvert$
8.00000	9.50000	6.24526	6.57208	0.32682
10.00000	12.50000	6.88066	8.49585	1.61519
15.00000	25.50000	15.65344	17.47017	1.81673
25.00000	27.50000	16.07635	18.87659	2.80024
35.00000	35.50000	21.12556	24.44513	3.31957
55.00000	59.80000	37.89507	41.37519	3.48012

For the two tests, we run the simulation up to time $T = 0.5$ seconds and we used for the downstream flow $h_2 = 0.5,\ q_2 = 0.0,\ q_1 = 2.5$

6.4.2 Dynamics with a small water height above the step

We consider a pooled stepped problem modeled as above with the data given by

$$U_l = (9.5, 2.5), \quad U_r = (1.5, 0.0), \quad H_1 = 8.0.$$

Table 6.2: *The water height at the dam obtained with the coupling conditions and the experiments. The Lax curves and the coupling conditions* (6.8),(6.13) *are used with* $\beta = 0.0002$

H_1	h_1	z^1_{dam} (simulation)	z^2_{dam} (experiments, (6.19))	$\lvert z^2_{\text{dam}} - z^1_{\text{dam}} \rvert$
8.00000	9.50000	6.23834	6.57140	0.33306
10.00000	12.50000	6.82623	8.48875	1.66252
15.00000	25.50000	15.65283	17.47009	1.81726
25.00000	27.50000	16.07545	18.87649	2.80104
35.00000	35.50000	21.12486	24.44506	3.3202
55.00000	59.80000	37.89465	41.37515	3.4805

We compute the dynamics of the water heights and that of the discharge $q = hu$ and we present the results in Figure 6.5. To gain more insight into the dynamics of the

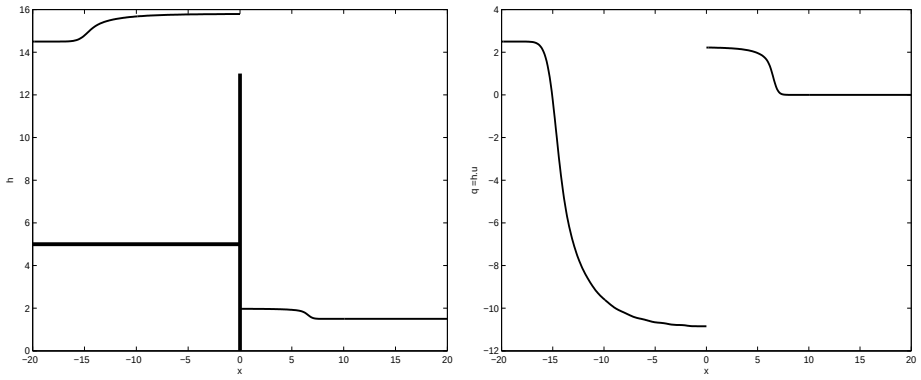

Figure 6.5: *Water height(left) and discharge (right) the solution of the Riemann problem at the dam with the coupling conditions* (6.8)-(6.9).

dam, we introduce a perturbation in the upstream reach of the river and investigate how it influences the flow downstream of the dam. From the data reported above, we replace the water height with a perturbation in the form

$$h'_l = h_l + \delta\xi_{[-6,-4]}$$

where ξ_A is the characteristic function taking the value 1 in the set A and zero elsewhere and with $\delta = 0.5$. We present in Figure 6.6 the water height and the discharge at the final time and in Figure 6.7 we plot the contour lines and the snapshot of the water height. We see that the introduced perturbation moves backwards and have a very small influence at the dam. From the perturbation, we have waves with considerable strength moving backwards and waves of very small strength that arrive at the dam. Those waves do not influence significantly the water height at the downstream reach which remains steady.

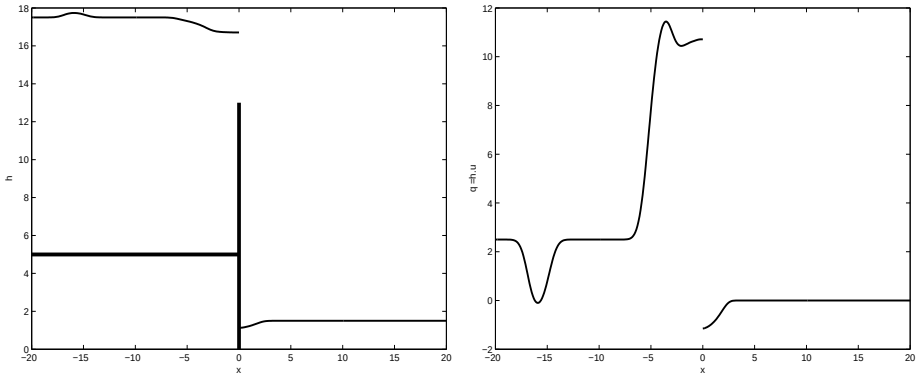

Figure 6.6: *Water height(left) and discharge (right) with a perturbation in the upstream river.*

6.4.3 The general case

Now we consider some data for the Riemann problem at the dam given as

$$U_l = (52.5, 2.5), \quad U_r = (0.5, 0.0), \quad H_1 = 25. \tag{6.20}$$

We expect the effect of the dam to be seen clearly. At the upstream reach, because of the small reaction of the dam and the free motion of water, there is a decrease in the water height upstream with a rarefaction wave that forms and moves backward. At the downstream reach, the water height increases because of the action of the water

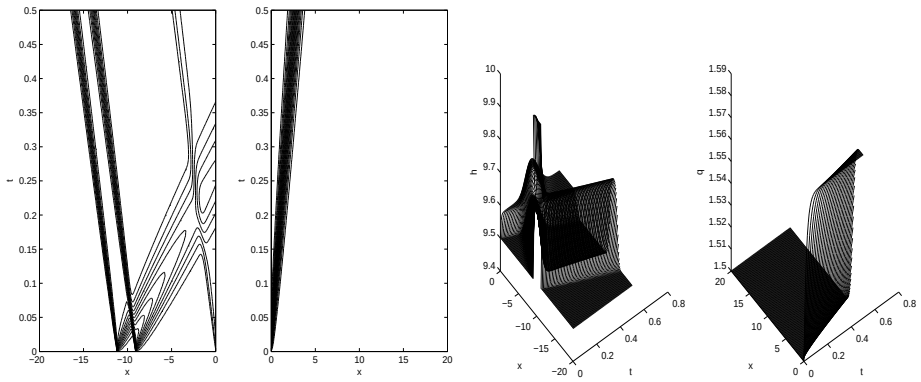

Figure 6.7: *Contour lines and snapshots of the water heights for the perturbed problem. The perturbations do not affect the dam.*

pouring. A shock wave originates there and moves downstream. The flow properties look steady far from the dam. The numerical results are depicted in Figure 6.8.

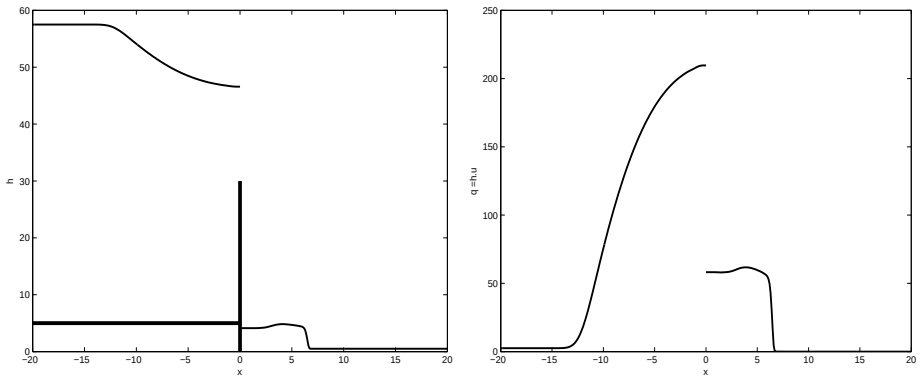

Figure 6.8: *Flow variables for the solution of the Riemann problem at the dam for the data in* (6.20).

Now we test a case where the water level in both rivers are nearly equal.

$$U_l = (52.5, 1.5), \quad U_r = (50.0, 0.0), \quad H_1 = 25. \tag{6.21}$$

The results are presented in Figure 6.9. The qualitative behavior of the solution is similar to that of the previous example.

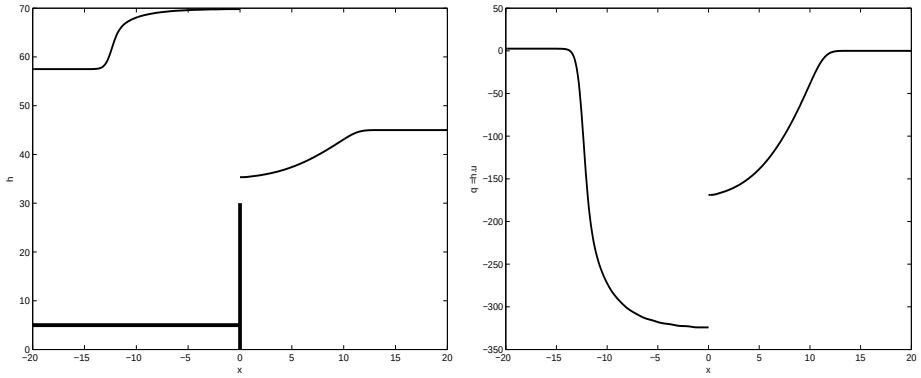

Figure 6.9: *Flow variables for the solution of the Riemann problem at the dam for the data in* (6.21).

For the two previous examples, we present the solution of the Riemann problem at the dam in the xt-plane in Figure 6.10. One sees clearly that the admissible solution has a shock wave moving backward (from the dam) and a rarefaction wave moving forward.

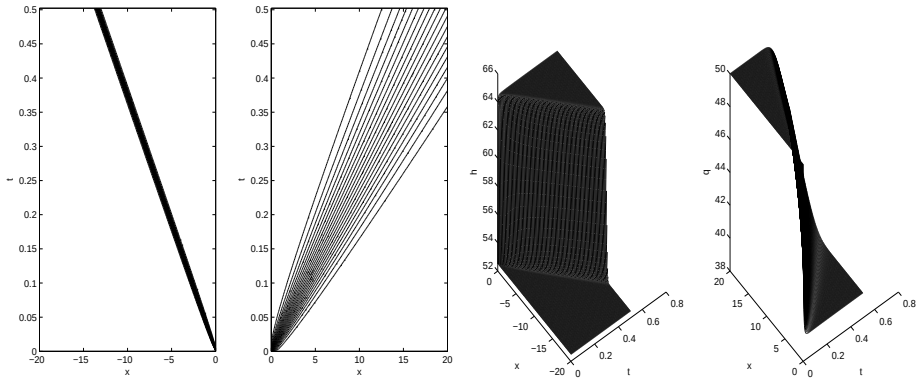

Figure 6.10: *Solutions of the Riemann problem at the dam in the xt-plane. The characteristic of the water height is plotted.*

6.5 Concluding Remarks

In this chapter, we have proposed a new approach to the simulation of pooled stepped chutes. We assume that the flow is governed by the shallow water equations and the dynamics are resolved by the use of some coupling conditions at each step or dam in the channel. The results presented here have been validated using an empirical formula obtained from experiments. In this chapter, we have concentrated on the case of one step in the channel. The results can be extended to the case of a channel with many steps in a straightforward way.

Part IV

Flow Optimization of Euler Systems

Chapter 7

A Multi-scale Approach to the Control of Systems Governed by Partial differential Equations

The treatment of control problems governed by a system of conservation laws poses serious challenges for the analysis and the numerical simulations. This is due mainly to wave interaction that occur in the solution of nonlinear systems of conservation laws. To solve that problem, we propose in this chapter the use of a linear approximation of the nonlinear system, specifically a lattice Boltzmann equations approach. The idea of the lattice Boltzmann approach is to retain the simplest microscopic description that gives macroscopic behavior of interest. By selecting appropriate number of speeds and the appropriate form of the equilibrium distribution function, one may match the equations that result from the lattice Boltzmann method with those of the traditional kinetic theory of interest to the desired level. In this work, we are concerned with the optimal control of systems governed by the Euler equations. We use an adjoint method and derive the optimality system using the lattice Boltzmann equation at the microscopic level. The result is obtained at the macroscopic limit using a multi-scale technique. Moreover, we consider the discrete form of the optimization problem and prove that the solution of the optimization

problems with the flow computed with first order and second order schemes are similar. This allows us to use the first order scheme to solve more robustly some practical test problems of interest. Part of the results presented in this chapter led to [86, 106].

7.1 Introduction

The control of systems governed by a system of conservation laws is of great interest, for example in aerodynamics [96, 66] and in shape optimization [90, 67, 91]. It is usually formulated as an inverse problem where given some flow properties at the final time T, one determines the initial flow that leads to the desired flow properties. In aerodynamics, the problem in general consists of determining the shape of a body (airplane, helicopter rotors) such that the lift is maximized or the drag is minimized, the flow surrounding the body being given by a system of conservation laws. It is known that in general the semi-group generated by a conservation law is non–differentiable in L^1 even in the scalar, one–dimensional case. A differential structure on general $BV-$solutions for hyperbolic conservation laws in one space dimension has been introduced and discussed in [12, 22, 25, 27, 104]. Based on the derived calculus first–order optimality conditions for systems have been given in [29]. Theoretical discussion on the resulting non–conservative equations can be found in [15, 16, 17]. Numerical results in the scalar, one–dimensional case with distributed control are also presented in [103, 104, 105]. Work on advection equations has been presented in [82]. Derivative-based approaches to control problems associated with partial differential equations follow the usual Lagrangian approach. [58]. They all start with a Lagrangian formulation and a formal derivation of the optimality system that consist in general of the original constraints (systems of conservation laws) which are recovered as the vanishing variation of the Lagrangian with respect to the Lagrange multipliers or adjoint variable, the adjoint system or co-state equations which are obtained when the variation of the Lagrangian with respect to the state variable vanishes and the optimality conditions which come from the variation of

the Lagrangian with respect to the control. For simple problems, one can solve "in one shot" the optimality system and obtain a solution of the control problem. This approach is considered as a solution of a control problem without optimization. The two other approaches are iterative methods which consist of solving iteratively the state equations and the adjoint equations or sensitivity equations and updating the control using the optimality conditions. The sensitivity approach is suitable when one has a finite and small number of controls [90] since one has as many sensitivity equations as the number of controls. In the other case, one uses the adjoint method for which one solves only one adjoint equation independently of the number of controls. It appears then that the adjoint method is suitable for problems with distributed controls that are effective in all the flow domain. For these iterative methods, the flow equations are solved forward in time and the adjoint system backward in time for unsteady problems. Due to the nonlinearity of the flux function, some wave interactions can occur in the solution of the flow equations and while solving the adjoint equations backward following the characteristics, the interaction point of the wave poses a serious problem to the backward solver. One might think of solving this problem by taking very small time steps that avoid these wave interactions. However, this leads to a stability problem since those small time steps can violate the CFL conditions.

In this chapter, we consider a control problem associated with the Euler equation and we propose for the solution of this problem the use of a linearization of the flow equation. It consists of replacing the Euler equations by its kinetic approximation in the form of the lattice Boltzmann equation (LBE) [92, 93, 71]. In [5], the same problem was considered for scalar conservation laws and a relaxation approach was used[11, 14, 69]. In general, the Lattice Boltzmann Method solves the kinetic equation of the discrete-molecular-velocity type such that the macroscopic variables satisfy the fluid dynamics type of equations. The lattice Boltzmann model differs from the macroscopic model in that it is linear in the transport term and therefore can resolve the problem of wave interactions. The nonlinear effect is captured in the so-called collision operator which appears as a source term in the LBE. The adjoint

approach to the control problem is derived at the microscopic level using the LBE and the macroscopic result is obtained at the hydrodynamic limit as the Knudsen number goes to zero. We obtained a robust method that works well for many test problems of interest.

The rest of this chapter is organized as follows. The formulation of the optimal control problem as an optimization problem with partial differential equations is presented in Section 7.2. We postulate that one can replace the PDE with its kinetics approximation formulated as a Lattice Boltzmann problem. For the Euler equation, more details on the finite velocities as well as the equilibrium distribution are given in Section 7.3. We briefly in the same section discuss the convergence of the kinetic model toward the hydrodynamic model. The derivation of the adjoint calculus using the microscopic model formulation is presented in Section 7.3.2. Numerical formulation of the optimization problem as well as the test of the method on practical problems of interest are documented in Section 7.5. Some concluding remarks and some future extensions are presented in Section 7.6.

7.2 Problem formulation

Here we consider the optimization problem

$$\underset{\mathbf{u}_0}{\text{Minimize}}\ \mathcal{J}(\mathbf{u}(T,.),\mathbf{u}_0;\mathbf{u}_d) \tag{7.1}$$

where $\mathcal{J}(\mathbf{u}(T,.),\mathbf{u}_0;\mathbf{u}_d)$ is a cost functional to be made precise later and $\mathbf{u}=(\rho,\rho u,\rho(bR\theta+u^2))$ solves the Euler equations in the form

$$\frac{\partial\rho}{\partial t}+\frac{\partial\rho u}{\partial x} = 0 \tag{7.2a}$$

$$\frac{\partial\rho u}{\partial t}+\frac{\partial(\rho u^2+p)}{\partial x} = 0 \tag{7.2b}$$

$$\frac{\partial\rho(bR\theta+u^2)}{\partial t}+\frac{\partial\left(\rho u(bR\theta+u^2)+2pu\right)}{\partial x} = 0 \tag{7.2c}$$

with the initial conditions

$$\mathbf{u}=\mathbf{u}_0\doteq(\rho_0,\rho_0u_0,\rho_0(bR\theta_0+u_0^2))\quad\text{at}\quad t=0, \tag{7.3}$$

where $t \in [0,T],\ x \in \mathbb{R},\ \rho_0,\ u_0,\ \theta_0$ are given initial density, velocity and temperature as function of the space variable x. In (7.1), $\mathbf{u}_d$ represents a desired state that needs to be approximately achieved at time $t = T$. We will denote the momentum as $m = \rho u$ and the energy as $E = \rho(b\theta + u^2)$. The cost functional $\mathcal{J}(\mathbf{u}(T,.), \mathbf{u}_0; \mathbf{u}_d)$ can then be written more explicitly as

$$\begin{aligned} \mathcal{J}(\mathbf{u}(T,.), \mathbf{u}_0; \mathbf{u}_d) &= \tfrac{1}{2}\int_{\mathbb{R}} \|\mathbf{u}(x,T) - \mathbf{u}_d(x)\|^2 dx \\ &= \tfrac{1}{2}\int_{\mathbb{R}} \big[(\rho(T,x) - \rho_d(x))^2 + (m(T,x) - m_d(x))^2 \\ &\quad +(E(T,x) - E_d(x))^2\big]\, dx. \end{aligned} \tag{7.4}$$

The solution of the optimal control problem (7.1) poses serious problems in practice due to wave interaction that can occur in the solution of the flow equation (7.2). These wave interactions are mainly due to the nonlinearity of the flow equations. We then suggest in this chapter the use of a linear approximation of the flow equation, the lattice-Boltzmann (LB) approximation, for the solution of the problem. This leads to a multiscale problem with the kinetic LB equation at the microscopic level and the Euler equation at the macroscopic level. We will derive the adjoint equations using the microscopic model and obtain the results at the macroscopic level by a multiscale technique.

7.3 A kinetic approximation of the Euler equation

In this section, we review for the purpose of the optimal control problem the Lattice Boltzmann approximation of the Euler equation proposed by Kataoka and Tsutahara [71]. In view of an extension of the problem for multidimensional situations, we consider the Euler equation in more than one dimension and we introduce the Greek subscripts $\alpha,\ \beta = 1, 2, \ldots, D$ for the space dimensions with $D = 1, 2, 3$. We

then write the Euler equations as

$$\frac{\partial \rho}{\partial t} + \frac{\partial \rho u_\alpha}{\partial x_\alpha} = 0 \tag{7.5a}$$

$$\frac{\partial \rho u_\alpha}{\partial t} + \frac{\partial \rho u_\alpha u_\beta}{\partial x_\beta} + \frac{\partial p}{\partial x_\alpha} = 0 \tag{7.5b}$$

$$\frac{\partial \rho(bR\theta + u_\alpha^2)}{\partial t} + \frac{\partial \left(\rho u_\alpha (bR\theta + u_\beta^2) + 2pu_\alpha\right)}{\partial x_\beta} = 0 \tag{7.5c}$$

where t is time, x_α is the spatial coordinate, ρ, u_α, θ and

$$p = \rho R\theta$$

are the density, the flow velocity in the x_α direction, the temperature and the pressure of a gas, respectively. The specific gas constant is denoted by R and $b = \frac{2}{\gamma - 1}$ is a given constant with γ the specific heat ratio. Recall that α and β are subscripts and the Einstein summation convention is used, i.e., repeated subscripts mean a summation over the space coordinates. The initial conditions are

$$\rho = \rho_0, \quad u_\alpha = u_{\alpha,0}, \quad \theta = \theta^0 \quad \text{at} \quad t = 0, \tag{7.6}$$

where ρ_0, $u_{\alpha,0}$, θ^0 are given function of the space variable x_α. A lattice-Boltzmann approximation to the compressible Euler equations (7.5) is described as follows. Let $N + 1$ be the number of particles. We denote by $\xi_{i\alpha}$ the molecular velocity of the $i-$th particle of density f_i in the x_α direction. We introduce the variable η_i to control the specific heat ratio and we denote by $f_i(t, x_\alpha)$ the velocity distribution function of the ith particle. The macroscopic variables ρ, u_α and θ are defined by

$$\rho = \sum_{i=0}^{N} f_i, \quad \rho u_\alpha = \sum_{i=0}^{N} \xi_{i\alpha} f_i \quad \text{and} \quad \rho(bR\theta + u_\alpha^2) = \sum_{i=0}^{N} (\xi_{i\alpha}^2 + \eta_i^2) f_i. \tag{7.7}$$

Now we denote as $f = (f_0, \ldots, f_{N-1})$ the vectors of all particles densities and we consider the initial-value problem for the kinetic equation

$$\frac{\partial f_i}{\partial t} + \xi_{i\alpha} \frac{\partial f_i}{\partial x_\alpha} = \Omega_i(f), \quad i = 0, \ldots, N. \tag{7.8}$$

where the collision operator $\Omega_i(f)$ is of the Bhatnager-Gross-Krook (BGK)-type

$$\Omega_i(f) = \frac{f_i^{eq}(\rho, u_\alpha, \theta) - f_i}{\tau}. \tag{7.9}$$

and the initial conditions are given by

$$f_i = f_i^{eq}(\rho^0, u_\alpha^0, \theta^0) \quad \text{at} \quad t = 0. \tag{7.10}$$

In (7.9), τ is a given constant called the *relaxation time* and the local equilibrium distribution function $f_i^{eq}(\rho, u_\alpha, \theta)$ is a given function of the macroscopic variables. One can integrate the Lattice Boltzmann model (7.8) along characteristics to obtain the classical form of the model [92]:

$$\frac{f_i(t + \Delta t, x_\alpha + \xi_{i\alpha}\Delta t) - f_i(t, x_\alpha)}{\Delta t} = \frac{f_i^{eq}(\rho, u_\alpha, \theta) - f_i}{\tau}, \tag{7.11}$$

where Δt is the discrete time step of order τ. In general, (7.11) is viewed as the two steps process made of a collision step

$$\tilde{f}_i(t, x_\alpha) = f_i(t, x_\alpha) + \Delta t \frac{f_i^{eq}(\rho, u_\alpha, \theta) - f_i}{\tau}, \tag{7.12}$$

and a propagation step

$$f_i(t + \Delta t, x_\alpha + \xi_{i\alpha}\Delta t) = \tilde{f}_i(t, x_\alpha). \tag{7.13}$$

The form (7.11) is only one finite difference discretization of the Lattice Boltzmann model (7.8). Therefore, for the purpose of deriving an adjoint calculus for the lattice Boltzmann model, we consider the general form (7.8) in the rest of the presentation. To recover from the lattice Boltzmann equation the Euler equation at the hydrodynamic limits, the following constraints are imposed on the moments of the local equilibrium distribution f_i^{eq} [71]:

$$\sum_{i=0}^{N} f_i^{eq} = \rho, \tag{7.14a}$$

$$\sum_{i=0}^{N} f_i^{eq}\xi_{i\alpha} = \rho u_\alpha, \tag{7.14b}$$

$$\sum_{i=0}^{N} f_i^{eq}\xi_{i\alpha}\xi_{i\beta} = p\delta_{\alpha\beta} + \rho u_\alpha u_\beta, \tag{7.14c}$$

$$\sum_{i=0}^{N} f_i^{eq}(\xi_{i\alpha}^2 + \eta_i^2) = \rho(bR\theta + u_\alpha^2), \tag{7.14d}$$

$$\sum_{i=0}^{N} f_i^{eq}(\xi_{i\beta}^2 + \eta_i^2)\xi_{i\alpha} = \rho(\left[(b+2)R\theta + \rho u_\beta^2\right] u_\alpha. \tag{7.14e}$$

It is convenient to use the non-dimensional form of the lattice Boltzmann model (7.8). For that purpose, let L, ρ_0 and θ_0 be a reference length, density, and the temperature,respectively. Then the non-dimensional variables are defined as

$$\begin{gathered}
\hat{t} = \frac{t}{L/\sqrt{R\theta_0}}, \quad \hat{x}_\alpha = \frac{x_\alpha}{L}, \quad \hat{\xi}_{i\alpha} = \frac{\xi_{i\alpha}}{\sqrt{R\theta_0}}, \quad \hat{\eta}_i = \frac{\eta_i}{\sqrt{R\theta_0}}; \\
\hat{f}_i = \frac{f_i}{\rho_0}, \quad \hat{f}_i^{eq} = \frac{f_i^{eq}}{\rho_0}; \\
\hat{\rho} = \frac{\rho}{\rho_0}, \quad \hat{u}_\alpha = \frac{u_\alpha}{\sqrt{R\theta_0}}, \quad \hat{\theta} = \frac{\theta}{\theta_0}, \quad \hat{p} = \frac{p}{\rho_0 R\theta_0}; \\
\hat{\rho}^0 = \frac{\rho^0}{\rho_0}, \quad \hat{u}_\alpha^0 = \frac{u_\alpha^0}{\sqrt{R\theta_0}}, \quad \hat{\theta}^0 = \frac{\theta^0}{\theta_0}, \quad \hat{p}^0 = \frac{p^0}{\rho_0 R\theta_0}.
\end{gathered} \tag{7.15}$$

The non-dimensional compressible Euler equations then read

$$\frac{\partial\hat{\rho}}{\partial\hat{t}} + \frac{\partial\hat{\rho}\hat{u}_\alpha}{\partial\hat{x}_\alpha} = 0, \tag{7.16a}$$

$$\frac{\partial\hat{\rho}\hat{u}_\alpha}{\partial\hat{t}} + \frac{\partial\hat{\rho}\hat{u}_\alpha\hat{u}_\beta}{\partial\hat{x}_\beta} + \frac{\partial\hat{p}}{\partial\hat{x}_\alpha} = 0, \tag{7.16b}$$

$$\frac{\partial\hat{\rho}(b\hat{\theta} + \hat{u}_\alpha^2)}{\partial\hat{t}} + \frac{\partial\left(\hat{\rho}\hat{u}_\alpha(b\hat{\theta} + \hat{u}_\beta^2) + 2\hat{p}\hat{u}_\alpha\right)}{\partial\hat{x}_\beta} = 0, \tag{7.16c}$$

where $\hat{p} = \hat{\rho}\hat{\theta}$ and the initial conditions are

$$\hat{\rho} = \hat{\rho}^0, \quad \hat{u}_\alpha = \hat{u}_\alpha^0, \quad \hat{\theta} = \hat{\theta}^0 \quad \text{at} \quad \hat{t} = 0. \tag{7.17}$$

The non-dimensional macroscopic variables are

$$\hat{\rho} = \sum_{i=0}^{N} \hat{f}_i, \quad \hat{\rho}\hat{u}_\alpha = \sum_{i=0}^{N} \hat{\xi}_{i\alpha}\hat{f}_i \quad \text{and} \quad \hat{\rho}(b\hat{\theta} + \hat{u}_\alpha^2) = \sum_{i=0}^{N} (\hat{\xi}_{i\alpha}^2 + \hat{\eta}_i^2)\hat{f}_i. \tag{7.18}$$

The kinetic equation (7.8) and its initial data in non-dimensional form are

$$\frac{\partial \hat{f}_i}{\partial_t} + \hat{\xi}_{i\beta}\frac{\partial \hat{f}_i}{\partial x_\beta} = \frac{\hat{f}_i^{eq}(\hat{\rho}, \hat{u}_\alpha, \hat{\theta}) - \hat{f}_i}{\varepsilon}, \quad i = 0, \ldots, N-1, \tag{7.19}$$

where $\varepsilon = \frac{\tau\sqrt{R\theta_0}}{L}$ is the Knudsen number and the initial conditions are given by

$$\hat{f}_i = \hat{f}_i^{eq}(\hat{\rho}^0, \hat{u}_\alpha^0, \hat{\theta}^0) \quad \text{at} \quad \hat{t} = 0. \tag{7.20}$$

The non dimensional equilibrium distribution $\hat{f}_i^{eq}$ satisfy similar constraints as in (7.14) with a hat on each flow variable and also on η_i. Moreover, the factor R is omitted in (7.14d) and (7.14e).

7.3.1 One dimensional lattice Boltzmann and the Euler equation

In this section and in the rest of this chapter, we restrict ourselves to the one dimensional model for the lattice Boltzmann model and we omit the subscripts α, β representing the space variables. Precisely, we consider the one dimensional and five velocities (D1Q5) model with the velocities given by

$$\hat{\xi}_i = \begin{cases} 0, & i = 0 \\ \nu_1 \cos[(i-1)\pi], & i = 1, 2 \\ \\ \nu_2 \cos[(i-1)\pi], & i = 3, 4. \end{cases} \tag{7.21}$$

The non-dimensional form of the constant η is given as

$$\hat{\eta}_i = \begin{cases} \eta_0, & i = 0 \\ 0, & i = 1, 2, 3, 4. \end{cases}$$

Therein ν_1 and ν_2, with $\nu_2 \neq \nu_1$, and η_0 are given nonzero constants. The equilibrium distribution is given in the form

$$\hat{f}_i^{eq} = \hat{\rho}(A_i + B_i\, \hat{u}\hat{\xi}_i), \tag{7.22}$$

where

$$A_i = \begin{cases} \frac{b-1}{\eta_0^2}\hat{\theta}, & i = 0, \\ \frac{1}{2(\nu_1^2-\nu_2^2)}\left[-\nu_2^2 + \left((b-1)\frac{\nu_2^2}{\eta_0^2}+1\right)\hat{\theta} + \hat{u}^2\right], & i = 1,2, \\ \frac{1}{2(\nu_2^2-\nu_1^2)}\left[-\nu_1^2 + \left((b-1)\frac{\nu_1^2}{\eta_0^2}+1\right)\hat{\theta} + \hat{u}^2\right], & i = 3,4, \end{cases} \tag{7.23a}$$

and

$$B_i = \begin{cases} 0, & i = 0, \\ \frac{-\nu_2^2+(b+2)\hat{\theta}+\hat{u}^2}{2\nu_1^2(\nu_1^2-\nu_2^2)}, & i = 1,2, \\ \frac{-\nu_1^2+(b+2)\hat{\theta}+\hat{u}^2}{2\nu_2^2(\nu_2^2-\nu_1^2)}, & i = 3,4. \end{cases} \tag{7.23b}$$

We show below that with this set of discrete velocities, the lattice Boltzmann equations (7.19) converges in the hydrodynamic limits toward an equilibrium distribution, whose macroscopic variables solve the Euler equations. We will consider from now on the non dimensional model and we will omit the hat on the non dimensional flow variables. The weak solution of the Euler equations (7.2) satisfies

$$\int_{-\infty}^{\infty} dx \int_0^{\infty} \left(\frac{\partial \psi}{\partial t} \begin{Bmatrix} \rho \\ \rho u \\ \rho(b\theta + u^2) \end{Bmatrix} + \frac{\partial \psi}{\partial x} \begin{Bmatrix} \rho \\ \rho u + p \\ \rho u(b\theta + u^2) + 2p\, u \end{Bmatrix} \right) dt + \int_{-\infty}^{\infty} \begin{Bmatrix} \rho^0 \\ \rho^0 u^0 \\ \rho^0(b\theta^0 + (u^0)^2) \end{Bmatrix} \psi(x,0) dx = 0, \tag{7.24}$$

where $\psi(t,x)$ is a smooth test function of t and x which vanishes for $t + |x|$ large enough. To obtain the weak solution of the Euler equation from the kinetic equation system (7.19), we consider as well the weak form of the lattice Boltzmann equation

(7.19) in the form

$$\int_{-\infty}^{\infty} dx \int_{0}^{\infty} \left[\left(\frac{\partial \psi}{\partial t} + \xi_i \frac{\partial \psi}{\partial x} \right) f_i + \frac{f_i^{eq}(\rho, u, \theta) - f_i}{\varepsilon} \psi \right] dt + \int_{-\infty}^{\infty} f_i^{eq}(\rho^0, u^0, \theta^0) \psi(0, x) dx = 0, \tag{7.25}$$

where ψ is a test function independent of ε. It was proven in [71] that the finite difference form of the kinetic equation (7.19) is consistent with the above integral form (7.25) even if the mesh width is of order $O(\varepsilon)$. According to the analysis of the Boltzmann equation, shock waves and contact discontinuities are not real discontinuities in the realm of lattice Boltzmann simulation, but thin layers of width $O(\varepsilon)$ across which the variable makes an appreciable variation [71]. The following result ensures that in the presence of shock and contact discontinuities, the weak form of the kinetic equation (7.25) converges in the hydrodynamic limit to the weak form of the Euler equations (7.24).

Proposition 7.1. *Consider a case where the solution f_i contains shock or contact discontinuities in some region where the order of variation of f_i in the space and time variable is $O(\varepsilon)$. In other regions, f_i has a moderate variation in the order of unity. Then the solution f_i of* (7.25) *in the limit $\varepsilon \to 0$ is given by $f_i = f_i^{eq}(\rho, u, \theta)$ whose macroscopic variable $\rho,\ u,\ \theta$ satisfy the weak form of the Euler equation given by* (7.24) *and its initial conditions.*

For completeness, we highlight the main ideas of the proof along the line of [71].

Proof. We will use the subscripts S and E for the flow variables in the region where the order of variation of f_i in space and time is $O(\varepsilon)$ and unity, respectively. The proof uses the Chapman-Enskog expansion of the microscopic and the macroscopic variables. This technique is also referred to as the multiscale technique. We expand the distribution $f_i,\ f_{iE},\ f_{iS}$ in the form

$$f_i = f_i^{(0)} + \varepsilon f_i^{(1)} + \varepsilon^2 f_i^{(2)} + \ldots, \tag{7.26}$$

where the components $f_i^{(m)}$ are of the same order as unity. Macroscopic variables are also expanded as

$$h = h^{(0)} + \varepsilon h^{(1)} + \varepsilon^2 h^{(2)} + \ldots \tag{7.27}$$

where h stands for ρ, ρu or E. The components functions here also have the magnitude of unity and moreover, they satisfy the equations of the form

$$\rho^{(m)} = \sum_{i=0}^{N} f_i^{(m)}, \tag{7.28a}$$

$$\rho^{(m)} u^{(m)} = \sum_{i=0}^{N} f_i^{(m)} \xi_i, \tag{7.28b}$$

$$\rho^{(m)} (u^{(m)})^2 + p^{(m)} = \sum_{i=0}^{N} f_i^{(m)} \xi_i^2, \tag{7.28c}$$

$$\rho^{(m)} (b\theta^{(m)} + (u^{(m)})^2) = \sum_{i=0}^{N} f_i^{(m)} (\xi_i^2 + \eta_i^2), \tag{7.28d}$$

$$\rho^{(m)} \left[(b+2)\theta^{(m)} + \rho^{(m)} (u^{(m)})^2 \right] u^{(m)} = \sum_{i=0}^{N} f_i^{(m)} (\xi_i^2 + \eta_i^2) \xi_i. \tag{7.28e}$$

where m is an integer. We substitute the expanded function f_i and f_i^{eq} in the kinetic equation (7.25) and collect the leading order terms to get

$$\begin{aligned} \int_{-\infty}^{\infty} dx \int_0^{\infty} (f_{iE}^{(0)} - f_{iE}^{eq(0)}) \psi dt &= 0, \\ \int_{-\infty}^{\infty} dx \int_0^{\infty} \left[\left(\frac{\partial \psi}{\partial t} + \xi_i \frac{\partial \psi}{\partial x} \right) f_{iE}^0 + (f_{iE}^{eq(1)}(\rho^{(0)}, u^{(0)}, \theta^{(0)}) - f_{iE}^{(1)}) \psi \right] dt & \\ + \int_{-\infty}^{\infty} f_{iE}^{eq(0)}(\rho^0, u^0, \theta^0) \psi(0, x) dx + & \\ \int \int_{D_S} \left[(f_{iS}^{(0)} - f_{iS}^{eq(0)}) - (f_{iE}^{(0)} - f_{iE}^{eq(0)}) \right] \psi dx dt &= 0, \end{aligned} \tag{7.29}$$

where D_S indicates where the variation of f_i in the xt plane is of the order of ε. From the leading order term we get

$$f_{iE}^{(0)} = f_{iE}^{eq(0)}(\rho_E^{(0)}, u_E^{(0)}, \theta_E^{(0)}). \tag{7.30}$$

The next-order equation can be seen as a linear inhomogeneous equation for $f_{iE}^{(1)}$. The constrains (7.28) apply also for the equilibrium particles. It follows that $\sum_{i=0}^{N-1} g_i (f_{iE}^{eq(1)} - f_{iE}^{(1)}) = 0$, where $g_i = 1, \xi_i, \xi_i^2, \xi_i^2 + \eta_i^2 \ldots$. Therefore, equation (7.29)

has a solution only when its inhomogeneous term satisfy the following solvability condition

$$\begin{aligned}\sum_{i=0}^{N-1} g_i \Bigg\{ \int_{-\infty}^{\infty} dx \int_0^{\infty} \left(\frac{\partial \psi}{\partial t} + \xi_i \frac{\partial \psi}{\partial x} \right) f_{iE}^0 dt \\ + \int_{-\infty}^{\infty} f_{iE}^{eq(0)}(\rho^0, u^0, \theta^0)\psi(0,x)dx + \\ \int\int_{D_S} \left[(f_{iS}^{(0)} - f_{iS}^{eq(0)}) - (f_{iE}^{(0)} - f_{iE}^{eq(0)}) \right] \psi dx dt \Bigg\} &= 0 \end{aligned} \tag{7.31}$$

Substituting (7.30) into (7.31) and using (7.28), we get the integral form of the Euler equation (7.24) for the leading order macroscopic variables $\rho_E^{(0)}$, $u_E^{(0)}$, $\theta_E^{(0)}$, and $p_E^{(0)}$.

■

For the rest of this chapter, the vector of conserved variables for the Euler equations is $\mathbf{u} = (\rho, \rho u, \rho(b\theta + u^2))$ which correspond to the nondimensional model.

7.3.2 Derivation of an adjoint calculus at the microscopic level

The Lagrangian at the microscopic level is given by

$$L(f, \lambda) = \mathcal{J}(\mathbf{u}(T, .), \mathbf{u}_0; \mathbf{u}_d) - \sum_{i=0}^{N} \int_0^T \int_{\mathbb{R}} \left[\partial_t f_i + \xi_i \partial_x f_i - \Omega_i(f) \right] \lambda_i dx dt, \tag{7.32}$$

where λ_i is the Lagrange multiplier or the *adjoint velocity distribution*. Integrating by parts, (7.32) becomes

$$\begin{aligned} L(f, \lambda) = \mathcal{J}(\mathbf{u}(T, .), \mathbf{u}_0; \mathbf{u}_d) + \sum_{i=0}^{N} \int_0^T \int_{\mathbb{R}} \left(f_i \left[\partial_t \lambda_i + \xi_i \partial_x \lambda_i \right] + \Omega_i(f) \lambda_i \right) dx dt \\ - \sum_{i=0}^{N} \int_{\mathbb{R}} \left(f_i(T, x)\lambda_i(T, x) - f_i^{eq}(\rho^0(x), u^0(x), \theta^0(x))\lambda_i(0, x) \right) dx. \end{aligned} \tag{7.33}$$

By taking the variation of the Lagrangian with respect to the state variable f_i and taking into account (7.7), we arrive at the adjoint system

$$-\partial_t \lambda_i - \xi_i \partial_x \lambda_i = \sum_{j=0}^{N-1} \frac{\partial \Omega_j(f)}{\partial f_i} \lambda_j \tag{7.34}$$

with a terminal condition

$$\lambda_i(T,\cdot) = (\rho-\rho_d)\frac{\partial \rho}{\partial f_i} + (m-m_d)\frac{\partial m}{\partial f_i} + (E-E_d)\frac{\partial E}{\partial f_i}, \quad x \in \mathbb{R}, \tag{7.35}$$

with

$$\frac{\partial \rho}{\partial f_i} = 1, \quad \frac{\partial m}{\partial f_i} = \xi_i, \quad \frac{\partial E}{\partial f_i} = \xi_i^2 + \eta_i^2. \tag{7.36}$$

The adjoint equation (7.34) has the same structure as the original model (7.8) and we can, therefore, call the term in the right hand side of (7.34) the *adjoint collision operator*. In the BGK formulation, the adjoint collision operator has the form

$$\sum_{j=0}^{N-1} \frac{\partial \Omega_j(f)}{\partial f_i}\lambda_j = \frac{1}{\varepsilon}\Big(\sum_{j=0}^{N-1} \frac{\partial f_j^{eq}}{\partial f_i}\lambda_j - \lambda_i\Big). \tag{7.37}$$

For the equilibrium functional given in (7.22), one can write that

$$\frac{\partial f_j^{eq}}{\partial f_i} = \frac{\partial f_j^{eq}}{\partial \rho}\frac{\partial \rho}{\partial f_i} + \frac{\partial f_j^{eq}}{\partial m}\frac{\partial m}{\partial f_i} + \frac{\partial f_j^{eq}}{\partial E}\frac{\partial E}{\partial f_i}. \tag{7.38}$$

The partial derivatives $\frac{\partial \rho}{\partial f_i}$, $\frac{\partial m}{\partial f_i}$, $\frac{\partial E}{\partial f_i}$ are already given in (7.36) and then we remain with the partial derivatives of the equilibrium functional with respect to the macroscopic variables. They can be obtained as

$$\frac{\partial f_j^{eq}}{\partial \rho} = A_j + \rho\frac{\partial A_j}{\partial \rho} + m\xi_j\frac{\partial B_j}{\partial \rho}, \tag{7.39}$$

$$\frac{\partial f_j^{eq}}{\partial m} = \rho\frac{\partial A_j}{\partial m} + \xi_j B_j + \xi_j m\frac{\partial B_j}{\partial m}, \tag{7.40}$$

$$\frac{\partial f_j^{eq}}{\partial E} = \rho\frac{\partial A_j}{\partial E} + \xi_j m\frac{\partial B_j}{\partial E}. \tag{7.41}$$

with

$$\frac{\partial A_j}{\partial \rho} = \begin{cases} -\frac{b-1}{\eta_0^2}\frac{E\rho-2m^2}{b\rho^3}, & j=0, \\ \frac{1}{2(\nu_1^2-\nu_2^2)}\left(\left(\frac{\nu_2^2(b-1)}{\eta_0^2}+1\right)\frac{2m^2-E\rho}{b\rho^3} - \frac{2m^2}{\rho^3}\right), & j=1,2, \\ \frac{1}{2(\nu_2^2-\nu_1^2)}\left(\left(\frac{\nu_1^2(b-1)}{\eta_0^2}+1\right)\frac{2m^2-E\rho}{b\rho^3} - \frac{2m^2}{\rho^3}\right), & j=3,4; \end{cases} \tag{7.42a}$$

$$\frac{\partial B_j}{\partial \rho} = \begin{cases} 0, & j = 0, \\ \frac{1}{2\nu_1^2(\nu_1^2-\nu_2^2)}\frac{4m^2+E\rho}{b\rho^3}, & j = 1,2, \\ \frac{1}{2\nu_2^2(\nu_2^2-\nu_1^2)}\frac{4m^2+E\rho}{b\rho^3}, & j = 3,4, \end{cases} \tag{7.42b}$$

$$\frac{\partial A_j}{\partial m} = \begin{cases} -\frac{b-1}{\eta_0^2}\frac{2m}{b\rho^2}, & j = 0, \\ \frac{1}{2(\nu_1^2-\nu_2^2)}\left(-(\frac{\nu_2^2(b-1)}{\eta_0^2}+1)\frac{2m}{b\rho^2}-\frac{2m^2}{\rho^2}\right), & j = 1,2, \\ \frac{1}{2(\nu_2^2-\nu_1^2)}\left(-(\frac{\nu_1^2(b-1)}{\eta_0^2}+1)\frac{2m}{b\rho^2}-\frac{2m^2}{\rho^2}\right), & j = 3,4, \end{cases} \tag{7.42c}$$

$$\frac{\partial B_j}{\partial m} = \begin{cases} 0 & j = 0, \\ -\frac{1}{\nu_1^2(\nu_1^2-\nu_2^2)}\frac{m}{b\rho^2}, & j = 1,2, \\ -\frac{1}{\nu_2^2(\nu_2^2-\nu_1^2)}\frac{m}{b\rho^2}, & j = 3,4, \end{cases} \tag{7.42d}$$

$$\frac{\partial A_j}{\partial E} = \begin{cases} \frac{b-1}{\eta_0^2}\frac{1}{b\rho}, & j = 0, \\ \frac{1}{2(\nu_1^2-\nu_2^2)}(\frac{\nu_2^2(b-1)}{\eta_0^2}+1)\frac{1}{b\rho}, & j = 1,2, \\ \frac{1}{2(\nu_2^2-\nu_1^2)}(\frac{\nu_1^2(b-1)}{\eta_0^2}+1)\frac{1}{b\rho}, & j = 3,4, \end{cases} \tag{7.42e}$$

and

$$\frac{\partial B_j}{\partial E} = \begin{cases} 0, & j = 0, \\ \frac{1}{\nu_1^2(\nu_1^2-\nu_2^2)}\frac{b+2}{b\rho}, & j = 1,2, \\ \frac{1}{\nu_2^2(\nu_2^2-\nu_1^2)}\frac{b+2}{b\rho}, & j = 3,4. \end{cases} \tag{7.42f}$$

We can then define the *adjoint equilibrium distribution* as

$$\lambda_i^{eq} = \sum_{j=0}^{N-1} \frac{\partial f_j^{eq}}{\partial f_i}\lambda_j. \tag{7.43}$$

Now at the microscopic level, one can solve the lattice-Boltzmann equations, and obtain solutions f_i. One then takes the moments to obtain the macroscopic variables at any time $0 \leq t \leq T$. These are then used to solve backward in time the microscopic adjoint equation (7.34) for the adjoint variable λ_i. These are eventually used together with the optimality condition to obtain the gradient of the cost function with respect to the control $\mathbf{u}_0$.

7.3.3 Hydrodynamic limits of the adjoint microscopic model

In this section, we find the hydrodynamic limit of the microscopic adjoint equations. We introduce the following notations for the macroscopic adjoint variables

$$\lambda = \sum_{i=0}^{N} \lambda_i, \quad \lambda\tilde{u} = \sum_{i=0}^{N} \xi_i \lambda_i, \tag{7.44}$$

where $\tilde{u}$ is an adjoint velocity. Recall that the equilibrium distribution was found as

$$\lambda_i^{eq} = \sum_{j=0}^{N-1} \frac{\partial f_j^{eq}(\rho, u, \theta)}{\partial f_i} \lambda_j.$$

Applying $\sum_{i=0}^{N}$ to (7.34), leads to the equation

$$-\partial_t \lambda - \partial_x \lambda\tilde{u} = \frac{1}{\tau}(\sum_{i=0}^{N} \lambda_i^{eq} - \lambda). \tag{7.45}$$

Therefore, if one needs a "conservation of mass" at the adjoint level, the adjoint equilibrium distribution in (7.43) should satisfy the constraint

$$\sum_{i=0}^{N} \lambda_i^{eq} = \lambda. \tag{7.46}$$

Similarly, applying multiplying (7.34) by ξ_i and taking the sum over i from 0 to N leads to the equation

$$-\partial_t \lambda\tilde{u} - \partial_x \sum_{i=0}^{N} \xi_i^2 \lambda_i = \frac{1}{\tau} \left(\sum_{i=0}^{N} \xi_i \lambda_i^{eq} - \lambda\tilde{u} \right), \tag{7.47}$$

As above if we want exact conservation of momentum, the equilibrium distribution needs to satisfy

$$\sum_{i=0}^{N} \xi_i \lambda_i^{eq} = \lambda\tilde{u}. \tag{7.48}$$

In order to close the adjoint system, we postulate that the adjoint equilibrium distribution satisfies (7.46), (7.45) and the relations

$$\sum_{i=0}^{N} \xi_i^2 \lambda_i^{eq} = \tilde{p} + \lambda \tilde{u}, \tag{7.49a}$$

$$\sum_{i=0}^{N} (\xi_i^2 + \tilde{\eta}_i^2) \lambda_i^{eq} = \lambda (b\tilde{\theta} + \lambda \tilde{u}^2), \tag{7.49b}$$

$$\sum_{i=0}^{N} \xi_i (\xi_i^2 + \tilde{\eta}_i^2) \lambda_i^{eq} = \lambda \left[(b+2)\tilde{\theta} + \lambda \tilde{u}^2 \right] \tilde{u}, \tag{7.49c}$$

where $\tilde{p}$, $\tilde{\theta}, \tilde{\eta}$ are some adjoint pressure, temperature and a constant similar to η. To close the momentum equation, we assume as for the flow equations that

$$\sum_{i=0}^{N} \xi_i^2 \lambda_i \approx \sum_{i=0}^{N} \xi_i^2 \lambda_i^{eq} = \tilde{p} + \lambda \tilde{u}$$

and we obtain

$$-\partial_t \lambda \tilde{u} - \partial_x (\tilde{p} + \lambda \tilde{u}) = \frac{1}{\tau} \left(\sum_{i=0}^{N} \xi_i \lambda_i^{eq} - \lambda \tilde{u} \right), \tag{7.50}$$

By multiplying (7.34) by $\sum_{i=0}^{N} (\xi_i^2 + \tilde{\eta}_i^2)$, we obtain, using similar closure law as above,

$$\begin{aligned} -\partial_t \left[\lambda (b\tilde{\theta} + \lambda \tilde{u}^2) \right] - \partial_x \left\{ \lambda \left[(b+2)\tilde{\theta} + \lambda \tilde{u}^2 \right] \tilde{u} \right\} \\ = \tfrac{1}{\tau} \left(\lambda (b\tilde{\theta} + \lambda \tilde{u}^2) - \sum_{i=0}^{N} (\xi_i^2 + \tilde{\eta}_i^2) \lambda_i \right) \end{aligned} \tag{7.51}$$

The final conditions at time $t = T$ are given as

$$\left\{ \begin{array}{rcl} \lambda & = & N(\rho - \rho_d) + (E - E_d) \sum_i (\eta_i^2 + \xi_i^2), \\ \lambda \tilde{u} & = & (m - m_d) \sum_i \xi_i^2 + (E - E_d) \sum_i \xi_i \eta_i^2, \\ \lambda \tilde{\theta} + \lambda \tilde{u}^2 & = & (\rho - \rho_d) \sum_i (\eta_i^2 + \xi_i^2) + (m - m_d) \sum_i \xi_i \eta_i^2 \\ & & + (E - E_d) \sum_i (\eta_i^2 + \xi_i^2)^2, \end{array} \right. \quad \text{at } t = T. \tag{7.52}$$

Note that in the previous equation, the flow variables are obtained from the solution of the flow equation at time T. They should then be seen as $\rho(T, \cdot)$, $\theta(T, \cdot)$ and so

on. We remark that the hydrodynamic limits of the adjoint microscopic system leads to a nonlinear system of conservation laws with source term. The source term can vanish if the adjoint equilibrium functional satisfies the constraints proposed in (7.46), (7.48) and (7.49). One has now to solve that system for the adjoint variables λ, $\tilde{u}$ and $\tilde{\theta}$.

7.3.4 The formal macroscopic adjoint system

In this section, we consider the Euler equation in one dimension (7.16) in its conservative form given by

$$\begin{aligned} \partial_t \rho + \partial_x m &= 0, \\ \partial_t m + \partial_x \left[\tfrac{E}{b} + \tfrac{m^2(b-1)}{b\rho} \right] &= 0, \\ \partial_t E + \partial_x \left[\tfrac{mE}{\rho} + \tfrac{2m(\rho E - m^2)}{b\rho^2} \right] &= 0, \end{aligned} \tag{7.53}$$

where the conservative variables $\mathbf{u} = (\rho, m, E)$ are related to the primitive variables (ρ, u, θ) by

$$m \doteq \rho u, \quad E \doteq \rho(b\theta + u^2). \tag{7.54}$$

Equation (7.53) can be written in a compact form as:

$$\mathbf{u}_t + f(\mathbf{u})_x = 0 \tag{7.55}$$

where the flux function $f(\mathbf{u})$ can be easily extracted. The Jacobian matrix of $f(\mathbf{u})$ with respect to $\mathbf{u}$ is given by

$$f'(\mathbf{u}) = \begin{bmatrix} 0 & 1 & 0 \\ -\frac{m^2(b-1)}{b\rho^2} & \frac{2m(b-1)}{b\rho} & \frac{1}{b} \\ -\frac{m(\rho E(b+2)-4m^2)}{b\rho^3} & \frac{\rho E(b+2)-6m^2}{b\rho^2} & \frac{m(b+2)}{b\rho} \end{bmatrix}. \tag{7.56}$$

The system (7.53) is strictly hyperbolic since the eigenvalues of the Jacobian matrix $f'(\mathbf{u})$,

$$\lambda_1(\mathbf{u}) = \frac{m}{\rho} - \frac{1}{b\rho}\sqrt{(b+2)(\rho E - m^2)}, \quad \lambda_2(\mathbf{u}) = \frac{m}{\rho}, \quad \lambda_3(\mathbf{u}) = \frac{m}{\rho} + \frac{1}{b\rho}\sqrt{(b+2)(\rho E - m^2)}$$

are real and distinct.

To derive the adjoint system, we assume that $\mathbf{u}$ is a column vector and we introduce the column matrix of Lagrange multipliers $\eta = [\eta_1, \eta_2, \eta_3]^t$ and write the Lagrangian as

$$L(\mathbf{u}(T,\cdot), \mathbf{u}_0; \mathbf{u}_d, \eta) = \mathcal{J}(\mathbf{u}(T,\cdot), \mathbf{u}_0; \mathbf{u}_d) - \int_0^T \int_{\mathbb{R}} \eta^t \left[\mathbf{u}_t + f(\mathbf{u})_x\right] dxdt.$$

The superscript ^{t} stand for the matrix transpose[1] so that $u^t v$ denote the usual dot product of the column vector u and v. We keep a matrix notation throughout this section. One can integrate by part the integral in the Lagrangian expression to have that

$$\begin{aligned} L(\mathbf{u}(T,\cdot), \mathbf{u}_0; \mathbf{u}_d, \eta) = \mathcal{J}(\mathbf{u}(T,\cdot), \mathbf{u}_0; \mathbf{u}_d) + \int_0^T \int_{\mathbb{R}} \eta_t^t \mathbf{u} + \eta_x^t f(\mathbf{u}) dxdt \\ - \int_{\mathbb{R}} \left[\eta(T,x)^t \mathbf{u}(T,x) - \eta(0,x)^t \mathbf{u}(0,x)\right] dx. \end{aligned}$$

By taking formally the variation of the Lagrangian with respect to the flow variable $\mathbf{u}$, we obtain the adjoint equation

$$-\eta_t - f'(\mathbf{u})^t \eta_x = 0. \tag{7.57}$$

We assume for the sake of generality that the cost functional has the integral form

$$\mathcal{J}(\mathbf{u}(T,\cdot), \mathbf{u}_0; \mathbf{u}_d) = \int_{\mathbb{R}} \psi(\mathbf{u}(T,x)) dx,$$

where $\psi : \mathbb{R}^3 \to \mathbb{R}^+$ is a given functional which depends possibly on some other function. The final condition for the adjoint equation can then be written as

$$\eta(T,\cdot) = \left(\frac{\partial \psi}{\partial \mathbf{u}}(\mathbf{u}(T,\cdot))\right)^t. \tag{7.58}$$

One can specify in a straightforward way this adjoint system for the Euler equations. We point out that we performed the above computation only formally since in general the flow generated by a system of conservation laws is not differentiable, see [29].

[1] Remark that this notation can be conflicting with that of the time t, but the difference between the two is clear from the context.

7.4 Relation between the microscopic-adjoint and the macroscopic-adjoint equations

In this section, we investigate the commutativity of the diagram given in Figure 7.1. In the previous section, we have derived formally the adjoint system related to the optimization of Euler flows. We obtained a backward linear system of conservation laws in the adjoint variables (7.57). On the other hand, we considered the moments of the adjoint Lattice Boltzmann system and obtained the microscopic-macroscopic adjoint system (7.45, 7.47, 7.51). The result is a nonlinear system of conservation laws with a source term which depends on the moments of the adjoint equilibrium distribution. With a suitable choice of the adjoint equilibrium distribution, this

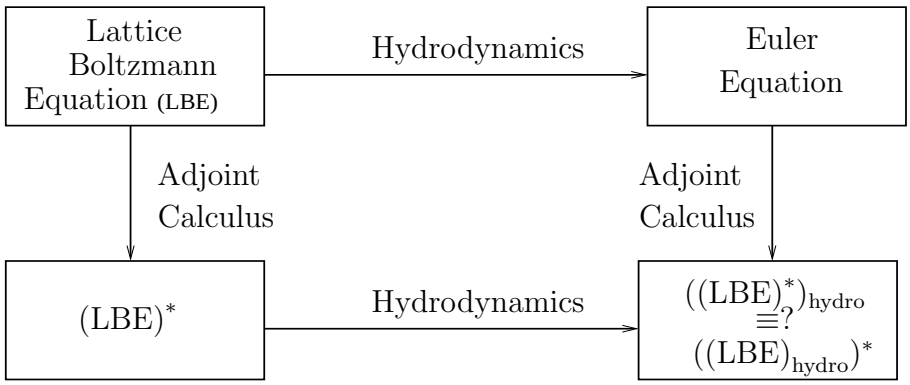

Figure 7.1: *Microscopic and macroscopic model: do they agree?*

source term can vanish. This amounts to require for example that $\lambda = \sum_{i=0}^{N-1} \lambda_i^{eq}$. However, one does not have many degrees of freedom in the choice of the equilibrium distributions. It is important to keep in mind that in general, the equilibrium distribution functional is found as a minimum of the entropy function under the constraints of conservation of mass and conservation of momentum [31, 30]. Since the adjoint collision operator is found as a linear combination of the derivatives of the equilibrium distribution functional, f_j^{eq}, with respect to the velocity distributions function f_i, this amounts to impose some constraints on both the equilibrium and

its derivatives. We found that this is meaningful only if the equilibrium functional is linear in the density and molecular velocities. But this case is not of much interest in practical problems.

7.5 Numerical Results

7.5.1 Solution of the flow equations

We point out that, for each particle i with speed ξ_i, the lattice Boltzmann equations (7.8) and its adjoint form (7.34) are transport equation with the source term. Therefore, we discretize them in the finite volume framework with a second order integration in time and a second order upwind integration in space with the minmod slope limiters [79] as briefly described below. We consider the advection equation in the general form

$$\begin{cases} v_t + a v_x &= g(v), \quad (x,t) \in [0,1] \times [0,T], \\ v(0,x) &= v^0(x), \quad x \in [0,1], \end{cases} \tag{7.59}$$

where a is the wave speed and $g(v)$ is a source term. We discretize the space domain $[0,1]$ with a uniform mesh as in Section 2.4. In the finite volume framework, we consider a second order scheme in the semi-discrete form [79]

$$\frac{dv}{dt} = -\frac{F_{j+\frac{1}{2}} - F_{j-\frac{1}{2}}}{\Delta x} + g_j, \tag{7.60}$$

where g_j is the cell average of the source term, and the numerical flux is given by

$$F_{j+\frac{1}{2}} = a^- v_{j+1} + a^+ v_j + \frac{1}{2}|a| \left(1 - |\frac{a\Delta t}{\Delta x}|\right) \sigma_{j+\frac{1}{2}}, \tag{7.61}$$

where $a^+ = \max\{a, 0\}$ and $a^- = \min\{a, 0\}$ and the slope limiters $\sigma_{j+\frac{1}{2}}$ are defined as

$$\sigma_{j+\frac{1}{2}} = \begin{cases} \text{Minmod}\,(v_j - v_{j-1}, v_{j+1} - v_j) & \text{if } a \geq 0, \\ \text{Minmod}\,(v_{j+1} - v_j, v_{j+2} - v_{j+1}) & \text{if } a < 0, \end{cases} \tag{7.62}$$

with

$$\text{Minmod}(x,y) \doteq \frac{1}{2}(\text{sgn}(x) + \text{sgn}(y)) \cdot \min(|x|, |y|).$$

The mesh size in time is set as $\Delta t = \varepsilon/4$ where ε is the Knudsen number. This choice ensures that the CFL condition is satisfied for appropriate values of the Knudsen number. For the numerical results, we used $\varepsilon = 10^{-4}$. For the source term, we use the mid-point rule quadrature.

We test the proposed flow solver on solution of the Lax shock tube problem described as follows: A tube is filled with a gas initially divided by a membrane into two sections. The gas has a higher density and pressure in one half of the tube than in the other, with zero velocity everywhere. At time $t = 0$, the membrane is suddenly removed and the gas is allowed to flow. We expect a net motion in the direction of the lower pressure. Assuming uniform flow across the tube, there is variation only in one direction and the 1-D Euler equations apply. For the lattice Boltzmann simulations, the initial macroscopic variables are taken as

$$\mathbf{u}_0(x) = \begin{cases} (1, 0, 3) & \text{for } x < 0 \\ (3, 0, 15) & \text{for } x > 0 \end{cases} \tag{7.63}$$

As a reference solution, we use the second order in space and time central scheme of Kurganov and Tadmor [75] computed on a grid of $N = 400$ points with $CFL = 0.74$. We present the numerical solution obtained with the lattice Boltzmann model and the relaxation method in Figure 7.2 computed up to time $t = 0.15$. The solution obtained with a D1Q5 lattice Boltzmann model (circle) compares well with that obtained in the central scheme of Kurganov (solid line), the shock, contact discontinuity and the rarefaction waves are well resolved. Also, a comparison with the scheme presented in [85, 78, 75] proves satisfactory.

7.5.2 Grid convergence analysis

In this section, we investigate the convergence of the lattice Boltzmann method when the grid size increases. This is important since we want the result of solution of the flow equation computed with the LBE to reproduce the hydrodynamic behavior independently of the mesh used. For this purpose, we solve numerically approximation of the Euler equation given by the LBE equation using the finite

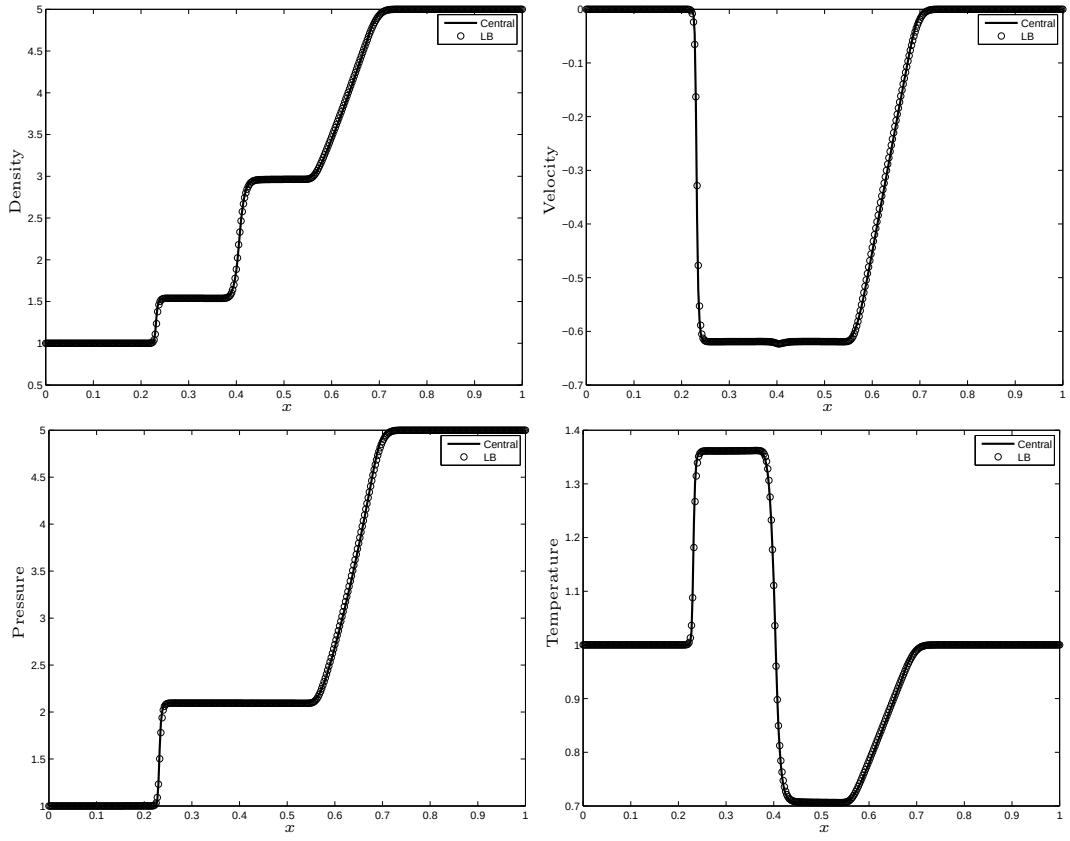

Figure 7.2: *Plot of the density, velocity, pressure and temperature computed at time* $t = 0.15$ *with a central scheme and the D1Q5 lattice Boltzmann model for the Euler equations.*

volume scheme discussed above for meshes of size $N \in \{80, 160, 320, 640\}$ and we compute the reference solution with a finer grid of $N = 1280$ points. We use the following Riemann data:

$$\mathbf{u}_0(x) = \begin{cases} (0.445, 0.311, 8.928) & \text{for } x < 0.5, \\ (0.5, 0.10, 1.4275) & \text{for } x > 0.5. \end{cases} \tag{7.64}$$

This problem can be described physically as the Lax shock tube problem, with a gas with non-zero velocity on each side of the membrane. We show in Figure 7.3 the profile of the conservative variables given by the density, the momentum, the

energy as well as the pressure.

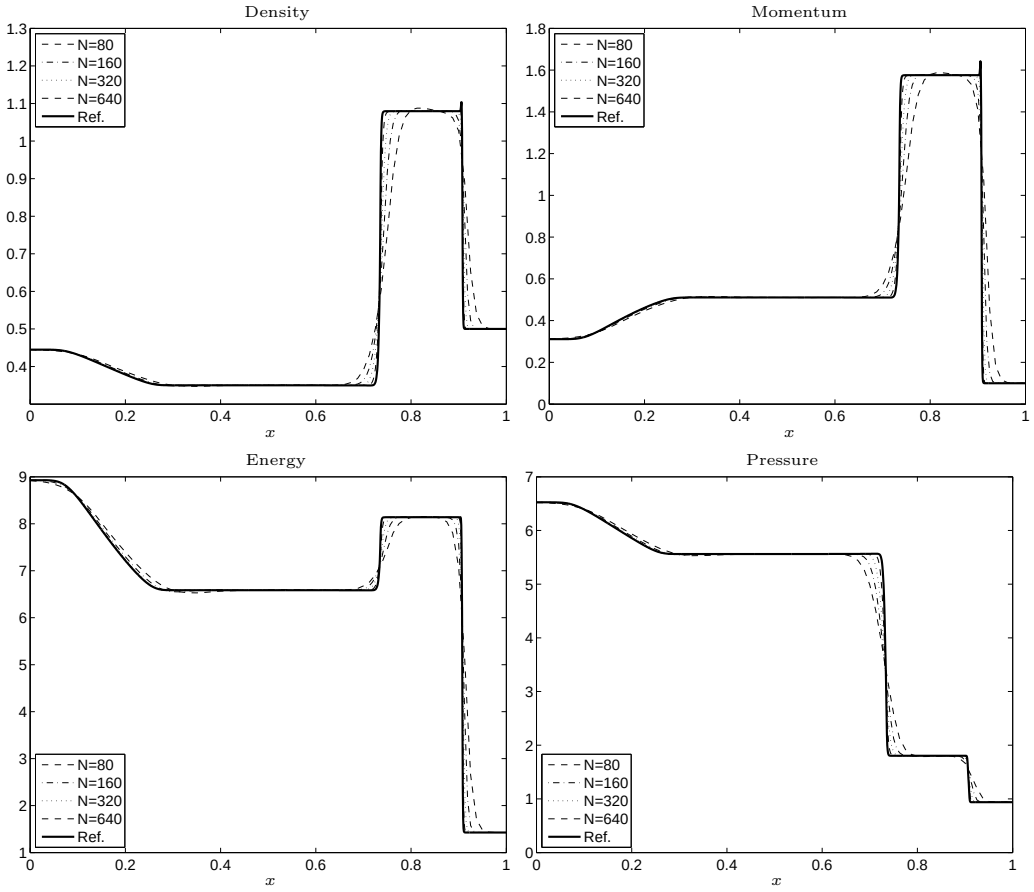

Figure 7.3: *Plot of the density, momentum, energy and pressure computed at time* $t = 0.15$ *with meshes of multiple sizes.*

The LBE flow solver used here is convergent and, as the grid is refined, the solution is more and more accurate. Moreover, the solutions obtained with the different grid as depicted in Figure 7.3 have the same qualitative behavior, that is, an expansion or rarefaction wave moving to the left, a contact discontinuity wave in the middle and a shock wave moving to the right.

7.5.3 The discrete form of the optimization problem

With the space and time discretization described above, the discrete form of the objective function can then be written as

$$\mathcal{J}(\mathbf{u}(\cdot,T),\mathbf{u}_0,\mathbf{u}_d)=\Delta x\sum_{i=1}^{K}\|\mathbf{u}_i^H-\mathbf{u}_{d\,i}\|^2.$$

Recall that the vector $\mathbf{u}=(\rho,m,E)$ contains the conservative variables which are the density, the momentum and the energy. For a given initial data $\mathbf{u}_0$, one can solve numerically the flow equations for the state variable $\mathbf{u}(T,\cdot)(\mathbf{u}_0)$ using the lattice Boltzmann method and the optimization problem (7.1) can be re-written as an unconstrained minimization for the reduced cost functional $\tilde{\mathcal{J}}=\mathcal{J}\left(\mathbf{u}(T,\cdot)(\mathbf{u}_0);\mathbf{u}_d\right)$. One can then compute the gradient of this reduced cost using the finite difference method. At each grid point, the gradient of the cost functional is computed using the adjoint method proposed in the previous sections. From the optimality conditions, we obtain that the gradient of the reduced cost functional satisfies

$$\nabla_{v_{0,i}}\tilde{\mathcal{J}}=\Delta x\sum_{j=0}^{N-1}\frac{\partial f_j^{eq}(\rho^0,u^0,\theta^0)}{\partial\mathbf{u}_{0,i}}\lambda_j(0,x_i). \tag{7.65}$$

Using this gradient information, we can compute the solution of the optimization problem using a descent algorithm with a line search algorithm. Here we used the Armijo line search algorithm [72, 88]. The test for convergence is done as

$$|\mathcal{J}(\mathbf{u}(\cdot,T),\mathbf{u}_0,\mathbf{u}_d)|<\text{tol},$$

where $\text{tol}\ll 1$ is a given tolerance.

7.5.4 An example with smooth data

We start the numerical investigations with the case of smooth data in the domain $[0,1]\times[0,T]$. We are searching for an optimal control (initial data) such that the flow properties at time T match the flow initially given by

$$\rho_{d,0}(x)=6x^2-7x+3.2,\ m_{d,0}(x)=1.2,\ E_{d,0}=x+1.2 \text{ for } x\in[0,1]. \tag{7.66}$$

We start the optimization algorithm with the initial data

$$\rho^0(x) = 6x^2 - 7x + 3,\ m^0(x) = 1.0,\ E^0(x) = x + 1.0 \text{ for } x \in [0, 1]. \tag{7.67}$$

The optimization problem is solved with a tolerance tol $= 10^{-4}$. The initial, target and optimized states are presented in Figure 7.4. The target state is attained and the optimization routine presented here performs very well on this simple problem.

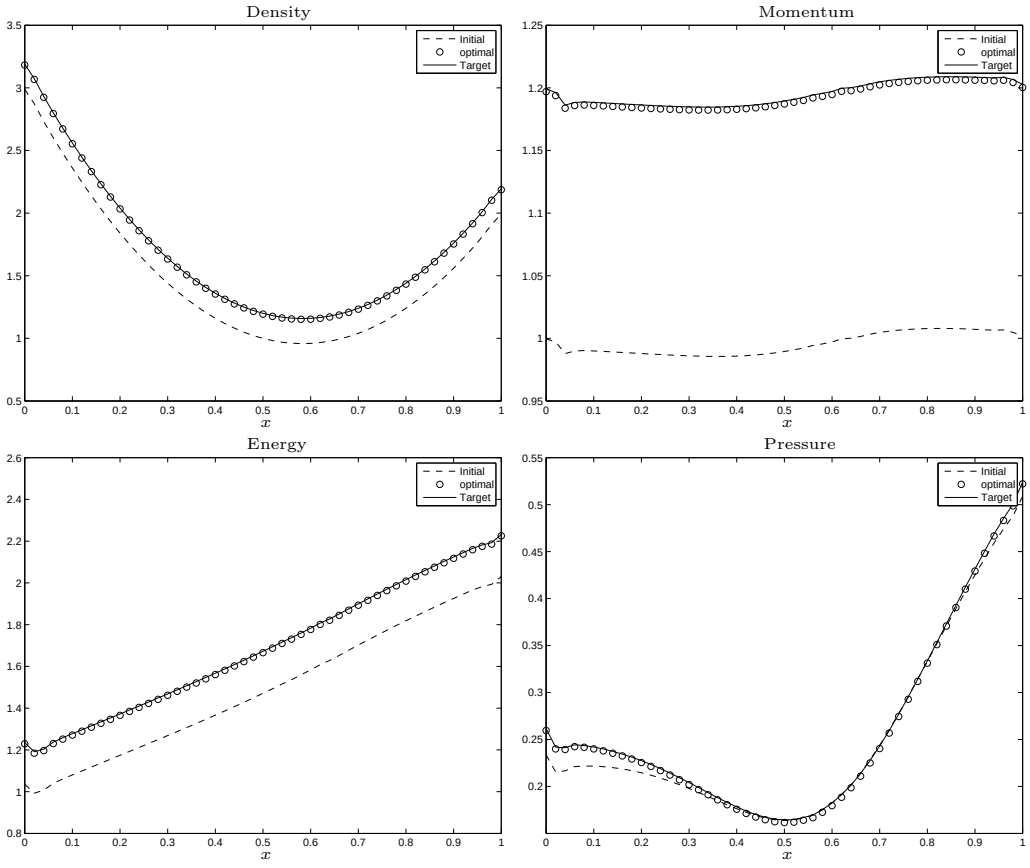

Figure 7.4: *Density, momentum, energy and pressure: Initial, target and Optimized values at time* $T = 0.01$ *for the example with smooth data.*

7.5.5 The inverse design of flow in a shock tube

The examples presented in this section involve the inverse design of a flow in a 1D shock-tube. Given a set of measurements of some actual flow at time $t = T$, determine the best estimate for the initial state that leads to the observed flow behavior at the final time. This problem has been explored before by many authors [64, 58, 66], but unlike them, we use the lattice Boltzmann approach for the solution of the flow equation and the derivation of the adjoint calculus based on the microscopic variable. We now consider numerical example derived from the Sod shock tube problem. The target flow is obtained as the solution of a Riemann problem. This is mainly for consistency because the objective function is evaluated only in the "dual" space which here is , the space of solution of the flow equation computed at time T. For the optimal control of the Sod problem, we consider the initial data and desired initial data given as

$$\mathbf{u}_0 = \begin{cases} (1.0,\, 0,\, 3.0) & \text{if } x < 0.5, \\ (0.125,\, 0,\, 0.375) & \text{if } x > 0.5, \end{cases} \tag{7.68a}$$

and

$$\mathbf{u}_{d,0} = \begin{cases} (1.1,\, 0,\, 3.3) & \text{if } x < 0.5, \\ (0.2,\, 0,\, 0.6) & \text{if } x > 0.5, \end{cases} \tag{7.68b}$$

respectively. We consider a time horizon of $T = 0.03$ in non-dimensional units and we solve the control problem related to the Sod problem with data in (7.68). We used a second order scheme as described in Section 7.5.1 with a mesh size of $N = 300$ cells. The results of the optimization problem are presented in Figure 7.5.

We used a tolerance tol $= 10^{-4}$. We see that the optimization routine performs very well and the optimum is reached after 38 design iterations with a fix optimization step of $\alpha = 0.047$. We solve the same problem with the first order scheme switching off the limiters $\sigma_{i+\frac{1}{2}}$ in the numerical fluxes (7.61). We present in Figure 7.6 the profile of the density and pressure.

The contact discontinuity wave in the solution of the flow equations is not well resolved due to the smearing that usually appears with first order schemes. Nevertheless, the values of the gradients and the objective function, presented in Figure 7.7

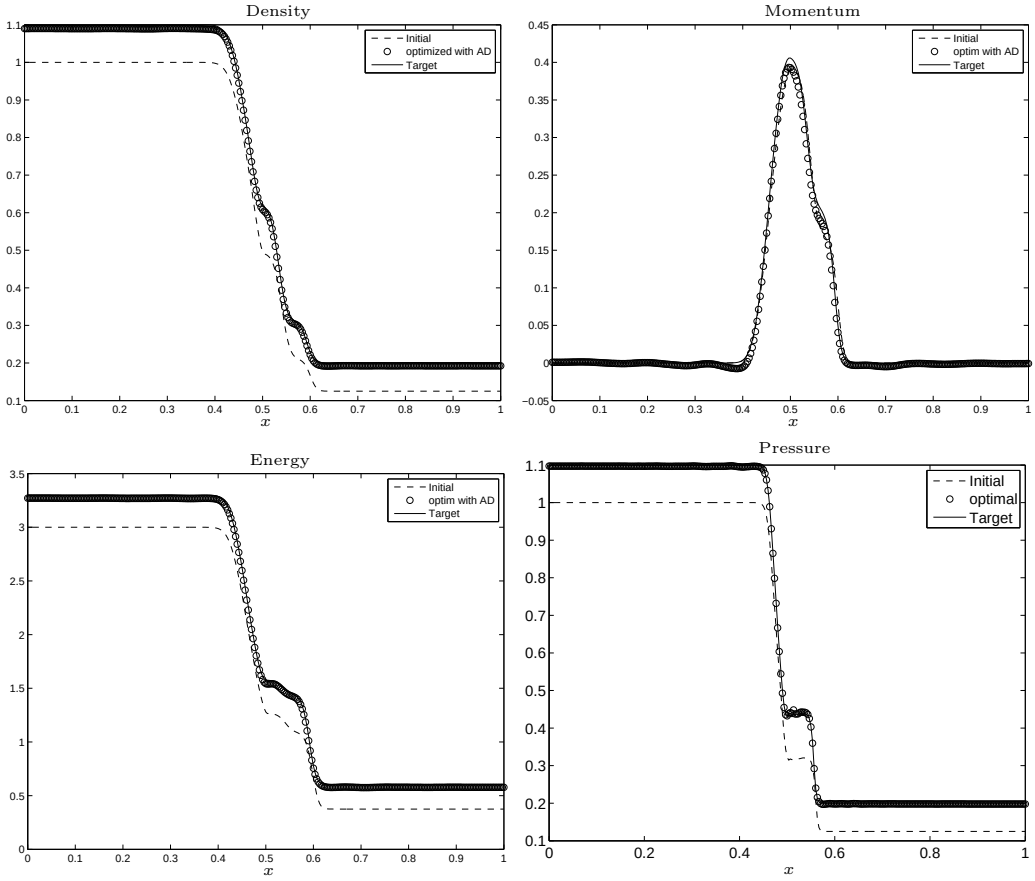

Figure 7.5: *Density, momentum, energy and pressure: initial, optimized and target flow variables at* $t = 0.03$. *for the inverse design of flow in a shock tube problem.*

show that the first order and second order scheme lead to similar values of the cost functional. This is important to notice because the optimization method failed for some test problems to compute the solution when the second order scheme was used. We remark also that the distributed gradient of the objective function have the same qualitative behavior for both schemes even if the exact values are not always the same. In Figure 7.8 we display the gradients of the cost functional at time $T = 0.03$ in term of the flow variable.

The failure of the second order scheme was pointed out by Banda and Herty [5] and Ulbrich [104] for scalar conservation laws. The second order schemes neverthe-

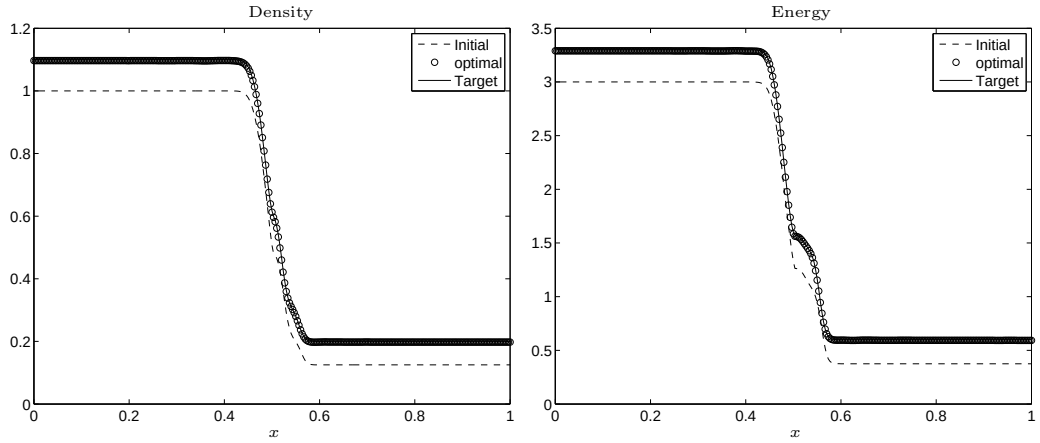

Figure 7.6: *Profile of the density(left) and energy(right) for the optimization problem with data* (7.68) *with the flow equation computed with a first order scheme.*

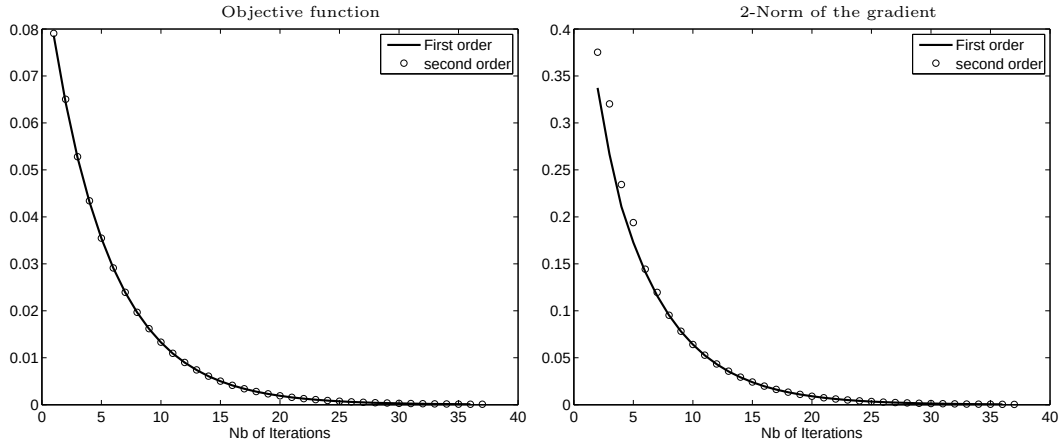

Figure 7.7: *Values of the objective function and the* $\mathbf{L}^2$ *norm of the gradient computed with the first order and second order scheme.*

less performs well for the solution of the optimization problem. The drawback is that it works only for small times. Moreover, we solved the Sod problem for a longer time $T = 0.15$ with the first order scheme as it was done by Homescu and Navon [64]. The profile of the density and energy are presented in Figure 7.9.

The results presented here compare very well with those obtained in [64].

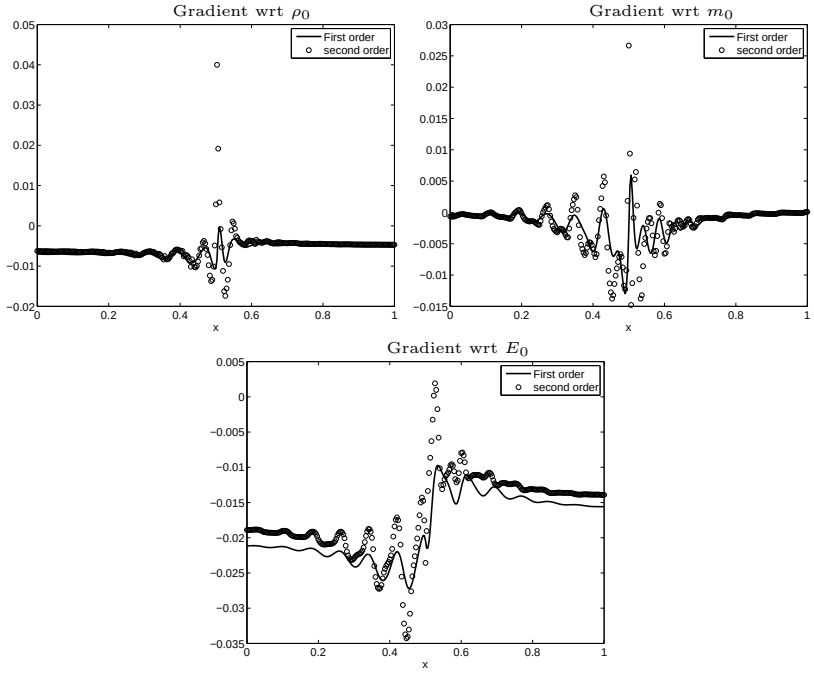

Figure 7.8: *Gradients of the cost functional with respect to the control variables at time* $T = 0.03$.

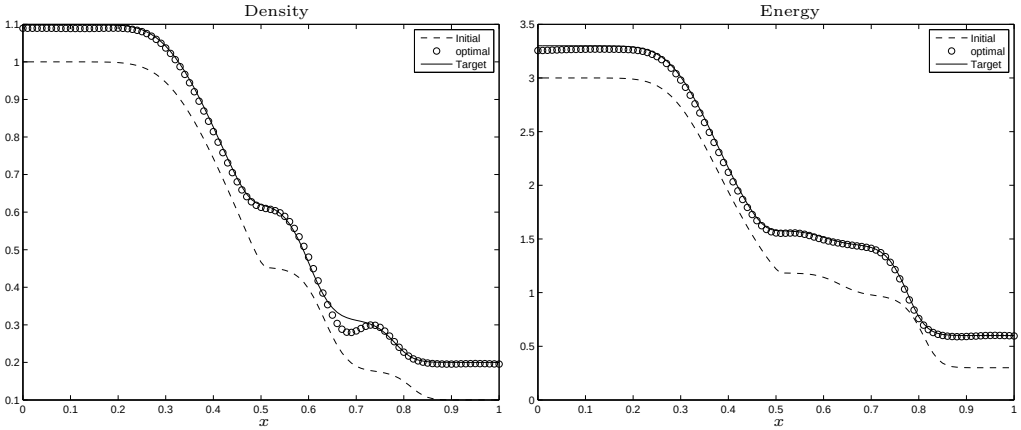

Figure 7.9: *Profile of the density and energy for the optimization problem at time* $T = 0.15$ *with the flow equation computed with a first order scheme.*

Note that we consider as control variables here, the conservative variables $\mathbf{u}_0 = (\rho_0, m_0, E_0)$ which are distributed along the flow domain. In [64], only the densities and the pressures were considered as control variables.

7.5.6 Convergence and CPU time

Here we investigate the convergence of the optimization method using the lattice Boltzmann method in terms of the number of grid points for a given tolerance. We consider here the example on the inverse design of flow in a shock tube with initial data (7.68). For a tolerance of tol $= 10^{-4}$ we compute up to the time $T = 0.03$ the solution of the optimal control problem related to the Euler equation with the grid size in $\{50, 100, 150, 200, 250, 300\}$. The value of the cost function, the $\mathbf{L}^2$ norm of the gradient of the cost functional, the number of optimization iterations (Nb It.) and the CPU time are presented in Table 7.1. The notable observation is that the number of optimization iterations does not depend on the grid size. This shows that the LB method does not depend on the chosen lattice. The differences in the values of the objective function are mainly due to the error related to the solution of the flow equation.

N	$\mathcal{J}(\mathbf{u}(T,\cdot), \mathbf{u}_0; \mathbf{u}_d)$	$\|\nabla\tilde{\mathcal{J}}(\mathbf{u}(T,\cdot), \mathbf{u}_0; \mathbf{u}_d)\|$	Nb It.	CPU time (in sec.)
50	9.088619e-05	3.814747e-04	37	6.426500e+02
100	9.186854e-05	3.797603e-04	37	1.087600e+03
150	9.199552e-05	3.781883e-04	37	1.497710e+03
200	9.310957e-05	3.813341e-04	37	1.916500e+03
250	9.211987e-05	3.805600e-04	37	2.322430e+03
300	9.049610e-05	3.430007e-04	37	2.823490e+03

Table 7.1: *Convergence and CPU time for the solution of the inverse design of flow in a shock tube.*

7.6 Concluding Remarks

We have presented in this chapter an adjoint calculus for the optimization of Euler flows using the Lattice Boltzmann Equations. We have proved that the LBM converges to the Euler equations using the Chapman-Enskog expansion. We studied the hydrodynamic limits of the adjoint system and propose some closure relations in order to have a consistent system in the macroscopic adjoint variables. This method is easy to implement and allows extension to higher order and multidimensional problems. An interesting fact about the results proposed here is that the number of optimization iterations needed to achieve convergence does not depend on the grid size. The numerical results compare well with those obtained by Rumpfkeil and Zingg [96], Homescu and Navon [64] on a similar problem. Moreover, it appears clear that the approach presented here, using the lattice Boltzmann model has no problem dealing with discontinuity such as shocks, rarefaction or contact discontinuities in the solution of the flow equations. There is no need for us to detect the discontinuity in the solution or to consider the shock position as a control variable as was done in [64] to solve the problem. This is an improvement on the results presented by Homescu and Navon [64].

Chapter 8

Summary and Future Work

In this thesis, we presented some classical results pertaining to the analysis and numerical integration of systems of conservation laws. We presented basic definitions and the construction of the solution to the standard Riemann problem. Some basic results and the general assumptions for the solution of the Cauchy problem at the junction were introduced. We briefly presented the upwind and central schemes and emphasized the conservative properties and the stability of these schemes for the numerical solution of systems of conservation laws.

Our first application was the study of the *drift-flux* model in a network of pipes. We derived the model equations from the *two-fluid* model and the assumption of vanishing *slip-function* and source term. We solved the Riemann problem at the junction for a simple pressure law and then did the same for a general pressure law by deriving carefully the Lax curves. We proposed, for a network of pipes, suitable coupling conditions for the solution of the Riemann problem at the junction. We proved a well-posedness result for the Riemann problem at the junction. Our constructive proof led to the numerical simulation of some junctions of interest. We used an upwind second order relaxation scheme for the solution of the flow equations and the Newton method to find the zeros of our *coupling conditions map*.
As future work in this direction, one can consider the Cauchy problem at the junction. Based on previous work on the p-system and on the Euler equation by Colombo

et al. [33, 41], it might be possible to develop a complete theory for the solution of the Cauchy problem at the junction for the drift-flux model. In order to drop the no-slip condition, one might have to go back to the two-fluid model and rather consider a 4×4 system of conservation laws.

Our second application dealt with the dynamics of the shallow water equations in a network of rivers. We first introduced the model equations for the flow and presented some general properties of the flow. We discussed the solution of the Riemann problem at junction for the shallow water equations in a network of rivers. We presented numerical results for the case of a confluence of three connected rivers, that of a river and a tributary and that of a storage basin. Still in this part, we considered the dynamics of pooled stepped chutes, a geometry used in dams to discharge flood water. Our approach here was to compute independently the water flow between the horizontal stepped chutes and to couple the dynamics with suitable coupling conditions. We compared the water height at the dam computed with our method with that obtained in the hydraulic community via experiments. The two results agreed and we then obtained a validation of our coupling conditions.

Finally, as a preliminary step for the control of fluid in networks, we solved an optimization problem with an objective function of a matching type and with constraints being the Euler equations. The novelty here was the linearization of the flow equations using the lattice Boltzmann equations (LBE). We derived the optimality condition using the microscopic model, the LBE, and we obtained our optimal macroscopic states using a multiscale technique. Precisely, we considered the hydrodynamic limit of our microscopic result as the Knudsen number goes to zero. We then obtain a new method for the solution of the optimization problems with the Euler equation as constraints on the flow. We implemented our method and we used it to solve some interesting problems in fluid mechanics. Future work in this area may consist of using the same method to solve two dimensional or three dimensional control problems related to the Euler equations. The analysis done here for the one dimensional case can be use with some straightforward changes. Also, one might attempt to solve control problems related to the Euler equations in a

network of pipes using the LBE method presented here. The big question is how can the coupling conditions, that are given in terms of the macroscopic variables, be included in the microscopic model? As demonstrated in this thesis, an open mind to the offerings of different points of view can serve to strengthen our ability to confront these open problems in our future work.

Bibliography

[1] D. Amadori and A. Corli. On a model of multiphase flow. *SIAM J. Math. Anal.*, 40(1):134–166, 2008.

[2] E. Audusse, F. Bouchut, M.-O. Bristeau, R. Klein, and B. Perthame. A fast and stable well-balanced scheme with hydrostatic reconstruction for shallow water flows. *SIAM J. Sci. Comp*, 25:2050–2065, 2004.

[3] M. K. Banda. *Kinetic-based numerical schemes in fluid dynamics*. Shaker Verlag, Aachen, 2004.

[4] M. K. Banda and M. Herty. Multiscale modeling of gas flow in pipe networks. *Mathematical Methods in the Applied Sciences*, 31(8):915–936, 2008.

[5] M. K. Banda and M. Herty. Adjoint IMEX–based schemes for Control Problems Governed By Hyperbolic Conservation Laws. *preprint*, 2009.

[6] M. K. Banda, M. Herty, and A. Klar. Coupling conditions for gas network governed by the isothermal Euler equations. *Networks and Heterogeneous media*, 1(2):295–314, June 2006.

[7] M. K. Banda, M. Herty, and A. Klar. Gas flow in pipeline networks. *Networks and Heterogeneous media*, 1(1):41–56, March 2006.

[8] M. K. Banda, M. Herty, and J. M. T. Ngnotchouye. Coupling the drift-flux models with unequal sonic speeds. *Mathematical and Computational Applications*, 15(4):574–584.

[9] M. K. Banda, M. Herty, and J. M. T. Ngnotchouye. Modelling and simulating multiphase drift-flux model in a networked domain. In L. Wiryanto and S. Pudjaprasetya, editors, *Proceedings of the Int. Conf. on Industrial and Appl. Math.*, pages 127–133. Institut Teknologi Bandung, Indonesia, 2010.

[10] M. K. Banda, M. Herty, and J. M. T. Ngnotchouye. Towards a mathematical analysis of multiphase Drift-Flux model in networks. *SIAM J. Sci. Comp*, 31(6):4633–4653, 2010.

[11] F. Berthelin and F. Bouchut. Relaxation to isentropic gas dynamics for a BGK system with single kinetic entropy. *Meth. and Appl. of Analysis*, 9(2):313–327, 2002.

[12] S. Bianchini. On the shift differentiability of the flow generated by a hyperbolic system of conservation laws. *Discrete Contin. Dynam. Systems*, 6(2):329–350, 2000.

[13] R. M. Boes and W. H. Hager. Hydraulic design of stepped spillways. *Journal of Hydraulic engineering*, 129(9):671–679, 2003.

[14] F. Bouchut, F. Golse, and M. Pulvirenti. *Kinetic equations and asymptotic theory.* Series in Appl. Math. Gauthiers-Villars, 2000.

[15] F. Bouchut and F. James. One-dimensional transport equations with discontinuous coefficients. *Nonlinear Anal.*, 32:891–933, 1998.

[16] F. Bouchut and F. James. Differentiability with respect to initial data for a scalar conservation law. In *Hyperbolic problems: theory, numerics, applications.* Internat. Ser. Numer. Math, Birkhuser, Basel, 1999.

[17] F. Bouchut and F. James. Duality solutions for pressureless gases, monotone scalar conservation laws, and uniqueness. *Comm. Partial Differential Equations*, 24:2173–2189, 1999.

[18] F. Bouchut and T. Morales. A subsonic-well-balanced reconstruction scheme for shallow water flows, 2009. (Preprint).

[19] A. Bressan. *Hyperbolic systems of Conservation laws*, volume 20 of *Oxford Lectures Series in Mathematics and its Applications*. Oxford University Press, 2000.

[20] A. Bressan and S. Bianchini. Vanishing viscosity solutions of nonlinear hyperbolic systems. *Annals of Mathematics*, 161:223–342, 2005.

[21] A. Bressan and P. Goatin. Oleinik type estimates and uniqueness for n×n conservation laws. *J. Differential Equations*, 156:26–49, 1999.

[22] A. Bressan and G. Guerra. Shift-differentiability of the flow generated by a conservation law. *Discrete Contin. Dynam. Systems*, 3(1):35–58, 1997.

[23] A. Bressan and P. Lefloch. Uniqueness of weak solutions to system of conservation laws. *Arch. Rational Mech. Anal.*, 140:301–317, 1997.

[24] A. Bressan and P. Lefloch. Structural stability and regularity of entropy solutions to hyperbolic systems of conservation laws. *Indina Univ. Math. J.*, 48:43–84, 1999.

[25] A. Bressan and M. Lewicka. Shift differentials of maps in BV spaces. In *Nonlinear theory of generalized functions (Vienna, 1997)*, volume 401 of *Chapman & Hall/CRC Res. Notes Math.*, pages 47–61. Chapman & Hall/CRC, Boca Raton, FL, 1999.

[26] A. Bressan, T. P. Liu, and T. Yang. l^1 stability estimates for n×n conservation laws. *Arch. Rational Mech. Anal.*, 149:1–22, 1999.

[27] A. Bressan and A. Marson. A variational calculus for discontinuous solutions to conservation laws. *Communications Partial Differential Equations*, 20:1491–1552, 1995.

[28] A. Bressan, B. Piccoli, and G. Grasta. Well psedness of the Cauchy problem for n×n systems of conservation laws. *Amer. Math. Soc. Memoir*, 694, 2000.

[29] A. Bressan and W. Shen. Optimality conditions for solutions to hyperbolic balance laws. *Control methods in PDE-dynamical systems, Contemp. Math.*, 426:129–152, 2007.

[30] S. Chen and G. D. Doolen. Lattice Boltzmann method for fluid flows. *Annu. Rev. Fluid Mech.*, 30:329–364, 1998.

[31] S. S. Chikatamarla and I. V. Karlin. Lattices for the lattice Boltzmann method. *Physical Review*, E 79(046701), 2009.

[32] R. M. Colombo and M. Garavello. A well posed riemann problem for the p-system at a junction. *Networks and Heterogeneous Media*, 1(3):495–511, 2006.

[33] R. M. Colombo and M. Garavello. On the cauchy problem for the p-system at a junction. *SIAM Journal of Mathematical Analysis*, 39(5):1456–1471, 2008.

[34] R. M. Colombo and M. Garavello. On the 1D modeling of fluid flowing through a junction, 2009. Preprint.

[35] R. M. Colombo and A. Groli. On the optimization of a conservation law. *Calculus of Variation and PDEs*, 19(3):269–280, 2004.

[36] R. M. Colombo and A. Groli. On the optimization of the initial boundary value problem for a conservation law. *Journal of Mathematical Analysis*, 291(1):82–99, 2004.

[37] R. M. Colombo, G. Guerra, M. Herty, and V. Sachers. Modeling and optimal control of networks of pipes and canals. Technical report, Milano Bicocca University, 2008.

[38] R. M. Colombo, M. Herty, and V. Sachers. On 2×2 conservations laws at a junction. *SIAM Math. Anal.*, 40(2):605–622, 2008.

[39] R. M. Colombo and F. Marcellini. Coupling conditions for the 3×3 euler system, 2010. preprint.

[40] R. M. Colombo and F. Marcellini. Smooth and discontinuous junctions in the p-system. *Journal of Mathematical Analysis and Applications*, 361:440–456, 2010.

[41] R. M. Colombo and C. Mauri. Euler system for compressible fluids at a junction. *Journal of Hyperbolic Differential equations*, 5(3):547–568, September 2008.

[42] C. M. Dafermos. *Hyperbolic conservation laws in continum physics*, volume 325 of *Grundlehren der mathematischen Wissenschaften*. Springer, 2 edition, 2005.

[43] M. de Saint-Venant. Théorie du mouvement non permanent des eaux, avec application aux crues des rivières et à l'introduction des marées dans leur lit. *Acad. Sci. Comptes Rendus,*, pages 147–154,237–240, 1871.

[44] A. I. Delis. Improved application of HLLE riemann solver for the shallow water equations with source terms. *Communications in Numerical Methods in Engineering*, 19:59–83, 2003.

[45] A. I. Delis and T. Katsounis. Relaxation schemes for the shallow water equations. *Int. J. Numer. Meth. Fluids*, 41:605–719, 2003.

[46] E. Duret, I.Faille, M. Gainville, V. Henriot, H. Tran, and F. Willien. Two models for the simulation of multiphase flows in oil and gas pipelines. Mathematical and Numerical Aspects of Low Mach Number Flows, June 2004. Institut Françcais du Pétrole, 1 et 4 avenue de Bois Préau, 92852 Rueil Malmaison.

[47] S. Evje and K. Fjelde. Relaxation schemes for calculation of two phase flow in pipes. *Elsevier science Ltd*, 2002.

[48] S. Evje and T. Flåtten. Hybrid flux-splitting schemes for a common two-fluid model. *Journal of computational physics*, 192:175–210, 2003.

[49] S. Evje and T. Flåtten. Hybrid central-upwind schemes for numerical resolution of two-phase flows. *ESAIM: Math. Mod. Num. Anal*, 39(5):1449–1484, 2005.

[50] S. Evje and T. Flåtten. A WIMF scheme for the drift-flux two-phase flow model. *SIAM Journal of Scientific Computing*, 26:1449–1484, 2005.

[51] S. Evje and T. Flåtten. On the wave structure of the two-phase flow models. *SIAM Journal of Applied Mathematics*, 67(2):487–511, 2007.

[52] S. Evje and K. H. Karlsen. Global existence of solution for a viscous two-phase model. *J. Differential Equations*, 245(9):2660–2703, 2008.

[53] L. V. Fausett. *Applied numerical analysis using Matlab*. Pearson Prentice hall, 2 edition, 2008.

[54] F. França and R. L. Jr. The use of drift-flux techniques for the analysis of horizontal two-phase flows. *International Journal of Multiphase flow*, 18:787–801, 1992.

[55] J. Glimm. Solutions in the large for nonlinear hyperbolic systems of equations. *Comm. Pure Appl. Math.*, 18:697–715, 1965.

[56] S. Gottlieb, C.-W. Shu, and E. Tadmor. Strong stability preserving high-order time discretization methods. *SIAM rev.*, 43:89–112, 2001.

[57] N. Goutal and F. Maurel. Dam break wave simulation. EDF, Laboratoire National d'Hydraulique, France.

[58] M. D. Gunzburger. *Perspective in Flow control and Optimization*. SIAM, 2002.

[59] P. Hartman. *Ordinary differential equations*. Society of industrial and applied mathematics, 2 edition, 2002.

[60] B. Haut. *Modelling and control of road traffic networks*. PhD thesis, UCL. - FSA/INMA - Département d'ingénieurie mathématique, 2007.

[61] M. Herty. Coupling conditions for networked systems of Euler equations. *SIAM J. Sci. Comp.*, 30(3):1596–1612, 2007.

[62] M. Herty and M. Rascle. Coupling conditions for a class of second order models for traffic flow. *SIAM J. MATH. ANAL*, 38(2):592–616, 2006.

[63] H. Holden, N. H. Risebro, and H. Sande. The solution of the Cauchy problem with large data for a model of a mixture of gases. Preprint, November 2007.

[64] C. Homescu and I. M. Navon. Optimal control of flow with discontinuities. *Journal of Computational physics*, 187(2):660–682, 2003.

[65] L. Iritz. Rainfall input in an adaptative river flow forecast. *Hydrological Sciences-Journal des sciences hydrauliques*, 37(6):607–619, 1992.

[66] A. Jameson. Aerodynamic design via control theory. In *Recent advances in computational fluid dynamics*. Springer, Berlin, 1989.

[67] A. Jameson. Aerodynamic shape optimization using adjoint method, 2003. Lectures note at the Von Karman Institute, Brussels.

[68] S. Jin. Runge-Kutta methods for hyperbolic conservation laws with stiff relaxation terms. *J. Comput. Phys.*, 122:51–67, 1995.

[69] S. Jin and Z. Xin. The relaxation schemes for systems of conservation laws in arbitrary space dimensions. *Comm. Pure Appl. Math.*, 48:235–276, 1995.

[70] S. Karni, E. Kirr, and A. K. G. Petrova. Compressible two-phase flows by central and upwind schemes. *M2AN Math. Model. Numer. Anal.*, 38:477–493, 2004.

[71] T. Kataoka and M. Tsutahara. Lattice Boltzmann method for compressible Euler equations. *Physical Review*, E(3)69(056702), 2004.

[72] C. T. Kelly. *Iterative methods for Optimization*. Frontiers in applied mathematics. SIAM, 1999.

[73] S. Kruzkhov. First order quasilinear equations with several independent variables. *Mat. Sb. (N.S.)*, 123:228–255, 1970. English translation: Math USSR Sbornik 10 (1970), 217-273.

[74] A. Kurganov and G. Petrova. A second order well balanced positivity preserving central-upwind scheme for the Saint-Venant system. *Commun. Math. Sci*, 5(1):133–160, 2007.

[75] A. Kurganov and E. Tadmor. New high resolution central schemes for nonlinear conservation laws and convection-diffusion equations. *J. Comp. Phys.*, 160:241–282, 2000.

[76] T. Lange, M. K. Banda, and J. M. T. Ngnotchouye. Time domain simulations of the dynamics of rivers networks. In D. P. Mason, editor, *Proceedings of the mathematics in industry study group*, pages 41–61. The university of the Witwatersrand, 2008.

[77] G. Leugering and E. J. P. G. Schmidt. On the modelling and stabilization of flows in networks of open canals. *SIAM J. Control Optim*, 41(1):164–180, 2002.

[78] R. J. LeVeque. *Numerical methods for conservation laws*. Birkhäuser Verlag, 1992.

[79] R. J. LeVeque. *Finite volume methods for hyperbolic problems*. Cambridge texts in applied mathematics. Cambridge Unviversity Press, 2002.

[80] T. P. Liu. The entropy condition and the admissibility of shocks. *J. Math. Anal. Appl.*, 53:78–88, 1976.

[81] T. P. Liu. The deterministic version of the Glimm scheme. *Comm. Math. Phys.*, 57:135–148, 1977.

[82] Z. Liu and A. Sandu. On the properties of discrete adjoints of numerical methods for the advection equation. *Int. J. for Num. Meth. in Fluids*, 56:769 – 803, 2008.

[83] M. Mercier. *Étude de différent aspects des* EDP *hyperboliques*. PhD thesis, Université de Lyon I, 2009.

[84] R. L. Mott. *Applied fluid mechanics*. Pearson Prentice Hall, New Jersey, 2006.

[85] H. Nessayahu and E. Tadmor. Non-oscillatory central differencing for hyperbolic conservation laws. *Journal of Computational Physics*, 87(2):408–463, April 1990.

[86] J. M. T. Ngnotchouye, M. Herty, and M. K. Banda. A multi-scale approach to the flow optimization of systems governed by the Euler equations. In L. Wiryanto and S. Pudjaprasetya, editors, *Proceedings of the Int. Conf. on Industrial and Appl. Math.*, pages 121–126. Institut Teknologi Bandung, Indonesia, 2010.

[87] J. M. T. Ngnotchouye, M. Herty, S. Veelken, and M. Banda. Relaxation approaches to the optimal control of the Euler equations. Computational and Applied Mathematics, 2011. (To appear).

[88] J. Nocedal and S. J. Wright. *Numerical Optimization*. Springer series in Operational research. Springer, 1999.

[89] S. Osher. Riemannsolvers,the entropy condition, and difference approximations. *SIAM J. Numer. Anal.*, 21:217–235, 1984.

[90] G. Pingen, A. Evgrafov, and K. Maute. Adjoint parameter sensitivity analysis for the hydrodynamic lattice Boltzmann method with applications to design optimization. *Computers and Fluid*, 38:910–923, 2009.

[91] J. A. Primbs. *Nonlinear optimal control: A receding horizon approach.* PhD thesis, California Institute of technology, 1999.

[92] Y. Qian, D. d'Humières, and P. Lallemand. Lattice BGK models for Navier-Stokes equation. *Europhys. Lett.*, 17:479–484, 1992.

[93] Y. H. Qian. Simulating thermohydrodynamics with lattice BGK models. *J. Sci. Comput*, 8(3):231–242, 1993.

[94] C. Rissoan, N. Goutal, and R. Herlédan. 1D hydraulic simulation of a dam break wave on the Rhone river. EDF-R&D, National Hydraulics and Environmental Laboratory, France.

[95] J. Rüdiger, J. Schiebelbein, R. Lunderstädt, and J. Horn. A new algorithm for gas network simulation. In *MIC'06: Proceedings of the 25th IASTED international conference on Modeling, indentification, and control*, pages 103–109, Anaheim, CA, USA, 2006. ACTA Press.

[96] M. P. Rumpfkeil and D. Zingg. A general framework for the optimal control of unsteady flows with applications. *AIAA paper 2007-1128*, 2007. 45th AIAA Aerospace Meeting and Exhibit, Reno, Nevada, USA.

[97] M. Schulz and G. Steinebach. Two-dimentional modelling of the river Rhine. *Journal of Computational and Applied Mathematics*, 145:11–20, 2002.

[98] G. Simpson and S. Castelltort. Coupled model of surface water flow, sediment transport and morphological evolution. *Computers & Geosciences*, 32:1600–1614, 2006.

[99] G. Steinebach, S. Rademacher, P. Rentrop, and M. Schulz. Mechanism of coupling in river flow simulation systems. *Journal of Computational and Applied Mathematics*, 168:459–470, 2004.

[100] P. K. Sweby. High resolution schemes using flux limiters for hyperbolic conservation laws. *SIAM Journal on Numerical Analysis*, 21(5):995–1011, 1984.

[101] J. Thorwarth. *Hydraulisches Verhalten von Treppengerinnen mit eigetieften Stufen-Selbstinduzierte Abflussinstationaritäten und Energiedissipation.* PhD thesis, Institut für Wasserbau und Wasserwirtschaft der RWTH Aachen, 2008.

[102] E. F. Toro. *Riemann solvers and numerical methods for fluid dynamics.* Spinger-Verlag, 2 edition, 1999.

[103] S. Ulbrich. *Optimal Control of Nonlinear Hyperbolic Conservation Laws with Source Terms.* Technische Universitaet Muenchen, 2001.

[104] S. Ulbrich. A sensitivity and adjoint calculus for discontinuous solutions of hyperbolic conservation laws with source terms. *SIAM J. Control Optim.*, 41:740, 2002.

[105] S. Ulbrich. Adjoint-based derivative computations for the optimal control of discontinuous solutions of hyperbolic conservation laws. *Systems & Control Letters*, 3:309, 2003.

[106] S. Veelken, M. Herty, J. M. T. Ngnotchouye, and M. Banda. Optimal control of the Euler equations via relaxation approaches. In *Proc. Appl. Math. Mech.*, volume 10, pages 595–596.

[107] A. I. Vol'pert and S. I. Hudjaev. *Analysis in classes of discontinuous functions and equations of mathematical physics*, volume 8 of *Mechanics: Analysis.* Martinus Nijhoff Publishers, Dordrecht, 1985.

[108] S. Vukovic and L. Sopta. Upwind schemes with exact conservation property for one-dimensional open channel flow equations. *SIAM J. Sci. comput*, 24(5):1630–1649, 2003.